Durham E-Theses

A neutron scattering study of adsorbed gases and some model compounds

Howard, J.

A NEUTRON SCATTERING STUDY OF ADSORBED GASES

AND SOME MODEL COMPOUNDS

BY

J. HOWARD B.Sc.

A thesis submitted in partial fulfilment of the requirements for

the degree of Doctor of Philosophy in the University of Durham.

October 1976
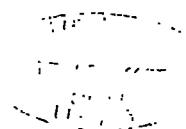
PREFACE

The work described in this thesis is original except where specifically stated to the contrary. It has not previously been submitted either wholly, or in part, for a degree at this or any other university.

To my family – with
thanks for all that
they have done.

Science is a first rate piece of furniture for
a man's upper chamber if he has common sense
on the ground floor.

O.W. Holmes

ACKNOWLEDGEMENTS

I would like to express my thanks to Professor T.C. Waddington, under whose guidance this research was undertaken, for considerable encouragement, advice and discussion.

The experimental work, relevant to this thesis, was carried out at Durham, A.E.R.E. Harwell and I.L.L. in Grenoble, and in consequence I have received help from a large number of people - far too numerous to thank by name. May I, however, thank the technical staff at Durham for their help and in particular Mr. R. Coult for preparing many of the organometallic complexes. My thanks also go to my colleagues in the neutron scattering group.

At Harwell the co-operation and assistance of the university support section is appreciated, especially of Mr. D.H.C. Harris, Mr. G. Haines and Mr. S. Stevens. I gratefully acknowledge the award of a research studentship from Harwell and the resulting "special consideration" I have received.

At Grenoble my thanks go primarily to Dr. J. Tomkinson, without whose unselfish help far less would have been accomplished.

A special word of thanks also to Mrs. B. McGonigle for transforming my dissordered script into the typed form here presented.

My deepest thanks are due to my wife, Anne, for all of the help and encouragement she has given, and for tolerating, without complaint, my long and frequent absences from home while I was engaged in experimental work.

ABSTRACT

Neutron scattering theory and spectrometers are described and the relevance of neutron scattering to surface science discussed. Low frequency vibrational modes of hydrogeneous ligands were studied, mainly by incoherent inelastic neutron scattering.

Complexes containing ethylene were investigated and their torsional vibrations assigned. The in-phase and out-of-phase torsions have been observed in the case of complexes containing more than one ethylene ligand, and models have been proposed for the interaction between the ethylene groups. The experimentally observed frequencies have been expressed in terms of constants derived from these models.

π-bonded complexes (π-allyls, norbornadienes and cyclobutadiene iron tricarbonyl) have been studied, their low frequency modes assigned and their effective torsional force constants calculated. However, there remains an anomaly in the assignments of the norbornadiene complexes.

Studies of square planar Pd and Pt ammines have shown that there is just a single torsional mode in each case. It has previously been suggested that the NH_3 ligands in trans complexes (particularly Pt) could couple via the "d" orbitals. No evidence of such coupling was found. From the momentum transfer dependence of the i.n.s. spectrum, and the temperature dependence of the i.r. spectrum, evidence for a significant metal-metal interaction in cis-$Pt(NH_3)_2Cl_2$ was obtained. In the case of sulfur complexes containing NH_3 and NH_2 groups, the torsions have been assigned. Comparison of their i.n.s. spectra with that of disilver sulfamide, has shown that the latter does not contain an NH_2 group.

C_2H_4 adsorbed on a silver exchanged zeolite (Ag-13X) at two different coverages was studied. From the observed i.n.s. intensities and shifts on deuteration (C_2D_4 and trans-$C_2D_2H_2$) assignments of the vibrational modes of the ethylene relative to the surface was possible. In the higher coverage case interaction between ethylenes on two different sites was observed. The i.n.s. spectrum of ethylene adsorbed on the sodium form of 13X was indicative of a much more weakly held species and an analysis of the quasi-elastic scattering confirmed this.

I.N.S. spectra of C_2H_2 and C_2D_2 adsorbed on Ag-13X were obtained and the acetylene-surface vibrations were assigned. From the shifts on deuteration it appears that the adsorbed molecule is non-linear. The i.n.s. spectra of C_2H_2 adsorbed on Na-13X was too poorly resolved for definite conclusions to be drawn.

Hydrogen adsorbed (at $200^{\circ}C$) on Pt black was studied in the region $0 \rightarrow 4000$ cm^{-1}. The adsorption conditions produced just one surface state (δ) and the adsorption was shown to be dissociative. A vibration of the hydrogen, relative to the surface, was observed at 403 cm^{-1}. In fact the spectra are best interpreted as being due to co-adsorbed H_2O and H. Higher energy peaks were obtained (including one assigned to the ν_2 vibration of water) but could not be definitely assigned. This project is not yet complete and further experimental work is required before full assignments can be made.

CONTENTS

Chapter 1   General Introduction

Section 1:   Neutron Spectroscopy

When a neutron enters a sample there are three possible occurrences, the neutron either

a) passes through without interaction

b) is absorbed

c) is scattered with or without exchanging energy with the sample.

This thesis is concerned with neutron scattering (c) and absorption will only be considered in so far as it influences the intensities of the observed spectral features.

Thermal neutrons are a unique probe for studying the dynamics of matter. This uniqueness stems from

1. the close similarity between the energy of the neutrons and the spacings of energy levels in the samples.

2. there are no electromagnetic selection rules to be obeyed and in principle all modes of motion are active. This point will be considered in more detail later.

3. neutrons transfer momentum to molecules along with energy. This is a consequence of the similarity between the mass of the neutron and the mass of the scattering atom. The transfer of momentum is not usually important in optical spectroscopy. Momentum transfers between 0.1 and 10Å^{-1} are common in neutron scattering and angular dependent intensities and peak widths follow from this. Analysis of the spectra can yield vibrational frequencies, vibrational amplitudes, diffusion coefficients etc. If a mode is dispersive its peak position will vary with momentum transfer $(\underline{Q})$ and the exchange of momentum varies with scattering angle.
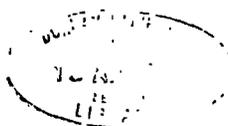
This is of particular importance for lattice modes because internal modes normally show little dispersion. In particular an acoustic lattice mode has a dispersion curve which indicates that at zero momentum transfer it has zero energy transfer:- consequently it is inactive in optical spectra but it will be active in a neutron spectrum.

4. the neutron scattering cross section of an atom depends upon the nature of the nucleus - it varies from element to element and isotope to isotope. This enables useful experiments involving isotopic substitutions to be done.

Thus thermal neutron scattering experiments combine, in the same experiment, both the spatial measurements that can be made with X-rays and the vibrational measurements obtainable with infra-red and Raman spectroscopy. Figs. 1a,b show the Q and energy range of some standard techniques[1] and plots of energy against wavelength for photons, neutrons and electrons.

In a typical experiment a monoenergetic beam of neutrons is incident on a sample and after scattering the energies of the neutrons are analysed at several angles of detection. We thus obtain, in the first instance, graphs of detected neutrons against energy. Peaks are obtained corresponding to neutron energy loss or gain.

The interaction of thermal neutrons with nuclei which are tightly bound in a solid results in an energy spectrum which consists of two parts; a sharp line at energy transfer zero (elastic scattering) and a region due to interaction with the molecular vibrations (inelastic scattering). If the scattering nuclei can undergo some diffusive process then as a result of this the sharp elastic line is broadened (quasi-elastic scattering). This quasi-elastic broadening is a feature

3.

b) Energy/λ Plots for electrons, neutrons and x-rays

Log(Å)

X-RAYS

NEUTRONS
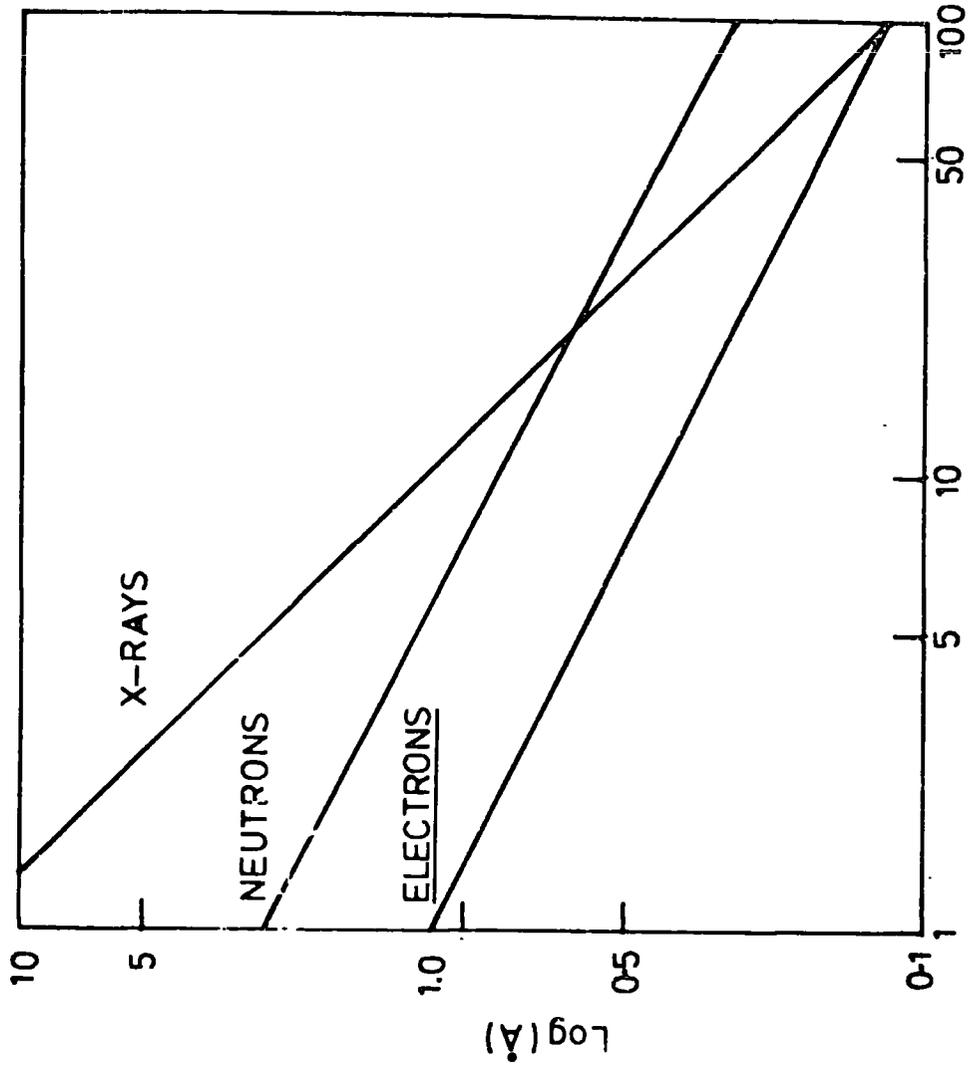
ELECTRONS

Electrons 100eV, Photons keV, Neutrons .01eV

Fig. 1   a) Q/ω Range of Some Techniques

X-RAY.
ELECTRON.

$Log_{10}(Å^{1})$

NEUTRONS

$Log_{10}(eV)$

R S

B S

S

X S

R S : Raman Scattering

B S : Brillouin Scattering

X S : X-Ray Scattering

of random rather than oscillatory motions and it can yield information

on the rate and geometry of such motions. Study of the inelastic

region yields information on the molecular vibrations and lattice modes.

In general when neutrons are scattered by a sample they do not

encounter a uniform scattering potential but one which varies from point

to point because of the different isotopes and spin orientations in the

sample. The scattering from a single nucleus can be characterised by a

single parameter b called the scattering length. The total scattering

cross section per atom σ_T is the effective area presented to an in-

coming neutron by the atom. It is given by

$$\sigma_T = 4\pi\, b^2$$

When a neutron encounters an array of nuclei the mean scattering potential

gives rise to interference effects (coherent scattering) and the

deviation from the mean leads to scattering which cannot have inter-

ference effects (incoherent scattering) because the deviations are

randomly distributed. Elements with predominantly one isotope and no

spin will therefore have no incoherent cross section (e.g. C and O).

The majority of elements and their isotopes have small incoherent cross

sections ($< 10 \times 10^{-24}$ cm^2). Hydrogen has an anomolously large

incoherent cross section (80×10^{-24} cm^2). This is due to the random

distribution of spin states and it is not isotopic in origin. All

other factors being equal, the inelastic neutron scattering spectrum of

a sample which contains hydrogen will be largely incoherent and it will

be dominated by those modes which involve motion of the hydrogen atoms.

This "effective" selection rule is the basis of the present study. The

incoherent cross section of deuterium is 2.0×10^{-24} cm^2 and this fact

is used extensively in isotopic substitution studies in two ways

1. selective deuteration will cause a reduction in intensity of modes associated with the deuterated fragment when compared to the spectrum of the undeuterated material.

2. complete deuteration enables frequency shifts to be measured. Table 1 lists the scattering cross sections for some elements.[2]

Table 1   Cross sections of some elements

Element	σ_{COH}*	σ_{INCOH}*
H	1.8	79.7
D	5.6	2.0
C	5.6	0.0
N	11.1	0.3
O	4.23	0.0
F	3.98	0.0
Si	2.16	0.0
Cl[+]	11.50	3.5
Ge	8.42	1.0
Br	5.79	0.3
I	3.50	0.4
Pd	4.50	0.3
Pt	11.30	0.7
Ag^{+}	4.48	1.8

*) Units of 10^{-24} cm^2 (barns)

+) average value

The double differential cross section $\left(\dfrac{d^2\sigma}{d_{\Omega}dE}\right)$ defined by

$$\frac{d^2\sigma}{d_{\Omega}dE} = \frac{\text{number of neutrons/sec. with energy E to E + dE scattered into solid angle } d_{\Omega}}{d_{\Omega} \times dE \times \text{incident flux}}$$

is the quantity that is observed in many neutron scattering experiments. This quantity can be derived from first order perturbation theory and Van Hove[3] has shown that it is intimately connected with some correlation functions and these, in the classical limit, permit interpretation in terms of simple physical models. Table 2 summarises some of the data available from neutron scattering experiments.

Table 2   Information available from neutron scattering experiments

	ELASTIC	INELASTIC
Coherent	Crystal and Magnetic Structures	Dispersion Relations
Incoherent	Study of the temperature variation is a test of models for the frequency distribution function. Diffusion Coefficients	Frequency Distribution Function

It can be shown (chapter II) that for molecular vibrations

$$\left(\frac{d^2\sigma}{d_{\Omega}dE}\right)_{inc} = \frac{k'}{k} \sum_{\nu} \frac{\sigma_{inc}}{4\pi} \frac{Q^2}{2M} \left(n_s + \frac{1}{2} \pm \frac{1}{2}\right) \exp(-2W) \frac{Z(\omega)}{\omega} \qquad (1)$$

k   the wave vector of the incident neutron $(k = |\underline{k}| = \frac{2\pi}{\lambda})$

k'   the wave vector of the scattered neutron

$\underline{Q}$ momentum transfer $(\underline{Q} = \underline{k} - \underline{k}')$

$Q^2 = \underline{Q}.\underline{Q}$

σ_{inc} the incoherent cross section

$\langle u^2 \rangle$ the mean square amplitude of vibration of the atom

$Z(\omega)$ the density of states in the system

ω the frequency of the mode (radians $\sec^{-1}$)

W the Debye Waller Factor $W = \frac{1}{3}Q^2 \langle u^2 \rangle$ where $\langle u^2 \rangle$ is the mean square vibrational amplitude of the atom

n_s $n_s = \left[\exp(\frac{\hbar\omega}{KT}) - 1 \right]^{-1}$

M the mass of the scattering atom.

The upper sign in $\pm\frac{1}{2}$ refers to neutron energy loss (down scattering) and the lower sign to neutron energy gain (up scattering).

We can see, therefore, that the differential cross section is weighted in favour of those atoms with large incoherent cross sections and large amplitudes of vibration. As mentioned earlier the value of σ_{inc} for hydrogen is more than an order of magnitude greater than for most other elements and furthermore because of its small mass the amplitude of vibration will be large.

Section II: General Aims

The object of this work was to apply the unique properties of neutrons to problems in molecular spectroscopy and in particular to the study of adsorbed species. Some of the most difficult data to collect by other techniques are the lower energy vibrational modes of adsorbed molecules and of organometallic complexes. The large incoherent scattering cross section of hydrogen has been utilised by studying hydrogeneous gases adsorbed on various surfaces. Two essentially different types of system have been studied

a) gases adsorbed on ion-exchanged zeolites

b) hydrogen adsorbed on Pt black.

The zeolite systems have the advantage of large surface areas so that large quantities of gas can be adsorbed (typically $40 cm^3 g^{-1} (C_2H_4)$) and the surface is relatively easily cleaned. Metal powders, on the other hand, have much lower surface areas and present a much more difficult cleaning problem.

In order to assist in the interpretation of the inelastic neutron scattering (i.n.s.) spectra of the adsorbed species, as well as for their general spectroscopic interest, we have also investigated a series of model compounds. The most important of these, in connection with the surface work actually discussed in this thesis, are the metal complexes which contain ethylene. π-complexes are thought to exist on many surfaces[4] and we have also investigated π-allyls, norbornadienes and cyclobutadiene iron tricarbonyl with this in mind. Also, in part as preparation for the study of adsorbed ammonia, we have investigated metal ammine and amido complexes. Our experience is that such data is very valuable in the evaluation of experimental data on adsorbed species.

Section III: Application of neutron scattering to surface science

Neutrons are not, in the usual sense, a surface probe. Applications of neutron scattering to the study of adsorbed (hydrogeneous) species rely primarily on the relative transparency of the support material when compared to the large cross section of the adsorbed species. Usually there are many more substrate than adsorbed atoms and this of course reduces the signal (i.e. counts from the adsorbed species) to background (i.e. counts from the substrate) ratio. One further feature,

not so far discussed, indicates that even so we should be able to obtain reasonable signal/background ratios. Equation 1 shows that the double differential scattering cross section is inversely proportional to the mass of the scattering atom. Obviously therefore, for a heavy substrate atom e.g. Pt, $\frac{d^2\sigma}{d_{\Omega}dE}$ will be reduced by a very large factor compared to the scattering from a proton.

It is obviously desirable that the substrate have as small a value of $\frac{\sigma_{inc}}{M}$ as possible. Table 3 lists values of $\frac{\sigma_T}{M}$ and $\frac{\sigma_{inc}}{M}$ for some elements.

Table 3: Calculated Values of $\left(\frac{\sigma_T}{M}\right)$ and $\left(\frac{\sigma_{inc}}{M}\right)$ for some metals

	σ_T	$\frac{\sigma_T}{M}$*	σ_{inc}	$\frac{\sigma_{inc}}{M}$
Ni	18.0	0.305	4.7	0.080
Pd	4.8	0.045	0.3	0.003
Pt	12.0	0.061	0.7	0.004
Cu	8.5	0.133	1.2	0.019
Fe	12.8	0.229	0.4	0.007
W	5.7	0.031	2.8	0.015
H	81.5	81.5	79.7	79.7

* a) σ_T and σ_{inc} in barns

   b) M in a.m.u.

We do,however,require a fairly large surface area sample and the greater the surface area the more successful the experiment is likely to be. The following is a calculation of the likely surface area necessary.

Metals typically have 10^{15} sites per cm^2.

We will assume the most favourable case i.e. a monolayer of H adsorbed on the metal. Considering 1 cm^2 of beam area and suppose we have an y% scatterer

y = number of hydrogens x cross section x 100

$y = n \times 80 \times 10^{-24} \times 100$

Usually we wish y $\approx$ 10%

Thus $n = 1.25 \times 10^{21}$

This is equivalent to 125 m^2 of surface/cm^2 of beam area. Thus for a beam 5 cm x 2.5 cm we require 1563 m^2 of surface area. If the metal powder has a surface area of $10m^2g^{-1}$ this means that we require 156g of powder. The incoherent scattering from this quantity of clean Pt powder would be 2.6%.

A metal powder is unlikely to have a surface area of 10^2mg^{-1} after heating at elevated temperatures for a period of time. $4 \rightarrow 5m^2g^{-1}$ is probably a more reasonable figure but to compensate for this we can obtain good i.n.s. spectra with less than 10% scatterers particularly if we count for longer times.

Section 1V: Neutron Scattering and Other Techniques

Many techniques have been applied to the study of adsorbed molecules though few of them can give information concerning the normal

modes of vibration.

I.R. has been used mainly for the study of molecules adsorbed on materials which are, at least, translucent to i.r. radiation e.g. zeolites or silica/alumina[5,6] etc. Adsorption on metals has mainly been studied using supported samples[7,8,9] though there are problems associated with high absorption of radiation by the support material, particularly in the lower frequency region, and with the influence of the support on the adsorbed species e.g. hydrogen spillover.[10] It is not obvious that results obtained with supported samples, are directly transferable to bulk materials though, of course, the study of supported samples is an important and interesting one in its own right. Reflection-absorption infrared is well suited to the study of well-defined metal surfaces e.g. single crystal faces or metal films. The theory and practical basis of the method have been established by Greenler[11,12,13] who was able to show that only those vibrations with dipole moment changes perpendicular to the surface would be i.r. active. The method would not appear to be universally applicable and Greenler has discussed the conditions and sample properties required for a successful experiment.[13] There are several excellent texts and reviews relating to the use of infrared spectroscopy in the study of surfaces [5,6,7,8,9] and Sheppard et al. have discussed recent results concerning the chemisorption of hydrocarbons on metals.[14]

The application of Laser Raman Spectroscopy to the study of adsorbed species has been recently reviewed by Cooney et al.[15] It appears that the majority of this work is directed to the study of systems where silica, zeolites etc. are the substrates. The major difficulty here seems to be the occurrence of fluorescence and in no

case has a surface-molecule vibration been observed. Low energy electron scattering has been used successfully in the study of adsorbed gas on metal ribbons. For instance vibrations of hydrogen on W were observed at 77 and 135 meV.[16] These are probably vibrations of hydrogen atoms parallel and perpendicular to the surface.

To summarise, although several techniques yield information on the vibrations of adsorbed molecules, each and every technique has its own advantages and difficulties and sphere of most suitable application. In particular the observation of the low frequency modes of gases adsorbed on unsupported metal powders is difficult by optical techniques. This is perhaps the region where neutron scattering can be applied most usefully. It must be pointed out, however, that neutron scattering has its own difficulties amongst which are

1. relatively poor resolution

2. fairly long experimental period - typically two days for a sample and two days for the background.

3. lack of ready access to spectrometers. This is a <u>very</u> important point from the point of view of an experimentalist. Although it is perhaps not too difficult to obtain scheduled time on a domestic spectrometer, applications are made well (3 months) in advance and time is allocated for specific dates. Problems with samples or spectrometers or even the need for additional time to finish an experiment may mean that an experiment cannot be repeated or completed for several months. This can be, at the very least, very frustrating!

Factors (1) and (2) are obviously related and they are both mainly dependent on the intensity of the neutron source. The advent of the

high flux reactor at Grenoble has lead to considerable improvements in
both of these factors.

References

1. P.A. Egelstaff, J. Stretton Downes and J.W. White "Molecular Sieves" Society of Chemical Industry, 306, (1968).

2. B.T.M. Willis (Ed), Chemical Applications of Thermal Neutron Scattering, Oxford University Press, 1973.

3. L. Van Hove, Phys. Rev., 95, 249, (1954).

4. G. Webb, Surface and Defect Properties of Solids, The Chemical Society, London (1971), Vol. 3.

5. M.L. Hair, Infrared Spectroscopy in Surface Chemistry, Marcel Dekker Inc., New York, (1967).

6. A.V. Kiselev and V.I. Lygin, Infrared Spectra of Surface Compounds, John Wiley and Sons, New York, (1975).

7. C.H. Rochester, Powder Technology, 13, 157, (1976).

8. R.P. Eishens, Acc. Chem. Res., 5, 74, (1972).

9. L.H. Little, Infrared Spectra of Adsorbed Species, Academic Press, London and N.Y., (1966).

10. P.A. Sermon and G.G. Bond, Catal. Rev., 8(2), 211, (1973).

11. R.G. Greenler, J. Chem. Phys., 44, 310, (1966).

12. R.G. Greenler, J. Chem. Phys., 50, 1963, (1969).

13. R.G. Greenler, Proc. 2nd Int. Conf. on Solid Surfaces, 1974, Jap. J. Appl. Phys. Suppl. 2 Pt.2, 1974, p.265.

14. N. Sheppard, D.H. Chenery, A. Lesiunas, J.D. Prentice, H.A. Pearce and M. Primet, Molecular Spectroscopy of Dense Phases, Proc. of 12th European Conf. on Molec. Spect., Strasbourg 1975, p.345.

15. R.P. Cooney, G. Curthoys and Nguyan The Tam, Advan. Catal., 24, 293, (1975).

16. F.M. Propst and T.C. Piper, J. Vac. Sci. Technol., 4(2), 53, (1967).

Chapter II: Theoretical Background

Introduction

The theory of neutron scattering is now well documented.[1,2,3,4,5] The purpose of the present chapter is to put into perspective some of the equations which we will use for later data analysis and to derive some relationships of particular relevance to this thesis. We will also describe the equations used in our calculations of torsional barriers.

Section I: Neutron Scattering

a)   Scattering by a Single Fixed Nucleus (elastic scattering)

The cause of the scattering is the nuclear force and this is known to be of short range (10^{-14}m) compared with the wavelengths of thermal neutrons (10^{-10}m). As a result it can be shown that for a single fixed nucleus the distribution of scattered waves is spherically symmetrical i.e. the scattering is isotropic. We consider a model which consists of a planar wave form for the incident neutron and scattering from a point nucleus; we define

a)   the wave vector of the incident neutrons is $\underline{k}$ ($k = \left|\underline{k}\right| = \frac{2\pi}{\lambda}$)

b)   the wave vector of the scattered neutrons is $\underline{k}'$

c)   the wave function of the incident neutrons is $e^{i\underline{k}\cdot\underline{r}}$

d)   the wave function of the scattered waves is $\frac{f}{|\underline{r}|}e^{i\underline{k}'\cdot\underline{r}}$

where f is a function called the Scattering Amplitude and λ is the wavelength of the neutrons. The total wave function at some point $\underline{r}$ is therefore

$$\psi(r) = e^{i\underline{k}\cdot\underline{r}} + \frac{f}{|\underline{r}|}e^{i\underline{k}'\cdot\underline{r}} \tag{1}$$

where $\underline{r}$ is the position vector of the point of observation and the scattering nucleus is at the origin. In this particular case $\left|\underline{k}\right| = \left|\underline{k}'\right|$

because the nucleus is fixed and we ignore the possibility of internal

excited states. f is determined by the properties of the nucleus and

it may be complex in which case neutron absorption takes place, and if

f is real it can be either positive or negative depending upon the

relative phases of the incident and scattered waves. Unless otherwise

stated we shall assume f is real. f can be written as a series in the

neutron energy (E)

$$f = -b + a_1E + a_2E^2 \ldots\ldots$$

but below 10KV the terms in E above are negligible. Thus we have

f = -b where b is called the <u>Scattering Length.</u> The value of b varies

from element to element and is a function of the spin state of the

nucleus, at present it is an empirical quantity.

Equation 1 can be derived more thoroughly by solving the

Schroedinger Equation for the system, neutron plus nucleus. The

problem is solved within first order perturbation theory by assuming

that the interaction between the neutron and nucleus is a small

perturbation. If the spherically symmetrical scattering potential is

written V($\underline{r}$) the solution for large distances $|\underline{r}-\underline{r}'|$ is [1]

$$\psi(\underline{r}) = e^{i\underline{k}\cdot\underline{r}} - \frac{e^{i\underline{k}'\cdot\underline{r}}}{|\underline{r}|}\left[\frac{m}{2\pi\hbar^2}\int e^{i(\underline{k}-\underline{k}')\cdot\underline{r}'}V(\underline{r}')d\underline{r}'\right] \qquad (2)$$

where m is the mass of the neutron, $\underline{r}'$ is the position of the nucleus

and $\underline{r}$ is the point of observation.

Comparing equations (1)' and (2) we can see that

$$f = -\left[\frac{m}{2\pi\hbar^2}\int_{-\infty}^{+\infty} e^{i(\underline{k}-\underline{k}')\cdot\underline{r}'}V(\underline{r}')d\underline{r}'\right] \qquad (3)$$

In fact $V(\underline{r}\,')$ is of very short range so that the $\exp(i(\underline{k}-\underline{k}\,').\underline{r}\,')$ term has hardly begun to deviate from unity before the scattering potential has declined to zero. The scattering amplitude can thus be written

$$f = -\frac{1}{4\pi} \int_{nucleus} \frac{2m}{\hbar^2} V(\underline{r}\,')d\underline{r}\,'$$

so that the scattering is independent of $\underline{Q}$ i.e. it is isotropic ($\underline{Q} = \underline{k} - \underline{k}\,'$).

The scattering amplitude is therefore proportional to the Fourier Transform of the scattering potential. The Fourier Transform $G(t)$ of a function $(f(\nu))$ is defined by

$$G(t) = \int_{-\infty}^{\infty} f(\nu) \exp(-2\pi i \nu t)d\nu$$

Calculation of $d\sigma/d\Omega$

$\frac{d\sigma}{d\Omega}$ is defined by; $\frac{d\sigma}{d\Omega} = \dfrac{\text{number of neutrons scattered into a solid angle}}{\text{solid angle x time x incident flux}}$
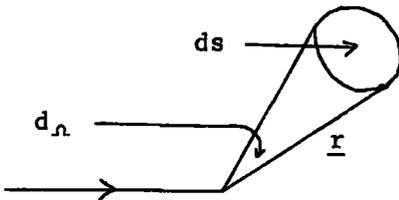
For the scattered wave $\psi_{sc}(\underline{r}) = e^{i\underline{k}.\underline{r}}$

For the incident wave $\psi_{inc}(\underline{r}) = \dfrac{b}{|\underline{r}|}e^{i\underline{k}\,'.\underline{r}}$

And from the diagram $d\Omega = \dfrac{ds}{|\underline{r}^2|}$

Number of neutrons through ds/sec = velocity x density x ds

$$= V \times \frac{b^2}{r^2} \times ds$$

$$= Vb^2 d\Omega$$

Note density $= |\psi|^2$

Thus $\dfrac{d\sigma}{d\Omega} = \dfrac{V \times b^2 \times d\Omega}{d\Omega \times \text{incident flux}}$

But   incident flux   = V x density

                                                 = V

Therefore $\dfrac{d\sigma}{d\Omega}$ = b^2 (4)

From which $\sigma = \displaystyle\int_{4\pi} \left(\dfrac{d\sigma}{d\Omega}\right) = 4\pi b^2$ (5)

and σ = $\dfrac{\text{total number of neutrons scattered/sec}}{\text{incident flux}}$

Returning to equations (1) and (2) it appears that if the form of V($\underline{r}$) is known then the scattering amplitudes and lengths can be calculated. Unfortunately, the detailed form of V($\underline{r}$) is not known, but Fermi suggested[1] choosing an equation for V($\underline{r}$) of the form

$$V(\underline{r}) = B\delta(\underline{r})$$ (6)

where $\delta(\underline{r})$ is the Dirac Delta Function (see Appendix 1) and B is a constant for a particular nucleus. The object is to choose a value for B so that the experimental and calculated values are identical, therefore by substituting (6) into (3) we obtain

$$f = \frac{-m}{2\pi\hbar^2}\ B$$

but $f = -b$

$\therefore$ $V(\underline{r}) = \dfrac{2\pi\hbar^2 b}{m}\ \delta(\underline{r})$ (7)

For the treatment of a free nucleus it is necessary to use centre of mass co-ordinates so that m is to be replaced by the reduced mass μ where $\mu = \dfrac{mM}{m+M}$

and M is the mass of the nucleus. We thus obtain the "free atom scattering length" "a" where a = $\left(\dfrac{M}{m+M}\right)$b and b is called the "bound atom scattering length".

For a rigidly bound nucleus no energy transfer can take place, while for a totally free nucleus translational energy transfer is possible. In reality the nuclei of a solid are neither totally free nor rigidly bound and whether or not they can be regarded as being in either of these two extreme states or intermediate between them depends on the incident energy of the neutron.

Scattering from an Array of Nuclei

The scattering potential, for an array of bound mono-isotopic nuclei, may be written

$$V(\underline{r}) = \frac{2\pi\hbar^2}{M} \sum_{L} b_L \; \delta(\underline{r}-\underline{R}_L) \tag{8}$$

where $\underline{R}_L$ and b_L are the position vectors and scattering lengths of the Lth nucleus. In first order perturbation theory the transition probability per unit time from a state i to f is given by

$$\left| \int dr \; \psi_f^*(\underline{r})V(\underline{r}) \; \psi_i \; (\underline{r}) \right|^2$$

which is written $|< f \,|V\,|i >|^2$

This can be shown[1] to lead to

$$\frac{d\sigma}{d\Omega} = \left(\frac{m}{2\pi\hbar}\right)^2 \; |< f \,|V\,|i >|^2 \tag{9}$$

which by comparison with equation (7) shows that the scattering amplitude is proportional to the transition probability. Since not all scattering is elastic the cross section becomes energy dependent and in this case equation (9) must be summed over all the final states of the nuclei and averaged over the initial states.[7]

$$\frac{d^2\sigma}{d\Lambda dE} = \frac{k'}{k} \left(\frac{m}{2\pi\hbar^2}\right)^2 \sum_{\lambda_i} P_{\lambda_i} \sum_{\lambda_f} |< f|V|i >|^2 \delta(\hbar\omega + E_{\lambda_i} - E_{\lambda_f}) \qquad (10)$$

where P_{λ_i} is the probability of the initial state λ_i $\left(\sum_{\lambda_i} P(\lambda_i) = 1 \right)$

and the δ function ensures conservation of energy in the system

neutron plus nucleus. To simplify the notation we have omitted

parameters involving the spin dependence of the scattering. By

substituting the equation for $V(\underline{r})$ (equation 8) into (10) more explicit

expressions for the cross section can be obtained, however, these do not

<u>clearly</u> relate the experimental quantity $\left(\frac{d^2\sigma}{d\Lambda dE}\right)$ to the fundamental

properties of the scattering centres. The formalism for doing this was

developed by Van Hove[6] who expressed the cross sections in terms of

correlation functions.

Coherent and Incoherent Cross Sections

Essentially by substituting equation 8 into equation 10 and

changing from a Schroedinger to a Heisenberg representation the cross

section can be written[7]

$$\frac{d^2\sigma}{d\Lambda dE} = \frac{k'}{k} \frac{1}{2\pi\hbar} \int_{-\infty}^{\infty} dt \, \exp(-i\omega t) \sum_{LL'} \overline{b_L b_L}' < \exp(-iQ.\hat{R}_L(0)\exp(iQ.\hat{R}_{L'}(t)) > \quad (11)$$

$\hat{R}_L(0)$ and $\hat{R}_L(t)$ are time dependent Heisenberg operators related to the

position vectors R_L of the L'th nucleus i.e.

$$\exp(iQ.\hat{R}_L(t)) = \exp\left(\frac{iHt}{\hbar}\right) \exp(iQ.R_L) \exp\left(\frac{-iHt}{\hbar}\right)$$

where H is the Hamiltonian of the target system.

$< \exp(-iQ.\hat{R}_L(0)) \exp(iQ.\hat{R}_{L'}(t)) >$ is the thermal average of the

expectation value of the time-dependent operators within the brackets

and where

$$\overline{b_L b_{L'}} = \left|\overline{b}\right|^2 + \delta_{LL'} \left(\overline{\left|b\right|^2} - \left|\overline{b}\right|^2\right)$$

Thus if $L = L'$

$$\overline{b_L b_{L'}} = \overline{\left|b\right|^2}$$

if $L \neq L'$ $\overline{b_L b_{L'}} = \left|\overline{b}\right|^2$

and $\overline{\left|b\right|^2} - \left|\overline{b}\right|^2 \equiv \overline{\left|b - \overline{b}\right|^2}$

Therefore $\overline{b_L b_{L'}}$ is the average of $b_L b_{L'}$ over random spin orientations and random isotope distributions. Also, for instance, if we consider the scattering lengths to be independent of spin, then if b_I is the scattering length of isotope I and C_I its concentration

$$\overline{b} = \sum_I C_I b_I$$

$$\overline{\left|b\right|^2} = \sum_I C_I \left|b_I\right|^2$$

The effect of defining these averages is to allow a separation of the cross section (equation 11) into the sum of two parts.[7] If we consider a system with only a single chemical species ($\overline{\left|b\right|^2} = \overline{b^2}$ and $\left|\overline{b}\right|^2 = \overline{b}^2$)

$$\frac{d^2\sigma}{d\Omega dE} = \left(\frac{d^2\sigma}{d\Omega dE}\right)_{inc} + \left(\frac{d^2\sigma}{d\Omega dE}\right)_{coh} \tag{12}$$

and

$$\left(\frac{d^2\sigma}{d\Omega dE}\right)_{coh} = N \frac{k'}{k} \overline{b^2} S_{coh}(\underline{Q}, \omega) \tag{13}$$

$$\left(\frac{d^2\sigma}{d\Omega dE}\right)_{inc} = N \frac{k'}{k} \left|b - \overline{b}\right|^2 S_{inc}(\underline{Q}, \omega) \tag{14}$$

where[7] in future we let $\frac{\sigma_c}{4\pi} = \overline{b}^2$ and $\frac{\sigma_{inc}}{4\pi} = \overline{\left|b - \overline{b}\right|^2}$, and where $\underline{Q} = \underline{k} - \underline{k}'$

$$S_{inc}(\underline{Q}, \omega) = \frac{1}{2\pi\hbar N} \int_{-\infty}^{\infty} dt \ \exp(-i\omega t) \sum_{L} < \exp(-i\underline{Q}.\hat{R}_L(0))\exp(i\underline{Q}.\hat{R}_L(t))> \quad (15)$$

and

$$S_{coh}(\underline{Q}, \omega) = \frac{1}{2\pi\hbar N} \int_{-\infty}^{\infty} dt \ \exp(-i\omega t) \sum_{LL'} < \exp(-i\underline{Q}.\hat{R}_L(0))\exp(i\underline{Q}.\hat{R}_{L'}(t))> \quad (16)$$

L and L′ are the L'th and L''th nuclei. $S_{inc}(\underline{Q}, \omega)$ depends only on

terms where L = L′ and so it behaves as if one had scattered from N

independent nuclei. $S_{coh}(\underline{Q}, \omega)$ on the other hand involves terms due to

scattering from different atoms. Coherent and incoherent scattering

are profoundly different. Coherent scattering involves strong inter-

ference between the waves scattered from each nucleus and strict

geometrical conditions are required for it to take place. For incoherent

scattering no interference takes place. $S(Q, \omega)$ is called the

"Scattering Law." We have separated the cross section into the sum of

incoherent (inc) and coherent (coh) parts. The physical significance

of this separation was discussed further in chapter 1. It is incoherent

scattering that is the main topic of this thesis. As we shall also see,

the assumption that we are dealing with a sample containing only a

single chemical species is a good approximation for any hydrogeneous

sample. As defined $S(\underline{Q}, \omega)$ is not symmetrical in ω but a new function

$\tilde{S}(Q, \omega)$ can be defined[1] by

$$S(\underline{Q}, \omega) = e^{\frac{-\hbar\omega}{2KT}} \ \tilde{S}(\underline{Q}, \omega)$$

and this is symmetrical in ω.

Correlation Functions

A clearer physical picture[1,7] can be obtained by considering

$S(\underline{Q}, \omega)$ as the double Fourier transform (in two variables) of a

function which is called $G(\underline{r}, t)$.

$$S(\underline{Q}, \omega) = \frac{1}{2\pi\hbar N} \iint \exp(-i(\omega t - \underline{Q}.\underline{r})) \, G(\underline{r}, t) \, d\underline{r}dt \qquad (17)$$

For $S_{inc}(\underline{Q}, \omega)$ we obtain the <u>Self Pair Correlation Function</u> $(G_s(\underline{r}, t))$ by[1,7] comparing equations (17) and (15) i.e.

$$G_s(\underline{r}, t) = \left(\frac{1}{2\pi}\right)^3 \int d\underline{Q} \, \exp(i\underline{Q}.\underline{r}) \, \frac{1}{N} \sum_L < \exp(-i\underline{Q}.\hat{R}_L(0))\exp(i\underline{Q}.\hat{R}_L(t))> \qquad (18)$$

with an analogous expression[1,7] for $G(\underline{r}, t)$ which on Fourier transformation yields $S_{coh}(\underline{Q}, \omega)$.

It can be shown that[1,7]

$$G_s(\underline{r}, t) = \frac{1}{N} \sum_L \int d\underline{r}' < \delta(\underline{r}-\underline{r}' + \hat{R}_L(0)) \, \delta(\underline{r}'-\hat{R}_L(t)> \qquad (19)$$

$G_s(\underline{r}, t)$ and $G(\underline{r}, t)$ are complicated functions because in general the operators $\hat{R}_L$ are non-commuting. The physical significance of the correlation functions can be appreciated by considering a <u>classical</u> system with all nuclei equivalent then[1,7]

$$G_s(\underline{r}, t) = < \delta(\underline{r} - R_L(t) + R_L(0))> \qquad (20)$$

and this is the probability that if an atom is at the origin at time $t = 0$ the same atom is at $\underline{r}$ at time t. $G(\underline{r}, t)$ can be similarly derived but in this case it represents the probability that if an atom is at the origin at time 0 then <u>some</u> atom (not necessarily the same one) is at $\underline{r}$ at time t. X-ray scattering gives information about $G(\underline{r}, t)$ and infra-red spectroscopy about $G_s(\underline{r}, t)$, however, even though the same functions are measured as in neutron scattering the ranges of Q and ω are different and so different information is obtained.

Neutron Scattering from Molecules

When the scattering occurs from molecules it is necessary to consider a more complex position vector than R_L. The usual assumption is that the vibrational, rotational and translational contributions to the scattering are separable i.e. the total wave function is separable $\psi = \psi(\text{translation}) \, \psi(\text{rotation}) \, \psi \, (\text{vibration})$. The position vector is written

$$R_L = C_L + d_L + U_L$$

where C_L is the co-ordinate of the centre of mass of the molecule, d_L is the mean position vector of the scattering atom relative to the centre of mass and U_L is the displacement of the nucleus from the mean. In practice both U_L and d_L are functions of the molecular orientation so that observation of vibrational motion also includes effects due to rotation. This is usually ignored in theoretical treatments so that we obtain

$$S(\underline{Q}, \omega) = \frac{1}{2\pi\hbar N} S_{trans}(\underline{Q}, \omega)^* S_{rot}(\underline{Q}, \omega)^* S_{vib}(\underline{Q}, \omega) \qquad (21)$$

where $*$ denotes convolution.

It is therefore possible to obtain the total scattering law by deriving expressions for the three components and convoluting them. As a result of this convolution the bands due to vibrations will be broadened; studies of broadening are, however, normally limited to the quasi-elastic region of the spectrum. Convolution, $H(\delta)$, of two functions $f(x)$ and $g(x)$ is defined by

$$H(\delta) = \int_{-\infty}^{\infty} f(x)g(\delta-x)dx = f(x) * g(x)$$

so that it produces a function of a new variable (δ). In effect every

value of $f(x)$ is multiplied by the corresponding value of $g(\delta-x)$ and

so a quantity is obtained which varies as δ varies (see fig).
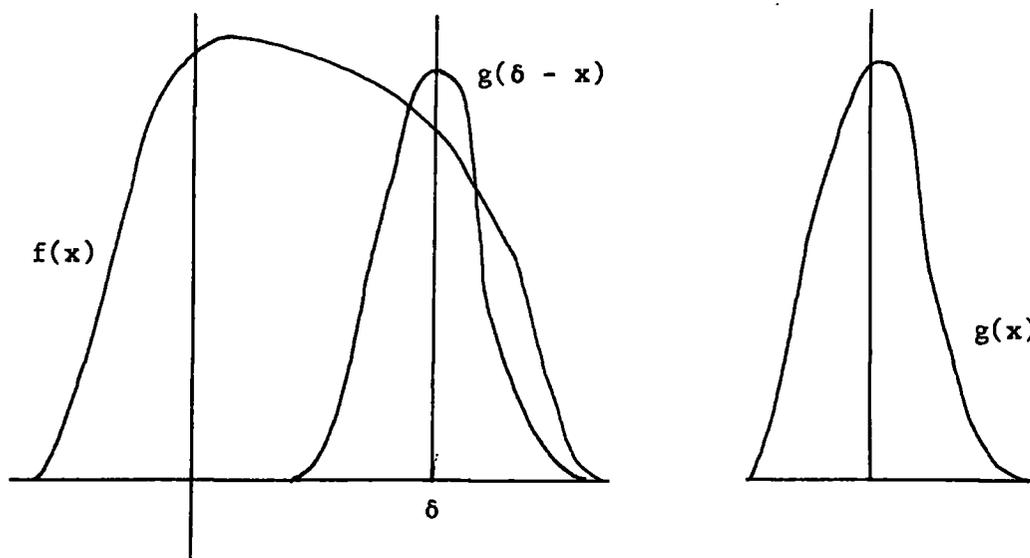
The physical significance of convolution can be illustrated if we

consider $f(x)$ to represent the distribution of intensity in the focal

plane of a spectrometer and $g(x)$ is the distribution in sensitivity

over the face of the detector which is slid across the focal plane.

The measured intensity when the detector is placed with its origin at

y is given by

$$\int_{-\infty}^{\infty} f(x)g(x-y)dx = f(x)*g(-x)$$

Scattering Law for Vibrations

The scattering law for vibrations has been discussed by Zermach

and Glauber[8] and we merely quote the result they obtained for an

assembly of identical harmonic oscillators.

$$\left(\frac{d^2\sigma}{d_\Omega dE}\right)_{inc} = \frac{k'}{k} \frac{1}{2\pi\hbar} \sum_L b^2 \; x \prod_\lambda \left[\exp(-(\underline{Q}.\underline{C}_L{}^\lambda)^2 \frac{\hbar}{2\, \omega_\lambda} \coth \frac{\hbar\omega_\lambda}{2KT})(\; |n_\lambda| \;)^{-1} \right.$$

$$\left. x \; \exp\left(-\frac{n_\lambda \hbar \omega_\lambda}{2KT}\right) \left(\frac{\hbar \; x \; (\underline{Q}.\underline{C}_L{}^\lambda)^2}{4 \; \omega_\lambda \; \sinh(\hbar\omega_\lambda/2KT)}\right)^{|n_\lambda|} x \; \delta(\hbar\omega - \hbar \sum_\lambda n_\lambda \omega_\lambda) \right] \qquad (22)$$

n   the number of quanta involved in a transition
$\begin{cases} n > 0 \text{ for neutron energy} \\ \text{gain} \\ n < 0 \text{ for neutron energy} \\ \text{loss} \end{cases}$

λ the normal mode

ω_λ frequency of each of the n quanta

M   mass of the L'th nucleus

K   Boltzmann's Constant

$\underline{C}_L{}^\lambda$ amplitude vector

We can make several immediate deductions from equation 22

a)   For elastic scattering $n_\lambda = 0$

Thus $\left(\frac{d^2\sigma}{d_\Omega dE}\right)_{\substack{inc \\ elastic}} = \frac{k'}{k} \frac{1}{2\pi\hbar} \sum_L b^2 \; \exp(-2W_L)$ \qquad (22a)

with $W_L = \frac{1}{4} \sum_\lambda \left(\frac{(\underline{Q}.\underline{C}_L{}^\lambda)}{\alpha_\lambda}\right)^2 \coth \left(\frac{\hbar\omega_\lambda}{2KT}\right)$

where $\alpha_\lambda{}^2 = \frac{\omega_\lambda}{\hbar}$

$\exp(-2W_L)$ is called the Debye-Waller Factor (D.W. factor). As $\underline{Q}$ increases the D.W. factor decreases so that the intensity of the quasi-elastic region decreases. The elastic incoherent scattering from a simple harmonic oscillator is therefore _not_ isotropic, however it has been shown[4] that provided the energy of incident neutron is small, compared to the energy levels of the oscillator, the scattering has only a very small angular dependence.

b)   For inelastic scattering ($n_\lambda \neq 0$) the intensity of an n quantum transition is governed by the factor $\left(\dfrac{\hbar(Q \cdot C_L{}^\lambda)^2}{4\ \omega_\lambda \sinh(\hbar\omega_\lambda/2KT)}\right)^{|n_\lambda|} \times \exp\left(\dfrac{-n_\lambda \hbar\omega}{2KT}\right)$

Because the term which is to be raised to the power $|n_\lambda|$ is _usually_ small this indicates that the single quantum transition will be much more intense than one involving two or more quanta. Likewise because of the product term $\prod_\lambda$ simultaneous transfer of single quanta to different normal modes again involves raising this term to the power n.

c)   Because of the delta function term the inelastic region should consist of a series of delta functions with zero intensity in between, however in practice this is not obtained because of the convolution mentioned earlier.

d)   It is possible to calculate the dependence of the intensity of first and second overtones on temperature and Q (Appendix 3). The single quantum cross section is therefore $\left(\text{with } A_\lambda = \exp\left(-\dfrac{\hbar\omega_\lambda}{2KT}\right)\right)$

$$\frac{d^2\sigma}{d\Omega dE} = \frac{k'}{k}\ \frac{1}{2\pi\hbar}\ \sum_L b^2\ \exp(-2W_L)\ \frac{A_\lambda}{1-A_\lambda}\ \frac{(Q \cdot C_L{}^\lambda)^2}{2\ \alpha_\lambda{}^2}\ \delta\ (\hbar\omega - \hbar\omega_\lambda) \qquad (23)$$

It can be seen that the intensity of a transition is a function of the incoherent cross section, the momentum transfer and also the amplitude vectors for each mode. The single quantum coherent cross section can also be written as[21]

$$\frac{d^2\sigma}{d\Omega dE} = \frac{k'}{k}\ \sum_\lambda \frac{\sigma_{inc}}{4\pi}\ \frac{Q^2}{2M}\ (n_s + \tfrac{1}{2} \pm \tfrac{1}{2}) \times \exp(-2W)\ \frac{Z(\omega)}{\omega} \qquad (24)$$

$Z(\omega)$ is the density of states spectrum $\displaystyle\int_0^\infty Z(\omega)d\omega = 1$

M   is the mass of the scattering atom

$2W = \tfrac{1}{3} <u^2> Q^2$

$n_s = \left(\exp\left(\dfrac{\hbar\omega}{KT}\right) - 1\right)^{-1}$

$<u^2>$ is the mean square vibrational amplitude of the atom.

From this we can easily see the advantages to be gained by using hydrogenous samples

a)   for hydrogen $\frac{\sigma_{inc}}{4\pi}$ is 40 times greater than any common element except Cl.

b)   because of its small mass $\frac{1}{M}$ for hydrogen atoms is large.

Furthermore because b for deuterium is small (2.0) partial isotopic substitution can be very useful in assigning normal modes.

Equations 23 and 24 use the approximation $(\underline{Q}.\underline{C}_L{}^\lambda)^2 = \frac{1}{3} Q^2$ which is strictly only valid for a system of cubic symmetry but which is thought to be a good approximation in general.[1,2]

Section II: Quasi-Elastic Scattering

As we have stated earlier the experimentally observed quantity in a neutron scattering experiment is closely related to $S(\underline{Q}, \omega)$ and this is the double Fourier Transform of the correlation function $G(\underline{r}, t)$. We consider three possible situations

a)   the scattering atom is freely diffusing so that $G(\underline{r}, \infty) = 0$ e.g. a gas. A typical case is shown in fig. 1a.
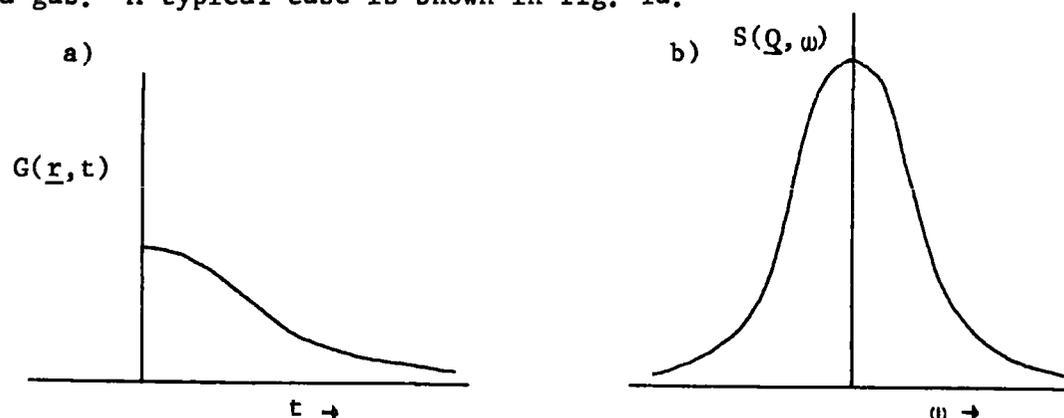
Fig. 1 a) $G(\underline{r}, t)$ and b) $S(\underline{Q}, \omega)$ for a freely diffusing atom.

The Fourier transform of this is a bell-shaped function (fig. 1b) so that typically we would expect a neutron scattering experiment, on a freely diffusing system, to yield a result similar to that shown in fig. 1b (quasi-elastic region).

b)   An important change in the spectrum takes place if we consider the scattering atom to be restricted to a finite volume of space e.g. a rotating molecule in a solid.

In this case $G(\underline{r}, \infty) \neq 0$ (fig. 2a)
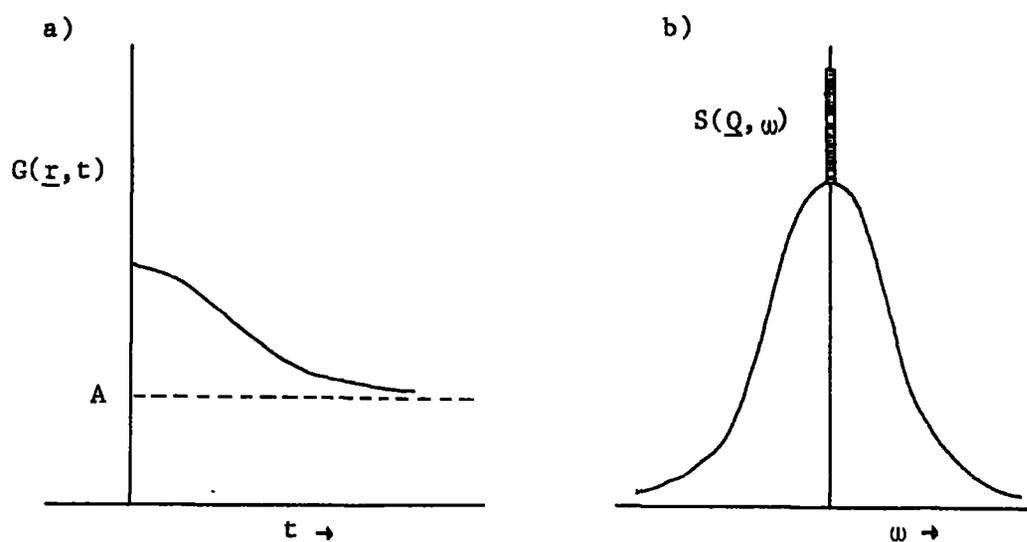
Fig. 2 a) $G(\underline{r},t)$ and b) $S(\underline{Q}, \omega)$ for an atom restricted in space.

$G(\underline{r}, t)$ is in this case assymptotic to some non-zero value A. We can write

$$G(\underline{r}, t) = G'(\underline{r}, t) + A$$

Because the Fourier Transform (F.T.) of a sum is the sum of the F.T.s of the components the final spectrum will contain a bell-shaped contribution (from $G'(r, t)$) similar to that discussed in case (a) (fig. 1b) and a δ function at the origin, which arises from the F.T.

of the constant. Therefore in this case the quasi-elastic region

contains two components of fundamentally different natures.

c)   A molecule in a liquid may undergo both translational diffusion

and random rotation so that a composite spectrum may be expected.

Naturally we have ignored the effects of experimental resolution.

In practice the sharp elastic peak and the whole spectrum will be

broadened as a result of the finite instrumental resolution available.

Several models have been proposed for calculating quasi-elastic

neutron spectra. It is not possible to analyse spectra directly in

detail. The normal procedure involves the following steps

1)   Selection of a model for the scattering process in the system.

2)   Formulation of this model in mathematical terms.

3)   Calculation of the scattering law.

4)   Fitting this scattering law to the observed spectra and testing to

     see if the fit is reasonable as a function of Q - with a fixed set

     of values for the fitting parameter(s).

The complications and difficulties involved in this process will be

discussed later.

A full discussion of quasi-elastic neutron scattering has been

given by Springer[9] and we shall discuss only those ideas relevant to

the work in this chapter.

A)   Free Rotation

This is not really possible in a solid, however, nearly free

rotation has been observed in solid hydrogen. Free rotation models

have been derived for gases e.g. NH_3, CH_4 etc.[3] The difference between

nearly free and free rotation is shown in fig. 3.
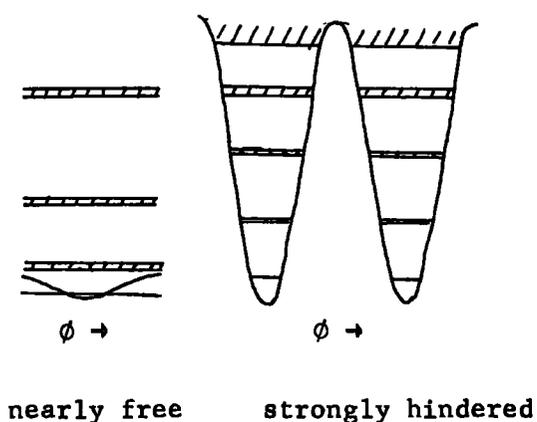
For nearly free rotation the energy states of the rotating molecule are far above the maximum of the hindering potential.

nearly free   strongly hindered

B)   Rotational Diffusion

In this case the rotational levels are completely blurred by interactions between the rotations and the thermal vibrations of the lattice. The motion is characterised by a single parameter:- the diffusion coefficient D_r.

C)   Jump Diffusion

This involves both libration and diffusion. The simplest, and most usual, case is to assume that the molecule librates in an equilibrium position for a time τ and then instantaneously rotates to a new equilibrium position by the shortest path. This model is clearly non-physical because it ignores the rotational energy involved as a result of the finite moment of inertia of the molecule.

Larson has proposed a more realistic model,[10] though he restricts his discussion to the case of a proton moving on the surface of a sphere. He associates two characteristic times to the motion

   τ_o the time spent librating

   τ_1 the time for which rotation occurs.

Phenomenologically Larson describes the model by assuming that the two modes of motion are linked to the microscopic density fluctuations in the material. Densities larger than average allow only damped librations and densities lower than average allow damped rotation. Obviously by judicial selection of the parameters this type of model could be used to describe the whole range of possibilities between free rotation and strongly hindered motion. The graph shown in fig. 4 shows the general case for <u>uniaxial</u> rotation
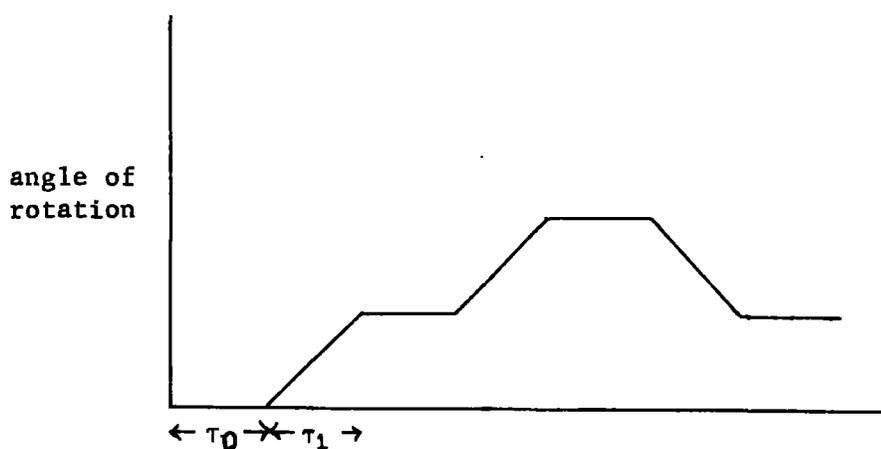
<u>Fig. 4</u> Angle of Rotation versus Time for Uniaxial Rotation.

a) $\tau_1 \to 0$ and τ_0 large   instantaneous jumps between deep wells.

b) $\tau_1 \neq 0$ but small and $\tau_0 \to 0$ rotational diffusion

c) $\tau_1 \to \infty$ and $\tau_0 = 0$ free rotation

d) $\tau_1 = 0$ and $\tau_0 \to \infty$ undamped libration

D)   <u>Random Walk Between N sites</u>

This is a special case of Jump Diffusion but the angle of rotation can be expressed as $\alpha = \dfrac{2\pi}{N}$ where N is an integer.

Uniaxial Motion

We will describe below the actual models used in this thesis. The theoretical work has been described in detail by Dianoux[11] and Springer.[9] The rotation is assumed to take place with the protons moving on a circle of fixed radius. If more than one radius exists in the molecule then the total scattering law is obtained by taking an average over the different radii of gyration.

a) Uniaxial Rotational Diffusion

If ϕ and ϕ_0 are the angular positions of the nuclei on a circle of radius "a" at times "t" and "0" respectively the probability distribution function is given by

$$\frac{\partial P_{rot}}{\partial t} = D_r \frac{\partial^2 P_{rot}}{\partial \phi^2}$$

The solution is

$$P_{rot}(\phi, \phi_0, t) = \frac{1}{2\pi} \sum_{n=-\infty}^{+\infty} \exp[in(\phi - \phi_0)] \exp(-D_r n^2 |t|) \qquad (25)$$

Where D_r is the rotational diffusion coefficient. The rotational scattering law is given by the powder average (over θ) of

$$S_{inc}^{rot}(\underline{Q}, \omega) = I_o^2(Q \, a \, \text{Sin} \, \theta)\delta(\omega) + \frac{2}{\pi} \sum_{n=1}^{\infty} I_n^2(Qa \, \text{Sin} \, \theta) \frac{D_r n^2}{(D_r n^2) + \omega^2} \qquad (26)$$

$I_i(Z)$ are the spherical Bessel functions. a is the radius of gyration of the proton.

Equation (26) has several important characteristics
a) the first term involves a δ function whose amplitude is a function of the molecular parameter "a". The existence of a δ function term, when $\hbar\omega = 0$, was predicted earlier.

b)   the second term represents the quasi-elastic scattering and it can be seen that it involves the sum of an infinite number of Lorentzian shaped curves.   The contribution of each Lorentzian to the total peak shape is determined by the Bessel function I_n. Furthermore the half width of a Lorentzian $\dfrac{d}{d^2+\omega^2}$ is "d" so the F.W.H.H. of each Lorentzian is $D_r n$.
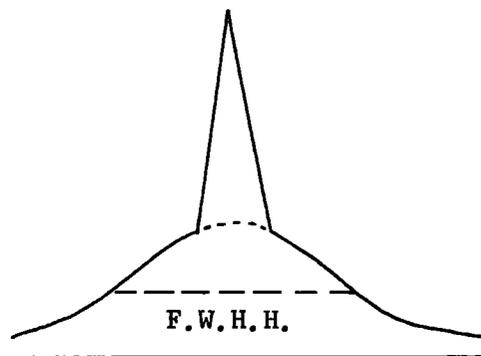
It has been shown that the major contribution to the quasi-elastic scattering comes in fact from the first Bessel function and the width of the quasi-elastic peak increases only slowly with Q until Qa = 3.

Composite Spectrum

Uniaxial Rotational Jump Model

In this case the assumption is made that the motion is by instantaneous jumps of angle α with a characteristic time τ between jumps.

It has been shown that the probability distribution function is given by

$$P_{rot}(\phi,\,\phi_0,\,t) = \frac{1}{2\pi} \sum_{n=-\infty}^{\infty} \exp[in(\phi-\phi_0)]\exp\left(-\frac{1 - \cos n\alpha}{\tau}\,|t|\right) \qquad (27)$$

This equation is very similar to eqn (25) i.e. each term consists of a phase factor multiplied by an amplitude factor. If we replace $D_r n^2$ by $\dfrac{1 - \cos n\alpha}{\tau}$ then the equations are identical. For very small jumps by setting $D_r n^2 = \dfrac{1 - \cos n\alpha}{\tau}$ one obtains $D_r = \dfrac{\alpha^2}{2\tau}$ and this serves as a definition of the rotational diffusion coefficient. The inverse

relationship between D_r and τ is what would be expected i.e. large time between jumps $\equiv$ small diffusion coefficient etc.

Random Walk Between N Equivalent Sites

The jump angle is now given by $\alpha = \dfrac{2\pi}{N}$ and the distribution function is still given by equation 27.

Defining $\tau_n = \dfrac{\tau}{1 - \cos n\alpha}$

then $\quad \tau_{n+pN} = \dfrac{\tau}{1 - \cos(n+pN)\alpha} = \dfrac{\tau}{1 - \cos(n\alpha+2\pi p)} = \dfrac{\tau}{1 - \cos n\alpha} = \tau_n$

where p is on integer.

The distribution function can be written in the form

$$P_{rot}(\phi, \phi_0, t) = \frac{1}{N} \sum_{n=0}^{N-1} \exp\left(-\frac{|t|}{\tau_n}\right) \exp[in(\phi-\phi_0)] \times \sum_{p=-\infty}^{\infty} \delta(\phi-\phi_0 - \frac{2\pi p}{N}) \qquad (28)$$

The delta function term ensures that the jump angle $(\phi-\phi_0)$ must be an integer multiple of α for it to have a non-zero probability. It is still true that $P_{rot}(\phi_0) = \dfrac{1}{2\pi}$ since the motions of different molecules are assumed uncorrelated.

The rotational scattering law is

$$S_{int}^{rot}(\underline{Q}, \omega) = A_0(Qa \sin\theta)\delta(\omega) + \frac{1}{\pi} \sum_{n=1}^{N-1} A_n(Qa \sin\theta) \frac{\tau_n}{1+(\omega\tau_n)^2} \qquad (29)$$

where $A_n(x) = \dfrac{1}{N} \displaystyle\sum_{p=1}^{N} I_0(2x \sin \frac{\pi p}{N}) \cos(n \frac{2\pi p}{N})$

and $\quad \tau_n = \dfrac{\tau_1 \sin^2(\pi/N)}{\sin^2(n\pi/N)} \qquad\qquad \tau_1 = \dfrac{\tau}{1 - \cos(2\pi/N)} \qquad (30)$

For N $\rightarrow \infty$ these equations become identical to the rotational diffusion

model with $D_r = \dfrac{1}{\tau_1}$. In fact for N > 6 and Qa $\leq$ 3 the two models are

almost identical. The advantage of (29) is that the powder average may

be obtained analytically which is not the case for (26). This makes the

computations easier and involves a saving of a factor of 10 in computing

time when N = 10 compared to the rotational diffusion model.

The result of taking the powder average is

$$S_{inc}^{rot} (\underline{Q}, \omega) = I_0(Qa)\delta(\omega) + \frac{1}{\pi} \sum_{n=1}^{N-1} B_n(Qa) \frac{\tau_n}{1+(\omega\tau_n)^2} \qquad (31)$$

where $\quad B_n(Qa) = \dfrac{1}{N} \sum_{p=1}^{N} I_0(2Q \, a \, \sin \frac{\pi p}{N}) \cos n \left(\frac{2\pi p}{N}\right)$

Once again we have a purely elastic line and this time a quasi-elastic

contribution consisting of a sum of N Lorentzians. It is important to

note that it is usual to assume that translational, rotational and

vibrational motions are uncorrelated. In this case in the quasi-

elastic region the vibrations contribute only through the Debye-Waller

factor so that on Fourier Transformation to obtain $S(\underline{Q}, \omega)$ the result

will be a convolution of the rotational and translational parts

multiplied by the Debye-Waller factor.

Section III: Comparison between optical and i.n.s. data

A t. of f. spectrum measures the intensity of scattered neutrons

both as a function of ω and $\underline{Q}$ and so it is not suitable for direct

comparison with optical spectra. A suitable function, for this

purpose, derived from i.n.s. data is $\rho(\omega)$[12] where

$$\rho(\omega) = \frac{4M\omega}{\hbar} \sin h \left(\frac{\hbar\omega}{2KT}\right) \left(\frac{\widetilde{S}(Q, \omega)}{Q^2}\right)_{Q\to0} \qquad (32)$$

and

$$\rho(\omega) = 2\beta \sin h \left(\frac{\beta}{2}\right) \left(\frac{S(\alpha, \beta)}{\alpha}\right)_{\alpha\to0} \qquad (33)$$

where $\alpha = \frac{\hbar^2 Q^2}{2MT}$ and $\beta = \frac{\hbar\omega}{KT}$ $\qquad (34)$

We also have

$$P(\alpha, \beta) = \frac{KT}{\hbar} \rho(\omega) \qquad (35)$$

The determination of $\rho(\omega)$ therefore involves extrapolating $\frac{\widetilde{S}(Q, \omega)}{Q^2}$ to

zero momentum transfer for fixed values of ω. It has the advantage of

using the data from all the angles of detection. Difficulty arises

because on many t. of f. neutron spectrometers, really small values of

$\underline{Q}$ are not obtainable. This means that a really reliable extrapolation

cannot be performed, particularly because $\frac{S(Q, \omega)}{Q^2}$ vs Q is not in fact

linear over the full Q range.

By substituting equation 24 into equation 32 we can see that $\rho(\omega)$

is in fact an amplitude weighted density of states. Thus we can write

(for neutron energy gain)

$$n_s = \frac{1}{e^{\frac{\hbar\omega}{KT}} - 1} = \frac{e^{-\frac{\hbar\omega}{2KT}}}{e^{\frac{\hbar\omega}{2KT}} - e^{\frac{\hbar\omega}{2KT}}}$$

$$= \frac{e^{-\frac{\hbar\omega}{2KT}}}{2 \sin h \left(\frac{\hbar\omega}{2KT}\right)}$$

Thus

$$\rho(\omega) = \frac{4M\omega}{\hbar} \sin h \left(\frac{\hbar\omega}{2KT}\right) e^{+\frac{\hbar\omega}{2KT}} \frac{1}{2M} e^{-\frac{\hbar\omega}{2KT}} e^{-2W} \frac{Z(\omega)}{\omega} \times \frac{1}{2\sinh\left(\frac{\hbar\omega}{2KT}\right)}$$

$$\rho(\omega) \alpha \qquad Z(\omega) e^{-2W}$$

Such an extrapolation procedure is not possible for results obtained using the B.F.D. spectrometer where data is collected at just one angle but Wright and White have shown[13] that the counts are approximately proportional to the unnormalised density of states though there is no provision for extrapolation to zero momentum transfer.

Section IV: Momentum Transfer Dependence of i.n.s. Bands

i.n.s. spectra involve appreciable momentum transfers (Q) and the value of Q varies with the angle of detection. Therefore, if a mode is dispersive the peak position will vary with angle. The magnitude of this variation will depend upon the angles of detection and the shape of the dispersion curve. Furthermore, as stated in equation 24, the value of $\frac{d^2\sigma}{d\Omega dE}$ is a function of the density of states ($Z(\omega)$). It has been shown that, for one dimension and for a value of Q, $Z(\omega)$ is inversely proportional to the gradient of the dispersion curve at that point.[14] If a mode is dispersive the gradient will change from point to point so that the intensity of the associated i.n.s. band will also vary. Obviously the greatest intensity region occurs where the dispersion curve is almost flat. If a mode is non-dispersive then $Z(\omega)$ is constant as is the peak position.

Lattice modes usually show a much greater degree of dispersion than do internal modes and so they can often be identified in the i.n.s. spectrum by their variations in intensity and peak position.

Section V: Time-Scales

A neutron scattering experiment performs a F.T. of the correlation functions $G_s(\underline{r}, t)$ and $G(\underline{r}, t)$ in space and time. The frequency and wave vector of the components are defined by the energy and momentum

transferred during the scattering process.

From the theory of Fourier Integrals it is well known that a phenomenon of duration "t" is represented by a frequency distribution of width not less than $\delta v \approx \frac{1}{2\pi t}$. That is, the behaviour of the original function at large arguments is responsible for the transformed function at small arguments and vice versa.

The Heisenberg Uncertainty Relation may be written

$$\Delta E . \Delta t > \hbar$$

$$\text{or} \quad \Delta v . \Delta t > \frac{1}{2\pi}$$

$$\text{or} \quad \Delta x . \Delta p \approx \hbar$$

$$\text{or} \quad \Delta x . \Delta Q \approx 1$$

Therefore

a) measurements at large momentum transfers implies information over small distances and vice versa

b) measurements involving large energy transfers implies information over short times.

Table 1 lists time scales for some techniques.

Table 1   Time scales for some scientific techniques

technique	Time scale (secs)
X-ray and electron diffraction	10^{-18}
u.v.	10^{-15}
Visible	10^{-14}
I.R. and R	10^{-13}
Neutron diffraction and I.N.S.	10^{-13}
E.S.R.	$10^{-4} \rightarrow 10^{-8}$
N.M.R.	$10^{-1} \rightarrow 10^{-9}$
N.Q.R.	$10^{-1} \rightarrow 10^{-8}$

Section Vl: Barrier Calculations

Choice of Potential Function

For the most general case the potential function is a Fourier Series in terms of the angle of rotation (θ) of one group relative to another, or to the framework i.e.

$$V(\theta) = \sum_{n} (V_n \cos n\, \theta + V_n{}' \sin n\, \theta) \qquad (36)$$

In many cases the symmetry of the molecule can be used to achieve some simplification; for instance if the barrier is repeated m times on rotation through 2π then

$$V(\theta) = \sum_{n} \frac{V_{nm}}{2} (1 - \cos nm\, \theta) \qquad (37)$$

Usually there is insufficient data to determine more than a very few of the coefficients V_{nm} and so the series is truncated at some small value of n, and in the simplest model the first term only is taken i.e.

$$V(\theta) = \frac{V_m}{2} (1 - \cos m\, \theta) \qquad (38)$$

V_m = barrier height in this case.

The influence of the second term has been discussed by several workers and in fact V_{2m} has usually found to be very small for methyl group rotations ($\sim 1\%$ of V_m).[15] Because of its periodicity the effect of a small second term is to change the shape of the well without altering its depth. If the second term is not small, however, a more complex situation arises with the production of a metastable well.

Equations of Motion

Once the form of the potential function has been selected it

remains to solve the resulting Schroedinger equation. If we consider

the case where $V(\theta)$ is given by equation 38 then

$$\frac{1}{I_r} \frac{d^2 \psi(\theta)}{d\theta^2} + \frac{8\pi^2}{\hbar^2} \left[E - \frac{V_n}{2} (1 - \cos n\theta) \right] \psi(\theta) = 0 \qquad (39)$$

where I_r = reduced moment of inertia (see Appendix 2). This is directly

related to Mathieu's equation

$$\frac{d^2 y}{dx^2} + (b - s \cos^2 x)y = 0 \qquad (40)$$

with $s = \dfrac{4V_n}{Fn^2}$ $\qquad F = \dfrac{h^2}{8\pi^2 Ir}$

$b = \dfrac{4E_{v\sigma}}{Fn^2}$ $\qquad E_{v\sigma} = \left(E - \dfrac{V_n}{2} \right)_{v\sigma}$

where v is the principle torsion quantum number

σ is the sublevel designation.

The solution of equation 40 is laborious but tables of solutions

are available. We have used those due to Herschbach.[16] For the case

n = 3 each energy level is split into an A and an E level with different

periodicities. This splitting is a consequence of tunnelling through

the barrier and so with an infinite barrier no such splitting should

occur. If $\Delta E_{v\sigma}$ $v;0 \rightarrow 1$ is observed and I_r is known then V_n can be

calculated.

There are two limiting cases for equation 36 for which solutions are

obtained more simply.

a)   Low barrier approximation

If $V_n \rightarrow 0$ $\qquad b_{v\sigma} \gg S$

$$\therefore \quad \frac{d^2 y}{dx^2} + b_{v\sigma} y = 0$$

The solutions are $y = e^{\pm ikx}$ $k = 0, 1, 2, 3$ etc.

The condition $\psi(\theta) = \psi(\theta + \frac{2\pi}{n})$ requires in fact that $k = 0, 2, 4, 6$ and we find that

$$E_k - \frac{V_n}{2} = \frac{n^2 h^2 k^2}{32 \pi^2 I_r}$$

which is similar to the expression for a free rotor.

b)   <u>High Barrier Approximation</u>

$$\text{Cos } n\ \theta = 1 - \frac{n^2 \theta^2}{2!} + \frac{n^4 \theta^4}{4!} - \frac{n^6 \theta^6}{6!} \quad \text{etc.}$$

If the barrier is high and the rotor is confined to small oscillations then terms in θ^4 and higher can be ignored. Thus

$$\frac{1}{I_r} \frac{d^2 (\psi(\theta))}{d\theta^2} + \frac{8\pi^2}{h^2} \left[E_t - \frac{V_n n^2}{4} \theta^2 \right] \psi(\theta) = 0$$

This is the equation of a simple harmonic oscillator with eigenvalues

$$E_t = (t + \tfrac{1}{2}) \left\{ \frac{n^2 h^2 V_n}{8\pi^2 I_r} \right\}^{\frac{1}{2}} \quad\quad t = 0, 1, 2, 3$$

For the $0 \to 1$ transition

$$\bar{V}_n = \frac{8\pi^2 c I_r}{n^2 h} \bar{\nu}^2$$

     $\bar{V}_n$ = barrier height in cm^{-1}

     $\bar{\nu}$ = frequency in cm^{-1}

It is generally stated that this gives a useful estimate of the barrier if the barrier is greater than 10 kJ mol^{-1}.

Das Approximation

Das[17] has developed an approximation to the solution of the Mathieu equation which has proved to be quite good for high and intermediate barriers. The accuracy of the solution can be improved by including an increasing number of terms and the first three cases are (for $0 \rightarrow 1$ transition)

1) $V_n = \bar{\nu}^2/K$

2) $V_n = (\bar{\nu} + K/4)^2/K$

3) $V_n^2 - (\bar{\nu}^2 + 3K^2/16 + \bar{\nu}K/2)\dfrac{V_n}{K} + (K/16)^2 = 0$

where $K = \dfrac{n^2 h}{8\pi^2 c I_r}$

The first term is equivalent to the expression calculated using the simple harmonic approximation. The Das approximation is particularly useful where Herschbachs' tables are not of the correct periodicity or where they do not extend far enough. In practice using three terms usually give a solution in good agreement with that obtained using Herschbachs' tables.

Multiple Top Molecules

We have used a classical description to determine the modes of vibration in a molecule which contains several interacting rotors. In order to do this the potential energy of each rotor is written as the sum of two terms; one involving the interaction with the framework etc. in the absence of the other rotors and the second involving only the potential energy variation as a result of interaction with the other rotors. (These can be regarded as the external and internal fields respectively.

The resulting equations for the kinetic and potential energies are substituted into Lagranges' Equation

$$\left(\frac{d}{dt}\left(\frac{\partial KE}{\partial \dot{x}_i}\right) + \frac{\partial V}{\partial x_i} = 0\right)$$

after making the approximation $\cos\theta = 1 - \frac{\theta^2}{2}$. From the resulting equations the vibrational frequencies and the angular variations associated with them can be determined. Detailed examples of such calculations are given in later chapters.

The following table is derived from the results of Ratcliffe and Waddington[18] and it summarises the number of torsional modes expected for a pair of rotors under various conditions of the internal and external fields.

Internal barrier	External barrier	Number of torsional modes
Non-zero	Non-zero	two
Non-zero	zero	one
zero	Non-zero	one

Appendix 1

The Dirac Delta Function is defined by

$$\delta(x) = 0 \quad \text{if } x \neq 0$$

$$\delta(x) = +\infty \quad \text{if } x = 0$$

$$\text{and} \quad \int_{-\infty}^{+\infty} \delta(x)dx = 1$$

It has the important properties that for a function $f(x)$

$$\int_{-\infty}^{+\infty} f(x)\delta(x-x_o)dx = f(x_o)$$

$$\delta(ax) = \frac{1}{|a|}\delta(x)$$

and

$$\delta(x) = \frac{1}{2\pi} \int_{-\infty}^{+\infty} e^{ixt} dt$$

Appendix 2

Reduced Moment of Inertia

$$I_r = I_A[1 - I_A \sum_g \lambda^2_g / I_g]$$

I_A = Moment of inertia of a rotor about its axis.

λ_g = Cosine of angle between the axis of the rotor and the g'th

principal axis of the whole molecule.

I_g = g'th principal moment of inertia.

I_r = reduced moment of inertia.

Appendix 3   Intensities in i.n.s. spectra

PART I: Neutron Energy Loss Spectroscopy

A)   Intensity of Fundamentals on the B.F.D. Spectrometer

We have by definition

$$\frac{d^2\sigma}{d_\Omega dE} = \frac{k'}{k} \frac{\sigma_{inc}}{4\pi} S(\underline{Q}, \omega) \tag{B1}$$

where for B.F.D. Spectroscopy $k' \approx$ constant.

Spectra are normalised by counting for a constant number of monitor counts for each incident energy. The monitor efficiency is energy dependent and in fact it is inversely proportional to v, where v is the velocity of the incident neutrons. Also $\frac{1}{v} \alpha \frac{1}{k}$ hence

$$\text{detected counts } \alpha \frac{d^2\sigma}{d_\Omega dE} \times k \tag{B2}$$

$$\alpha \ S(\underline{Q}, \omega) \tag{B3}$$

We also have[1]

$$\frac{d^2\sigma}{d_\Omega dE} = N \frac{k'}{k} b^2 Q^2 \frac{Z(\omega)}{M\omega} \exp(-2W) \tag{B4}$$

Substituting (B4) into (B2) we obtain

$$\text{detected counts } \alpha \ Q^2 \frac{Z(\omega)}{M_\omega} \exp(-2W) \tag{B5}$$

Q is defined by $\underline{Q} = \underline{k} - \underline{k}'$ and for B.F.D. spectra $|\underline{k}'| \approx 0$ hence

$$Q^2 \ \alpha \ k^2 \ \alpha \ \omega \tag{B6}$$

because

$$\hbar\omega = \frac{\hbar^2 k^2}{2m} \tag{B7}$$

where m is the mass of the neutron.

Substituting (B6) into (B5) we have

$$\text{detected counts} \propto \frac{Z(\omega)}{M} \exp(-2W) \tag{B8}$$

so that the detected counts are proportional to the density of states

(weighted by b^2 and $\frac{1}{M}$).

B) <u>Intensity of Overtones</u>

Consider a harmonic oscillator with fundamental ω_0 and an overtone ω

with $\omega = n\omega_0$ then from equation B7 we have (with $\underline{k}_n$ the wave vector

associated with the incident neutron involved in the energy transfer ω).

$$\hbar\omega_0 = \frac{\hbar k_0^2}{2m}$$

$$\text{and} \quad \hbar\omega = \frac{\hbar k_n^2}{2m} = n\hbar\omega_0 \tag{B9}$$

$$\therefore nk_0^2 = k_n^2$$

Marshall and Lovesey[1] have given the following formula, for $S_n(\underline{Q}, \omega)$, for

a harmonic oscillator, where $S_n(\underline{Q}, \omega)$ is the scattering law for the

transfer of n quanta each of energy $\hbar\omega_0$.

$$S_n(Q, \omega) = \exp\left(\frac{\hbar Q^2}{2M\omega_0} \coth\left(\frac{\hbar\omega_0}{2KT}\right)\right) \exp\left(n\frac{\hbar\omega_0}{2KT}\right) I_n(y) \tag{B10}$$

where

$$y = \frac{\hbar Q^2}{2M\omega_0} \operatorname{cosech}\left(\frac{\hbar\omega_0}{2KT}\right)$$

and

$$I_n(y) = \frac{(\frac{1}{2}y)^n}{n!}$$

n > 0 for neutron energy loss

n < 0 for neutron energy gain

$$\left\{\text{N.B. } I_n(y) = I_{-n}(y)\right\}$$

For large ω_0 and small T; $\frac{\hbar\omega_0}{2KT} \gg 1$ {typical of a B.F.D. experiment} and so

$$\coth\left(\frac{\hbar\omega_0}{2KT}\right) = 1$$

And $Q^2 = k^2_n = nk^2_o$

Thus (B10) can be written

$$S_n(\underline{Q}, \omega) \propto \exp\left\{-\frac{\hbar Q^2}{2M\omega_0}\right\} \left\{\exp\left(\frac{\hbar\omega_0}{2KT}\right)\right\}^n \left(\frac{\hbar Q^2}{2M\omega_0}\right)^n \times \frac{1}{2^n} \times \frac{1}{n!} \times \left\{\frac{2}{e^{\frac{\hbar\omega_0}{2KT}} - e^{\frac{-\hbar\omega_0}{2KT}}}\right\}^n \tag{B11}$$

$$S_n(\underline{Q}, \omega) \propto \exp\left(\frac{-\hbar Q^2}{2M\omega_0}\right) \left(\frac{\hbar Q^2}{2M\omega_0}\right)^n \times \frac{1}{n!} \times \left\{\frac{1}{1 - e^{\frac{-\hbar\omega_0}{KT}}}\right\}^n \tag{B12}$$

and $e^{\frac{-\hbar\omega_0}{KT}} \approx 0$

$$S_n(\underline{Q}, \omega) \propto \exp\left\{\frac{-\hbar Q^2}{2M\omega_0}\right\} \left(\frac{\hbar Q^2}{2M\omega_0}\right)^n \times \frac{1}{n!} \tag{B13}$$

But we also have

$$\frac{\hbar k^2_o}{2m} = \frac{\hbar Q^2}{2m} = \omega_0$$

So that

$$S_n(\underline{Q}, \omega) \propto \left\{\exp\left(\frac{-nm}{M}\right) \left(\frac{nm}{M}\right)^n \times \frac{1}{n!}\right\} \propto \left\{\frac{n^n}{n!} \left(\frac{m}{M} \exp\left(\frac{-m}{M}\right)\right)^n\right\} \tag{B14}$$

Consider ethylene so that M = 28m. This approximation will only be valid provided that the energy of the neutron is such that it cannot excite an internal C_2H_4 mode.

$$S_n(\underline{Q}, \omega) \propto \frac{n^n}{n!} \left(\frac{1}{28} \exp\left(\frac{-1}{28}\right)\right)^n \tag{B15}$$

The following were calculated from this equation.

	$\dfrac{S_i(Q, \omega)}{S_3(Q, \omega)}$	$\dfrac{S_i(Q, \omega)}{S_1(Q, \omega)} \times 100$
$S_1(Q, \omega)$	187.1	100
$S_2(Q, \omega)$	12.89	6.9
$S_3(Q, \omega)$	1	0.5

The relative intensities of fundamental and overtones is obviously dependent on the ratio $\dfrac{m}{M}$. An important limiting case is the scattering from a proton (e.g. dissociatively adsorbed hydrogen). Then

$$S_n(Q, \omega) \; \alpha \; \exp(-n) \; \frac{n^n}{n!}$$

	$\exp(-n) \; \dfrac{n^n}{n!}$	$\dfrac{S_i(Q, \omega)}{S_1(Q, \omega)} \times 100$
$S_1(Q, \omega)$	.368	100
$S_2(Q, \omega)$	.271	73
$S_3(Q, \omega)$	.224	61

These results indicate that overtones of intense modes, involving light ligands, should be readily observed provided that $\dfrac{\hbar\omega_o}{2KT} \gg 1$. This is of greatest importance for the IN1B Spectrometer (see chapter III). The observed peak heights will not have the ratios calculated above because both the Debye-Waller Factor and the resolution function of the instrument will tend to broaden higher energy modes. When comparing intensities it is necessary to use the integrated intensity of each peak.

PART II: Energy Gain Spectroscopy

With t. of f. experiments it is not possible to make some of the assumptions that were made in the previous section. For instance it is no longer true that $\underline{Q} \approx \underline{k}$ or usually that $\frac{\hbar\omega_0}{2KT} \gg 1$. The population factor will cause the intensity to fall as the energy transfer increases. If we once again use equation (B10) (with $-n$) and repeat the steps involved in deriving (B13)

$$S_n(\underline{Q}, \omega) = \frac{1}{n!} \exp\left\{\frac{-\hbar Q^2}{2M\omega_0} \coth \frac{\hbar\omega_0}{2KT}\right\}\left\{\frac{\hbar Q^2}{2M\omega_0}\right\} \left\{\frac{1}{e^{\frac{\hbar\omega_0}{KT}}-1}\right\}^n \qquad \text{(B16a)}$$

If $e^{\frac{\hbar\omega_0}{KT}} = 1 + \frac{\hbar\omega_0}{KT}$

$$S_n(\underline{Q}, \omega) = \frac{1}{n!} \exp\left(\frac{-\hbar Q^2}{2M\omega_0} \coth\left(\frac{\hbar\omega_0}{2KT}\right)\right) \left(\frac{\hbar Q^2}{2M\omega_0}\right) \left(\frac{KT}{\hbar\omega_0}\right)^n \qquad \text{(B16b)}$$

A) Momentum Transfer Dependence

If ω_0 and T are constant

$$S_n(\underline{Q}, \omega) \; \alpha \; (Q^2)^n \, \exp(-BQ^2) \qquad \text{(B17)}$$

where $B = \frac{-\hbar}{2M\omega_0} \left(\frac{\hbar\omega_0}{2KT}\right) = <u_\lambda^2>$

Thus a plot of

$$\log\left(\frac{S_n(\underline{Q}, \omega)}{\exp(-BQ^2)}\right) \; \text{v.s.} \; \log(Q^2) \qquad \text{(B18)}$$

will have a gradient of n.

B) Temperature Dependence

If Q and ω_o are constant

$$S_n(Q, \omega) \propto T^n \exp\left\{-\frac{Q^2\hbar}{2M\omega_o} \coth\left(\frac{\hbar\omega_o}{2KT}\right)\right\}$$

The temperature dependence is therefore fairly complex, however, if M is large the exponential term varies slowly with temperature. For instance with $M = 28$, $Q^2 = 3$ and $\omega_o = 40 \text{ cm}^{-1}$ the exponential term is .85 at 100K and .72 at 200K so that a 100% change in T produces a 15% change in the exponential term. To a first approximation we therefore have

$$S_n(Q, \omega) \propto T^n \qquad (B19)$$

Thus a plot of log $(S_n(Q, \omega)$ v.s. T will have a gradient of n.

C) $P(\alpha, \beta)$

We have

$$P(\alpha, \beta) = 2\beta \, \text{Sinh}\left(\frac{\beta}{2}\right) \frac{S(\alpha, \beta)}{\alpha}$$

and $e^{-\frac{\beta}{2}} S(\alpha, \beta) = KTS(Q, \omega)$

Hence

$$P(\alpha, \beta) = \frac{4MT\omega_o}{Q^2} \, e^{\frac{\beta}{2}} \, \text{Sinh}\left(\frac{\beta}{2}\right) S(Q, \omega)$$

Substituting eqn. B16 we obtain

$$P_1(\alpha, \beta) \propto T \times \exp\left\{-\frac{\hbar Q^2}{2M\omega_o} \coth\left(\frac{\hbar\omega_o}{2KT}\right)\right\}$$

i.e. $P_1(\alpha, \beta) \propto Te^{-Q^2 <u^2>}$

and

$$P_2(\alpha, \beta) \propto T \exp\left(-\frac{\hbar Q^2}{2M\omega_0} \coth \frac{\hbar\omega_0}{2KT}\right) \exp\left(\frac{-\hbar Q^2}{2KT}\right)\left(\frac{\hbar Q^2}{2M\omega_0}\right) \times \frac{1}{\sinh\left(\frac{\hbar\omega_0}{2KT}\right)}$$

$$\propto T \times \frac{\hbar Q^2}{2M\omega_0} \exp\left(-\frac{\hbar Q^2}{2M\omega_0} \coth\left(\frac{\hbar\omega_0}{2KT}\right)\right) \times \frac{e^{-\frac{\hbar\omega_0}{2KT}}}{\sinh\left(\frac{\hbar\omega_0}{2KT}\right)}$$

$$\propto T \times \frac{\hbar Q^2}{2M\omega_0} \exp\left(\frac{-\hbar Q^2}{2M\omega_0} \coth\left(\frac{\hbar\omega_0}{2KT}\right)\right) \times \frac{2}{e^{\frac{\hbar\omega_0}{KT}}-1}$$

Thus considering only the temperature dependence (and remembering our earlier remarks concerning the exponential term $\exp(-BQ^2)$) we have

$$P_2(\alpha, \beta) \propto \frac{T}{e^{\frac{\hbar\omega_0}{KT}}-1} \tag{B20}$$

or with $e^{\frac{\hbar\omega_0}{KT}} = 1 + \frac{\hbar\omega_0}{KT}$

$$P_2(\alpha, \beta) \propto T^2 \tag{B21}$$

Fig. 5 shows plots of

$$\log_e\left[\frac{T}{e^{\frac{\hbar\omega_0}{KT}}-1}\right] \quad v.s. \quad \log_e T$$

Equation (B21) indicates that a plot of log (Intensity) vs $\log_e T$ should have a gradient of 2, however, we can see from Fig. 5 that the more exact solution (eqn. B20) yields a straight line of gradient greater than two.

PART III:-General Points

It is not very meaningful to compare peak intensities from a t.of.f. spectrum because
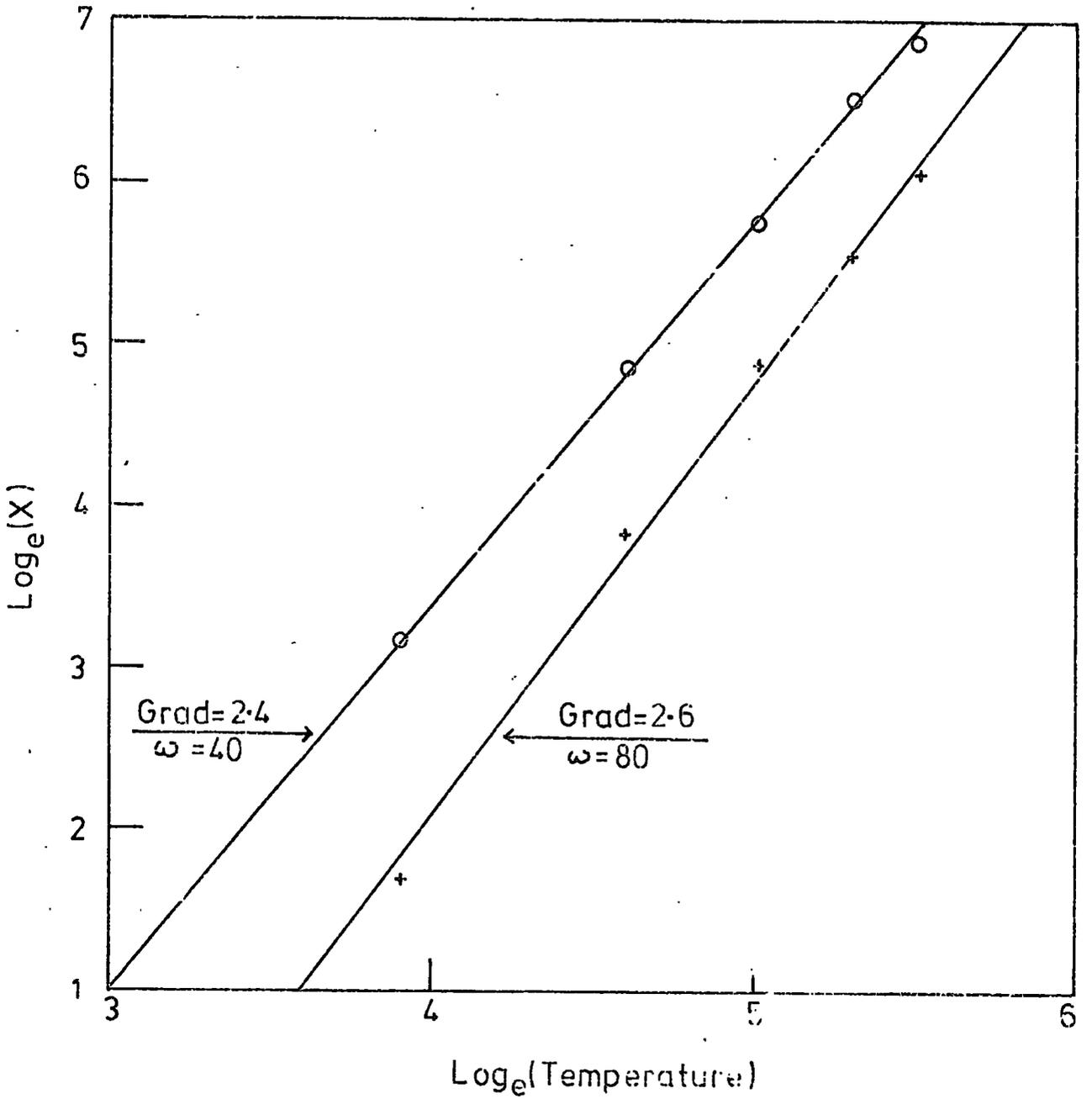
$$X = \frac{T}{\left[e^{\frac{\hbar\omega}{KT}} - 1 \right]}$$

FIG. 5.

1. the Boltzmann Factor reduces the intensities of the bands as energy transfer increases.

2. the resolution function of the instrument changes with ω.

3. the energy scale is non-linear.

For a typical (6H) t.of.f. experiment the following graphical output is available

a) corrected counts vs t.of.f.   (9 graphs)

b) corrected counts vs cm^{-1} (9 graphs)

c) $P(\alpha, \beta)$ v. cm^{-1} (9 graphs)

d) $\rho(\omega)$ and $2\beta Sinh(\frac{\beta}{2}) \frac{P(\alpha, \beta)}{\alpha}$ (2 graphs)

Obviously it is not possible to present all of this data here and so we have shown typical pieces of data, though in some cases this does mean that the trends are no longer quite so obvious as when all of the data is available.

References

1. W. Marshall and S.W. Lovesey, Theory of Thermal Neutron Scattering, Oxford University Press, 1971.

2. B.T.M. Willis (Ed), Chemical Applications of Thermal Neutron Scattering, Oxford University Press, 1973.

3. P.A. Egelstaff (Ed), Thermal Neutron Scattering, Academic Press, 1965.

4. V.F. Turchin, Slow Neutrons, Israel Program for Scientific Translations, Jerusalem 1965.

5. A.K. Ghatak and L.S. Kothari, An Introduction to Lattice Dynamics, Addison-Wesley Pub. Co., London 1972.

6. L. Van Hove, Phys. Rev., 95, 249, (1954).

7. G. Allen and J.S. Higgins, Rep. Prog. Phys., 36, 1073, (1973).

8. A.C. Zemach and R.J. Glauber, Phys. Rev., 101(1), 118, (1956).

9. T. Springer, Springer Tracts in Modern Physics Vol. 64, Ed. G. Höhler, Springer-Verlag, Berlin 1972.

10. K.E. Larsson, J. Chem. Phys., 59(5), 4612, (1973).

11. A.J. Dianoux, F. Volino and H. Hervet, Molec. Phys., 30(4), 1181, (1975).

12. P.A. Egelstaff, Inel. Scat. Neutrons, Solid, Liq., Proc. Symp., Vienna 1960.

13. C.J. Wright, Ph.D. Thesis, University of Oxford 1971

14. C. Kittel, Introduction to Solid State Physics, John Wiley and Sons, New York, 1971.

15. W.G. Fateley and F.A. Miller, Spectrochim. Acta., 17, 857, (1961).

16. D.R. Herschbach, 'Tables for the Internal Rotation Problem', Dept. Chem. Harvard Univ.

17. T.P. Das, J. Chem. Phys., 25, 896, (1956).

18. C.I. Ratcliffe, Ph.D. Thesis, University of Durham, 1975.

Chapter III: <u>Techniques and Instrumentation</u>

<u>Introduction</u>

The object of this chapter is to introduce the main features of the spectrometers used, the details of sample preparation and handling and a brief description of the standard computer programs available for data analysis.

<u>Section I: Optical Spectra</u>

The optical spectrometers used are relatively standard and by now well characterised, they were

<u>Near Infrared</u>   Perkin Elmer 457

               "   "   577 grating spectrometers

<u>Far Infrared</u>   Beckman-RIIC FS720 Interferometer

<u>Raman</u>   Cary 82 using:

     Spectra-Physics Model 125 He/Ne laser at 15,802 cm^{-1} (red)

     "   "   Model 164 Ar/Kr laser at 19436.3 cm^{-1} (green)

The punched paper tape output from the FS720 was processed on the N.U.M.A.C. computer using programmes developed by Symon[1] and Jinks.[2]

Low temperature spectra were obtained using cells of conventional design. The window materials were a) Polythene for the far i.r. spectra b) CsI for the near i.r. c) glass for the Raman cell. For the low temperature Raman spectra samples were sublimed onto a copper block and the same facility for subliming samples was available on the i.r. cells. I.r. samples were also run as nujol mulls smeared onto a polythene disc or pressed between two CsI plates as appropriate. After evacuation the cell dewar was filled with liquid nitrogen.

Section II: Neutron Spectrometers

The spectra presented in this thesis were obtained using spectrometers located at A.E.R.E. Harwell or the I.L.L. in Grenoble. Both of these centres have continuous flux reactors and the Maxwellian distribution of the neutron energies can be modified by inserting in the reactor either "hot" or "cold" sources which shift the distribution to either shorter or longer wavelengths respectively.

The design and characteristics of neutron spectrometers have been extensively documented[3,4,5] though because instrumentation for neutron scattering is less well-known than that for optical spectroscopy we will discuss it in more detail here.

1. Monochromators

Because neutrons emerge from the reactor with a broad range of energies it is necessary to select a narrow band of energies using a monochromator. There are three basic types of monochromator used in neutron spectrometers.

a) Mechanical Velocity Selectors

"White beam"

Pulsed
Monochromatic
Beam
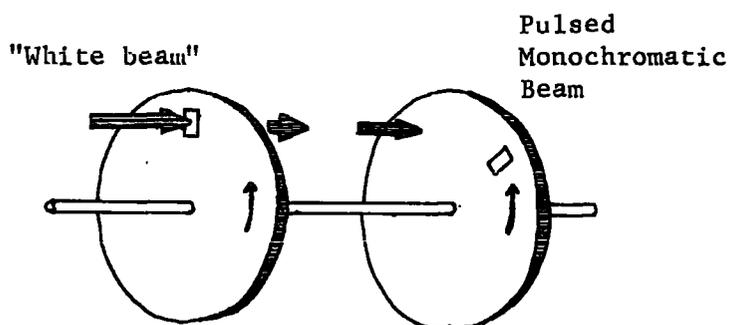
Fig. 1a Principle of Mechanical velocity of selector[4]
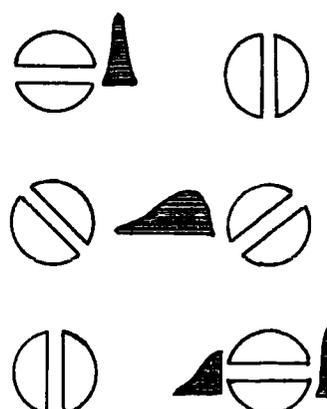
Fig. 1b Time-Spread of Neutrons

Fig. 1a shows the principle of this method. The material of the velocity selectors (choppers) is opaque to neutrons. They do, however, contain curved slots so that as the rotors spin, only those neutrons within a narrow velocity range are transmitted. The transmitted pulse broadens and further wavelength selection is achieved by the second rotor (fig. 1b).

b) Diffraction

Neutrons impinging on a single crystal will be diffracted to give specific wavelengths at scattering angles of 2θ according to

$$\lambda = 2d \, \sin\theta$$

where d is the interplanar spacing. Thus by selecting d and θ a wide range of values of λ is accessible. Perfect crystals are not used because of their low reflectivity. Order contamination (i.e. simultaneous reflection of neutrons with wavelengths λ, $\lambda/2$, $\lambda/3$ etc.) can present difficulties though to a certain extent filters can be used to reduce the problem. If the crystal is rotated rapidly then a pulsed mono-chromatic beam is obtained:- this system is analogous to the mechanical velocity selector technique. The rotating crystal spectrometer has the advantage of very low backgrounds since the monoenergetic beam is deflected away from the line of the initial beam. Very high resolution can also be obtained.

c) Filters

Because, in a polycrystalline material, there is a maximum spacing between planes (d_{max}) there is a maximum wavelength which can be reflected i.e. $\lambda = 2d_{max}$. There is therefore a wavelength above which

Bragg scattering does not take place. Beryllium has a cut off at

3.96Å and so only neutrons with energies in the region 0 - 5.2 meV are

transmitted through a beryllium block.

2. Analysis of the Scattered Neutrons

Thermal neutron velocities fall in a very convenient region

$(10^{-5} \rightarrow 10^{-3}$ $\mu s/m)$ for them to be separated by the time taken for them

to travel from the sample to the detector. For each pulse produced by

either rotating crystals or choppers the time of arrival of neutrons at

the detector is recorded in say 6μs channels with approximately 500

channels to each pulse. If the incident wavelength of the neutrons is

known the average wavelength of neutrons arriving in a particular

channel (time of flight channel) can be calculated from the time of

arrival and the known geometry of the instrument. The data collection

rate is very high because data can be collected at several angles

simultaneously and analyses of energy and momentum transfer are performed

simultaneously.

Analysis of the scattered neutrons can also be achieved by using a

single crystal and a detector though this is not of direct relevance to

this work and by using a filter - this will be described in more detail

later.

3. The Spectrometers

a) Time-of-Flight Spectrometers (t.of.f)

Four t.of f. spectrometers were used i.e. 6H,[6] 4H5,[7] 7H[8] at A.E.R.E.

Harwell, and IN4 at I.L.L. Grenoble.

The Harwell instruments all have mechanical choppers and they differ

essentially only in the wavelengths corresponding to peak flux (table 1)

the angles of detection, the arrangement of the detectors and the length

of the flight path. Fig. 2 shows a detailed drawing of the 6H

spectrometer.

Table 1   Energy Corresponding to Peak Flux for the Harwell t.of f.

   Spectrometers

	λ (Å)	cm^{-1}
6H	4.2	37.4
7H	NOW OBSOLETE	
4H5	4.8	28.6

Because the incident energy is so low these spectrometers are used for

experiments in which the neutrons gain energy from the sample i.e. from

upper energy levels. For this reason it is fairly unusual, in inelastic

scattering experiments,using these spectrometers, to run very cold

samples. For 6H or 4H5 the sample is clamped over a hole in a metal

plate, which also has a space for an empty sample container to serve as

background, and a third space for a standard vanadium plate.[6] The

sample chamber can be evacuated or flushed with helium to reduce air

scattering. Samples can be run below room temperature by evacuating the

sample chamber and blowing nitrogen gas through tubes which are in

intimate contact with the metal base-plate. The lowest temperature

available with this system is c.a. 100K and the arrangement is such that

any pre-selected temperature can be maintained with good accuracy. The

three samples (background, sample, vanadium) are cycled periodically so

that each spends a pre-selected period in the beam during each cycle.

62.

Fig. 2 6H Time-of-Flight Spectrometer
(A.E.R.E. Harwell)

CORE CENTRE LINE

FLOODABLE COLIMATOR

TUNGSTEN SWITCH

BERYLLIUM

LIQUID N₂ COOLING
COILS

REACTOR SHIELDING

BISMUTH

COLLIMATOR

REACTOR SHIELDING

N₂ HEADER TANK

CONCRETE & IRON SHOT

CONCRETE & IRON SHOT

RED ROTOR

RESIN & IRON SHOT

BORAX & RESIN

BORAX & RESIN

BLUE ROTOR

MI

BORAX & RESIN

SAMPLE HOLDER

M2

BORAX & RESIN

DETECTOR

BORAX & RESIN

SCALE

FEET

3

0

MONITOR

M3

FLIGHT PATH

BEAM STOP

WITHDRAWABLE
SHIELDING

REACTOR FLOOR LEVEL

Fig. 3 Factors Effecting the Resolution of the 6H Spectrometer

Fig. 4 IN4 Spectrometer

amplifiers
high voltage
collimator
He^3 detector
Detector box

detectors

length of flightpath 4m

sample

helium flight path box

monoenergetic pulsed neutron-beam

double monochromator

collimatordrum

rot. crystal

rot. crystal

reactor beam
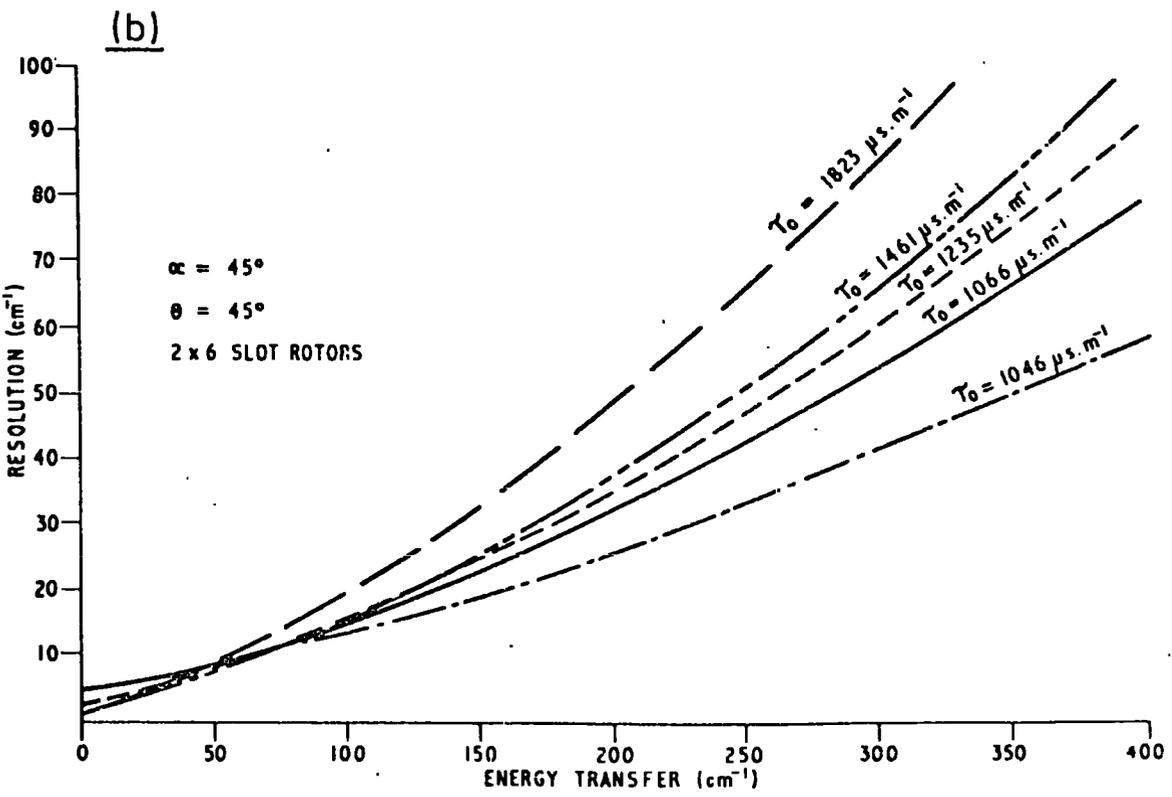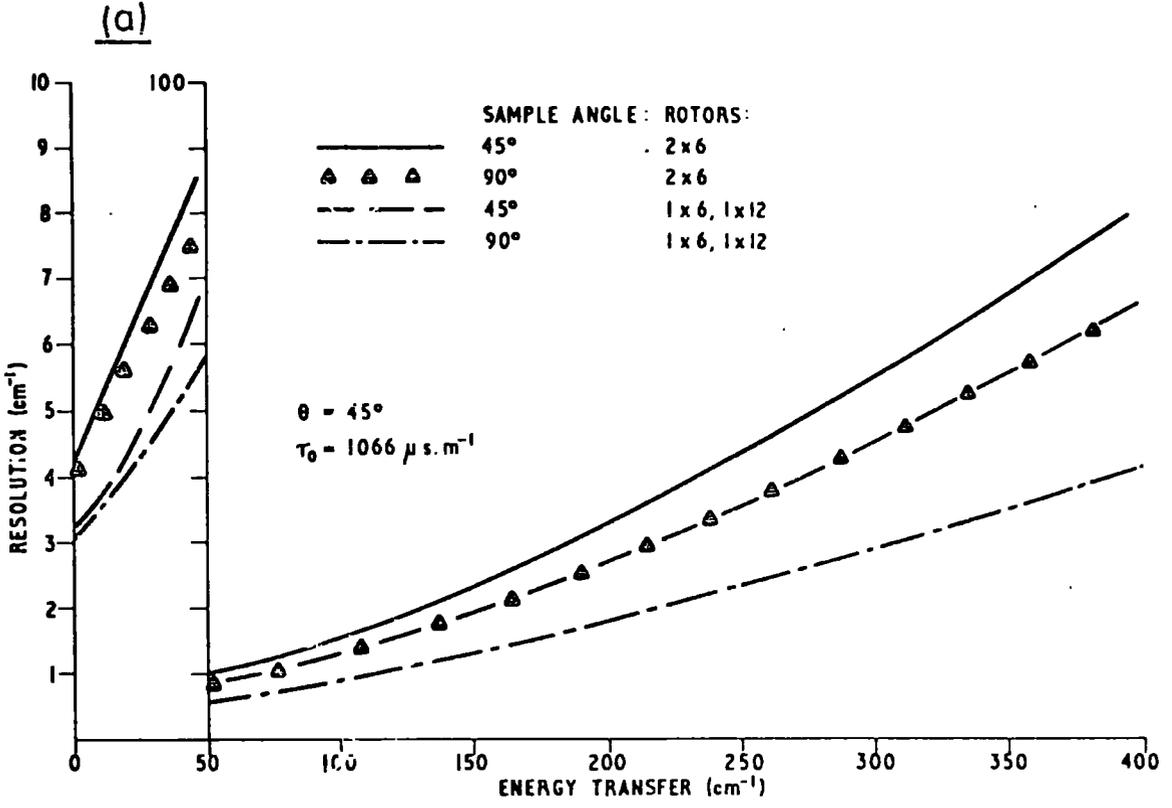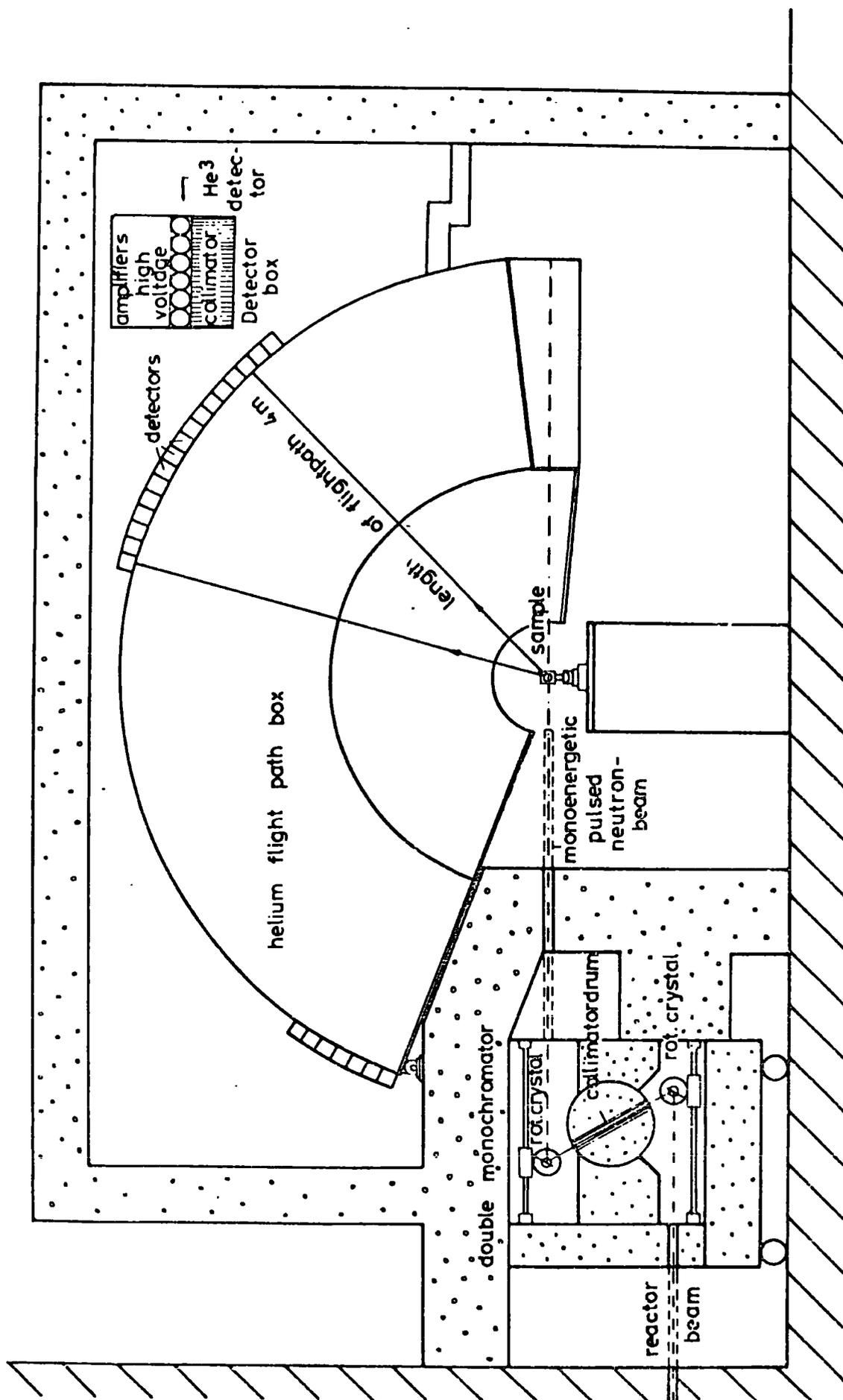
This cycling helps to smooth out effects due to changes in flux or more importantly, variable background. For 7H experiments a conventional centre-loading cryostat is used and no cycling is possible.

The resolution of these spectrometers has been discussed by Harryman and Hayter[9] and it is found to depend mainly upon

A)   the monochromation achieved by the rotors

B)   the angle of the sample to the beam

C)   the finite thickness of the detectors.

A) is the major factor so that in general there is nothing to be gained by collecting data in say 3μs channels instead of 6μs channels. Here the resolution of an instrument is defined as its response to a δ function input signal. There are two sets of rotors available - having six and twelve slots respectively. The effective resolution obtained using these and a combination of them is shown in figs. 3a,b.

Above 300 cm^{-1} the resolution of these spectrometers is very poor so that they are mainly used for the study of very low energy vibrations.

IN4 is a rotating crystal spectrometer (fig. 4) which has the advantage of very low backgrounds and it can be used in the down-scattering mode. Because the neutrons are losing energy to the sample the samples can be cooled to liquid helium temperature. The resolution is excellent compared to the Harwell spectrometers. In using this instrument it is necessary to select an energy window according to the region of special interest. This is because the neutrons, which have transferred greater energy, travel more slowly and because collection of data is by equal time channels the energy spread in a time channel is smaller (and hence the detected counts lower) towards the end of a

cycle. A very large number of time-of-flight channels therefore are necessary to cover an energy spread of 1 cm^{-1} as the kinetic energy of the scattered neutrons approaches zero, and the detected number of neutrons/channel is also very much reduced. In the practical situation it is therefore necessary, for down-scattering experiments, to select an incident energy such that after losing energy to a mode in the region of interest the neutron still has sufficient energy to reach the detectors in a reasonable time. The maximum incident energy is 85 meV.

b) <u>Beryllium Filter Detector Spectrometers</u>[10] (B.F.D.)

The principle of this type of spectrometer is very simple. Monochromation is achieved via a single crystal and the incident neutron beam loses energy to the sample. Some of the scattered neutrons pass into a cooled beryllium block but only those with energies below 5.2 meV are transmitted, and reach the detector bank (fig. 5). If the energy of the incident neutron is high then some neutrons may lose most of this energy in a scattering event. If the energy levels in the sample are such that the scattered neutrons have an energy of less than 5.2 meV then some of them will reach the beryllium filter and be transmitted to be detected in the counter bank. The incident energy is varied stepwise so that, unlike t. of f. methods, data for only one energy is collected at a time. Because the neutrons are virtually stopped the momentum transfer is relatively independent of angle of scattering and so the detector is usually placed at c.a. 90° to the incident beam on the sample in order to reduce background. The counter bank covers a large solid angle so that momentum resolution is poor.

A monitor is placed before the sample and normalisation is achieved by counting, at each energy, for the same number of monitor
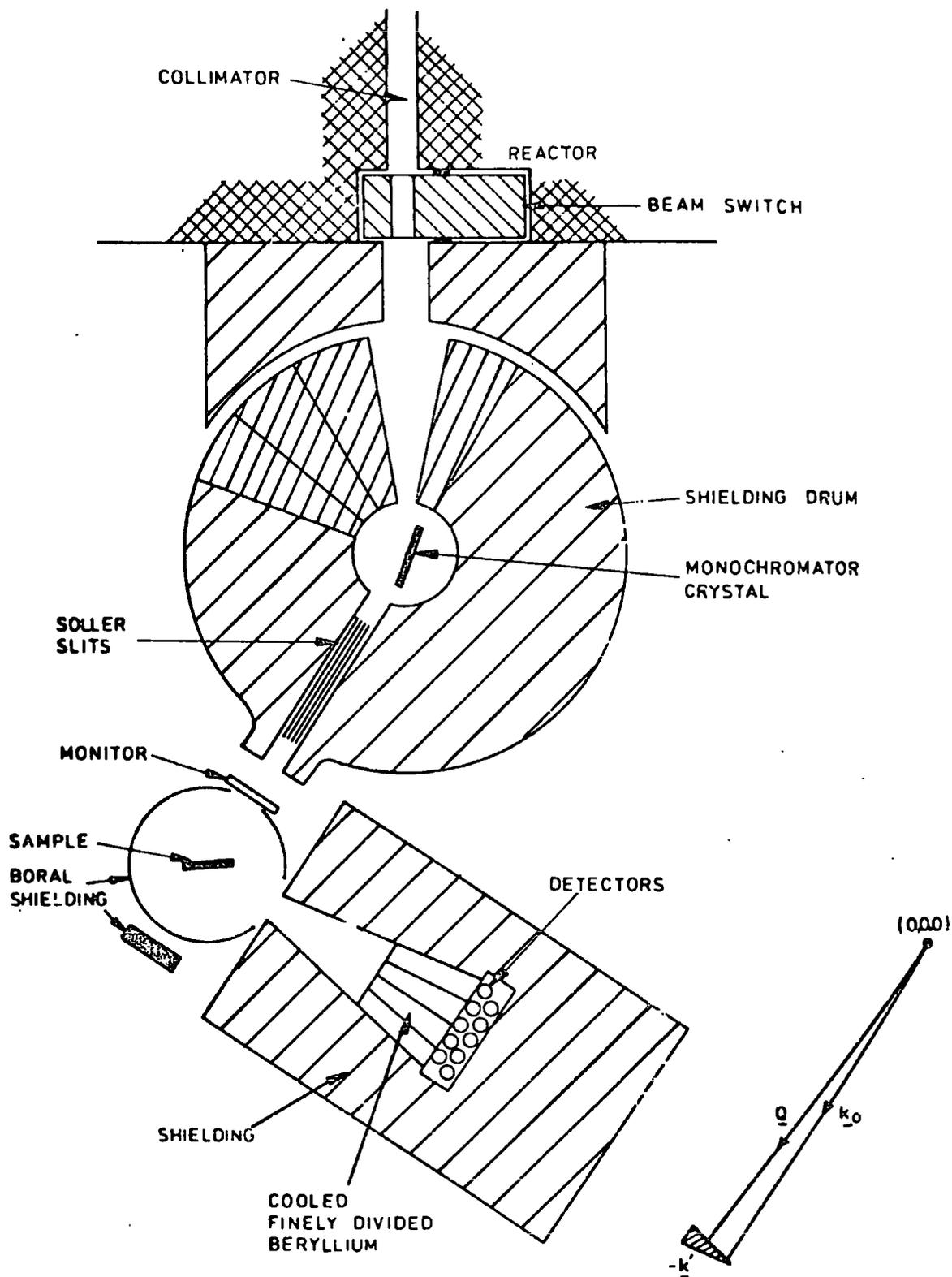
Fig. 5 Beryllium Filter Detector Spectrometer,
A.E.R.E. Harwell

counts. Under these conditions the spectrum obtained is directly proportional to the density of states.[11]

Samples are usually run at liquid nitrogen temperature in order to reduce the multiple quantum scattering, which as we have shown (chapter II), is approximately a function of T^2 and narrower bands are observed due to the reduced D.W. factor. This is particularly necessary because of the large Q values inherent in the use of this type of spectrometer. With IN1B (Grenoble instrument; fig. 6) the momentum transfers are particularly large because of its available energy range (300 cm^{-1} → 4500 cm^{-1}) and we have observed quite intense second and even third overtones (fig. 7). There is, therefore, a fundamental limit on the use of B.F.D. spectrometers at high energy transfers and this does not seem to have been realised in the design stage of IN1B.

For the Harwell instrument the available energy range is 60 cm^{-1} → 2000 cm^{-1} though above 1300 cm^{-1} the count rate is very low and the counting times unacceptably long.

The resolution and relationship between observed peak position and true mode frequency have been thoroughly discussed by Gamlen et al.[10]

It can be seen from fig. 8a that the cut-off for beryllium is not a simple rectangular function. The first cut off occurs at 42 cm^{-1} (96.5%) and the second at 52 cm^{-1} (100%). Furthermore the detector efficiency is energy dependent (fig. 8b). The result of these factors is that the response function of the instrument is as shown in fig. 8c. The mode frequency corresponds to the threshold value and not the peak maximum. Because the incident beam is not strictly monochromatic it is necessary to convolute the incident beam with the response function to obtain the observed spectrum. The distribution of incident energies is
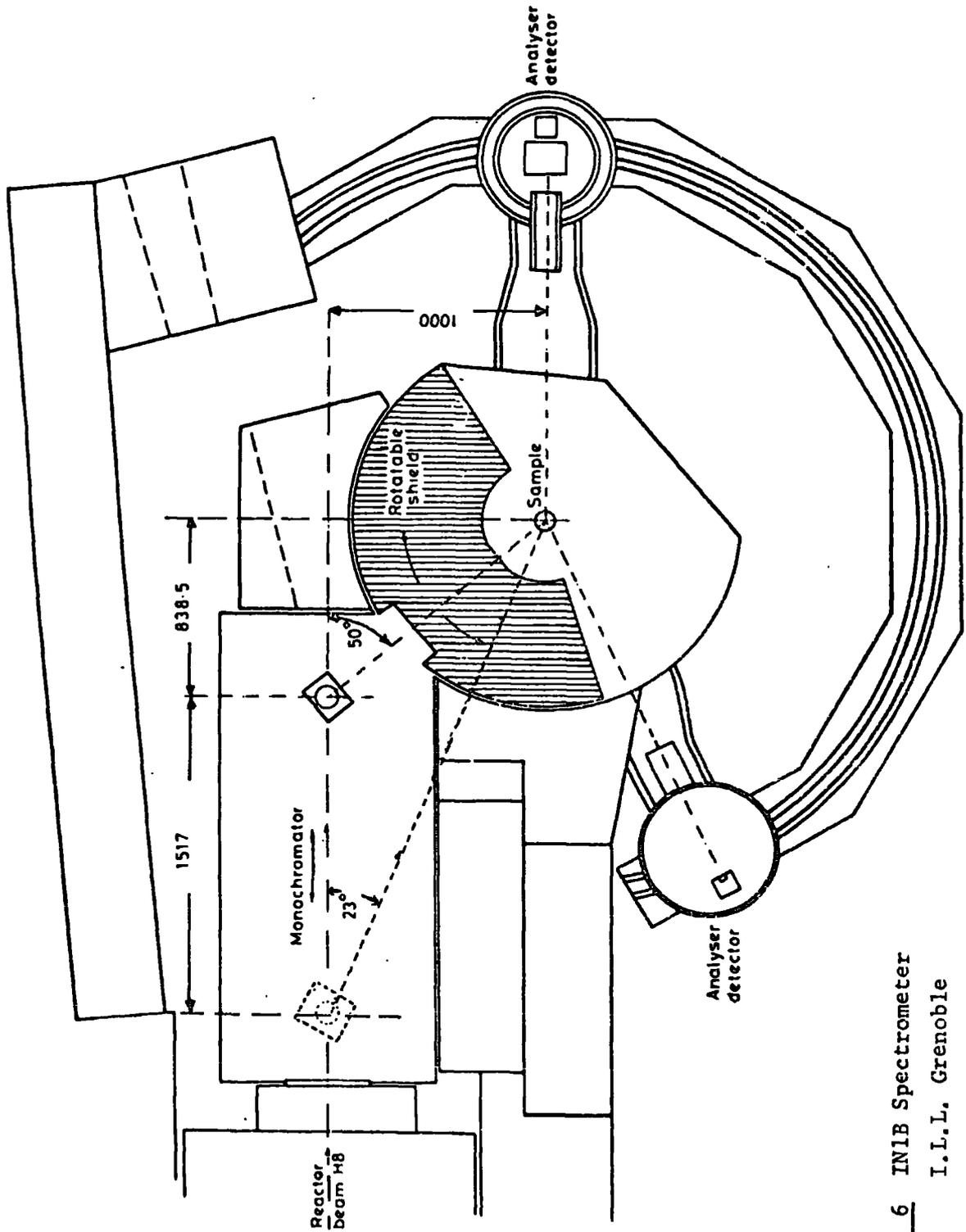
Fig. 6   IN1B Spectrometer
          I.L.L. Grenoble

Fig. 7 IN1B Spectrum of CsHCl₂ showing the observed overtones

71.
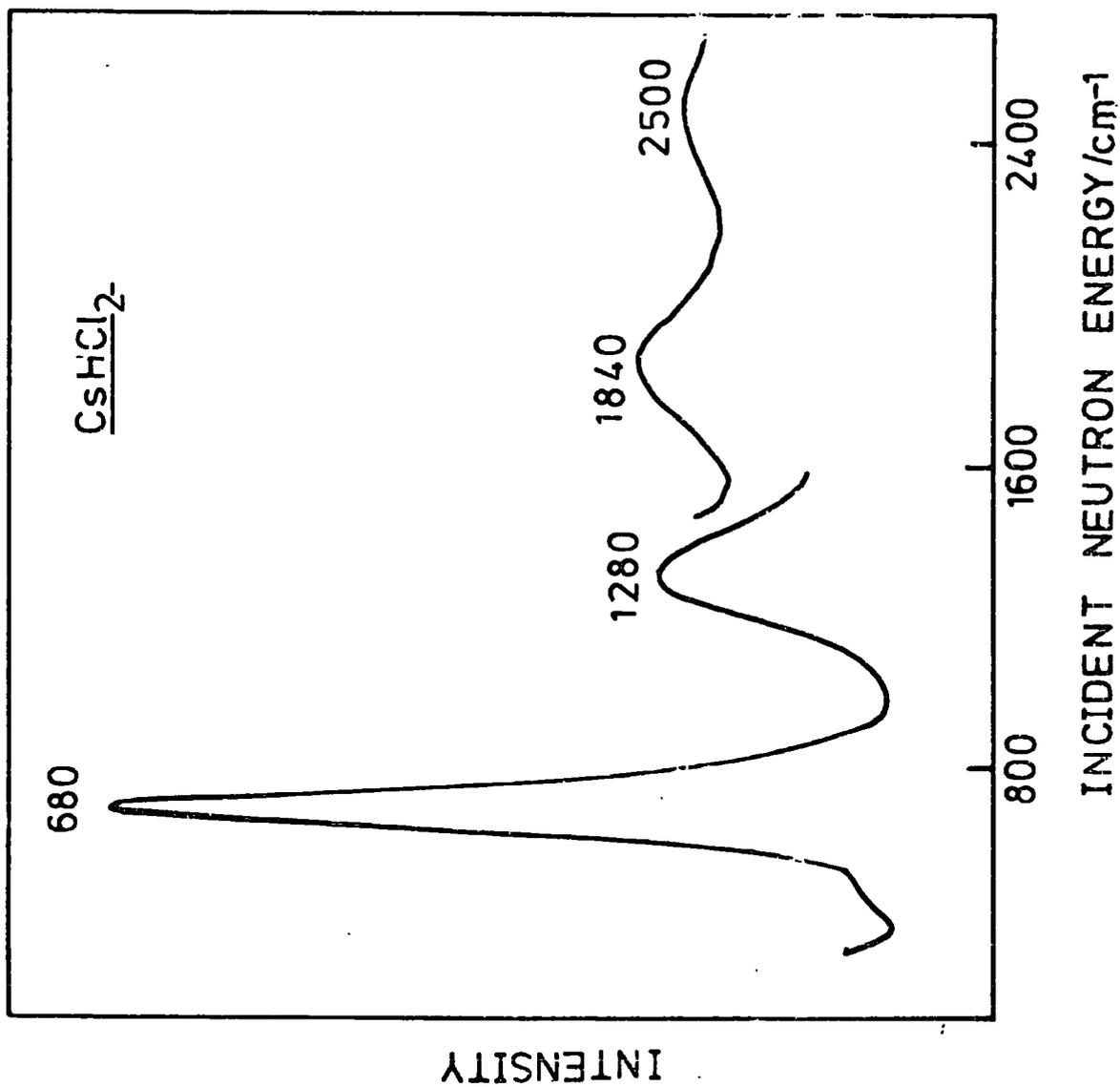
Fig. 8 Parameters of the B.F.D. Spectrometer   Fig. 9 Theoretical Line Shapes for B.F.D. Spectrometer
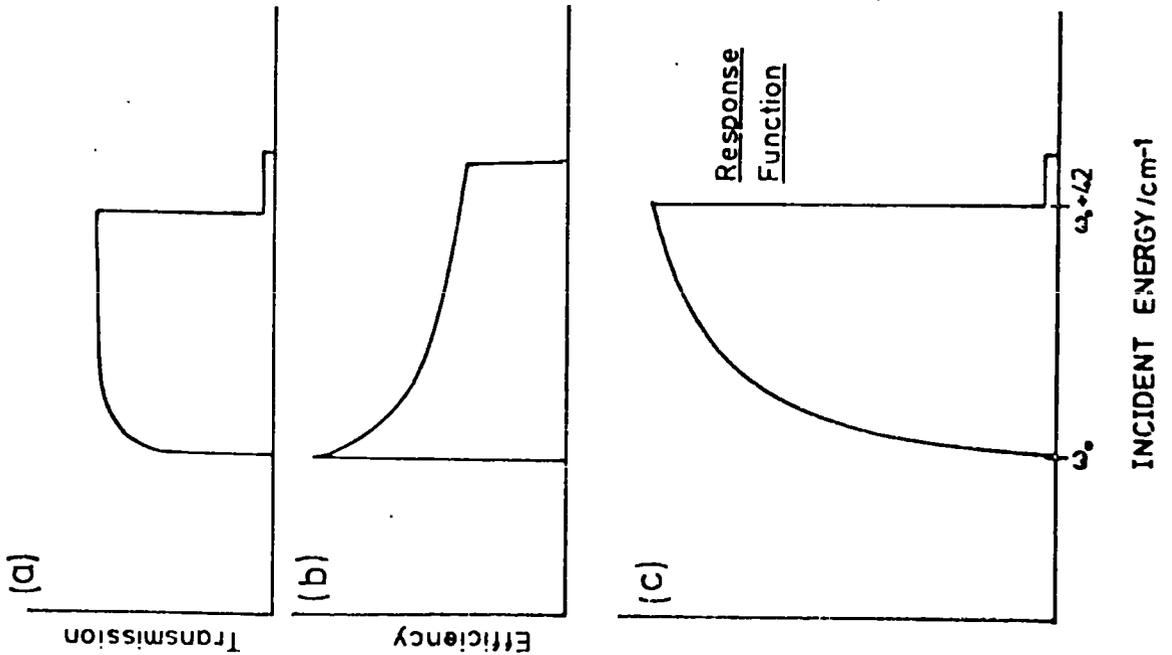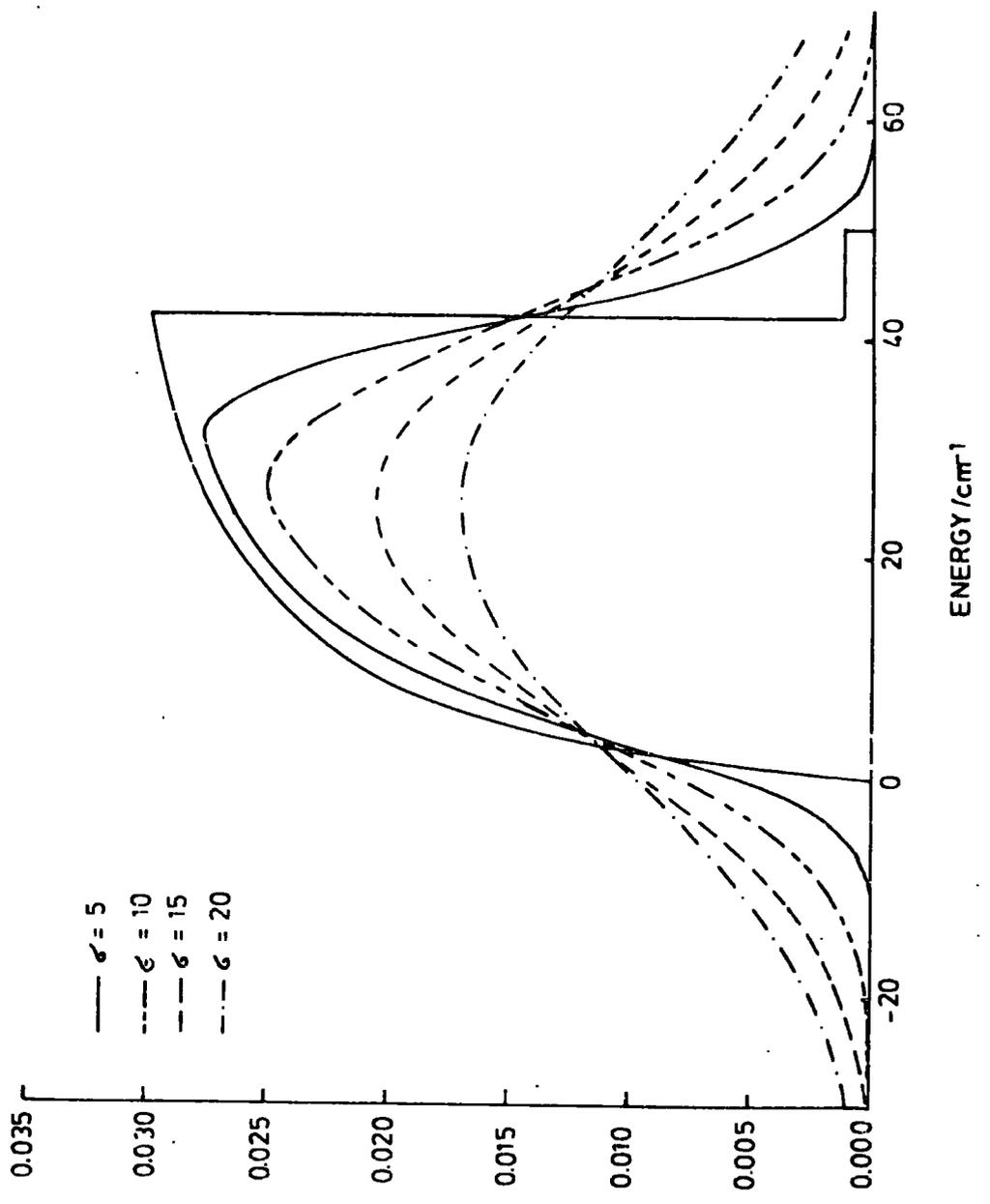
taken to be Gaussian.

$$f(E_i) = (2\pi\sigma^2)^{-\frac{1}{2}} \exp (-E_i^2/2\sigma^2) \qquad (1)$$

Fig. 9 shows that as σ increases the convoluted spectrum changes from asymmetric to symmetric shape. The displacement of the threshold from the peak maximum (Δ) decreases from 42 cm^{-1} to an assymptotic value of 24.5 cm^{-1}.

In order to calculate the mode frequency from the peak position it is necessary to know the value of σ. The major contribution to σ is the finite width of the Soller slits (dθ). From Braggs' Law we have

$$dE_i = 2E_i \text{Cot } \theta \text{ d } \theta$$

Thus if E_i, dθ, and Cot θ are known dE_i can be calculated. This value is equated with the F.W.H.H. of the gaussian in eqn. (1) i.e.

$$dE_i = 2\sigma \sqrt{2} \log_e 2 = 2.35\sigma$$

Plots of the displacement of the peak maximum above the threshold against E_i have been produced (fig.10,11) and to obtain the true mode frequency the value of Δ should be subtracted from the position of the observed peak.

The best resolution is obtained by using the lowest σ value available i.e. the highest order plane. It has been stated that as a rule-of-thumb one may expect to distinguish a doublet whose separation is greater than the F.W.H.H. expected at that σ.[10] I have found this view to be rather over optimistic. The resolution of the instrument is however, better than 42 cm^{-1} so that it is superior to 6H and 4H5 above 250 cm^{-1}. It has been shown, however, that the signal/noise ratio for

Fig. 10.
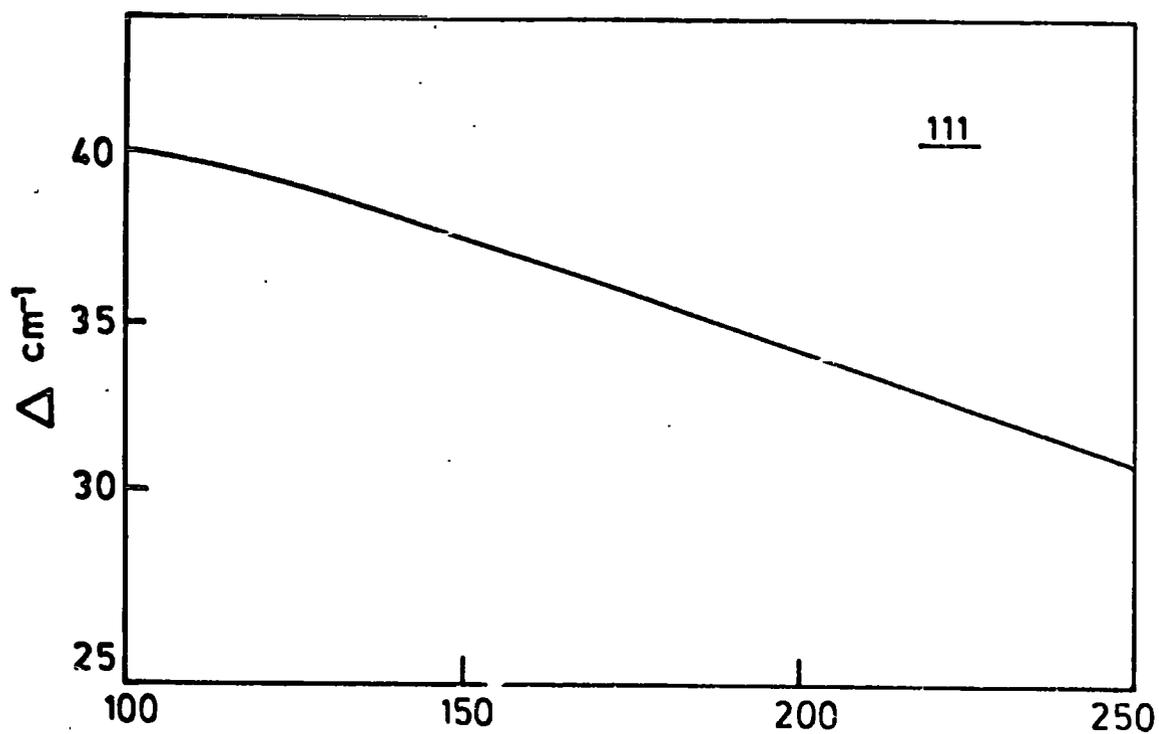
Fig. 11.

PEAK POSITION /cm⁻¹
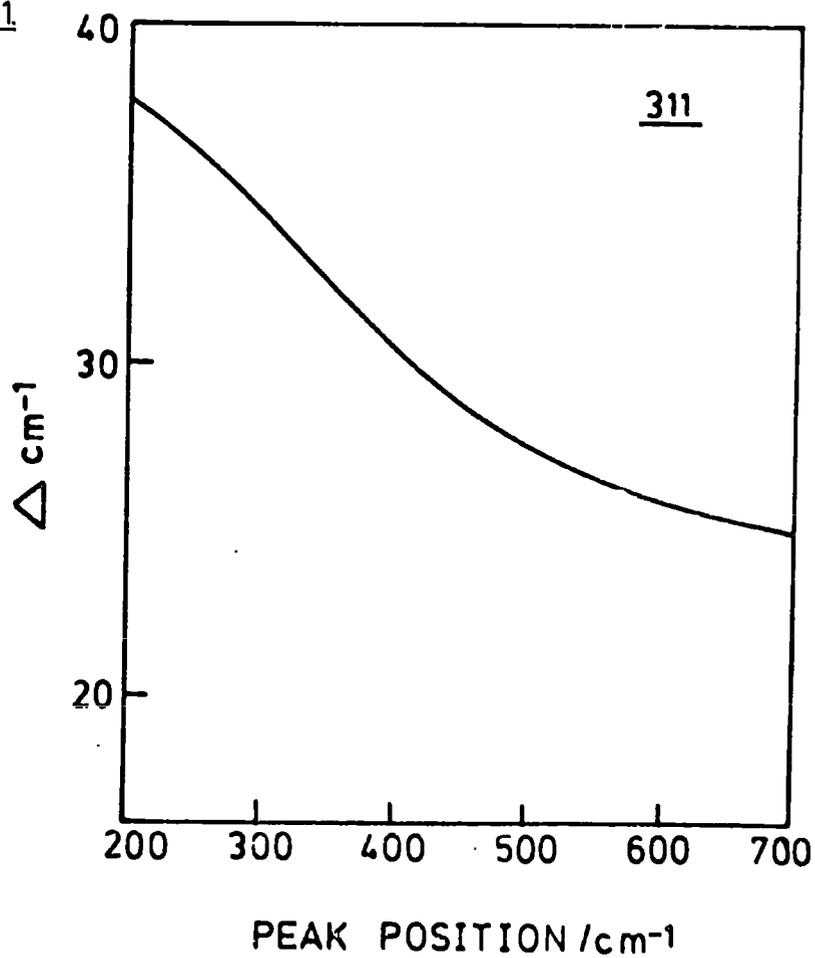
Figs. 10 and 11 Correction Factors for Harwell B.F.D. Spectrometer

sealed into thin-walled (.5 mm) silica cells using a picene coated

stopper. These cells are 5 cms. in diameter with a sample thickness in

the order of .5 mm. The samples were all less than 15% scatterers.

Silica is used because ordinary glass contains a boron isotope (^{10}B)

which is an efficient neutron absorber.

It is preferable to use thin aluminium sachets where possible

because the scattering and absorption by them is almost negligible.

The cross section of silica is greater than for Al and the silica has

to be thick for mechanical strength. The scattering from a silica cell

is therefore at least twelve times as great as that from an aluminium

sachet.

b)   Zeolites and Metal Powders

1.   Zeolites

Sample Preparation

Samples were placed in a wide-bore silica tube (7.5 cms) fitted

with a silica/pyrex graded seal. After sealing onto the glass vacuum

line the sample and sample cell were evacuated, at room temperature,

until the pressure fell below 10^{-6} torr (approx. 1 day). The pumping

system involved a trapped oil diffusion pump. The sample temperature

was then slowly raised to $450^{\circ}C$ while ensuring that the pressure

remained below 10^{-3} torr. When the pressure had again fallen below

5×10^{-6} torr the unit (fig. 12) consisting of sample cell and sample

was sealed off from the vacuum line. After tapping the sample into the

sample holder the sample cell was sealed off and finally removed from

the rest of the apparatus. This sample was then run as a background

before sealing the cell onto the vacuum line and carrying out the gas

adsorption to the required pressure. Gases were admitted through glass

a B.F.D. spectrometer is worse than that for t.of f. instruments.[11]

It is therefore desirable to use somewhat higher percentage scatterers

for B.F.D. experiments (15 → 20%) than for t.of f. measurements (10%).

It is possible in theory to improve the resolution of a B.F.D.

spectrometer by using two different filters. One possible arrangement

is shown below.

Detectors ⟶

BeO ⟶

Incident beam ⟶ Sample

Be ⟶
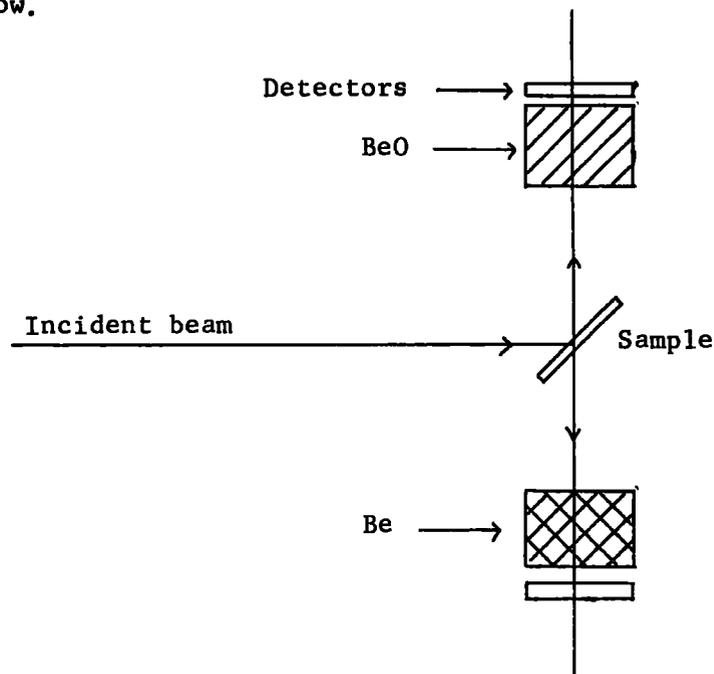
Beryllium Filter Difference Method

The two filters have different cut-offs so that by subtracting the two

counts one could obtain the intensity in the energy interval between

the two cut-offs. For instance using Be and BeO blocks the energy

interval would be c.a. 10 cm^{-1}. This facility is not yet available.

Section III: Sample Preparation and Sample Holders

a)   Model Compounds

Preparations are described in the relevant chapters.

Air-stable samples were contained in thin (.05 mm) aluminium

sachets for the neutron experiments. Unstable or reactive samples were
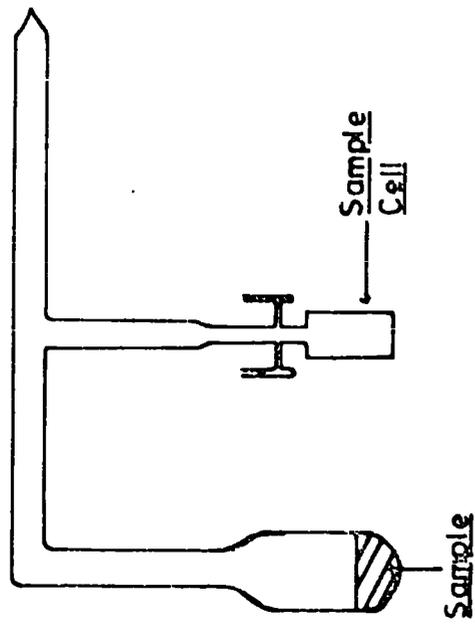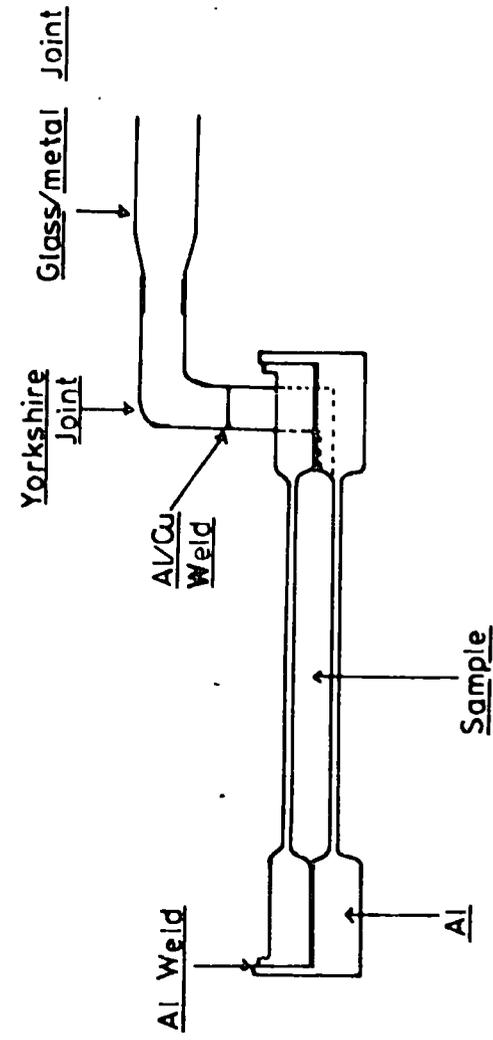
Fig. 13   Aluminium Cell Used For Zeolite Experiments

Fig. 12   Sample Unit Sealed Off from
Vacuum line

break seals fitted to the sample cell. Water was removed by passing the gases through a glass spiral surrounded by a CO_2/acetone mixture. Pressure measurements were made using a penning or bourdon gauge as required. The sample was then sealed off from the system once again.

Deuterated gases were obtained from Merck, Sharpe and Dohme Ltd. and the cylinder ethylene and acetylene were > 99.9% pure.

Sample cells

Thin walled aluminium cells (fig. 13) were used for the t.of f. experiments. The B.F.D. experiments were, however, normally carried out with silica sample holders (fig. 14).

2. Metal Powders

Sample Preparation

The technique used for the platinum powder was fairly similar to that used for the zeolites. The procedure was to

1. pump on the powder (which was dispersed in a wide bore tube) until the pressure fell below 10^{-5} torr

2. adsorb hydrogen and pump off the water formed

3. repeat step (2) four times

4. when the pressure had fallen below 10^{-5} torr the temperature was increased slowly to $200^{o}C$.

5. hydrogen was adsorbed and the system pumped several times

6. hydrogen adsorbed and finally the system pumped out to 10^{-2} torr at $200^{o}C$.

The baking chamber and sample cell were then sealed off from the pumping system and the powder tapped into the sample cell (fig. 15). The

Fig. 15   Aluminium Sample Cell

Glass

Glass/metal
seal

Cu

Al/Cu
Weld

Al

Fig. 14   Silica Sample Cell

Break
Seal
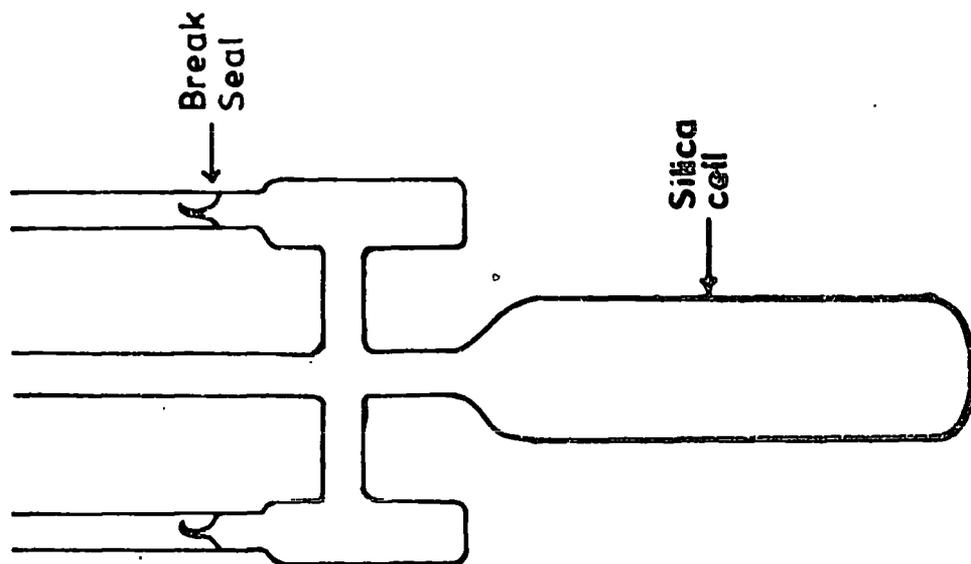
Silica
cell
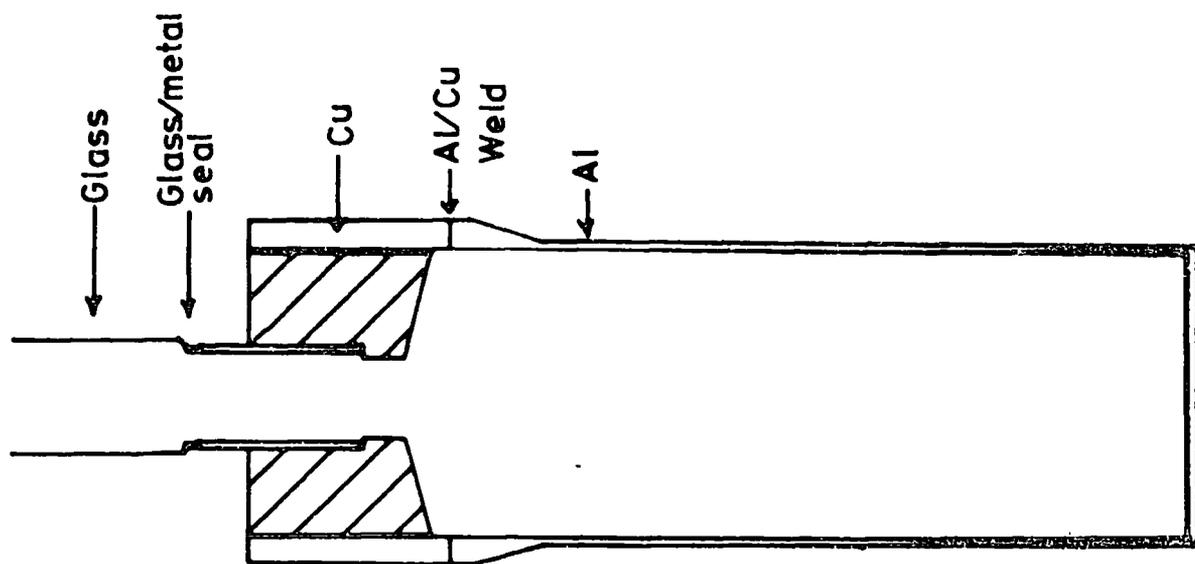
procedure was then identical to that used for the zeolites.

One variation that we have used is to clean the surface with deuterium in order to remove the possibility of scattering from adsorbed H_2O or H_2.

Our initial t.of f. experiments were carried out in a silica sample cell, however, this proved undesirable (see chapter IX). We have designed a vacuum-tight aluminium cell (fig. 15) and this was used for the later experiments. Hydrogen was purified by passing it through a deoxygenating unit.

Our experience now indicates that we require more rigorous cleaning conditions. We cannot use a higher temperature because of the sintering which would occur so we have improved the vacuum system. We have designed and built an ultra-high-vacuum (U.H.V.) system (shown schematically in fig. 16). After the initial evacuation (by trapped oil diffusion pump) the backing system is isolated via U.H.V. valves and pumping is via an ion pump (fig. 17) on a closed system. The system has so far reached 10^{-8} torr <u>unbaked</u> and should ultimately be capable of 10^{-10} torr. Further improvements are discussed in chapter IX.

Cryostat

In order to run our fairly large sample cells at low temperatures it was necessary to design and have built a centre loading cryostat with a large diameter neck. The full details are shown in fig. 18.

UV: U.H.V. Valve
LV: U.H.V. Leak valve
BV: Bakeable valve
UG: U.H.V. Gauge
S: Sample system
GS: Gas handling system
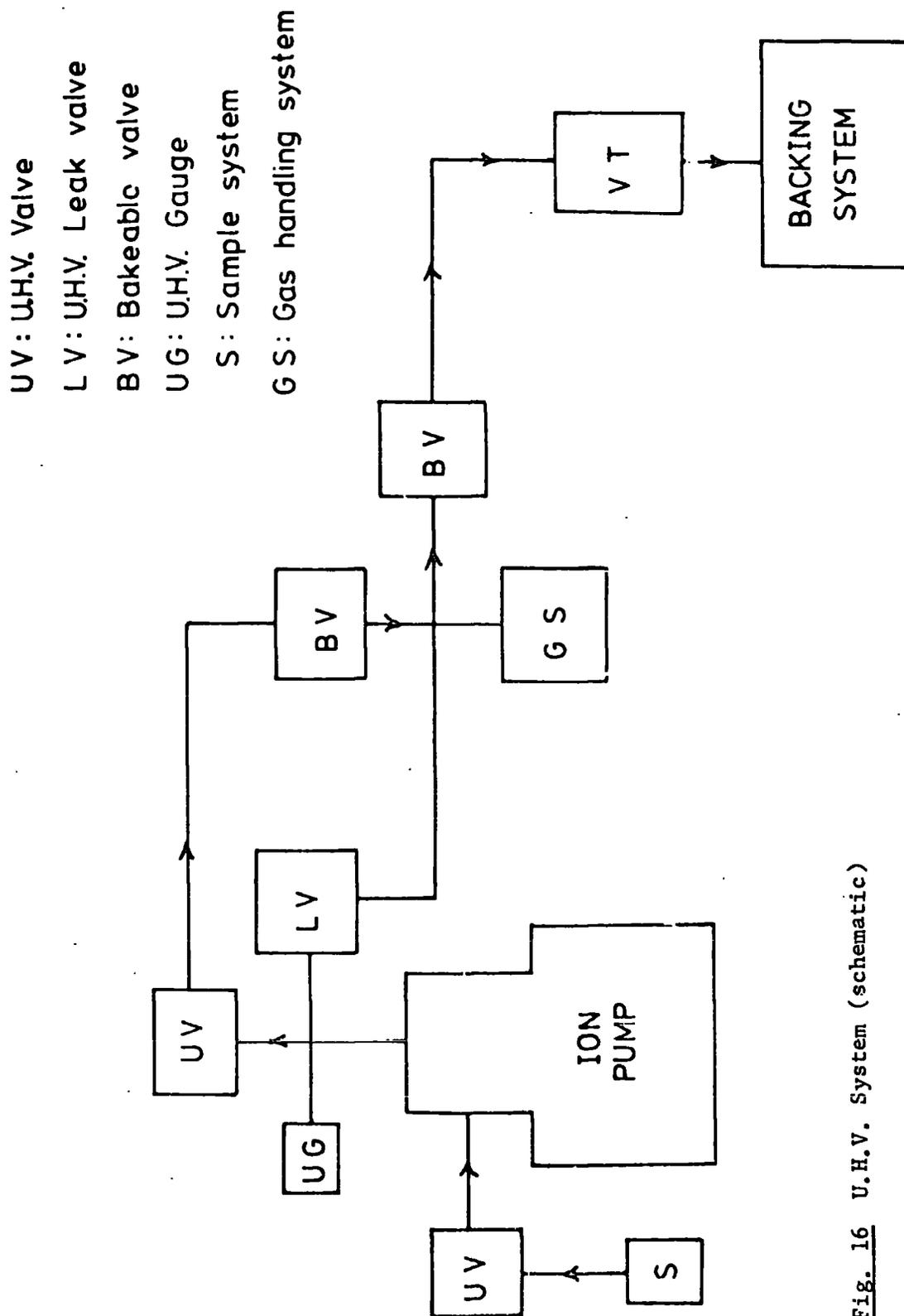
Fig. 16 U.H.V. System (schematic)

Fig. 18 Liquid Nitrogen Cryostat

Helium
Gas

Nitrogen Inlet

Cryogenic
Tubing

Sample
Space

Vacuum
Connector

Nitrogen
Chamber

Thin Al
"Windows"

Fig. 17 Ion Pump (schematic)

Cathode

Terminal

Anode
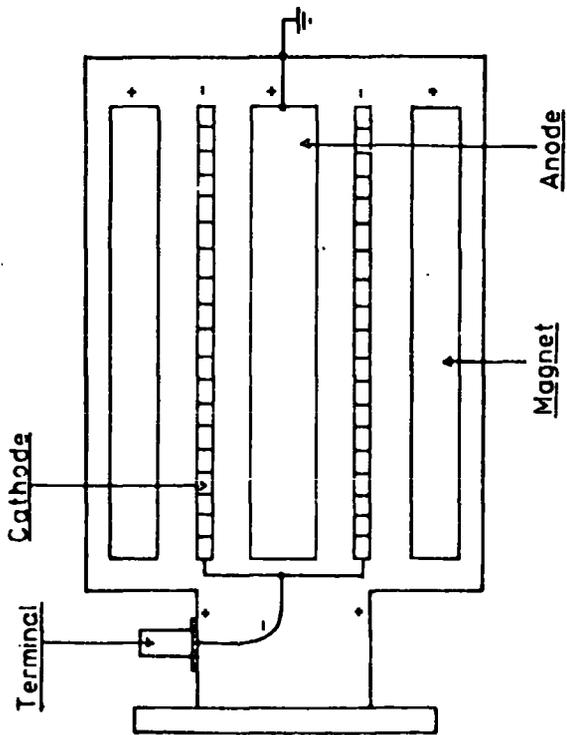
Magnet
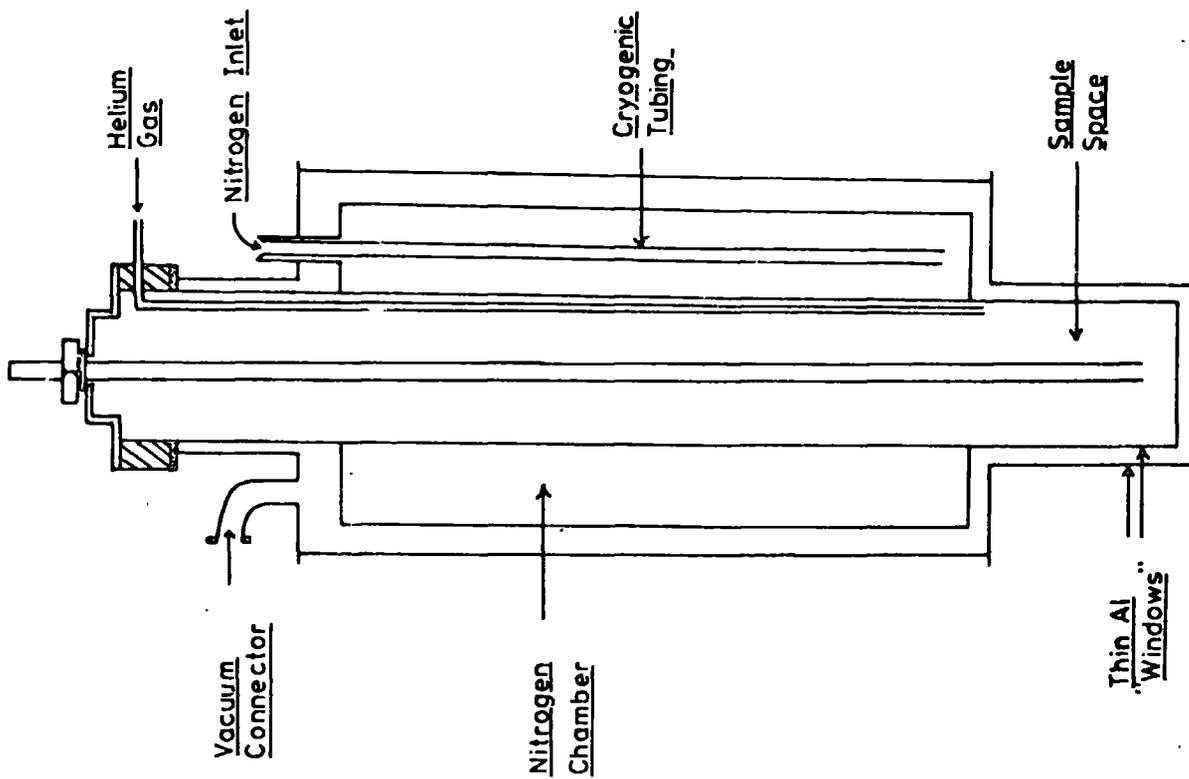
Section IV: Data Analysis

There are now well established computer programs[12,13] which can

be used for the analysis of data from t. of f. spectrometers. These are

described briefly below.

The first stage in the analysis involves the production of a line-

printer output containing the total counts in each time-channel for

each angle. Then the analysis of the data from the monitors (calculation

of incident time-of-flight) and from the standard vanadium plate is

performed to produce parameters required in further data reduction.[12]

Because the scattering cross section of vanadium is almost entirely

incoherent and it has no angular dependent scattering, other than that

resulting from a small Debye-Waller factor, the data from the standard

vanadium is used to correct for varying detector efficiency (from angle

to angle) and so normalise the results. Corrections are also made for

t he varying detector efficiency with energy. Scattering from the blank

sample holder or the background can then be subtracted and values of

$S(Q, \omega)$, $P(\alpha, \beta)$ etc. are calculated. Graphs are produced of the

corrected counts versus time of flight. There are then a series of

programmes[13] (Roundabout Programs) which can be used for further

analysis. A brief description follows.

a)   Dougal

Cubic splines are used to fit the spectrum with a smooth curve and

resulting peaks and shoulders are detected and listed for each angle.

b)   Dylan

Performs measurements on the quasi-elastic peak e.g. background

subtraction and measurement of area and full width at half height.

c)   <u>Florence</u>

This program performs the extrapolation involving $P(\alpha,\beta)$ (chapter II) and produces the resultant frequency distribution function.

d)   <u>Zebedy</u>

A general plotting program to plot pairs of variables e.g. $P(\alpha,\beta)$ v.s. cm^{-1} or $S(\alpha,\beta)$ v.s. cm^{-1} etc.

References

1. D.A. Symon, Ph.D. Thesis, University of Durham (1972).

2. M.J. Jinks, personal communication.

3. P.A. Egelstaff (Ed), Thermal Neutron Scattering, Academic Press, London and N.Y., 1965.

4. B.T.M. Willis (Ed), Chemical Applications of Thermal Neutron Scattering, Oxford University Press, 1973.

5. Instrumentation for Neutron Inelastic Scattering Research, International Atomic Energy Agency, Vienna, 1970.

6. L.J. Bunce, D.H.C. Harris and G.C. Stirling, Harwell Report R6246, H.M.S.O. (1970).

7. D.H.C. Harris, S.J. Cocking, P.A. Egelstaff and F.J. Webb, Proc. Symp. I.A.E.A. Vienna, p.107, (1963).

8. R.F. Dyer and G.G.E. Low, Harwell Report A.E.R.E. R. 3494.

9. M.B.M. Harryman and J.B. Haytor, Unpublished Harwell Report (1972).

10. P.H. Gamlen, N.F. Hall and A.D. Taylor, Unpublished Harwell Report (1974).

11. C.J. Wright, Ph.D. Thesis, University of Oxford (1971).

12. A.H. Baston, Harwell Report, A.E.R.E. M2570 (1972).

13. R.E. Ghosh, Unpublished Harwell Report (1974).

Chapter IV: Organometallic Complexes Containing Ethylene

Section I

a) Introduction

There has been considerable interest in the dynamics of complexes

containing simple π-bonded ethylene ligands. By studying the variable

temperature ^{13}C and ^1H n.m.r. spectra of a complex in which the two

ends of the C_2H_4 ligand were in different chemical environments,

Johnson and Segal,[1] were able to show conclusively that the olefin

rotation takes place about an axis through the centre of the C = C

bond and not about an axis joining the carbons.

J. Lewis et al. in a series of papers[2-5] have studied the effect

of substituents on the barrier to rotation of C_2H_4 in square planar Pt

complexes.

A theoretical study of the bonding in $Ag(C_2H_4)^+$ concluded that

the σ bond is much more important than the π bond, however, the effects

of varying the Ag-C distance and the geometry of the C_2H_4 ligand were

not studied.[6]

The vibrational modes of several π-bonded olefin complexes of Pt

and Pd have been studied previously using i.n.s.[7] The torsional mode

(torsioning about the axis joining the centre of the C = C bond to

the metal atom) was assigned in each case and, as predicted, it was

the most intense mode in the low energy spectrum. Fig. 1 shows the

neutron time-of-flight spectrum of Zeise's Salt [K $PtC_2H_4Cl_3 \cdot H_2O$] at

a scattering angle of 90°. Table 1 lists their results and assign-

ments for this complex and for all of the complexes studied. Table 2

(chapter V) lists the i.n.s., i.r. and Raman assignments for Zeise's

Salt and Dimer. The torsion is formally   infrared

Fig. 2 In-Phase and Out-of-Phase Torsions

i.p.

o.p.

Fig. 1 T.of.F. Data for Zeise's Salt

INTENSITY

TIME OF FLIGHT/μs/m

300   600   900
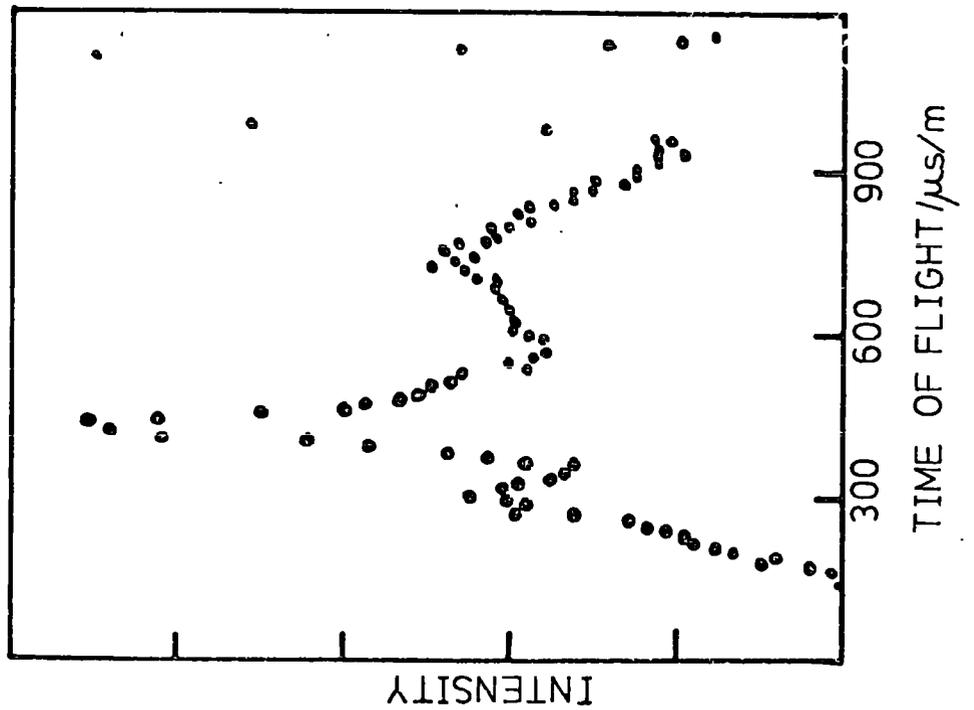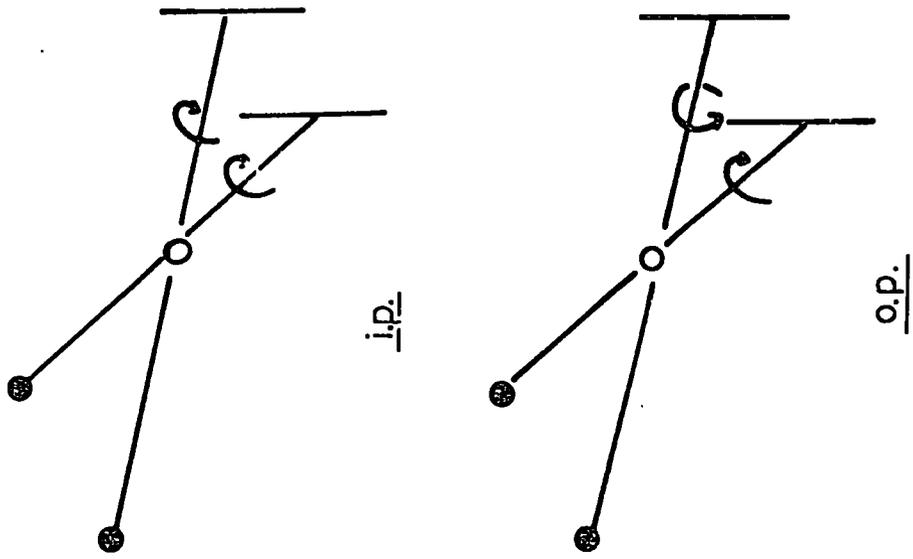
Table I I.N.S. Results for Metal-C_2H_4 Complexes[7]

	Torsion (cm^{-1})	$5V_o$ ($kJ\ mol^{-1}$)*
$Pt_2Cl_4(C_2H_4)_2$	170 ± 5	106
$Pd_2Cl_4(C_2H_4)_2$	155 ± 5	87.8
$K[PtCl_3C_2H_4]H_2O$	185 ± 5	118
$Cs[PtCl_3C_2H_4]$	190 ± 5	125

* $\omega = \sqrt{\dfrac{5V_o}{2I_r}}$

inactive. In order to reconcile the barriers to rotation calculated from n.m.r. and i.n.s. data it was necessary to write the potential function, for the rotation of the C_2H_4 about the C_2 axis, as

$$V(\theta) = \frac{V_o}{2} (1-\text{Cos } \theta) + \frac{V_4}{2} (1-\text{Cos } 4\theta)$$

where θ is the angle of rotation measured from the equilibrium position.

This function has a ground state minimum at $\theta = 0^o$ and a meta-stable minimum at $\theta = \frac{\pi}{2}$ (provided that $V_4 > 0$ and $V_4 > \frac{V_o}{4}$). These conclusions are in agreement with a molecular orbital calculation which predicted a metastable well when $\theta = \frac{\pi}{2}$.[8]

We have continued and extended this work and in order to obtain further information about the torsion potentials of ethylene molecules bound to metal atoms we have studied the vibrations of the ethylene groups in $\pi-C_5H_5Rh(C_2H_4)_2$, $[Rh(C_2H_4)_2Cl]_2$ and $\pi-C_5H_5Rh(C_2H_4)SO_2$ with inelastic neutron scattering (i.n.s.). These data will be of value in the interpretation of the spectra of adsorbed molecules. In the first two compounds the ethylene groups are bound in a cis configuration to their metal atoms and we have been able to observe the interactions between the groups through the splittings between their in-phase and out-of-phase torsions (fig. 2). These interactions have been expressed in terms of constants in the Fourier expansions of the potential energies of the rotating ethylene groups. Confirmation of our interpretation is provided by the spectrum of $\pi-C_5H_5Rh(C_2H_4)SO_2$. Ethylene rotation in the two cyclopentadiene compounds has also been studied with n.m.r.[9] and the combination of the i.n.s. and n.m.r. results leads to more detailed information than can be obtained from either method independently.

We have also obtained the low frequency (0-300 cm^{-1}) i.n.s. spectrum of $AgNO_3 \cdot \frac{1}{2} C_2 H_4$ and the higher frequency i.n.s. spectra (200-1500 cm^{-1}) of Zeise's Salt and Dimer, however, as these results are of particular relevance to our study of adsorbed $C_2 H_4$ they have been discussed with that work (chapter V).

Two complexes containing more than two ethylene ligands bonded to the same metal atom have been studied, however, experimental difficulties have meant that this work is somewhat incomplete.

b)   Experimental

[$Rh(C_2 H_4)_2 Cl$]$_2$ was purchased from Strem Chemicals Inc., π-$C_5 H_5 Rh(C_2 H_4)_2$ was kindly donated by Dr. R. Cramer and π-$C_5 H_5 Rh(C_2 H_4)$ SO_2,[10] $Ir(C_2 H_4)_4 Cl$[11] and [$Rh(C_2 H_4)_3 (CD_3 CN)_2$]$BF_4$[12] were prepared by literature methods.

All samples were handled in inert atmospheres and examined as polycrystalline powders. Both cyclopentadiene complexes were sandwiched between 0.05 mm. thick aluminium foil whereas the remaining samples were contained in thin-walled silica cells. The neutron spectra (except for the iridium complex) were obtained at room temperature on the 6H spectrometer. Because of its instability the spectrum of the iridium complex was obtained at nitrogen temperature using the 7H spectrometer. The higher energy spectra were obtained on the Beryllium Filter Detector Spectrometer with the sample at c.a. 90K.

Infrared measurements were made using a Beckman-RIIC FS720 Fourier Transform spectrophotometer. Samples were run as nujol mulls supported on a polythene disc. The Raman measurements we made with a Cary 82 Laser Raman spectrophotometer using a wavelength of 632.8 nm with approximately 10 mW power at the sample.

Section II: Interactions Between cis-Ethylene Ligands Studied by

Inelastic Neutron Scattering

a)   Results and Discussion

        Assignment of Spectra

        The frequency distributions $\rho(\omega)$, of $[Rh(C_2H_4)_2Cl]_2$, $Fe(\pi-C_5H_5)_2$,

$Rh(C_2H_4)_2(\pi-C_5H_5)$ and $Rh(C_2H_4)(SO_2)(\pi-C_5H_5)$, obtained from energy-gain

inelastic neutron scattering are shown in fig. 3-6, and the results

together with those from the Raman and infra-red spectra are

summarized in table 2.
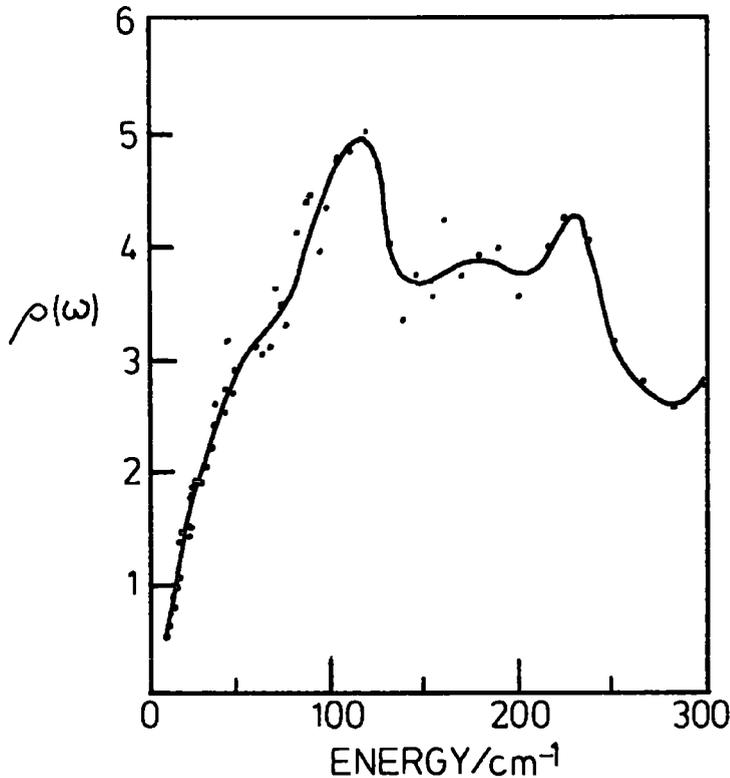
Fig. 3 Density of States of $[Rh(C_2H_4)_2Cl]_2$

To a first approximation each of the spectra of the cyclopentadiene

compounds is separable into the vibrations of its constituents, i.e.,

the scattering due to the cyclopentadienyl ring should be separable

from that due to the ethylene ligands. Such a separation procedure is

not, in general, possible with optical spectra because of the changes

in selection rules which may occur as a result of substitution;
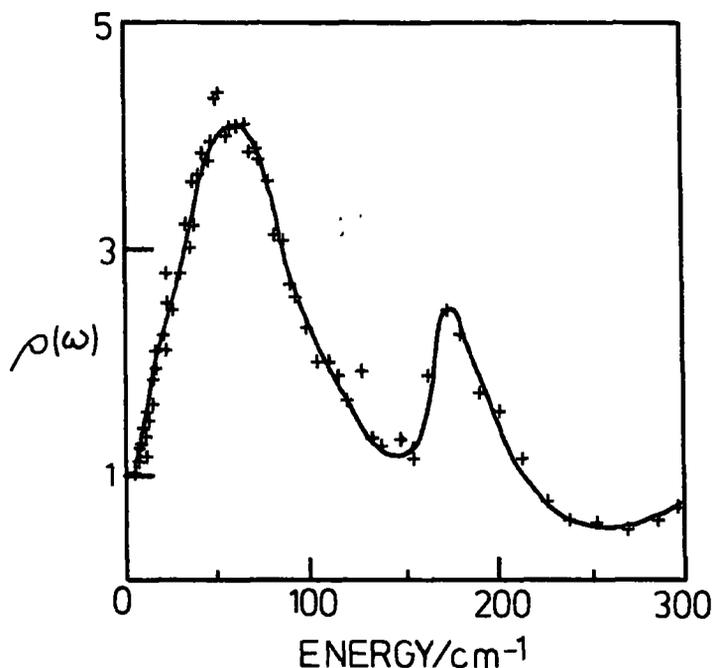
Fig. 4   Density of States of $(\pi\text{-}C_5H_5)_2Fe$

TABLE 2

$(\pi\text{-}C_5H_5)Rh(C_2H_4)_2$			$[(C_2H_4)_2RhCl]_2$			$\pi\text{-}C_5H_5Rh(C_2H_4)SO_2$		$(\pi\text{-}C_5H_5)_2Fe$		
i.n.s.	i.r.[a]	Raman	i.n.s.	i.r.[a]	Raman	i.n.s.	i.r.[a]	i.n.s.	i.r.[b]	Raman[a,c]
					21					
	30			29						
				39	40					48(?)
50	60		50	50	50	52		56		57
					60				60	65
									70	73
									83	82
					84					
100			112	118	123					
						125	124			
	140(?)			138			141			
				146						
165	166	171	160	172	170	175	185(sh)		174	179
230							197			186
	242	244	226	220						

[a] At liquid-nitrogen temperature;

[b] ref (14)   [c] ref (20)

however, this separation will be valid for the neutron spectra if there is no coupling between the motions of the C_5H_5 ring and the ethylene ligands. It is believed, from a variety of experimental evidence, e.g. n.m.r. work,[13] infrared results,[14] electron diffraction[15] and from a study of the number and type of acetylethylferrocene isomers[16] that the torsional
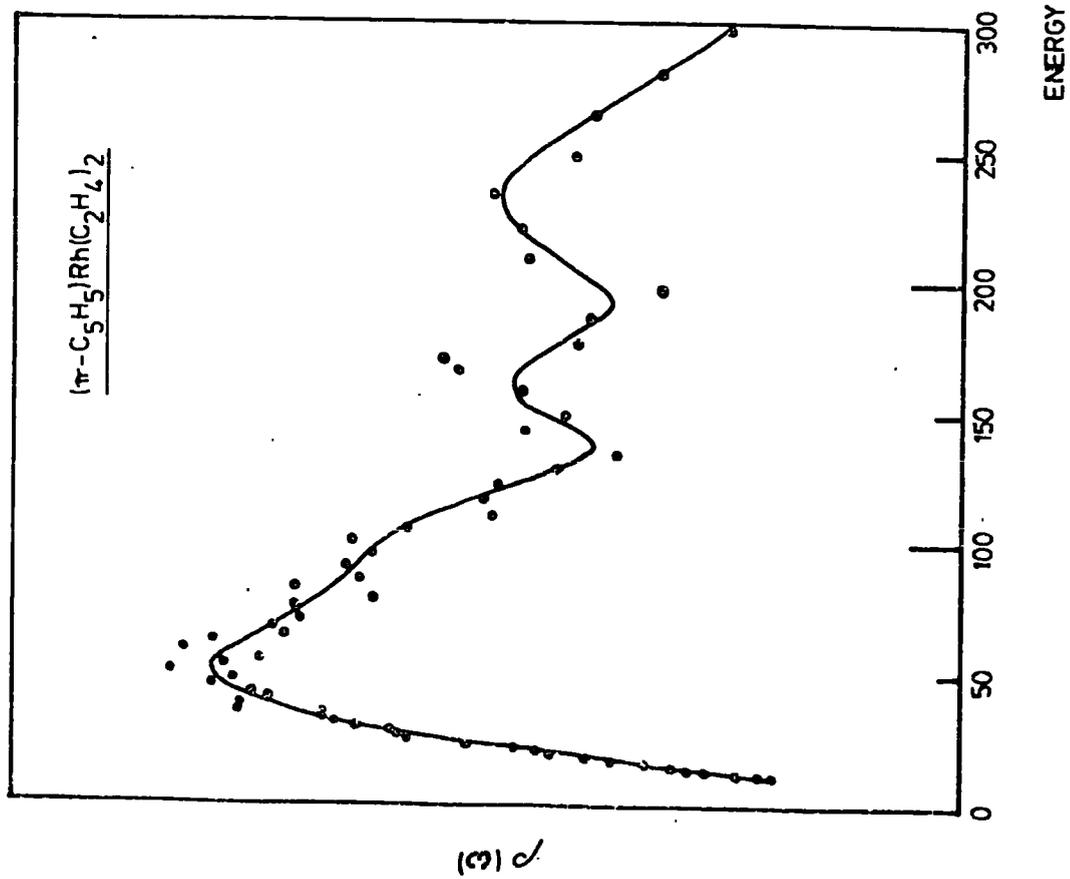
Fig. 6 Density of States Spectrum of $\pi-C_5H_5Rh(C_2H_4)SO_2$
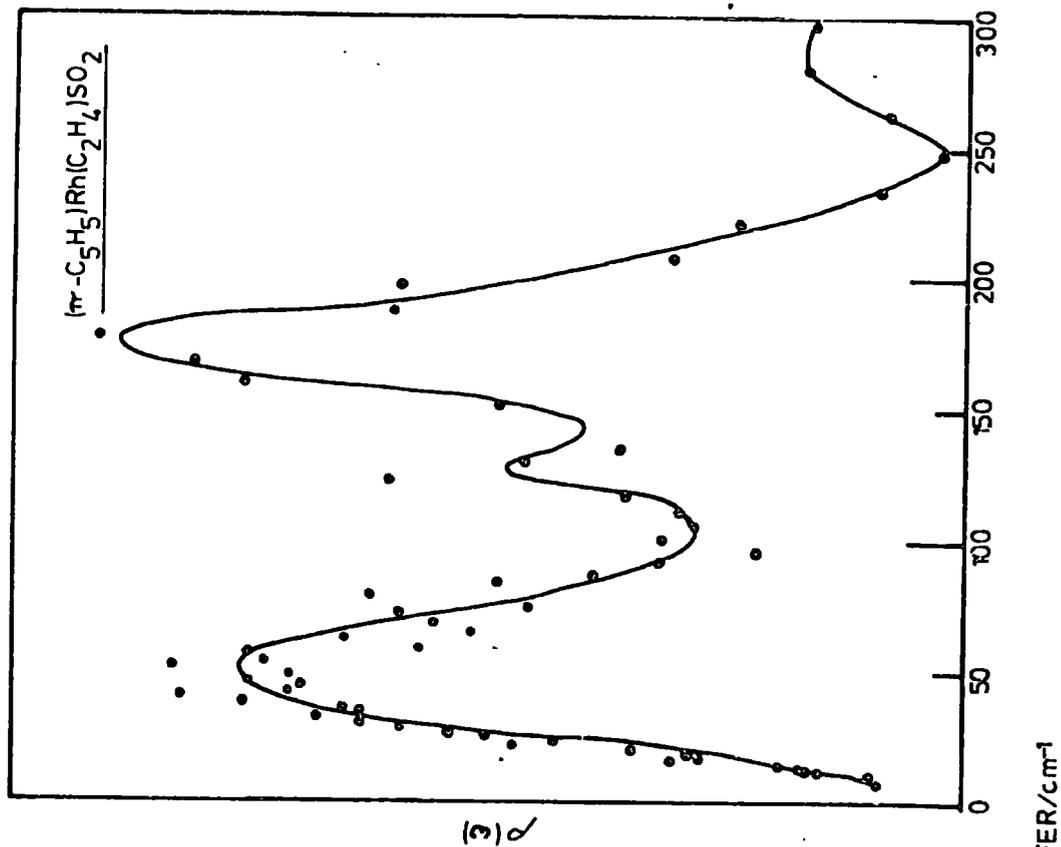
Fig. 5 Density of States Spectrum of $\pi-C_5H_5Rh(C_2H_4)_2$

ENERGY TRANSFER/cm⁻¹

motions of the C_5H_5 rings in $Fe(\pi-C_5H_5)_2$ are virtually free. We consider

that a similar situation obtains in $\pi-C_5H_5Rh(C_2H_4)_2$ and $\pi-C_5H_5Rh(C_2H_4)SO_2$.

The n.m.r.[10,17] results for these compounds show only a single absorption

for the protons on the C_5H_5 ring. The separation is further supported by

the similarity of the i.n.s. spectra of $Rh(\pi-C_5H_5)(C_2H_4)_2$ and

$[Rh(C_2H_4)_2Cl]_2$ in the low-frequency region. In the solid state the

formal number of electrons at the metal atom in $[Rh(C_2H_4)_2Cl]_2$ is identical

to that in $Rh(\pi-C_5H_5)(C_2H_4)_2$[18] because of the extra interactions between

metal atoms in neighbouring molecules. Consequently, it is not unexpected

that the ethylene vibrations in these two molecules are similar; rather

it gives additional confirmation to our assignments. Thus, in our analysis

we treat the C_5H_5 ring as a massive freely-rotating group. The scattering

from the ethylene ligands can be obtained from our results by separating

the spectrum of the $(\pi-C_5H_5)Rh$ group, a good description of which we

consider to be provided by ferrocene, $(\pi-C_5H_5)_2Fe$.[19]

The i.n.s. spectrum of ferrocene contains bands at 56 ± 5 and 174 ± 5

cm^{-1} in the low energy region. The peak at 174 cm^{-1} corresponds to an i.r.

band at 179 cm^{-1} which has been assigned to a ring-metal-ring bending

mode.[20] The peak at approximately 50 cm^{-1} in the spectra of the cyclo-

pentadiene compounds we thus assign to a vibration of the C_5H_5 ring by

analogy with the $(\pi-C_5H_5)_2Fe$ spectrum.

By analogy with the spectra of Zeise's salt and related compounds

the peak at 173 ± 5 cm^{-1} in the i.n.s. spectrum of the SO_2 compound can be

assigned to the ethylene torsion vibration. As predicted from consideration

of the moment of inertia and mass of the ethylene group,[7] only weak inten-

sity is seen in the regions 110-130 and 190-200 cm^{-1} where the rock and

wag vibrations are expected to occur[21,22,23] with intensity approximately

$\frac{1}{3}$ that of the torsion vibration. The peak at $125\overset{+}{-}5$ cm^{-1} is probably the wag and the rock is not resolved from the much stronger torsional peak.

The i.n.s. spectrum of $[(C_2H_4)_2RhCl]_2$ contains four features. The two most intense bands, at $112\overset{+}{-}5$ and $226\overset{+}{-}5$ cm^{-1}, we assign to the in-phase (i.p.) and the out-of-phase (o.p.) torsions respectively of the ethylene ligands. No assignment which omits i.p. and o.p. torsion vibrations can account for the similar intensities of the peaks in this spectrum. An assignment of one peak to a torsion vibration and another to a particular bending vibration of the ethylene-metal bond would be unacceptable on intensity grounds.

The i.n.s. spectrum of $Rh(\pi-C_5H_5)(C_2H_4)_2$ also has four bands. The band at 50 cm^{-1} we have already assigned to a vibration of the C_5H_5 ring by comparison with the spectra of ferrocene. The remainder of the spectrum is very similar to that of $[Rh(C_2H_4)_2Cl]_2$. Thus, for identical reasons, we assign the bands at 100 and 230 cm^{-1} to i.p. and o.p. torsions of the ethylene groups.

I.r. and Raman spectra (table 2) are not particularly helpful in confirming these assignments. Both diethylene compounds are of C_{2v} symmetry so that all vibrations are Raman active and only those of A_2 symmetry are i.r. inactive. Thus, we were unable to detect an i.r. band corresponding to the i.p. (A_2) torsion in $Rh(\pi-C_5H_5)(C_2H_4)_2$ as would be expected; however, we were also unable to detect a Raman signal close to this frequency. The o.p. torsion for $Rh(\pi-C_5H_5)(C_2H_4)_2$ (B_1) has corresponding i.r. and Raman bands as expected. The i.p. and o.p. torsions in $[Rh(C_2H_4)_2Cl]_2$ are of symmetry B_1 and A_1 respectively and we were unable to detect a Raman signal corresponding to the o.p. torsion.

$(\pi\text{-}C_5H_5)Rh(C_2H_4)SO_2$ is of C_s symmetry and so all modes should be i.r. and Raman active. We were unable to obtain the Raman spectrum of this complex.

b)   Calculation of Barriers from the Torsional Frequencies:
     Potential Energy Calculations

We now calculate how the potential energy of a pair of cis-ethylene ligands can be expected to vary during in-phase and out-of-phase rotation. We also obtain simple formulae for these potential functions which can then be used to interpret the assignments we have made.

If α_1 and α_2 are the clockwise rotational angular displacements of the two ethylene groups about the axes joining their midpoints to the metal atom, then the variation of the potential energy of the ethylene ligands, on rotation, may be written as

$$V_{total}(\alpha_1,\alpha_2) = V(\alpha_1,\alpha_2) + V_T(\alpha_1) + V_T(\alpha_2), \tag{1}$$

where $\alpha_1 = \alpha_2 = 0$ in the ground vibrational state conformation. $V(\alpha_1,\alpha_2)$ is the potential energy variation due to the cis-ethylene interactions and $V_T(\alpha_1)$ and $V_T(\alpha_2)$ are the potential energy variations due to interactions with the remainder of the molecule.

$\underline{V(\alpha_1,\alpha_2):}$

$V(\alpha_1,\alpha_2)$ is, in general, a complex function of α_1 and α_2 but for the in-phase ($\alpha_1 = \alpha_2$) and out-of-phase ($\alpha_1 = -\alpha_2$) motions the potential energy variations may be expressed as

$$V(\alpha, -\alpha) = \sum_{n=1}^{\infty} V_{2n}(1 - \cos 2n\alpha) \tag{2}$$

$$V(\alpha,\alpha) = \sum_{n=1}^{\infty} V_{2n}(1 - \cos 2n\alpha) + \sum_{n=1}^{\infty} \tfrac{1}{2}V'_{4n}(1 - \cos 4n\alpha). \quad (3)$$

For a discussion of this result see Appendix A.

We have numerically calculated values of $V(\alpha,\alpha)$ and $V(\alpha,-\alpha)$ for a cis-diethylene complex to decide where these series may be truncated. The calculations used the function,

$$V(R) = 11.094 \times 10^3 \exp(-3.74R) - 114.1R^{-6} \text{ kJ mol}^{-1}$$

due to Williams,[24] where R is the hydrogen-hydrogen separation in Å.

The intramolecular interaction potentials between hydrogens on the ethylenes and those on the C_5H_5 ring are approximately 1% of the potentials between hydrogens on the different ethylene ligands. The structural parameters used in this calculation were those determined for $\pi\text{-}C_5H_5Rh(C_2H_4)(C_2F_4)$[25] and the angle between the three-membered ethylene-metal ring was taken from this structure, but with less justification, as 95°. Plots of the calculated values of $V(\alpha,\alpha)$ and $V(\alpha,-\alpha)$ are shown in fig. 6a To determine the importance and size of the individual coefficients eqn (2) and (3) were fitted to these curves by the method of least squares. Because the exact geometry of the $\pi\text{-}C_5H_5Rh(C_2H_4)_2$ molecule is not known and the higher Fourier coefficients were found to be small and interdependent, it was decided that the simple potential functions shown below, which correctly reproduce the essential details of the calculated curves, would be used for further data analysis.

$$V(\alpha,-\alpha) = V_2(1 - \cos 2\alpha) + V_4(1 - \cos 4\alpha), \quad (4)$$

$$V(\alpha,\alpha) = V_2(1 - \cos 2\alpha) + V_4(1 - \cos 4\alpha) + \tfrac{1}{2}V'_4(1 - \cos 4\alpha)$$
$$+ \tfrac{1}{2}V'_8(1 - \cos 8\alpha). \quad (5)$$

The best fits of these functions to the calculated curves together
with the values obtained for the Fourier coefficients are also shown in
fig.6a. Our theory indicates that the first Fourier coefficients, for
the in-phase and out-of-phase motions, will be equal and from fig. 5
this can be seen to be the case.

$\underline{V_T(\alpha)}$:

We now find a value for $V_T(\alpha)$ by using the n.m.r. and i.n.s. data
for $\pi-C_5H_5Rh(C_2H_4)SO_2$ to determine the form of the potential function
for rotation of a single ethylene ligand. Using this form to describe
the situation for the diethylene complex when only a single ethylene
rotation is being observed, as in the n.m.r. experiment, we can use the
n.m.r. barrier to obtain $V_T(\alpha)$.

We assume that there is negligible steric hindrance to the
rotation of the ethylene ligand in $\pi-C_5H_5Rh(C_2H_4)SO_2$ and that the
torsion potential may be expressed as

$$V_{total}(\alpha) = V_T(\alpha) = \tfrac{1}{2}V^T(1 - \cos 2\alpha).$$

$V_2 = 16.5$, $V_4 = 22.1$ kJ mole^{-1}
$V_2 = 16.5$, $2V_2+V'_4 = 32.4$,
$V'_8 = -21.8$ kJ mole^{-1}
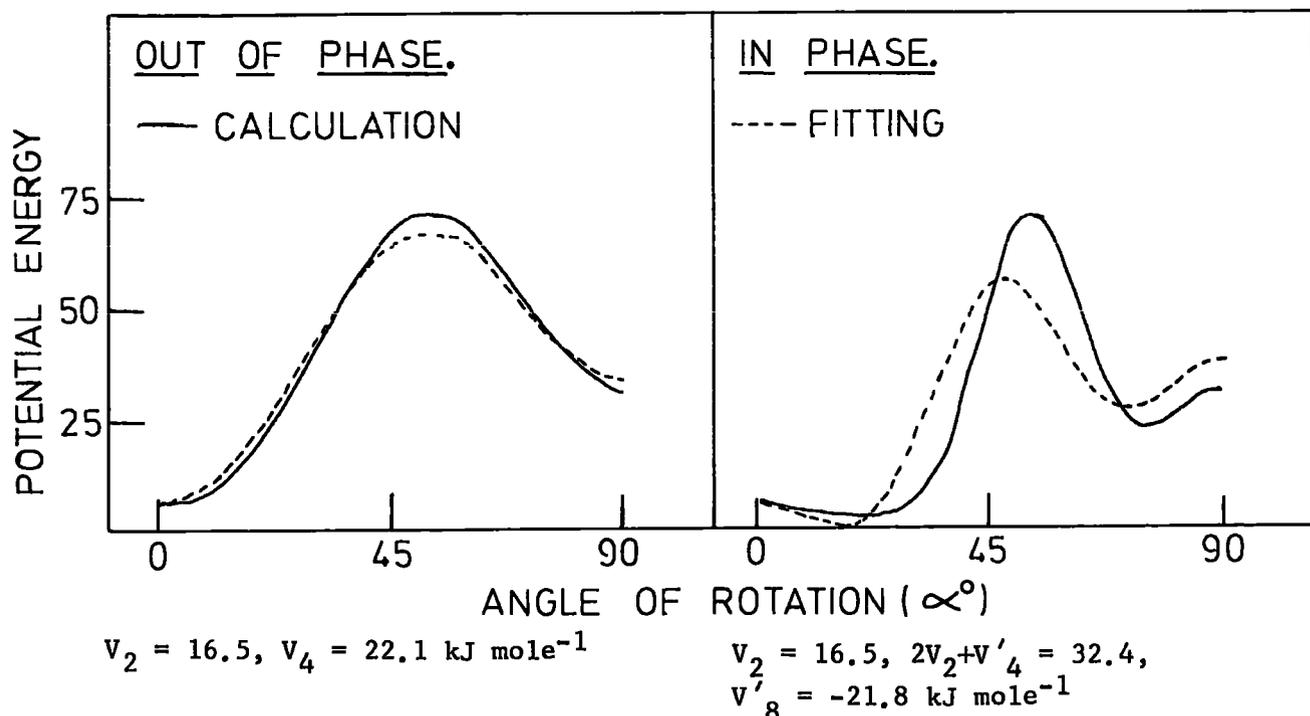
Fig. 6a Potential energies calculated for cis-ethylene ligands.

Using the simple harmonic oscillator formula, this simple two-fold potential leads to a value of V^T, obtained from the neutron data of 109.3 ± 6 kJ mol^{-1} which compares with the n.m.r. value of 51.1 kJ mol^{-1}. This discrepancy is expected since work on Zeise's salt[7] showed the necessity of including a four-fold term in the torsion potential in order to account for the increase in $d_\pi - p_\pi$ bonding after rotation of the ethylene group by 90° from the ground state position. By using an equation of the form

$$V_T(\alpha) = \tfrac{1}{2}V^T (1 - \cos 2\alpha) + (V^T/2x)(1 - \cos 4\alpha), \qquad (6)$$

we can effect agreement between the n.m.r. and i.n.s. data. This leads to a value for x of approximately $\frac{7}{2}$ and with this value the n.m.r. barrier to rotation is still numerically approximately equal to V^T. The four-fold contribution is smaller than that found for Zeise's salt but there is still a very small metastable minimum in $V_T(\alpha)$ at $\alpha = 90^o$.

We assume that eqn (6) (with $x = \frac{7}{2}$) may also be applied to the complex $\pi\text{-}C_5H_5Rh(C_2H_4)_2$ and that we may use its n.m.r. barrier (62.7 kJ mol^{-1}) for V^T.

This treatment neglects the effect of intermolecular interactions in the solid state. The justification for this is that good agreement between theoretical and experimental values of the barrier in Zeise's salt was found using this approximation.

c) Comparison with Experimental Results

By substituting eqn (4), (5) and (6) into eqn (1), we obtain analytic expressions for $V_{total}(\alpha,\alpha)$ and $V_{total}(\alpha, -\alpha)$. Again, using the harmonic oscillator formula, we obtain the following expressions for the energy separations of the 0-1 torsional transitions of the

ethylene groups:

$$\omega_{o.p.} = \frac{1}{I_r^{\frac{1}{2}}} (2V_2 + 8V_4 + 4.3V^T)^{\frac{1}{2}} \text{ for the out-of-phase rotation,}$$

(7)

$$\omega_{i.p.} = \frac{1}{I_r^{\frac{1}{2}}} (2V_2 + 8V_4 + 4V'_4 + 16V'_8 + 4.3V^T)^{\frac{1}{2}} \text{ for the}$$

in-phase rotation, (8)

where I_r is the reduced moment of inertia of an ethylene ligand. Substituting for the experimental values of $\omega_{o.p.}$ and $\omega_{i.p.}$ for $\pi\text{-}C_5H_5Rh(C_2H_4)_2$ and using the value of 62.7 kJ mol^{-1} for V^T enables us to calculate values for $V_2 + 4V_4$ and $V'_4 + 4V'_8$ these being 58.3 ± 7.5 and -78.2 ± 6 kJ mol^{-1} respectively. These values can be compared with those obtained by the curve fitting to the numerical calculation of 105 and -98.8 kJ mol^{-1} respectively.

As there is no simple method for the accurate determination of energy barriers of processes leading to the collapse of a AA'BB'X spin system to an A_4X system, approximate methods were employed in the determination of the barriers to rotation by n.m.r. The values we have quoted were calculated from computer line-shape analysis by a method which gives predicted line shapes which are in good agreement with the experimental data. The value for $C_5H_5Rh(C_2H_4)_2$ has also been calculated[26] (65.9 kJ mol^{-1}) by using an approximate equation which is subject to the limitations outlined by Raban et al.[27] This value is in reasonable agreement with the value calculated from the line shape analysis (62.7 kJ mol^{-1}).

Eqn (7) and (8) are sensitive to the experimental values of the n.m.r. barriers. For instance, if the value of 51.1 kJ mol^{-1} for the

$(\pi-C_5H_5)Rh(C_2H_4)SO_2$ compound were too low by more than 7% then the value of x, in eqn (6) would change and the metastable minimum at $\alpha = 90°$ would disappear. However, the n.m.r. barrier would still be approximately equal to V^T. The major change would be a reduction in the coefficient of V^T in eqn (7) and (8). This would not alter the value of $V'_4 + 4V'_8$ but it would lead to an increase in $V_2 + 4V_4$.

The "splitting interaction" -78.2 kJ mol^{-1}, which is determined straightforwardly from the difference in energy between the in-phase and out-of-phase torsion vibrations, agrees more favourably with the calculations than the other term which requires more assumptions in its determination.

Errors in the assumptions behind the above calculations are likely to arise from at least three sources: (i) a distortion of the ethylene ligand during rotation, (ii) the competition between the two ethylene groups for the d_{xy} electrons, of the metal atom, when $\alpha_1 = \alpha_2 = 90°$, and (iii) the intermolecular interactions mentioned earlier.

The bridging of the torsion frequency of the SO_2 compound by those of the diethylene complex can be seen to be caused by the opposing effects of $V_2 + 4V_4$ on the out-of-phase torsion and $V'_4 + 4V'_8$ on the in-phase torsion.

Section III: Complexes Containing Several Ethylene Ligands Bonded to the Same Metal Atom

Very few complexes containing more than two C_2H_4 ligands bonded to the same metal atom, have been prepared. As far as we are aware the only ones to exist are $Ni(C_2H_4)_3$,[28] $Pd(C_2H_4)_3$,[29] $Pt(C_2H_4)_3$[30] and $Pt(C_2H_4)_2(C_2F_4)$,[31] $Ir(C_2H_4)_4Cl$[11] and $[Rh(C_2H_4)_3(CH_3CN)_2]BF_4$.[12] The Ni, Pd and Pt complexes are very unstable and our efforts to prepare them, in sufficient quantity for an i.n.s. experiment, have so far been unsuccessful.

Crystal structure[12,31,32] data show that the arrangement of the ethylene ligands in the above complexes is very different from that found in Zeise's Salt[33] or $[Rh(C_2H_4)_2Cl]_2$. In each case the C_2H_4 ligands are arranged so that three of them have their double bonds in a plane (fig. 7). There has also been a theoretical study of the

(A)   (B)

o C
⊙ N
• H
⊕ Rh
O Cl
⊙ Ir
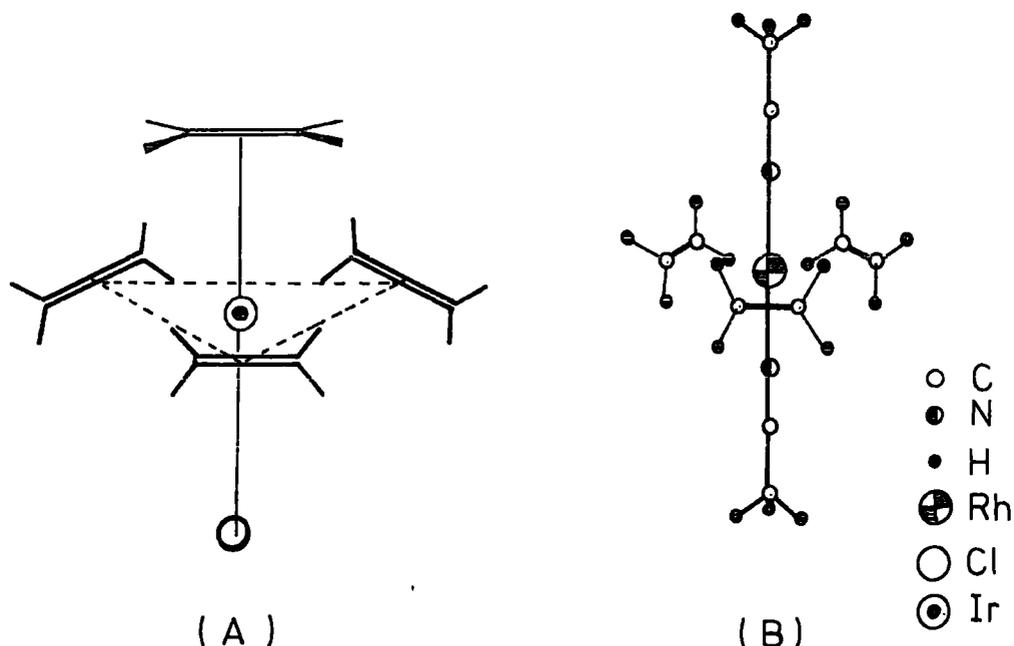
Fig. 7 Molecular Structures of (A) $Ir(C_2H_4)_4Cl$ and (B) $Rh(C_2H_4)_3(CH_3CN)_2^+$

molecular configuration and bonding in these complexes.[34]

a) $\underline{Ir(C_2H_4)_4Cl}$

Relevant previous work

This (white) complex is unstable at room temperature, even in a

C_2H_4 atmosphere, however, it decomposes into bright red $[Ir(C_2H_4)_2Cl]_2$

and so any decomposition is immediately apparent.

Its crystal structure has apparently been determined but full

details have not yet been published.[11] The molecular configuration is

shown in fig. 7 and it has been found that the iridium atom is

situated slightly out of the equatorial plane, of the three C_2H_4

ligands, towards the axial C_2H_4 ligand.

Infrared bands have been reported at[11] 505, 397, 372 cm^{-1} "in the

$\nu(Ir-C_2H_4)$ region" and 280 cm^{-1} (assigned to $\nu(Ir-Cl)$) with a shoulder

at 308 cm^{-1}.

Proton magnetic resonance spectra in chloroform solution (at -20°C)

show two sharp peaks (intensity ratio 1:3) due to axial and equatorial

C_2H_4 ligands respectively.[11] Broadening of the axial C_2H_4 resonance,

on admission of gaseous C_2H_4 indicates exchange with this particular

ligand.

Although no broadening of the resonances was observed on cooling

the chloroform solution it was found that the proton magnetic resonance

spectrum in toluene at -60°C exhibited an AA$'$ BB$'$ pattern due to the

equatorial ligands. A single sharp peak was found for the axial C_2H_4.

The AA$'$ BB$'$ pattern was shown to be consistent with the cis protons of

the equatorial ligand being equivalent. This corresponds with the

equatorial ligands being arranged with the double bonds in a plane
and hence agrees with the crystal structure.

In the solid state rotational barriers of 5.1 kcal mol^{-1}, for the
equatorial ligands and 1.6 kcal mol^{-1} for the axial ligand, have been
determined from magnetic resonance measurements as a function of
temperature.[35] The solid state n.m.r. results were interpreted in
terms of 180° jump rotations about the metal-alkene axis.

b) Theoretical

By using the methods already outlined for $[Rh(C_2H_4)_2Cl]_2$
(Appendix A) we can determine the number of torsional modes that we
may expect to observe as a result of interactions between the C_2H_4
ligands. A full discussion is given in appendix B, however, to
summarise we have defined
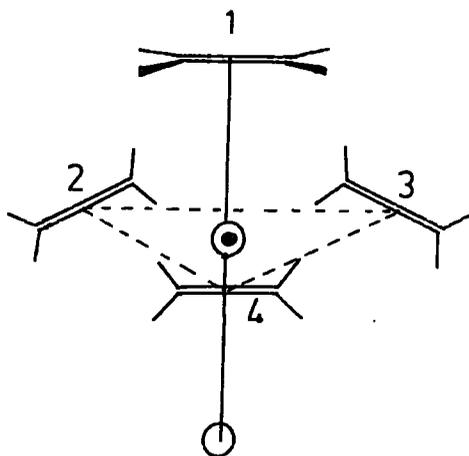
Fig. 8 Numbering of Ethylene Ligands

$$f_1 = V_1(1- \cos p\ \theta_1)$$

$$f_i = V_2(1- \cos n\ \theta_i) \quad i = 2,3,4$$

$$f_{1,i} = V_{1,2}(1-\cos m(\theta_1 + \theta_i)) \quad i = 2,3,4$$

$$f_{i,j} = V_{2,3}(1- \cos q(\theta_i + \theta_j)) \quad i,j = 2,3;\ 3,4;\ 2,4$$

where

f_k is the potential function representing the variation in potential energy of a single C_2H_4 ligand on rotation but which does not include potential energy variations as a result of interactions between ligands.

$f_{k,\ell}$ is the potential function which represents potential energy variations arising solely from interactions between ligands k and ℓ.

θ_s is the clockwise rotational angular displacement of the ligand from its equilibrium position.

p,n,m,q are the barrier periodicities (chapter II).

V_k and $V_{k,\ell}$ are the barrier heights.

Because the equatorial ligands are equivalent and different from the axial ligand we have

$$f_2 \quad = \quad f_3 \quad = \quad f_4$$
$$f_{1,2} \quad = \quad f_{1,3} \quad = \quad f_{1,4}$$
$$f_{2,3} \quad = \quad f_{2,4} \quad = \quad f_{3,4}$$

From these results we are able to show (appendix B) that there are three torsional modes which can be expressed as

$$\omega_1^2 = \left(\frac{\ell + k + s}{I}\right) \tag{9}$$

$$\omega_2^2 = \left(\frac{A + \sqrt{A - 4B}}{2I}\right) \tag{10}$$

$$\omega_3^2 = \left(\frac{A - \sqrt{A - 4B}}{2I}\right) \tag{11}$$

where $A = r + \ell + 4k + 4s$

$B = 4(r\ell + rk + 4rs + 3k\ell + 12ks)$

$\ell = n^2 V_2 \qquad k = m^2 V_{1,2} \qquad s = q^2 V_{2,3} \qquad r = p^2 V_1$

These expressions are very complex, however, the important conclusion is that we expect three modes one of which is doubly degenerate.

Note that $\omega_2{}^2 + \omega_3{}^2 = \left(\dfrac{A}{I}\right)$

Let us consider some special cases

Case 1

Set $V_{1,2} = 0$ i.e. the potential energy of the axial ligand is independent of the equatorial ligands and vice versa.

We then obtain

$$\omega_1{}^2 = \left(\frac{n^2 V_2 + q^2 V_{2,3}}{I}\right) \quad \text{doubly degenerate} \qquad (12)$$

$$\omega_2{}^2 = \left(\frac{n^2 V_2 + 4q^2 V_{2,3}}{I}\right) \qquad (13)$$

$$\omega_3{}^2 = \left(\frac{p^2 V_1}{I}\right) \qquad (14)$$

The single most important point to be derived from this is that, as one would expect, one of the vibrations (ω_3) is entirely concerned with the axial ligand. There are then two modes associated with the equatorial ligands.

By substituting the expressions for "ω" into equation B7 we can obtain the angular variations associated with each mode. For ω_1 the result is $\theta_1 + \theta_2 + \theta_3 = 0$ and for ω_2, $\theta_1 = \theta_2 = \theta_3$. Therefore ω_2 is

an in-phase mode (fig. 9a) and ω_3 is some sort of doubly degenerate out-of-phase vibration (fig. 9b), though the solution is very much less
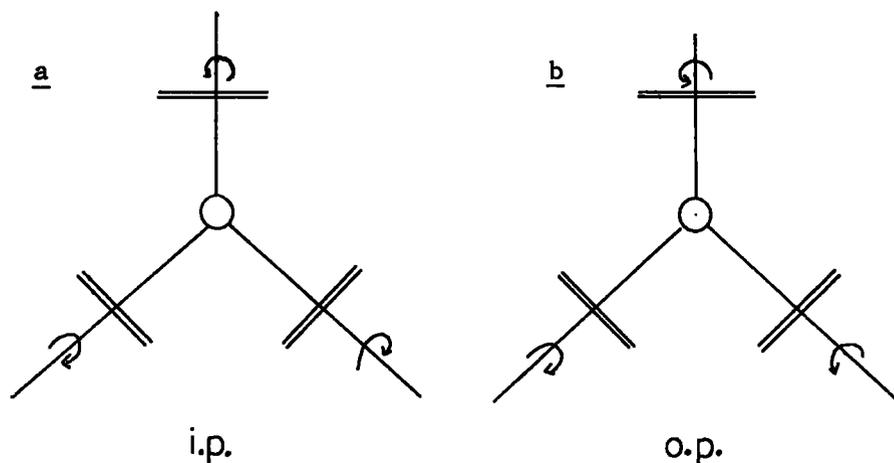
Fig. 9 In and out-of-phase torsions of $M(C_2H_4)_3$

restrictive, as far as rotation is concerned, than for the in-phase case.

Case 2

Set $V_{1,2} = 0$ and $V_1 = 0$ i.e. effectively we have the situation applicable to $M(C_2H_4)_3$ where the axial ligand is a free rotor and independent of the remainder of the molecule.

The solutions are obviously ω_1 and ω_2 above so that we expect two modes one of which is doubly degenerate.

Note that

$$\omega_1^2 - \omega_2^2 = \frac{-3q^2 V_{2,3}}{I}$$

$$4\omega_1^2 - \omega_2^2 = \frac{3n^2 V_2}{I}$$

The physical significance of ω_1 and ω_2 is shown in fig. 9.

Case 3

Set $V_{1,2} = V_{2,3} = 0$ i.e. the ligands do not interact. The solutions are then

$$\omega_1^2 = \frac{n^2 V_2}{I} \qquad \omega_2^2 = \frac{n^2 V_2}{I} \qquad \omega_3^3 = \frac{p^2 V_1}{I}$$

Again, as one would expect, we obtain just two torsional modes which correspond to the two different types of ligand present. Because they do not interact there are no in-phase or out-of-phase solutions.

The mathematical model therefore leads to solutions which are physically reasonable. One difficult point however is that, with reference to equations 12 and 13, because we would expect the out-of-phase motion to be of higher frequency than the in-phase motion the interaction term $V_{2,3}$ is negative. This type of result has been obtained previously for systems of interacting rotors.[38]

We have not used a fully symmetrical mathematical model in so far as we have included only an interaction term which involves the sum of the angles of rotation. To make the model fully symmetrical a term involving the difference of the angles would need to be included. This however leads to vast overparameterization of the physical situation and does not influence the basic conclusions e.g. the number of modes or their degeneracy.

c)   Results and Conclusions

The Beryllium Filter Detector Spectrum of $Ir(C_2H_4)_4Cl$ is shown in fig. 10 and the corrected frequencies are listed in table 3. The peak at 503 cm^{-1} corresponds to an i.r. band and by comparison with results

108.

Fig. 10 B.F.D. Spectrum of Ir(C₂H₄)₄Cl
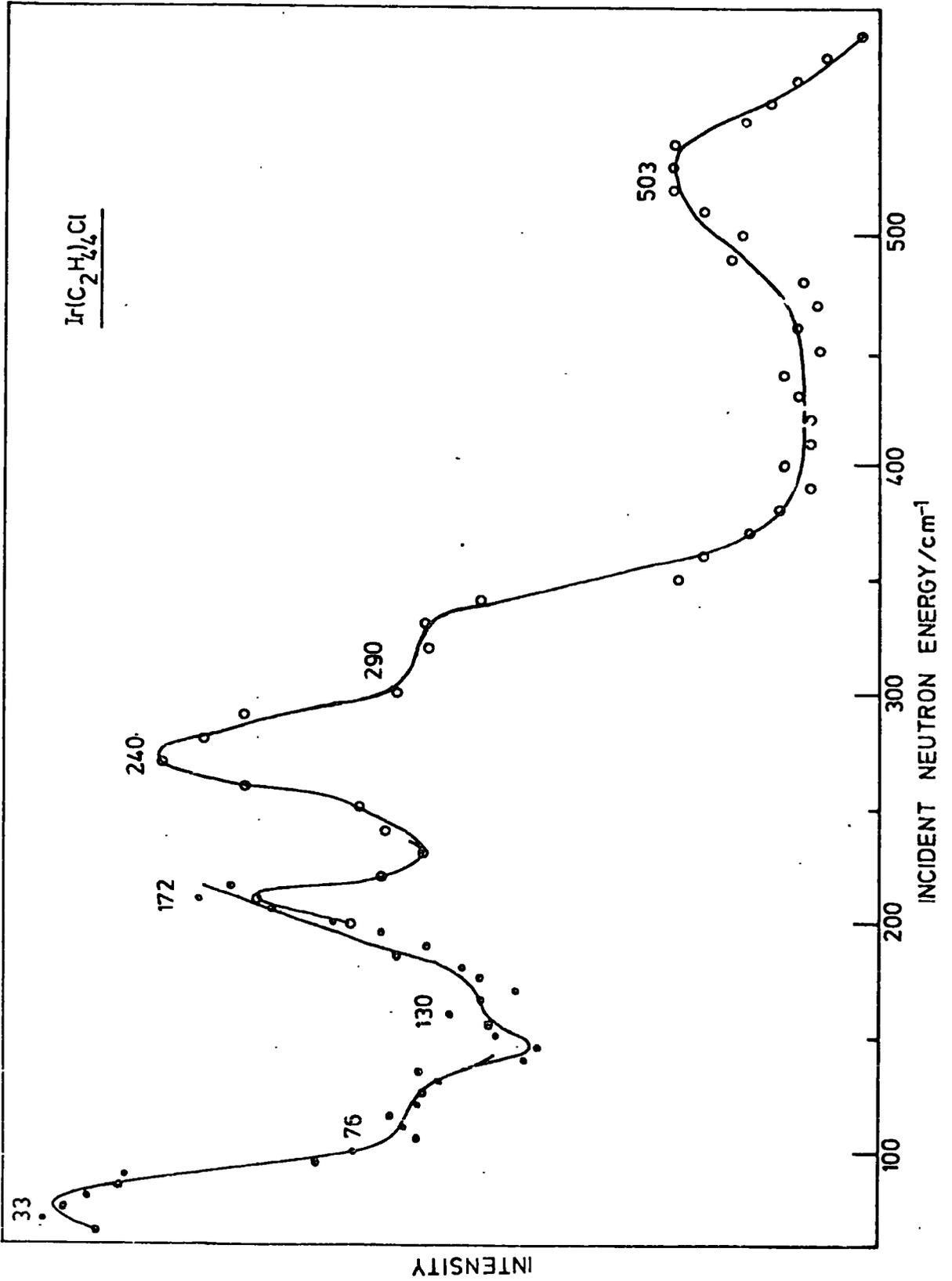
for other C_2H_4 complexes this must be an Ir - C_2H_4 stretching mode.

Table 3 I.N.S. Results of $Ir(C_2H_4)_4Cl$

FREQUENCY	ASSIGNMENT
503 $\pm$ 14	Ir - C_2H_4 stretch
290(sh) $\pm$ 14	
240 $\pm$ 14	out-of-phase torsion
172 $\pm$ 14	in-phase torsion
130 $\pm$ 14 ?	
76(sh) $\pm$ 14	
33 $\pm$ 14	torsion of axial C_2H_4 ligand

There are no bands in the i.n.s. spectrum corresponding to the i.r. bands at 372 cm^{-1} or 397 cm^{-1}. These must therefore mainly involve halogen motion.

There are three intense peaks, at 33 cm^{-1}, 172 cm^{-1} and 240 cm^{-1}. It is not possible to obtain relative intensities for all of these bands because the results were obtained using two different monochromator planes (chapter 3). The previous work on simple ethylene complexes confirmed that the torsions were always the most intense feature in the i.n.s. spectrum. In view of this it is very likely that these three modes are the ω_1, ω_2, ω_3 we have predicted. In particular the very low frequency of one of the modes is compatible with it being associated with the axial ethylene ligand and so perhaps our simplified treatment (case 1) is applicable to the molecule. The bands at 172 cm^{-1} and

240 cm^{-1} are then assigned to torsional modes of the equatorial ligands. In view of its greater intensity the band at 240 cm^{-1} must be the doubly degenerate out-of-phase vibration and this is the higher frequency mode as we would expect.

The frequencies of the in-phase and out-of-phase modes are both higher than those observed for $C_5H_5Rh(C_2H_4)_2$ and the barrier as determined from n.m.r. measurements is lower. It must be remembered, however, that the configuration of the ligands is very different and so the barrier multiplicities are probably very different too. We have shown that for a potential of the form $V = V_0/2 \ (\ 1 - \cos n\alpha)$ and using the harmonic approximation the barrier height is given by (chapter II)

$$V_o = \frac{8\pi^2 Ic}{n^2 h} \ \nu_L^2 .$$

The remaining features of the spectrum are a strong shoulder at 290 cm^{-1} and a much weaker shoulder at 76 cm^{-1} with perhaps another weak shoulder at 130 cm^{-1}. At present we do not have any sufficient information on which to assign these bands.

d) $[Rh(C_2H_4)_3(CD_3CN)_2]BF_4$
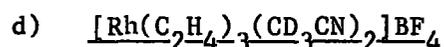
The crystal structure of $[Rh(C_2H_4)_3(CH_3CN)_2]BF_4$ has been determined and the molecular configuration is shown in fig. 7.[32] The C = C distance 1.34Å is practically identical with that found in free ethylene. This implies that there is a low degree of back donation of electrons to the ligand.

Results and Discussion

Our sample was a poor scatterer so that the background corrections were large compared to the scattering from the protons. We ran the

spectrum of $[Rh(C_2H_4)_3(CD_3CN)]BF_4$ in order to avoid complications due to the scattering from CH_3.

This work will need to be repeated and extended, however, the time-of-flight spectra are shown in fig. 12. There are peaks at 385 ± 25 cm^{-1}, 186 ± 12 cm^{-1} and 90 ± 5 cm^{-1}. The higher energy peak is almost certainly a C_2H_4 stretching mode. Corresponding modes were found in $[Rh(C_2H_4)_2Cl]_2$ at 417, 412 and 403 cm^{-1} in the infrared. The other i.n.s. modes can only be the two torsions that were predicted earlier (case 2).

The lower frequency for the stretching and torsional modes found for this complex as compared to $Ir(C_2H_4)_4Cl$ and $[Rh(C_2H_4)_2Cl]_2$ is possibly a reflection of the reduced back donation, which was indicated by the length of the $C = C$ bond.

The relative strengths of rhodium and iridium alkene bonds has been a controversial subject. Winkhaus and Singer[36] found the iridium complexes to be less stable than their rhodium analogues and they explained this by the more diffuse character of the atomic orbitals of iridium. Their conclusions conflict with the value of overlap integrals calculated by Brown and Fitzpatrick.[37]

Conclusion

Table 4 lists the contributions of the internal and external fields to the effective torsional force constants for the complexes discussed in this chapter. The values for the iridium complex were calculated with the assumption that there is no interaction between the axial and equatorial ligands (case 1). It can be seen that the values for the two diethylene complexes are very similar as expected, but that in
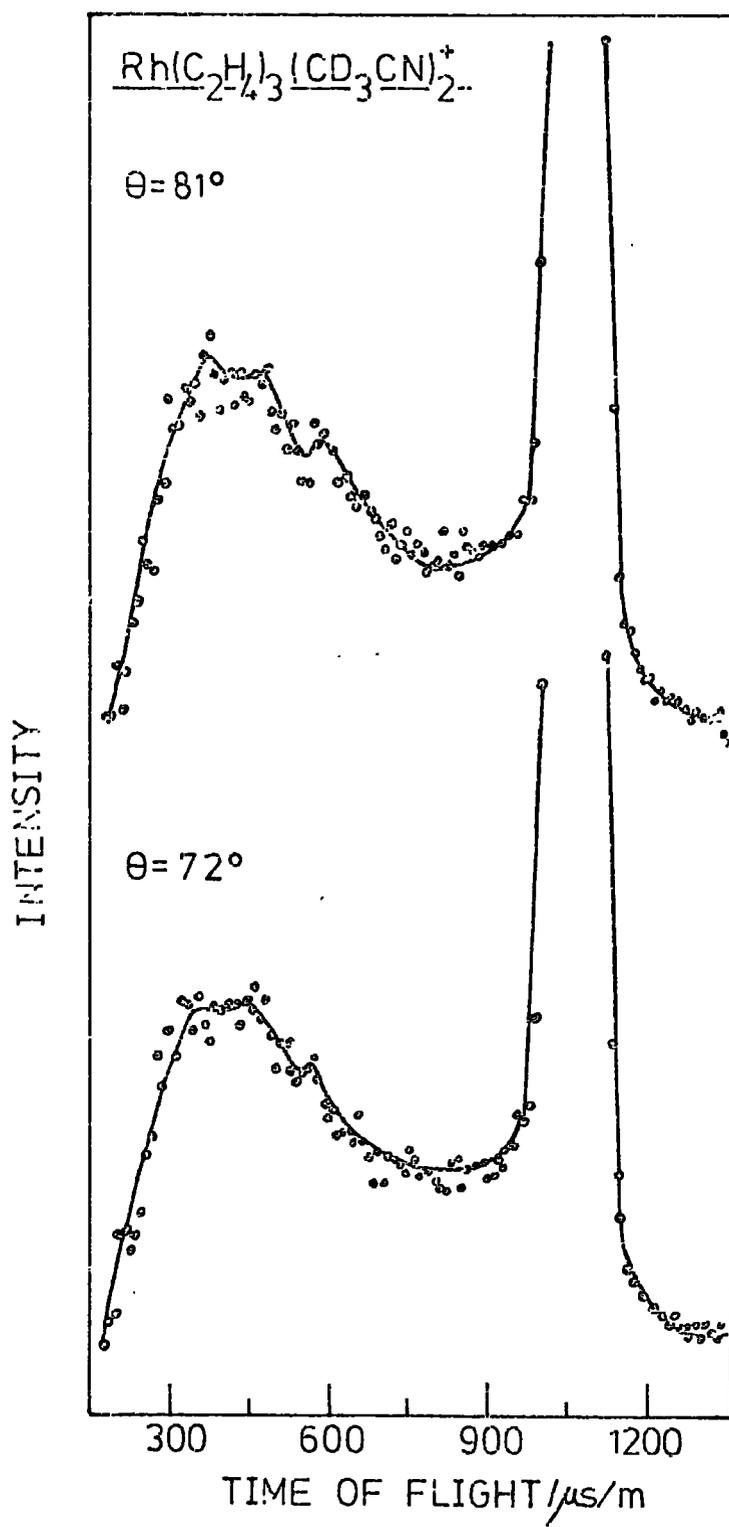
FIG.12.

Table 4 Contributions of the internal and external fields to the
effective torsional force constants [*] (kJ mol^{-1})

	n^2V_1	$q^2V_{2,3}$	m^2V_o
$[(C_2H_4)_2RhCl]_2$	373.4	-140.8	—
$(\pi-C_5H_5Rh(C_2H_4)_2)$	386.7	-156.8	—
$(\pi-C_5H_5Rh(C_2H_4)SO_2)$	—	—	250
$Ir(C_2H_4)_4Cl$			
equatorial	240.6	-24.33	—
axial	—	—	8.0
$[Rh(C_2H_4)_3(CD_3CN)]^+$	317.5	-64.56	—

modulus the values are very much lower for the complexes containing
three or four ethylene ligands. This is perhaps a reflection,
particularly in the case of $Ir(C_2H_4)_4Cl$ of the increased competition
for electron density. The low values for the iridium complex also
agrees with the low barriers found from solid state n.m.r.[35]

It is interesting to compare these results with the conclusion of
the theoretical study on $(C_2H_4)_3Ni$.[34] The authors concluded that
configuration A is favoured over B (fig. 13) by 0.74 eV. The rotational
potential energy curve shows a bump at $\theta = 30°$ due to steric hinderence.
They concluded that the preference for configuration A was due to the
relative importance of the π-bonding in the two configurations.

[*] Calculated using potential functions of the form $V = V'(1-Cosn\ \theta)$
and not $V = V'/2\ (1-Cosn\ \theta)$.

(A)
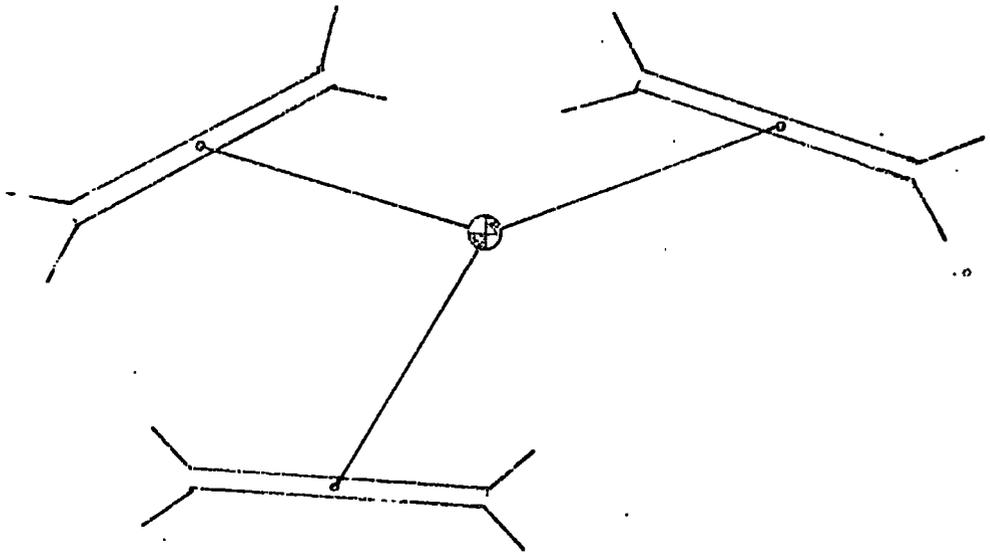
(B)
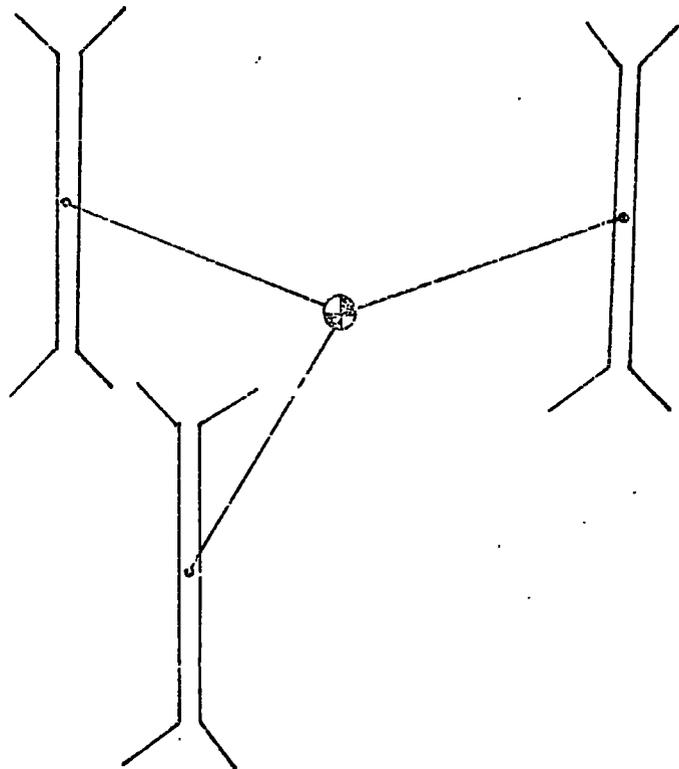
FIG. 13

APPENDIX A

$V_{total}(\alpha_1,\alpha_2)$ may be written

$$V_{total}(\alpha_1,\alpha_2) = f_1(\alpha_1) + f_2(\alpha_2) + f_{1,2}(\alpha_1 \overset{+}{_-} \alpha_2).$$

For the molecules under consideration molecular symmetry requires that

$$V_{total}(\alpha_1,\alpha_2) = V_{total}(-\alpha_1, -\alpha_2)$$

$$V_{total}(\alpha_1,\alpha_2) = V_{total}(\alpha_1+\pi,\alpha_2)$$

$$V_{total}(\alpha_1,\alpha_2) = V_{total}(\alpha_1,\alpha_2+\pi)$$

$$V_{total}(\alpha_1,\alpha_2) = V_{total}(\alpha_1+\pi,\alpha_2+\pi)$$

$$f_1(\alpha_1) = f_2(\alpha_1)$$

$$f_1(\alpha_1) = f_1(-\alpha_1)$$

$$f_{1,2}(\alpha_1 \overset{+}{_-} \alpha_2) = f_{1,2}(-\{\alpha_1 \overset{+}{_-} \alpha_2\})$$

$$f_1(\alpha) = f_1(\pi+\alpha).$$

We may therefore express f_1 and $f_{1,2}$ as Fourier series

$$f_1(\alpha_1) = f_2(\alpha_1) = \sum_{n=1}^{\infty} \tfrac{1}{2}\bar{V}_{2n}(1-\cos 2n\alpha_1), \qquad (A1)$$

$$f_{1,2}(\alpha_1 \overset{+}{_-} \alpha_2) = \sum_{n=1}^{\infty} \tfrac{1}{2}V'_{4n}(1-\cos 2n(\alpha_1 \overset{+}{_-} \alpha_2)), \qquad (A2)$$

where the factor 2 in the numerator of eqn (A2) is derived using $V_{total}(\tfrac{1}{2}\pi, \tfrac{1}{2}\pi) = V_{total}(\tfrac{1}{2}\pi,-\tfrac{1}{2}\pi)$. Considering only the case where $f_{1,2}$ is expressed as the sum of α_1 and α_2 and applying the simple harmonic oscillator approximation we obtain

$$V_{total}(\alpha_1,\alpha_2) = \sum_{n=1}^{\infty} \{(n^2\bar{V}_{2n}+n^2V'_{4n})\alpha_1^2+(n^2\bar{V}_{2n}+n^2V'_{4n})\alpha_2^2+2n^2V'_{4n}\alpha_1\alpha_2\}.$$

Writing

$$k = 2 \sum_{n=1}^{\infty} (n^2 \bar{V}_{2n} + n^2 \bar{V}'_{4n}),$$

$$k_{1,2} = \sum_{n=1}^{\infty} 2n^2 V'_{4n},$$

then the potential energy is

$$V_{total}(\alpha_1, \alpha_2) = \tfrac{1}{2} k \alpha_1^2 + \tfrac{1}{2} k \alpha_2^2 + k_{1,2} \alpha_1 \alpha_2.$$

Writing the kinetic energy as $\tfrac{1}{2} I_r \dot{\alpha}_1^2 + \tfrac{1}{2} I_r \dot{\alpha}_2^2$, where I_r is the reduced moment of inertia of a single ethylene ligand, and solving Lagrange's equations for the system we obtain

$$\omega^2 = \left(\frac{k \overset{+}{-} k_{1,2}}{I_r} \right).$$

Hence

$$\omega_1 = \left(\frac{k + k_{1,2}}{I_r} \right)^{\frac{1}{2}} = \left(\frac{\sum_{n=1}^{\infty} (2n^2 \bar{V}_{2n} + 4n^2 V'_{4n})}{I_r} \right)^{\frac{1}{2}},$$

$$\omega_2 = \left(\frac{k - k_{1,2}}{I_r} \right)^{\frac{1}{2}} = \left(\frac{\sum_{n=1}^{\infty} 2n^2 \bar{V}_{2n}}{I_r} \right)^{\frac{1}{2}},$$

$$\omega_1^2 - \omega_2^2 = \left(\frac{\sum_{n=1}^{\infty} 4n^2 V'_{4n}}{I_r} \right).$$

The solution ω_1 corresponds to motion where $\alpha_1 = \alpha_2$, and ω_2 to motion where $\alpha_1 = -\alpha_2$. We expect the in-phase motion ($\alpha_1 = \alpha_2$) to have the lower frequency.

Thus,

$$V_{total}(\alpha,\alpha) = \sum_{n=1}^{\infty} \bar{V}_{2n}(1 - \cos 2n\alpha) + \sum_{n=1}^{\infty} \tfrac{1}{2}V'_{4n}(1 - \cos 4n\alpha) \text{ for in-phase}$$

motion.

$$V_{total}(\alpha, -\alpha) = \sum_{n=1}^{\infty} \bar{V}_{2n}(1 - \cos 2n\alpha) \text{ for out-of-phase motion.}$$

$V_{total}(\alpha_1, \alpha_2)$ can be rewritten as the sum of the torsional interaction of the ethylene groups with the rest of the molecule $V_T(\alpha)$ and the "non-bonding" interactions between the ethylene groups $V(\alpha_1, \alpha_2)$.

Hence

$$V_{total}(\alpha_1, \alpha_2) = V(\alpha_1, \alpha_2) + V_T(\alpha_1) + V_T(\alpha_2)$$

where

$$V_T(\alpha_i) = \sum_{n=1}^{\infty} \tfrac{1}{2}V^T_{2n}(1 - \cos 2n\alpha_i), \qquad i = 1 \text{ or } 2,$$

$$V(\alpha_1, \alpha_2) = \sum_{n=1}^{\infty} \tfrac{1}{2}V_{2n}(1 - \cos 2n\alpha_1) + \sum_{n=1}^{\infty} \tfrac{1}{2}V_{2n}(1 - \cos 2\alpha_2) +$$

$$\sum_{n=1}^{\infty} \tfrac{1}{2}V'_{4n}(1 - \cos 2n(\alpha_1 + \alpha_2)),$$

and

$$V_{2n} = \bar{V}_{2n} - V^T_{2n}.$$

Thus,

$$V(\alpha,\alpha) = \sum_{n=1}^{\infty} V_{2n}(1 - \cos 2n\alpha) + \sum_{n=1}^{\infty} \tfrac{1}{2}V'_{4n}(1 - \cos 4n\alpha)$$

and

$$V(\alpha, -\alpha) = \sum_{n=1}^{\infty} V_{2n}(1 - \cos 2n\alpha).$$

APPENDIX B

We define

f_i :   the potential function which represents the variation in the
potential energy of ligand "i" on rotation, but which does not
include potential energy variations as a result of interaction
with other C_2H_4 ligands.

$f_{i,j}$ the potential function representing the potential energy
variations which result solely from the interaction between
ligands i and j.

From n.m.r. data it is known that the axial ligand is different from
the equatorial ligands, therefore we may write

$$f_2 = f_3 = f_4$$

$$f_{1,2} = f_{1,3} = f_{1,4}$$

$$f_{2,3} = f_{2,4} = f_{3,4}$$

We will write these potential functions in the form

$$f_i = V_i(1 - Cos\ n\ \theta_i)$$

and $$f_{i,j} = V_{i,j}(1 - Cos\ p(\theta_i + \theta_j))$$

where θ_k is the clockwise rotational angular displacement of the k th
ligand about the axis joining its mid point to the metal atom (see
fig. 8). The coefficient of θ i.e. n, p etc. is the periodicity of
the barrier in question (chapter II). Therefore we write

$$f_1 = V_1(1 - \cos p \; \theta_1)$$

$$f_i = V_i(1 - \cos n \; \theta_i) \qquad i = 2,3,4$$

$$f_{1,i} = V_{1,i}(1 - \cos m(\theta_1 + \theta_i)) \qquad i = 2,3,4$$

$$f_{i,j} = V_{i,j}(1 - \cos q(\theta_i + \theta_j)) \qquad i,j = 2,3; \; 3,4; \; 2,4$$

The periodicity (p) and barrier height (V_1) are different for ligand 1 because it is different from the equatorial ligands. The equatorial ligands are equivalent so a single periodicity and barrier height are required i.e. $V_2 = V_3 = V_4$. Similarily the interaction between any pair of equatorial ligands is the same as the interaction between any other pair thus $V_{2,3} = V_{3,4} = V_{2,4}$. By a similar argument we also get $V_{1,2} = V_{1,3} = V_{1,4}$.

The total potential energy is therefore

$$V_{TOTAL} = f_1(\theta_1) + f_2(\theta_2) + f_3(\theta_3) + f_4(\theta_4) + f_{1,2}(\theta_1 + \theta_2)$$

$$+ f_{1,3}(\theta_1 + \theta_3) + f_{1,4}(\theta_1 + \theta_4) + f_{2,3}(\theta_2 + \theta_3)$$

$$+ f_{3,4}(\theta_3 + \theta_4) + f_{2,4}(\theta_2 + \theta_4)$$

Using the equations above we obtain

$$V_{TOTAL} = V_2(3 - \cos n \; \theta_2 - \cos n \; \theta_3 - \cos n \; \theta_4) + V_1(1 - \cos p \; \theta_1)$$

$$+ V_{1,2}(3 - \cos m(\theta_1 + \theta_3) - \cos m(\theta_1 + \theta_2) - \cos m(\theta_1 + \theta_4))$$

$$+ V_{2,3}(3 - \cos q(\theta_2 + \theta_3) - \cos q(\theta_3 + \theta_4) - \cos q(\theta_4 + \theta_2))$$

Making the simple harmonic oscillator approximation

i.e. $\cos \theta = 1 - \dfrac{\theta^2}{2}$ we obtain

$$V_{TOTAL} = \frac{V_2}{2} (n^2 \theta_2^2 + n^2 \theta_3^2 + n^2 \theta_4^2) + V_1 \frac{p^2 \theta_1^2}{2}$$

$$+ V_{1,2} \left\{ m^2 \frac{(\theta_1 + \theta_2)^2}{2} + m^2 \frac{(\theta_1 + \theta_3)^2}{2} + m^2 \frac{(\theta_1 + \theta_4)^2}{2} \right\}$$

$$+ V_{2,3} \left\{ q^2 \frac{(\theta_2 + \theta_3)^2}{2} + q^2 \frac{(\theta_3 + \theta_4)^2}{2} + q^2 \frac{(\theta_2 + \theta_4)^2}{2} \right\}$$

Thus

$$V_{TOTAL} = \frac{\theta_1^2}{2} (p^2 V_1 + 3m^2 V_{1,2}) + \frac{\theta_2^2}{2} (n^2 V_2 + m^2 V_{1,2} + 2q^2 V_{2,3})$$

$$+ \frac{\theta_3^2}{2} (n^2 V_2 + m^2 V_{1,2} + 2q^2 V_{2,3}) + \frac{\theta_4^2}{2} (n^2 V_2 + m^2 V_{1,2} + 2q^2 V_{2,3})$$

$$+ m^2 V_{1,2} (\theta_1 \theta_3 + \theta_1 \theta_4 + \theta_1 \theta_2) + q^2 V_{2,3} (\theta_2 \theta_3 + \theta_2 \theta_4 + \theta_3 \theta_4) \quad \text{(B1)}$$

The total kinetic energy is T where

$$T = \tfrac{1}{2} I \dot{\theta}_1^2 + \tfrac{1}{2} I \dot{\theta}_2^2 + \tfrac{1}{2} I \dot{\theta}_3^2 + \tfrac{1}{2} I \dot{\theta}_4^2 \quad \text{(B2)}$$

and I is the reduced moment of inertia of a single ethylene ligand.

We make the following substitutions

$$n^2 V_2 = \ell \qquad m^2 V_{1,2} = k \qquad q^2 V_{2,3} = s \qquad p^2 V_1 = r$$

Thus

$$V_{TOTAL} = \frac{\theta_1^2}{2} (r+3k) + \frac{\theta_2^2}{2} (\ell+k+2s) + \frac{\theta_3^2}{2} (\ell+k+2s) + \frac{\theta_4^2}{2} (\ell+k+2s)$$

$$+ k(\theta_1 \theta_3 + \theta_1 \theta_4 + \theta_1 \theta_2) + s(\theta_2 \theta_3 + \theta_2 \theta_4 + \theta_3 \theta_4)$$

Applying Lagranges' Equations $\left(\frac{d}{dt} \frac{\partial T}{\partial \dot{q}_u} + \frac{\partial V}{\partial q_u} = 0 \right)$ for equations (B1) and (B2) we obtain

$$I\ddot{\theta}_1 + (r + 3k)\theta_1 + k(\theta_2 + \theta_3 + \theta_4) = 0$$

$$I\ddot{\theta}_2 + (\ell + k + 2s)\theta_2 + k\theta_1 + s(\theta_3 + \theta_4) = 0$$

$$I\ddot{\theta}_3 + (\ell + k + 2s)\theta_3 + k\theta_1 + s(\theta_2 + \theta_4) = 0$$

$$I\ddot{\theta}_4 + (\ell + k + 2s)\theta_4 + k\theta_1 + s(\theta_2 + \theta_3) = 0$$

Substitute $\theta_i = A_i \exp(i\omega t)$

$$-IA_1\omega^2 + (r + 3k)A_1 + k(A_2 + A_3 + A_4) = 0 \qquad (B3)$$

$$-IA_2\omega^2 + (\ell + k + 2s)A_2 + kA_1 + s(A_3 + A_4) = 0 \qquad (B4)$$

$$-IA_3\omega^2 + (\ell + k + 2s)A_3 + kA_1 + s(A_2 + A_4) = 0 \qquad (B5)$$

$$-IA_4\omega^2 + (\ell + k + 2s)A_4 + kA_1 + s(A_2 + A_3) = 0 \qquad (B6)$$

For a non-trivial solution we require

$$\begin{vmatrix} -I\omega^2 + r + 3k & k & k & k \\ k & -I\omega^2 + \ell + k + 2s & s & s \\ k & s & -I\omega^2 + \ell + k + 2s & s \\ k & s & s & -I\omega^2 + \ell + k + 2s \end{vmatrix} = 0$$

Substituting with $x = -I\omega^2 + r$ and $y = -I\omega^2 + \ell$ and expanding by cofactors we obtain

$$(y + k + s)^2 \{(x + 3k)(y + k + 4s) - 3k^2\} = 0$$

Thus either

$$y + k + s = 0$$

i.e. $-I\omega^2 + \ell + k + s = 0$

$$\omega^2 = \frac{\ell + k + s}{I}$$

or $(x + 3k)(y + k + 4s) - 3k^2 = 0$

This yields

$$\omega^2 = \frac{(r + \ell + 4k + 4s) \pm \sqrt{(r + \ell + 4k + 4s) - 4(r\ell + rk + 4rs + 3k\ell + 12ks)}}{2\,I}$$

substituting A = r + ℓ + 4k + 4s

B = 4(r ℓ + rk + 4rs + 3kl + 12ks)

we obtain

$$\omega^2 = \frac{A \pm \sqrt{A - 4B}}{I}$$

The three solutions are therefore

$$\omega_1^2 = \frac{\ell + k + s}{I} \qquad \text{doubly degenerate}$$

$$\omega_2^2 = \frac{A + \sqrt{A - 4B}}{2I}$$

$$\omega_3^2 = \frac{A - \sqrt{A - 4B}}{2I}$$

References

1. B.F.G. Johnson and J.A. Segal, J.C.S. Chem. Comm., 1312, (1972).

2. C.E. Holloway, G. Hulley, B.F.G. Johnson and J. Lewis, J. Chem. Soc.
    (A), 53, (1969).

3. C.E. Holloway, G. Hulley, B.F.G. Johnson and J. Lewis, J. Chem. Soc.
    (A), 1653, (1970).

4. J. Ashley-Smith, Z. Douek, B.F.G. Johnson and J. Lewis, J.C.S.
    Dalton, 16, 1776, (1972).

5. J. Ashley-Smith, Z. Douek, B.F.G. Johnson and J. Lewis, J.C.S.
    Dalton, 2, 128, (1974).

6. H. Basch, J. Chem. Phys., 56, 441, (1972).

7. R.E. Ghosh, T.C. Waddington and C.J. Wright, J.C.S. Faraday II,
    69, 275, (1973).

8. K.S. Wheelock, J.H. Nelson, L.C. Cusachs and H.B. Johnson, J. Amer.
    Chem. Soc., 92, 5110, (1970).

9. R. Cramer, I.B. Kleine and J.D. Roberts, J. Amer. Chem. Soc., 91,
    2519, (1969).

10. R. Cramer, J. Amer. Chem. Soc., 89, 5377, (1967).

11. A.L. Onderlinden and A. van der Ent, Inorg. Chim. Acta., 6(3), 420,
    (1972).

12. F. Maspero, E. Perrotti and F. Simonetti, J. Organometal. Chem.,
    38, C43, (1972).

13. L.N. Muloy, E.G. Rochow, E.O. Stejskal and N.E. Weliky, J. Inorg.
    Nuclear Chem., 16, 23, (1960).

14. F. Rocquet, L. Berreby and J.P. Marsault, Spectrochim. Acta., 29A,
    1101, (1973).

15. A. Haaland and J.E. Nilsson, Acta. Chem. Scand., 22, 2653, (1968).

16. M. Rosenblum and R.B. Woodward, J. Amer. Chem. Soc., 80, 5443,
    (1958).

17. R. Cramer, J. Amer. Chem. Soc., 89, 5377, (1967).

18. W.E. Oberhansli and L.F. Dahl, J. Organometal. Chem., 3, 43, (1965).

19. R.E. Ghosh and T.C. Waddington, unpublished results.

20. J.S. Bodenheimer and W. Low, Spectrochim. Acta., 29A, 1733, (1973).

21. M.J. Crogan and K. Nakamoto, J. Amer. Chem. Soc., 90, 918, (1968).

22. M. Adams and P.J. Chandler, J. Chem. Soc. A., 588, (1969).

23. J. Hiraishi, Spectrochim. Acta., 25A, 749, (1969).

24. D.E. Williams, J. Chem. Phys., 47, 4680, (1967).

25. L.J. Guggenberger and R. Cramer, J. Amer. Chem. Soc., 94, 3779, (1972).

26. R. Cramer and J.J. Mrowca, Inorg. Chim. Acta., 5(4), 528, (1971).

27. D. Kost, E. Carlson and M. Raban, Chem. Comm., 656, (1971).

28. K. Fischer, K. Jonas and G. Wilbe, Angew. Chem. Int. Ed., 12, 565, (1973).

29. P. Timms, Personal Communication.

30. M. Green, J.A.K. Howard, J.L. Spencer and F.G.A. Stone, J.C.S. Chem. Comm., 3, (1975).

31. M. Green, J.A.K. Howard, J.L. Spencer and F.G.A. Stone, J.C.S. Chem. Comm., 449, (1975).

32. G. Del Piero, G. Perego and M. Cesari, Cryst. Struct. Comm., 3, 15, (1974).

33. R.A. Love, T.F. Koetzle, G.J.B. Williams, L.C. Andrews and R. Bau, Inorg. Chem., 14, 2653, (1975).

34. N. Rösch and R. Hoffmann, Inorg. Chem., 13(11), 2656, (1974).

35. K. van Putte and A. van der Ent., Inorg. Chim. Acta., 7, 497, (1973).

36. G. Winkhaus and H. Singer, Chem. Ber., 99, 3610, (1966).

37. D.A. Brown and N.J. Fitzpatrick, J. Chem. Soc.(A), 315, (1967).

38. C.I. Ratcliffe, Ph.D. Thesis, University of Durham, 1975.

Chapter V: Ethylene Adsorbed on Type-X Zeolites

Section I

Zeolites, a General Introduction

Zeolites are one member of the general class of aluminosilicates. A zeolite has been defined[1] as "an aluminosilicate with a framework structure enclosing cavities occupied by large ions and water molecules, both of which have considerable freedom of movement, permitting ion exchange and reversible dehydration". They are very important industrial materials with applications to e.g. separation of paraffin hydrocarbons, cryopumping, removal of atmospheric pollutants and as cracking catalysts. There are several excellent texts dedicated to zeolites and their properties and uses.[2,3,4]

Structurally zeolites are based on infinite three-dimensional networks of SiO_4 and AlO_4 tetrahedra which are linked by sharing all of the oxygens. Their general formula is $M_{x/n} (AlO_2)_x (SiO_2)_y \omega H_2O$ where y/x is in the range 1 to 5 and "n" is the cation valency.

Zeolites are unusual in that each zeolite has a specific and uniform pore size, which is uniquely determined by its crystal structure. Other commercial adsorbents e.g. activated carbons, silica gel etc. do not have an ordered structure and hence the pores are non-uniform. Pore size is a function of many variables e.g. temperature, cation and type of zeolite.

Although over 130 types of zeolites are known only a few are of practical importance. For many of them total dehydration permanently alters the framework so that partial or total collapse occurs. In order to be used successfully, for instance as molecular sieves, their structure must remain intact on dehydration. Zeolite minerals can

vary considerably in chemical composition and so the synthetic zeolites, which have a greater degree of uniformity, are best suited for research and industrial applications. For our research work we chose an X type zeolite for reasons which will become apparent later. Na - 13X is a synthetic zeolite with unit cell contents Na_{86} $(AlO_2)_{86}$ $(SiO_2)_{106}$ xH_2O and which has the faujasite structure.[2,5,6,7,8] Members of this group have cubic symmetry and a framework based on combinations of truncated octahedra (β cages) and hexagonal prisms. Each of these octahedra (fig. 1a) is composed of 24 (Al, Si) ions, which are the vertices, interconnected with 36 oxygen atoms. Each truncated octahedron has 6 square faces and 8 hexagonal faces. Fig. 1b shows the tetrahedral arrangement of the octahedra, which are linked by their hexagonal faces through hexagonal prisms. These prisms consist of 12 (Si, Al) tetrahedra. This results in a series of wide cavities (supercages) each of which opens by common windows (8 → 9A diameter) into four, identical, tetrahedrally arranged cavities (fig. 2). This very stable structure in which the supercages have a diamond-like arrangement with respect to each other, contains the largest void space of any known zeolite (50% of the dehydrated crystal).

Cation Location

The substitution of an Al^{3+} ion for Si^{4+} necessitates the introduction of a cation in order to restore electrical neutrality. The maximum observed substitution corresponds to an Al/Si ratio of 1 : 1. The distribution of cations within a zeolite framework is a function of many parameters e.g. water content, Al/Si ratio and type of cation. Several different cation locations have been discovered for each zeolite framework[2] and in particular for NaX there are four sites.
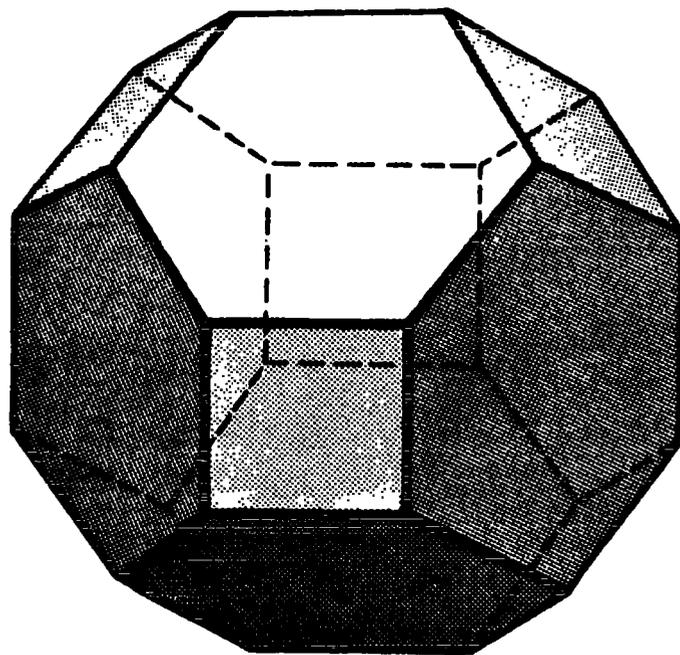
Fig. 1 a) Truncated Octahedron
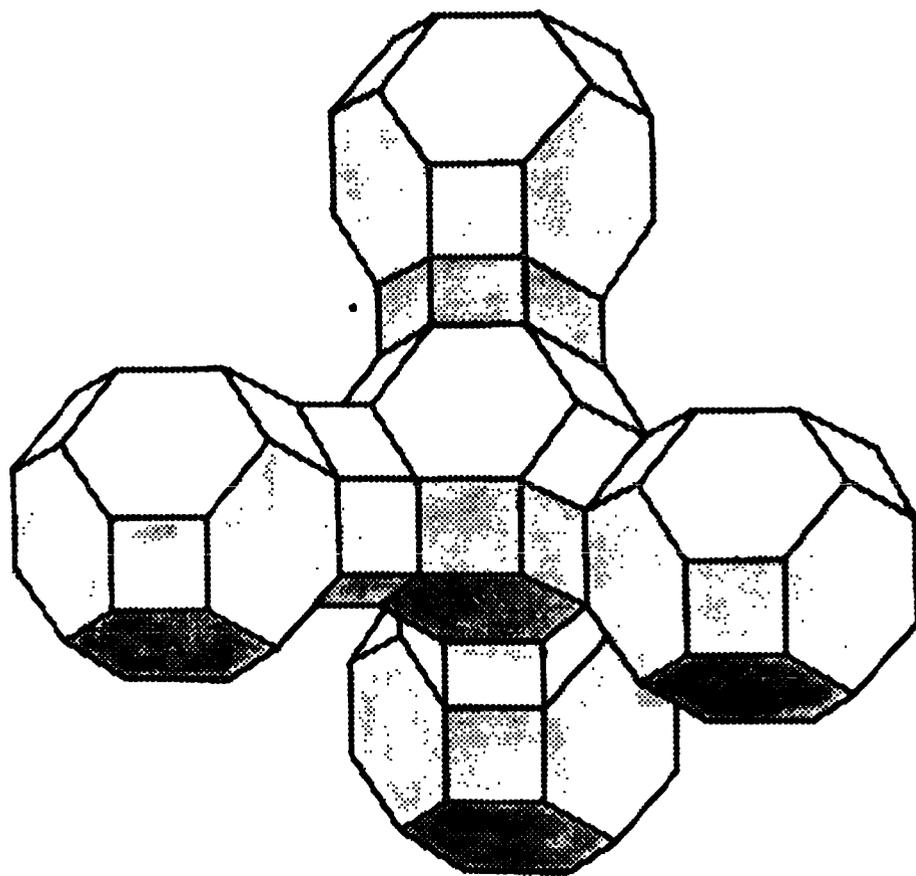
b) Tetrahedral arrangement of octahedra
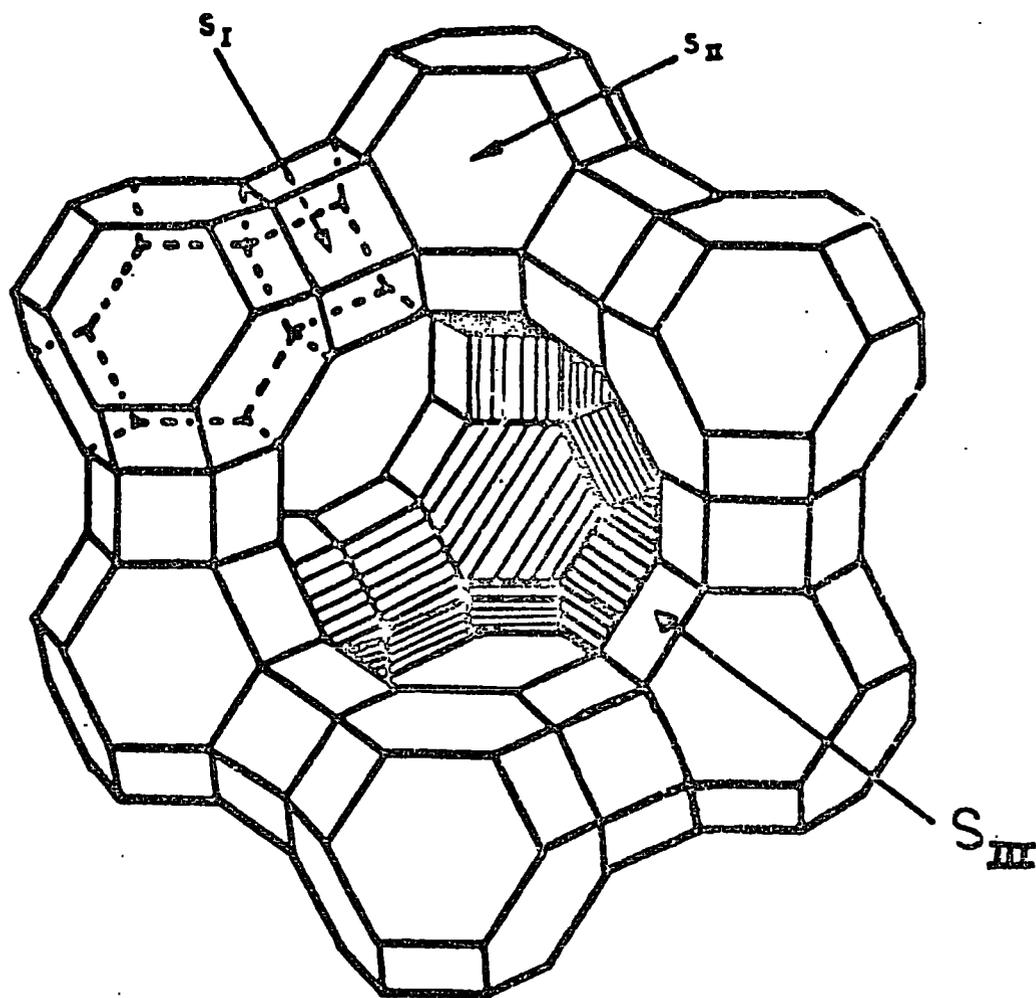
Fig. 2   Cation Positions in Faujasites

<u>Type I</u>   in the centre of a hexagonal prism.

<u>Type I'</u>   inside the sodalite unit.

<u>Type II</u>   in the six-membered rings, the unjoined hexagonal faces of the octahedra.

<u>Type III</u>   on the walls of the channels:- on the square faces of the octahedra.

Three of these are shown in fig. 2. The site occupancies for an X zeolite of composition Na_{80} [$(AlO_2)_{80}$ $(SiO_2)_{112}$] are given in table 1.

<u>Table 1   Cation Distributions in X zeolites</u>

Type of Site	Na - X		K - X
	Site occupancy	Available Sites	
I	4	16	9.2
I'	32	32	13.6
II	32	32	25.6
III	4	48	38.2

The crystal structure of dehydrated Ag-13X has not been determined. It has, however, been found that larger ions e.g. K^+ and Cs^+ occupy more sites III than do the cations in the sodium form.[8] It is therefore likely that for Ag-13X the number of site II sites occupied by cations is greater than for Na-13X. This is in agreement with the gravimetric and volumetric studies of Yates[9] who found two adsorbtion sites in

approximately equal numbers. Table 1 lists the cation distribution in dehydrated $K_{86.5}Al_{86.5}Si_{105.5}O_{384}$.[8]

Dehydration of type X Zeolites

Outgassing at 475°C in high vacuum produces no gross change in the crystal structure of Na-13X. The differential thermal analysis of zeolite Na-13X indicates a continuous loss of water over a broad range from just above room temperature to 350°C. Peaks at 772°C and 933°C indicate decomposition.[10] We obtained X-ray powder photographs of Ag-13X after

a) being dried, in air, overnight at 40°C

b) dehydration at 450°C.

The results showed that no collapse of the framework had taken place.

Ion Exchange

Ag^+ replaces Na^+ very easily and there is 100% exchange under appropriate conditions.[11] Ions of type I are, in general, the most difficult to exchange and in fact larger ions e.g. Rb^+ or Cs^+ cannot replace them because they are too large to pass through the small openings in the hexagonal prism.

Adsorption of Gases

The selectivity of zeolites is well known but, for example, an A-type zeolite at -196°C will freely adsorb O_2 but N_2 is excluded. The kinetic diameter of N_2 is only .2Å greater than that of O_2, but this is sufficient to prevent it entering the pores. The kinetic diameter σ is derived from a Leonard-Jones Potential Function

$$\phi(r) = 4\epsilon \left[\left(\frac{\sigma}{r}\right)^{12} - \left(\frac{\sigma}{r}\right)^{6} \right]$$

and it is used rather than the equilibrium diameter r_{min}. In fact r_{min} = $2^{1/6}\sigma$. Figure 3 shows that σ corresponds to the distance for which the potential is zero and r_{min} to the distance for which the energy of attraction is a maximum.
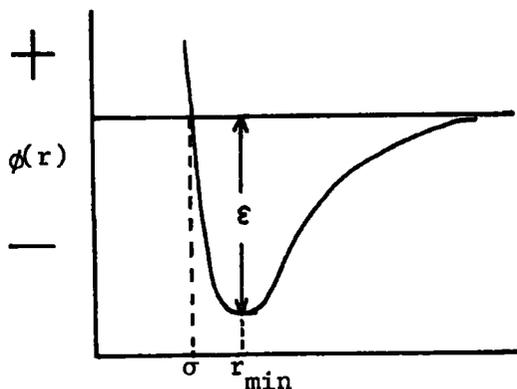
Fig. 3 Relationship between σ and r_{min}

The type III cations are thought to protrude further into the super-cage than ions of type II. Further-more as a result of their being bonded to a smaller oxygen ring it is expected that ions of type III will have their orbitals less fully occupied with bonding to the lattice than type II. It therefore appears that the adsorbed molecules will probably be more strongly bonded to the ions on the cage walls than to those on the windows.

Section II

Why Use Neutrons?

Raman studies of zeolites and particularly of zeolites containing adsorbed species have proven either very difficult or impossible. Zeolites give rise to very weak Raman scattering, but the fluorescence background is very high.[13] Successful spectra have been obtained only in a few cases.[12,13,14] The presence of even small amounts of transition metal ions usually leads to unacceptable levels of fluorescence.[12,13] Therefore, successful investigations were almost entirely limited to alkali or alkaline earth ion exchanged forms of the various zeolites.

Many near-infrared studies of zeolites and zeolites containing adsorbed species, have been published,[15] however, far-infrared studies have proven far more difficult.[16] The difficulties associated with obtaining optical spectra of zeolites e.g. fluorescence, absorption and the need to use very thin samples, do not arise when measuring neutron spectra. The zeolite background is relatively transparent to neutrons so that neutron scattering spectroscopy is particularly sensitive to the vibrations of the (hydrogeneous) adsorbed species.

Furthermore, as explained earlier, inelastic neutron scattering spectroscopy (i.n.s.) is free from optical selection rules so that from a combination of successful I.R., Raman and neutron studies it should be possible to observe all of the normal modes and to obtain complete vibrational assignments for the adsorbed molecules.

Section III

Relevant Previous Investigations

a) Crystal Structure Determinations

During the course of this work several crystal structures of zeolites containing adsorbed C_2H_4 or C_2H_2 have been published.[17,18,19] Zeolite A was used in every case, however, a variety of ion-exchanged forms have been investigated i.e. Co(11), Mo, Na. Three very important points arise from these investigations:

1. In all cases the data is consistent with the adsorbed gases being symmetrically bonded with the carbon atoms equi-distant from the metal ion.

2. The metal to carbon distances are longer than in comparable model compounds and so it appears that the interaction with the metal is relatively weak.

3. The adsorbed molecule makes no significant approach to the framework oxygens etc. For instance for the Co - C_2H_4 system in zeolite A the minimum C - O distance is 3.5Å. Although the hydrogen atoms were not located, they should lie approximately in the plane of the carbon atoms, which is parallel to the plane of the oxygen atoms. The minimum separation H - O cannot be less than 3.1Å so no C - H --- O hydrogen bonding occurs.

It seems reasonable to assume that similar considerations will apply to the structures of C_2H_4 and C_2H_2 adsorbed on Ag - 13X and Na - 13X. This is in agreement with infra-red studies.

b) Infrared Studies

Infrared spectroscopic studies (1300 → 3300 cm^{-1}) of ethylene

adsorbed by several ion-exchanged 13X zeolites, have been made by

Yates et al.[20] They found that for Na, Ca, Li, K and Ba exchanged

zeolites the ethylene was weakly held e.g. it could be removed by

evacuation at room temperature. This was not so for Ag or Cd exchanged

13X zeolites for which heating to > 200°C was necessary to remove all

of the adsorbed gas.

The absence of dissociative chemisorption was confirmed by the

presence of the C = C vibrational band in all of the spectra.

It was also possible to establish that, except for C_2H_4 on Ag13X,

the C_2H_4 was freely rotating about the C_2 axis. This was possible

because it was observed that narrow bands (∼4cm^{-1}) were obtained for

those vibrations for which the dipole moment change is perpendicular to

the surface and broad bonds (∼40 cm^{-1}) for vibrations associated with

dipole moment changes parallel to the surface. Free rotation about the

C_2 axis would modulate vibrations parallel to the surface and hence

produce broad bands. For C_2H_4 on Ag13X the v_{12} band is narrow hence

they postulate that the free rotation has become a torsion in this case.

If the rotation of adsorbed C_2H_4 about the C_2 axis is perfectly

free then some rotational fine structure may have been expected. None

was observed. Comparable results have been reported for CH_4 adsorbed

on silica.[21] The shape of the v_3 band for the adsorbed CH_4 is

compatable either with no free rotation taking place or with free

rotation about a single axis. The authors point out that interruption

of free rotation by vibration relative to the surface would broaden

the individual rotational bands, leading to non-resolution of the

discrete fine structure and the production of smooth wings as

observed. It is possible that fine structure was not observed in the

Ag13X + C_2H_4 case for the same reason.

A broadened band (A) as opposed to one with distinct P and R

branches (B) is further evidence that the adsorbed C_2H_4 has only one

—— Perpendicular Component

------ Parallel Component

$$cm^{-1} \rightarrow$$

A

$$cm^{-1} \rightarrow$$

B
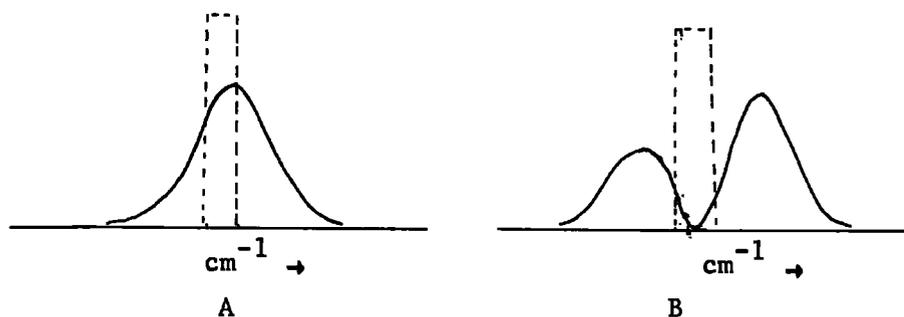
degree of rotational freedom. The relative intensities of the individual

lines are[22]

a)   for a rotor with one degree of freedom; for a perpendicular band

$$\text{Intensity} \; \alpha \; C \; \exp \left(\frac{-\bar{K}^2 h^2}{8\pi^2 IKT} \right)$$

$\bar{K} = 0, 1, 2, \ldots$

$C = 1$ if $K = 0$

$C = 2$ if $K > 0$

b)   for a rotor with three degrees of freedom

$$\text{Intensity} \; \alpha \; (2J + 1)^2 \; \exp \left(\frac{-J(J+1)h^2}{8\pi^2 IKT} \right) \qquad J = 0, 1, 2 \ldots$$

In the first case there is no maximum and the function decreases

monotonically. In the second case we have, as J increases, an

increasing pre-exponential factor but a decreasing value of the

exponential. This leads to a function with a definite maximum and

produces the characteristic P and R branches.

Finally from a study of the v_s(CH def.) band as a function of coverage it was also established that there are two different adsorbtion sites for C_2H_4 on Ag13X. This was later confirmed by gravimetric and volumetric studies.[9]

The infrared results quoted above, concerning hindered rotation of C_2H_4 on Ag13X, are relevant only to the low coverage case. It was not possible to make similar measurements for the high coverage situation because the bands were incompletely resolved.

N.M.R. Studies

Both wideline[23,24] and chemical shift[23] proton n.m.r. results have been published for ion exchanged zeolites containing ethylene (10 cms. pressure).

For C_2H_4 adsorbed in zeolites containing alkali metal cations it was found that the n.m.r. signal exhibited a simple temperature dependence. The linewidth broadened in a regular manner from room temperature to 77K (the lowest temperature studies). This indicates a general slowing down of molecular motion without loss of any degrees of freedom. With Ag-13X however, the line broadened rapidly until 178K at which temperature a double humped peak, characteristic of dipolar broadening, appeared. The second moment then remained constant between 178K and 77K.

These results indicate that the rapid reorientational motion, which is causing the band narrowing for C_2H_4 adsorbed on Ag-13X is quenched below -95°C. It can be seen that for M-13X + C_2H_4, where M

is an alkali metal, the infrared and n.m.r. results are in agreement.
For Ag-13X + C_2H_4 there is an apparent discrepancy because the infrared
results indicate that even at room temperature the C_2H_4 is restricted
in its rotation on Ag-13X. This descrepancy is possibly explained by
the time-scales of the two techniques which differ by several orders
of magnitude. (Chapter 3).

Section IV

Zeolite - Ethylene Interaction

The bonding between transition metals and alkenes is usually described in terms of the Chatt-Dewar model.[25] According to this model an initial σ bond is formed between the filled π orbitals on the alkene and on empty σ acceptor orbitals of the metal. Accumulated negative charge on the metal is then back-donated by d (or dp hybrid) π orbitals to a π acceptor orbital of the alkene. Because the π-acceptor orbital of the alkene is antibonding the C = C bond order may be decreased and the bond length increased (found 1.337 Å in gaseous ethylene and 1.375 Å in Zeise's Salt).[27] Without detailed knowledge of the bonding of the metal ions to the zeolite framework it is not possible to describe fully the bonding of the ethylene to the metal ions. However, it seems reasonable to assume that the situation will be similar to that found for model complexes and the infrared and i.n.s. results can in fact be rationalised by applying the Chatt-Dewar model to the adsorbed C_2H_4.

Consider firstly the Ag-13X zeolite. If the interaction between the silver ion and the framework were purely electrostatic then the C_2H_4 could only become directionally fixed in space as a result of interactions between e.g. its hydrogens and the framework oxygens. A degree of covalent bonding, however, necessarily fixes the silver d orbitals in space. Therefore the directional nature of the silver "d" orbitals is a consequence of the degree of interaction with the frame-work. Any strong interaction between these orbitals and the π^* orbitals of the olefin will effectively prevent the olefin freely rotating around the C_2 axis. The difference between silver and cadmium may simply be

one of ionic radii (Cd^{2+}, 0.98 Å; Ag^+, 1.26 Å) and so the filled 4d

orbitals of Cd may not extend far enough for effective π overlap with

the C_2H_4. Thus in the majority of the zeolites studied the bonding

is likely to be due solely to σ interaction. The barrier e.g. to torsion

about the C_2 axis will be a function of the amount of π bonding, and so

virtually free rotation is expected for C_2H_4 bonded to Na^+, Li^+ etc.

but hindered rotation is expected where significant π-overlap can take

place.

Section V

An Inelastic Neutron Scattering Study of Ethylene Adsorbed by Silver

Exchanged 13X Zeolite

a)   Introduction

Incoherent inelastic neutron scattering spectra of ethylene

adsorbed on Ag-13X zeolite have been measured. The degassed zeolite

is relatively transparent to neutrons but it will adsorb ethylene so

that the total sample scattering cross section increases by up to a

factor of twelve. The ethylene exists as discrete molecules within

the zeolite framework and at 110K the strong interaction between the

silver ions and the ethylene leads to sharp vibrational transitions

associated with the motion of the ethylene with respect to the surface.

The adsorption of an ethylene molecule introduces six new normal modes,

i.e. three hindered rotations and three hindered translations, to the

system (fig. 4). Corresponding modes have been observed, using i.n.s.

[28,29] infrared and Raman techniques,[30] in model compounds e.g.

K[Pt Cl_3 C_2 H_4]. Because of the weaker bonding of the ethylene to the

silver ion in the zeolite we would expect these transitions to occur

at lower frequencies than in the platinum model complexes. However,

the data from the model compounds can be used in the interpretation of

the spectra of the adsorbed species.

Infrared and gravimetric studies[9,20] demonstrate the existence of

two different adsorption sites for the ethylene, within the zeolite

framework. Under the experimental conditions used isotherm data[9]

indicates that 4.4 and 8 ethylene molecules respectively are adsorbed

per supercage. For several reasons, discussed later, it is expected

that C_2H_4 will be more strongly held on cations of type III. It was

141.

Fig. 4 Ethylene-Surface Modes: Notation
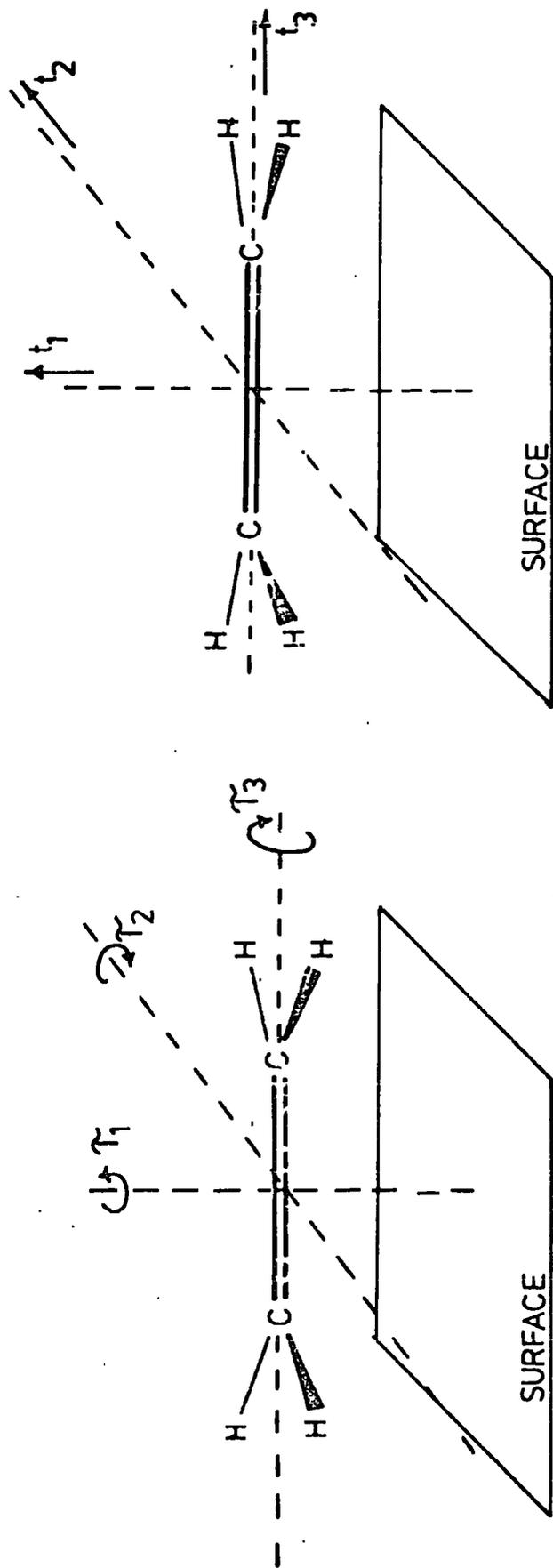
HINDERED ROTATIONS

τ_1: torsion one

τ_2: torsion two or antisymmetric stretch

τ_3: torsion three

HINDERED TRANSLATIONS

t_1 : symmetric stretch

t_2 : wagging mode

t_3 : rock

deduced that at the pressures used type III and types II and III sites respectively were occupied by the ethylene. Ions of type I are not able to adsorb C_2H_4 because the apertures in the hexagonal prism are too small to admit the molecule. The heats of adsorption of C_2H_4 on the type III and type II sites are 18.1 and c.a. 12.5 k cal mol^{-1} respectively.[20]

b) **Experimental**

Zeises' Salt was purchased from Alfa Inorganics Ltd. and Zeises' Dimer was prepared by a standard technique.[31] $AgNO_3 \cdot \frac{1}{2} C_2H_4$ was prepared by bubbling ethylene through a saturated $AgNO_3$ solution at $0^{o}C$. The white precipitate was dried on a glass sinter in a stream of ethylene and at no time was the temperature allowed to rise above $0^{o}C$. For the i.n.s. experiments these samples were enclosed in thin-walled silica containers. In order to avoid decomposition of the $AgNO_3 \frac{1}{2} C_2H_4$ the operations of transferring it to a silica container and loading it into a cryostat, were performed in a cold room ($-10^{o}C$). This procedure also avoided contamination of the sample with water.

The Ag-13X was obtained by repeatedly ion-exchanging Na-13X (Linde Lot No.1976300) with $AgNO_3$ solution.[32] The sample was washed thoroughly and then degassed to a pressure below 5×10^{-6} torr at $450^{o}C$ before being transferred, under vacuum, to either a silica or aluminium sample cell. The cell plus zeolite was then run as a background. Spectra were measured again when a pressure of 500 torr of ethylene had been introduced, at room temperature, via a glass break seal and again after the zeolite plus ethylene had been evacuated for 30 minutes at room temperature.

In order to obtain a satisfactory spectrum of the zeolite itself it was necessary to use five times as much sample as was used for the adsorption experiments. To ensure the removal of all "H" from the system, because even a small amount would produce a significant contribution to the spectrum, the sample was washed several times with D_2O before the baking procedure was started. The spectrum of this sample was obtained at ambient temperature.

During the heating and degassing procedure the Ag-13X zeolite turned bright yellow. In a test experiment it was found that the original off-white colour would return on exposing the zeolite to the atmosphere.

The i.n.s. measurements were made using the 6H[33] and 7H[34] time-of-flight and the Beryllium Filter Detector[35] Spectrometers at A.E.R.E. Harwell. The initial data analysis was performed using the Prescat, Circa[36] and Roundabout[37] programmes. All of the Beryllium Filter Detector measurements were made with the sample in a liquid nitrogen cryostat and the sample temperature was c.a. 90K. Time-of-flight spectra of the zeolite systems were obtained at several temperatures between ambient and 110K. All of the spectra shown have had the background subtracted.

c)   Model Compounds

We have obtained the i.n.s. spectra of Zeises' Salt, Zeises' Dimer and $AgNO_3 \cdot \frac{1}{2}C_2H_4$. These results and the assignments available from Raman and Infrared studies[30] are given in table 2 and fig   5.

The lower energy spectra (< 250 cm^{-1}) of the platinum complexes have been published elsewhere[28].

Table 2 Vibrational Assignments for Zeises' Salt and Zeises' Dimer (cm^{-1})

[PtCl$_3$C$_2$H$_4$]$^-$		[PtCl$_2$(C$_2$H$_4$)]$_2$		Assignment
I.R. + Raman[1]	I.N.S.[2,3]	I.R. + Raman[1]	I.N.S.[2,3]	
120	185	-	110	PtC$_2$ wag
-	190	201	170	torsion
219		405⎤ 415⎦	190	PtC$_2$ rock
403	400		400	Symmetric Stretch PtC$_2$
493	490	482⎤ 492⎦	487	Antisymmetric Stretch PtC$_2$
720	720	719⎤ 728⎦	718	CH$_2$ rock
814	840	814⎤ 818⎥ 828⎦	820	CH$_2$ rock
		972⎤ 977⎥ 982⎦	985	CH$_2$ wag
1010	1020	1021⎤ 1026⎥ 1036⎦	1030	CH$_2$ wag
1180		1176		CH$_2$ twisting
1243	1230	1231⎤ 1239⎦	1230	C = C stretch
1426	1440	1414	1400	CH$_2$ scissoring

1. Ref. 30 and 39.
2. Low frequency data from 28.
3. Higher frequency data; this work.
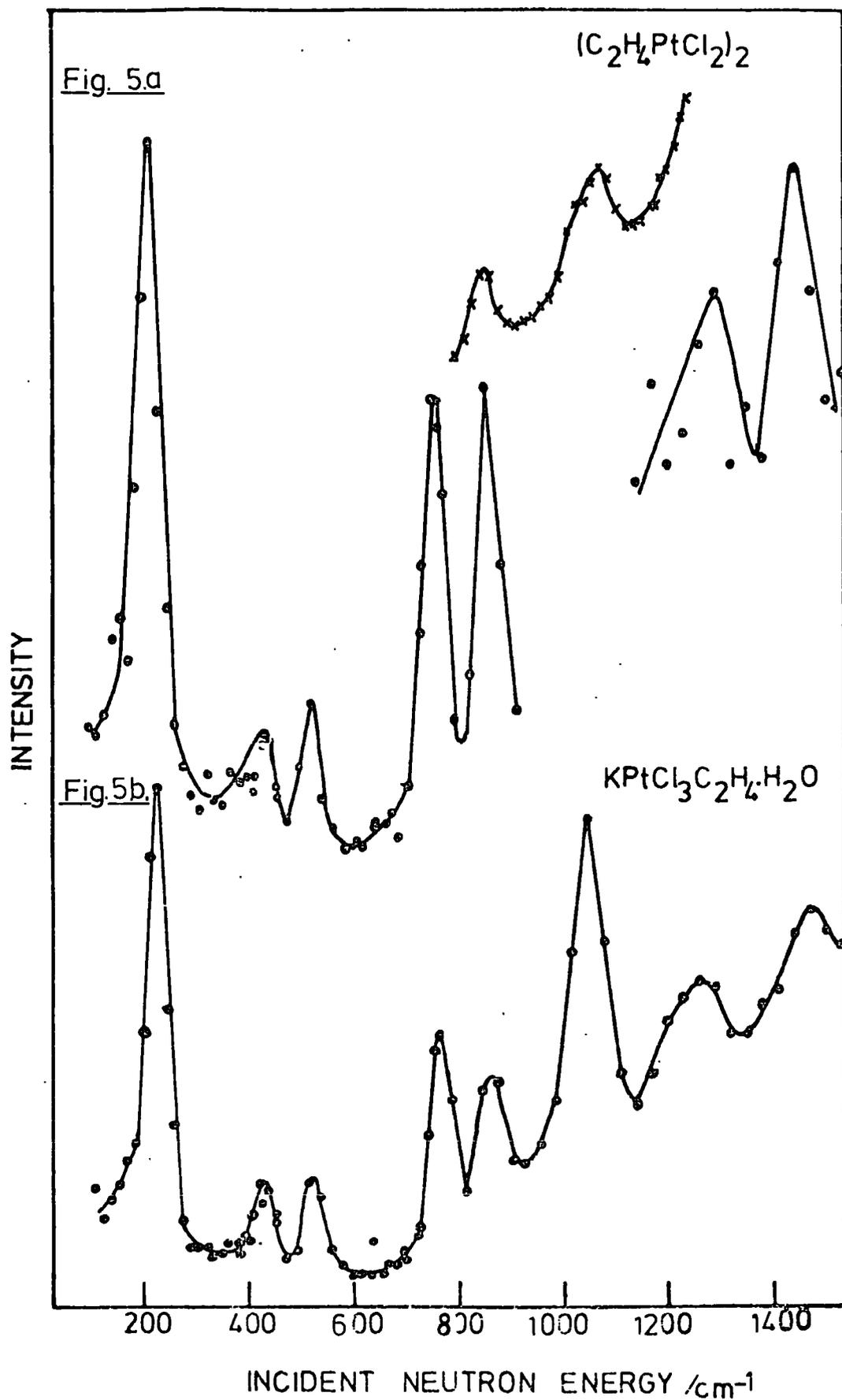
Fig. 5   B.F.D. Spectra of Zeise's Salt and Dimer

The two intense peaks, at ~ 720 and ~ 840 cm^{-1}, in the spectra of the complexes are absent from the i.n.s. spectra of the adsorbed species. This is understandable because these vibrations have been assigned to CH_2 rocks (v_{17} and v_{23})[30] and so with the greater double bond character of the C = C bond in the adsorbed species, we would expect them to occur at higher frequency. These modes have been assigned at 810 (v_{10}) and 1236 cm^{-1} (v_6) in gaseous C_2H_4.[38] Reference to figure 13 shows that there is a poorly resolved shoulder at ~ 800 cm^{-1} in the i.n.s. spectra of C_2H_4 on Ag13X which may correspond to the lower of these two rocks. Thus we expect all of the intramolecular modes of the adsorbed ethylene to occur above 800 cm^{-1} (C_2H_4) and 586 cm^{-1} (C_2D_4).

The i.n.s. spectra of the platinum complexes show three intense peaks below 600 cm^{-1} (table 2). The rock and wag modes are weak as predicted.[28] The torsion 1 (τ_1) mode (fig. 4) occurs above 1000 cm^{-1}. We can reasonably assume that the same modes i.e. τ_1, τ_2, τ_3 and the symmetric stretch will be intense in the i.n.s. spectra of the adsorbed ethylene. Because the bonding of the C_2H_4 to the Ag zeolite is weaker than to Pt the observed transitions should be at a lower frequency than in the model compounds. This is confirmed by the i.n.s. spectrum of $(AgNO_3)_2C_2H_4$ (fig. 6). The spectrum is very similar to those of the platinum complexes and the intense peak at 140 cm^{-1} can only be reasonably assigned to the τ_1 mode. The peak at 280 cm^{-1} is probably the first overtone of τ_1.

d) Time of Flight Results (0-300 cm^{-1})

The spectra in fig. 7 a, b, c, show the corrected neutron counts plotted as a function of scattered neutron time-of-flight for Ag-13X

Fig. 6 $S(\alpha, \beta)$ vs Energy for $AgNO_3 \cdot \frac{1}{2} C_2H_4$

$\theta = 68°$

ENERGY/CM^{-1}

$\theta = 90°$

$T = 110K$
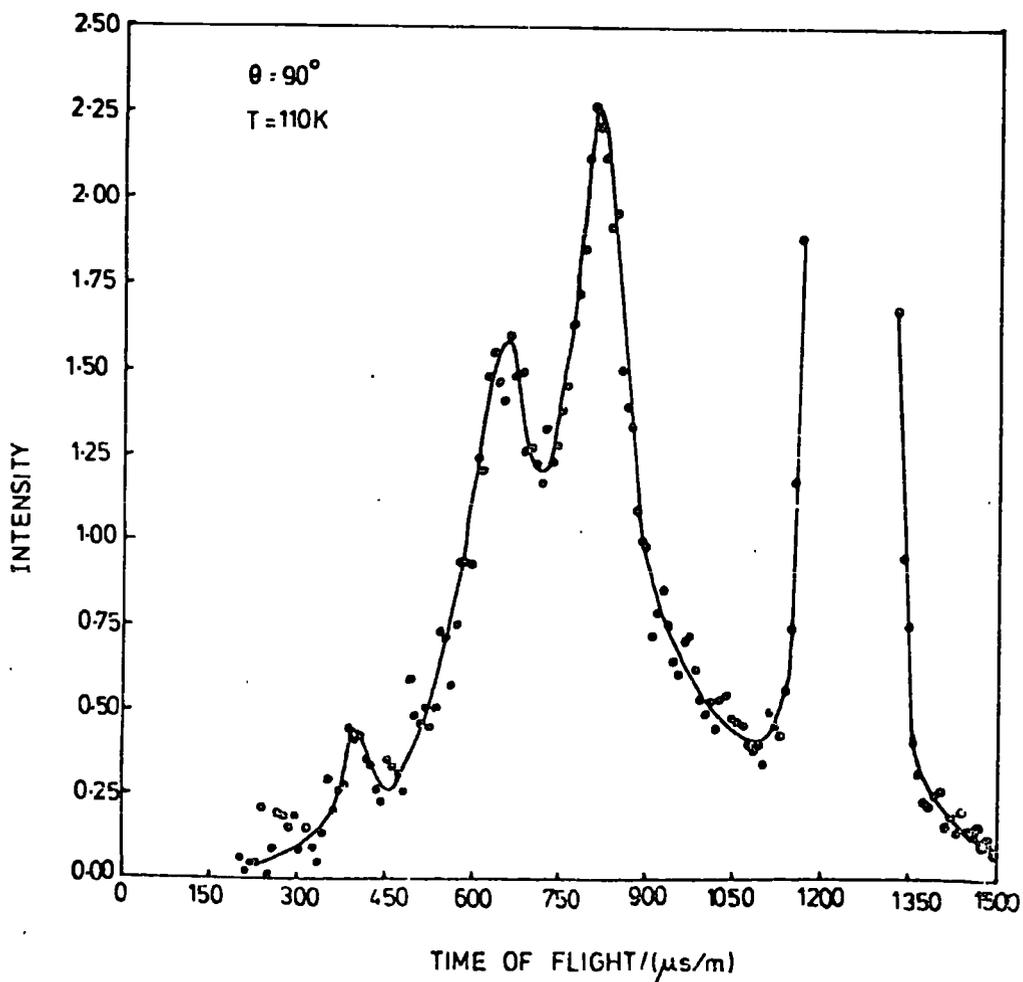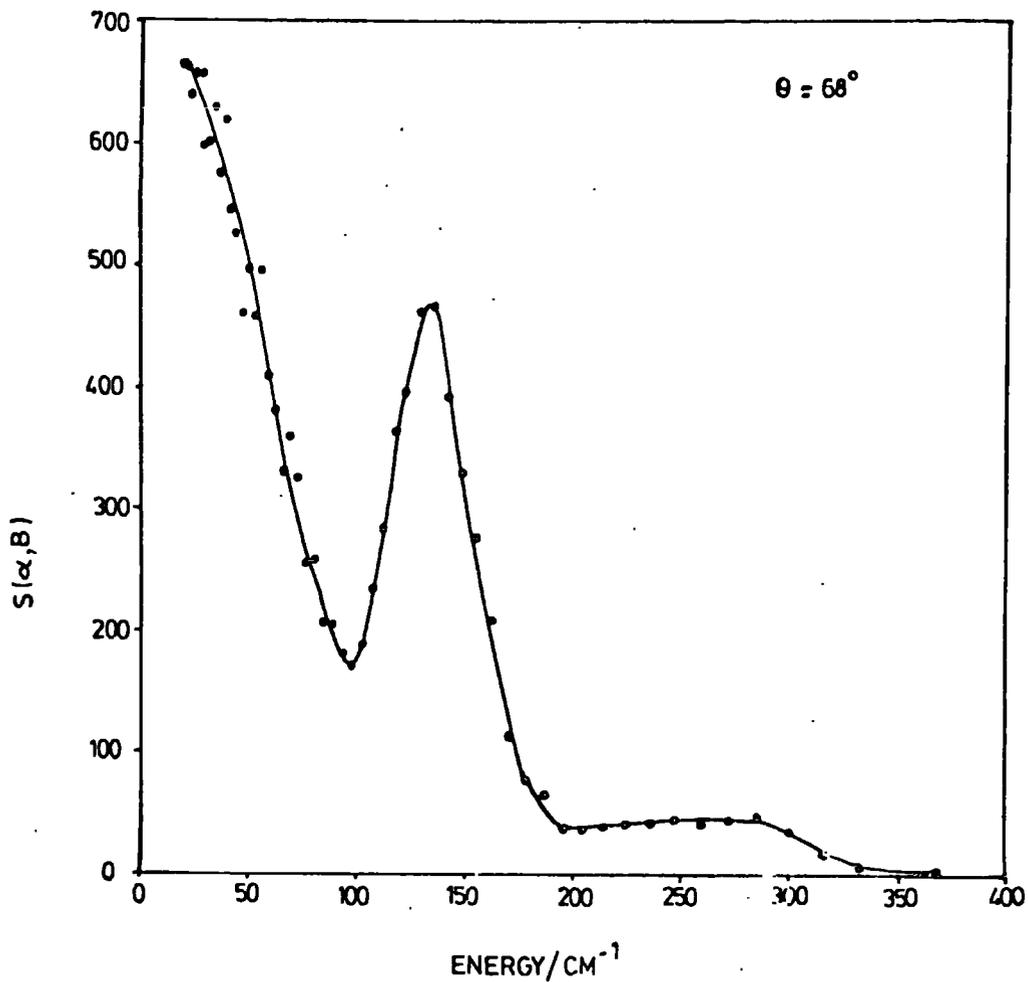
TIME OF FLIGHT/$(\mu s/m)$

Fig. 8 T.of.F. Spectrum of C_2D_4 + Ag13X (Low Coverage)
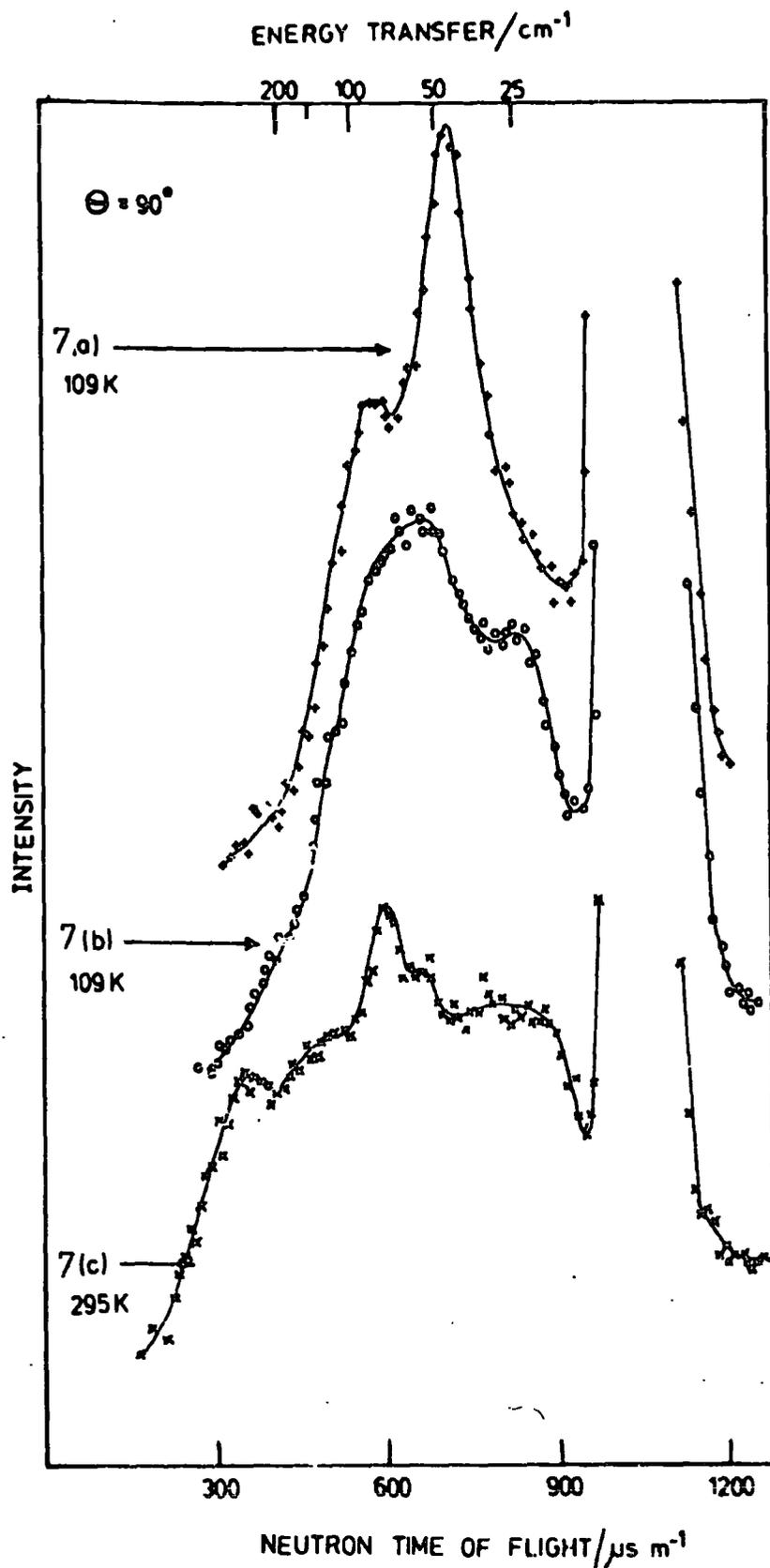
FIG.7 - Neutron time of flight spectra of

a) ethylene absorbed on Ag-13X zeolite at low pressure.

b) ethylene absorbed on Ag-13X zeolite at a pressure of 500 torr.

c) Ag - 13X zeolite.

and C_2H_4 adsorbed on Ag13X. These spectra were obtained at 110K. For the ethylene adsorbed at low pressure a transition is found at 40 cm^{-1} (fig. 7a). At the higher pressure of ethylene when type II sites are also occupied, transitions occur at 56 cm^{-1} and 22 cm^{-1} (fig. 7b). Our interpretation of these spectra is that a vibration of the more strongly bound species occurs at 40 cm^{-1}, however, on increasing the coverage this vibration shifts to 56 cm^{-1} and a new transition, associated with the more weakly bound species, occurs at 22 cm^{-1}. The shift in frequency is possibly associated with steric crowding within the supercage as a result of the increased coverage. We intended to test this hypothesis by first covering the stronger adsorption sites with C_2H_4 and then adsorbing C_2D_4 so that even with both sites covered we would be still obtaining the i.n.s. spectrum of the more strongly held species. The result of such an experiment would of course depend on the similarities or differences between the ethylene adsorbed on the two sites. In a test experiment, however, analysis of the gas phase of a sample prepared as described above, indicated that complete mixing had taken place.

We have also obtained the i.n.s. spectrum of C_2D_4 adsorbed on type III sites (low coverage) and this is shown in fig. 8. The most intense peak occurs at 35 $\pm$ 3 cm^{-1}. The peak position for C_2H_4 adsorbed on type III sites is 39.5 $\pm$ 3 cm^{-1}. This corresponds to a shift of .886. By comparison with the spectra of the model compounds we would expect the most intense low energy vibration to be τ_1. It is difficult to predict deuteration shifts for the adsorbed species because the exact geometry of the molecules is not known. However, we can consider two extreme situations

(A) The adsorbed molecules are planar and their structure is the same as observed in the gas phase.[26]

(B) The adsorbed molecules have the same geometry as the C_2H_4 ligand in Zeise's Salt.[27] In this case we may consider that the C-D distance is .01Å shorter than the C-H but the other parameters are identical.

The moments of inertia and expected shifts on deuteration are given in table 3.

If the band at 39.5 ± 3 cm^{-1} is the τ_1 mode then we can predict that it would occur at 32.1 ± 2.1 cm^{-1} (Alternative A) or 32.8 ± 2.5 cm^{-1} (Alternative B). Therefore on the grounds of intensity and shift on deuteration we assign this band to τ_1. An assignment to τ_2, though reasonable from the deuteration shift, would be unacceptable on intensity grounds (see table 5 and later discussion).

e) Separation of Fundamentals and Overtones

There is a peak at 80 cm^{-1} in the spectrum of C_2H_4 on type III sites and there exists a shoulder in the same region when both types II and III sites are covered, however, the occurrence of the peak at 56 cm^{-1} makes its position difficult to determine.

We have investigated the possibility that this peak at 80 cm^{-1} is an overtone of the peak at 39.5 cm^{-1}. From neutron scattering theory (chapter 2) it is known that if a fundamental and a first overtone both have the same frequency then

a) at different temperatures, if all other factors are equal, then for a fixed value of energy transfer (ω)

Table 3 Moments of Inertia and expected shifts $\left(\dfrac{\nu_{C_2H_4}}{\nu_{C_2D_4}}\right)$ for adsorbed C_2H_4 and C_2D_4

Gas-Like Geometry

	$I_{C_2H_4}$	$I_{C_2D_4}$	$\dfrac{I_{C_2H_4}}{I_{C_2D_4}}$
AXIS 1	20.432	30.093	.8240
AXIS 2	16.887	23.053	.8559
AXIS 3	3.546	7.040	.7097

Zeises Salt Structure

	$I_{C_2H_4}$	$I_{C_2D_4}$	$\dfrac{I_{C_2H_4}}{I_{C_2D_4}}$
AXIS 1	21.0375	30.4879	.8307
AXIS 2	17.7467	24.0049	.8598
AXIS 3	3.4766	6.8028	.7149

$$\text{Intensity of a fundamental} \propto T \tag{1}$$

$$\text{Intensity of an overtone} \quad \propto T^2 \tag{2}$$

T is the absolute temperature.

b)   at constant temperature and constant value of ω

$$\text{Intensity of a fundamental} = Q^2 A \exp(-Q^2 C) \tag{3}$$

$$\text{Intensity of an overtone} \quad = Q^4 B \exp(-Q^2 C) \tag{4}$$

Q is the momentum transfer

C is the mean square vibrational amplitude.

Fig. 9 shows the Boltzmanncorrected scattering $(P(\alpha,\beta))$ at 295K and 110K and it appears that the scattering at 80 cm^{-1} increases faster with temperature than that at 40 cm^{-1}. This is to be expected if a significant proportion of scattering at 80 cm^{-1} is due to a first overtone.

We have attempted to achieve a separation of one and two quantum scattering by taking $P(\alpha,\beta)$ data, obtained at different Q values but at the same ω value, and fitting it to the expression

$$\frac{\text{Experimental Intensity}}{Q^2} = (A + BQ^2)\exp(-Q^2 C) \tag{5}$$

The division of the experimental intensity by Q^2 simplifies the fitting problem.   Fig. 10 is a plot of "Q" versus "ω" for the 6H spectrometer. Our fitting procedure involved taking experimental data along lines parallel to the ordinate and fitting it to equation 5.

The value of C was calculated from the quasi-elastic peak data (chapter 2).   Fig. 11 is a plot of the calculated values of A and B for a temperature of 247K.   These plots have the correct characteristics

153.

Fig. 10   Plots of Q v.s. ω for the 6H Spectrometer
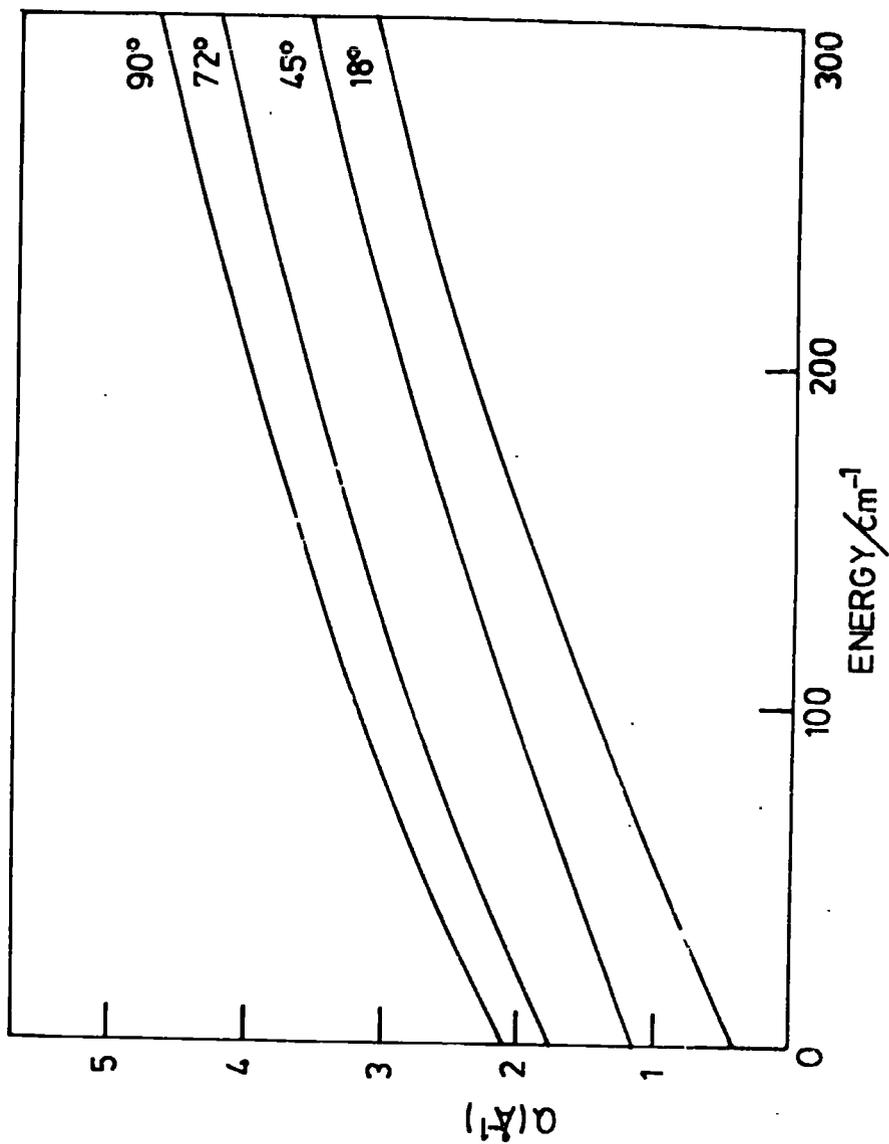
Fig. 9   Variation with temperature of
the i.n.s. spectra of Ag13X + C_2H_4

Fig. 11   Plots of A and B Factors for C_2H_4 + Ag13X
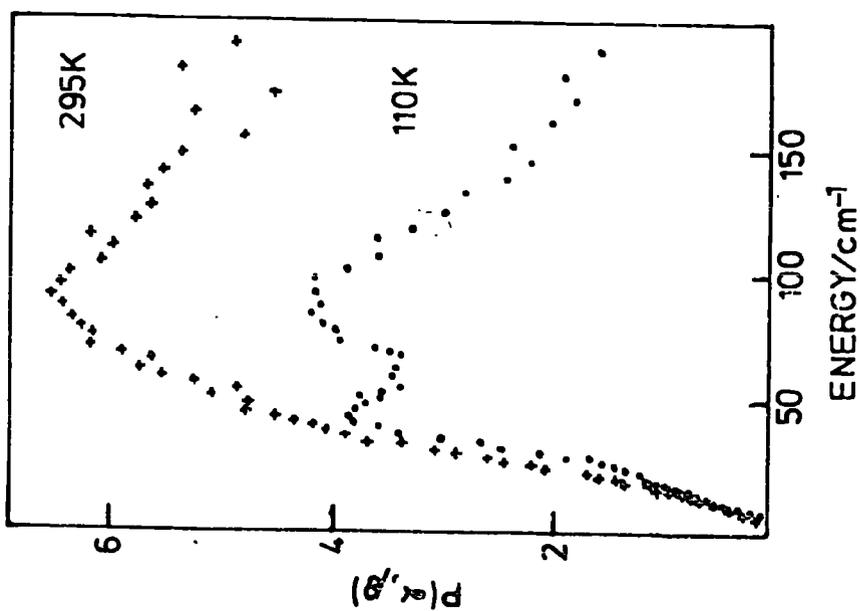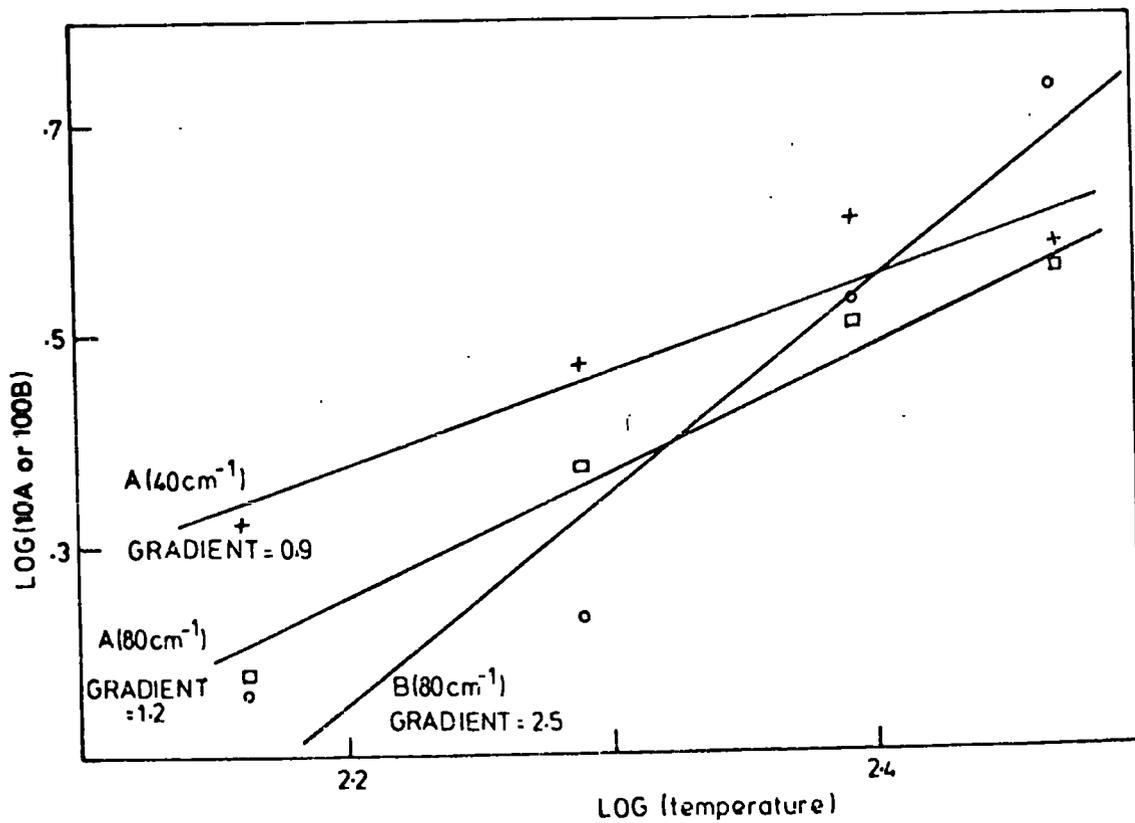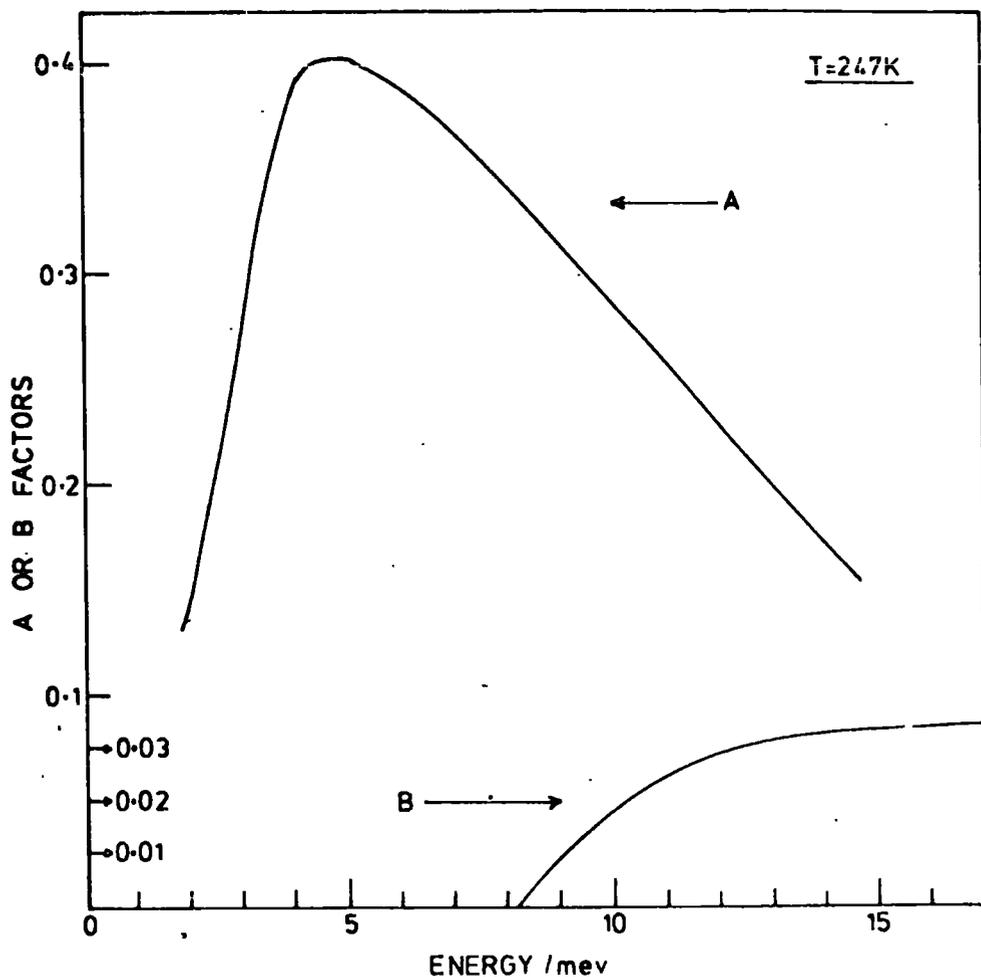
Fig. 12   Temperature Dependence of the A and B Factors

i.e. the B values are very small when "ω" is small. That the "B" values rise monotonically and do not "peak" at any particular value is probably due to the fact that we should include higher terms in the fitting equation e.g. $DQ^6 \exp(-Q^2C)$ to account for second overtones etc. Because we have only nine data points for each "ω" value and the resolution begins to worsen beyond 100 cm^{-1} it was considered that further analysis along these lines was not justified.

From equations 1 and 2 it can be seen that a plot of log (intensity) vs log (T) should be a straight line for both fundamentals and first overtones but that the gradients should be one and two respectively. In order to see if our separation has been performed correctly we have plotted logarithm of the measured "A" and "B" values, for the peak heights, against log (temperature). The results obtained were

	80 cm^{-1} peak		40 cm^{-1} peak	
	Gradient	Correlation Coefficient	Gradient	Correlation Coefficient
A values	1.21	.978	.92	.949
B values	2.50	.94	—	—

As expected the "B" values for the lower energy peak were extremely small (less than 1% of the A values) and so a reliable gradient could not be obtained.

Although the results are not really good enough to enable exact quantitative statements to be made it does appear that both a fundamental and a first overtone occur at $\sim 80 \text{ cm}^{-1}$ and that at 110K their intensities are approximately equal.

f) Beryllium Filter Detector Results (> 60 cm^{-1})

Using the Beryllium Filter Detector spectrometer bands were observed at 258 $\pm$ 21 cm^{-1} and 418 $\pm$ 28 cm^{-1} for ethylene adsorbed on Ag-13X. Although the number of transitions may have been expected to double on increasing the coverage the positions of the bands are identical in both spectra (fig. 13), however the intensity of each peak is doubled. There are three possible explanations for these observations.

a) the resolution of the instrument is ~ 35 cm^{-1} (chapter 3) and so each of the bands, in the spectrum of the high coverage case, may be an unresolved doublet.

b) the vibrations may be the same frequency on both sites.

c) we may be observing surface vibrations which are being amplified as a result of the ethylene molecules mirroring their motion.

In order to assign these vibrations we have obtained the i.n.s. spectra of Ag-13X and of C_2D_4 and trans - $C_2D_2H_2$ adsorbed on it. The results are shown in Table 4 and figures 14 and 15. Time-of-flight spectra of adsorbed trans $C_2D_2H_2$ were not measured because it was expected that the shifts would be too small to measure with meaningful accuracy.

Alternative "b" is unlikely because infrared and gravimetric evidence indicates that there are two distinct adsorbed species.[9,20]

The full width at half height (F.W.H.H.) of the peaks is ~ 100 cm^{-1} and it does not appear to change on increasing the coverage.

Fig. 13   B.F.D. Spectra of C_2H_4 + Ag13X
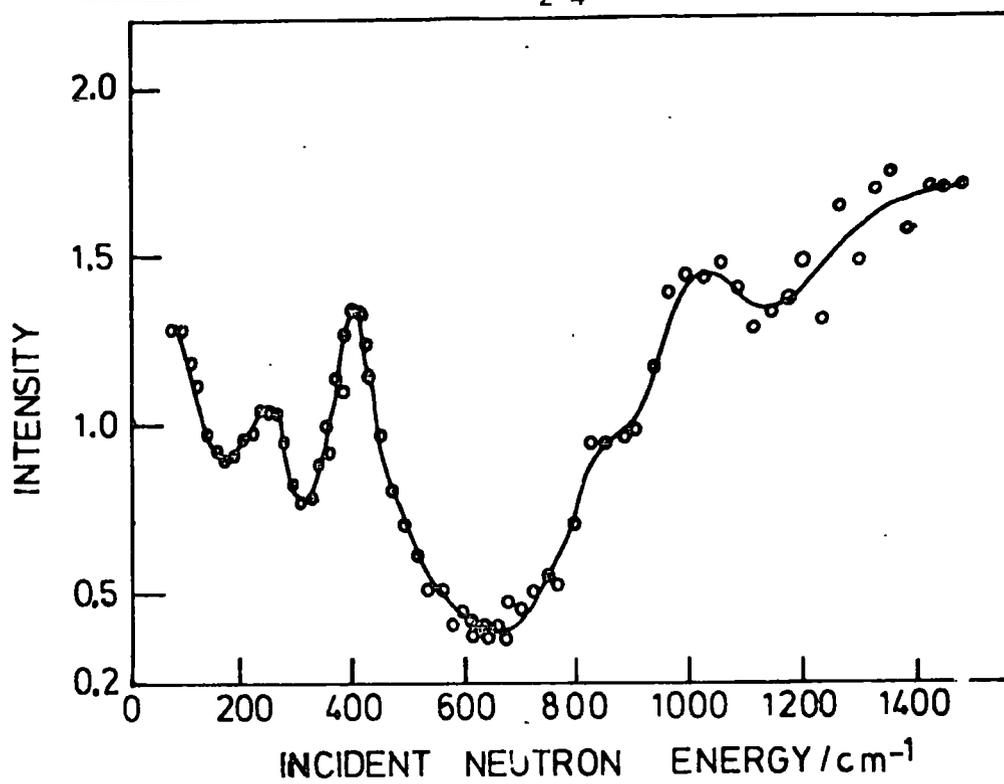
a)   at high coverage
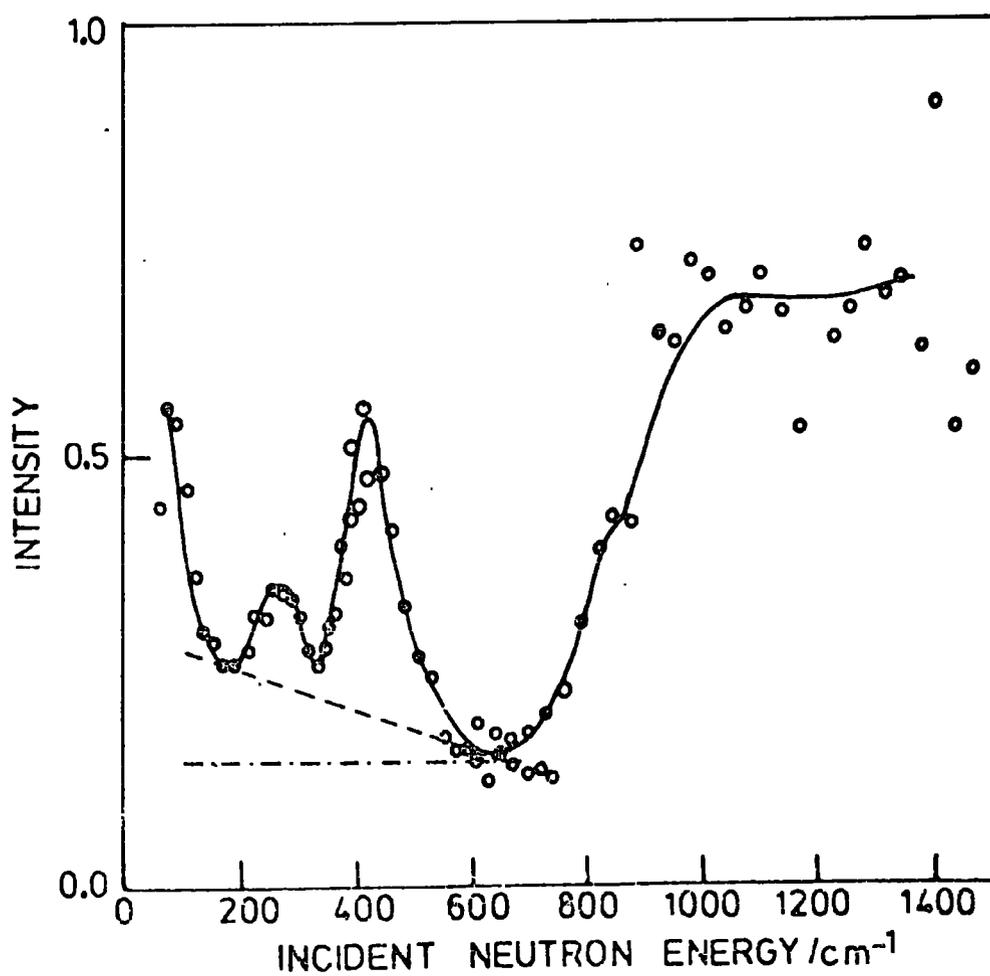
b)   at low coverage

Table 4 I.N.S. Results for C_2H_4, trans-$C_2D_2H_2$ and C_2D_4 adsorbed on Ag-13X at low coverage

Observed C_2H_4	C_2D_4			trans $C_2D_2H_2$				Assignment
	Predicted A[a]	Predicted B[b]	Observed	Predicted A	Predicted 1* B	Predicted 2* B	Observed	
39.5 ± 3	32.5 ± 2.5	32.8 ± 2.5	35 ± 3	Data not available				τ_1
~ 80	~ 75	~ 75	75 ± 5					Hindered translation t_1
258 ± 21	220.8 ± 18	221.8 ± 18	199 ± 20	235 ± 19	235 ± 19	235 ± 19	270 ± 14	τ_2
							338 ± 14	
418 ± 28	296.5 ± 20	298.8 ± 20	276 ± 20	353.6 ± 23.7	252.9 ± 23.6	349.9 ± 23.4	380 ± 14	τ_3

a) Calculated using gas geometry

b) Calculated using Zeises Salt Configuration

* Two configurations because the C-D bonds are not all equivalent in Zeises salt.

159.

Table 5: Predicted Relative Intensities for Ethylene-Zeolite Modes

	Gas-Like Geometry			Zeise's-Salt Geometry		
	C_2H_4	C_2D_4	trans $C_2D_2H_2$	C_2H_4	C_2D_4	trans $C_2D_2H_2$
τ_1	3.3	2.6	2.8	3.1	2.5	2.8
τ_2	2.6	2.1	1.8	2.5	2.1	1.9
τ_3	7.0	4.0	7.6	6.9	4.0	7.3
Mass Sensitive Modes	1.0	1.0	1.0	1.0	1.0	1.0

Fig. 14 B.F.D. Spectra of C_2D_4 + Ag13X a) at high coverage and b) low coverage

(a) 8:1, C_2D_4

(b) 4:1, C_2D_4

INCIDENT NEUTRON ENERGY/cm^{-1}

INTENSITY
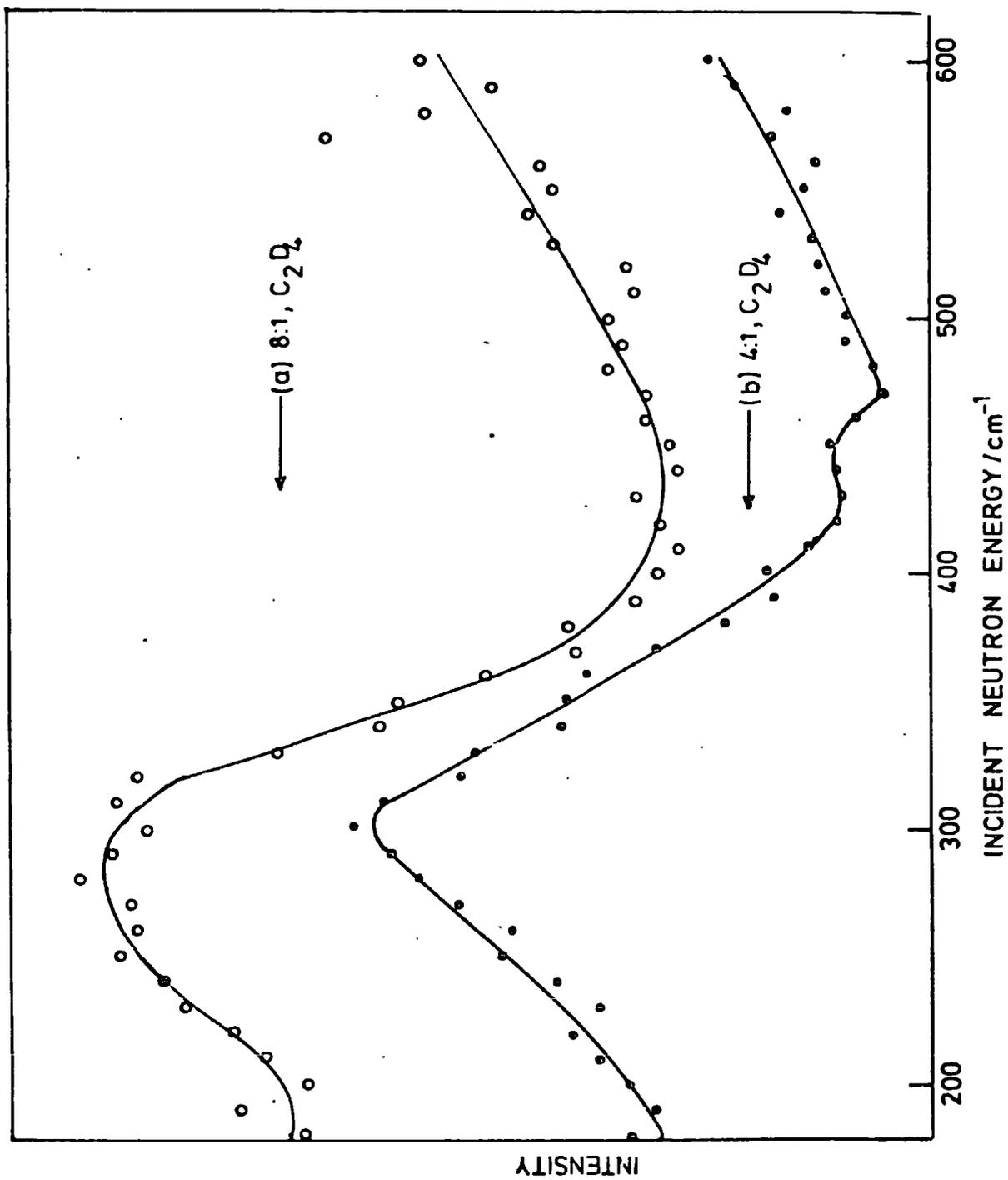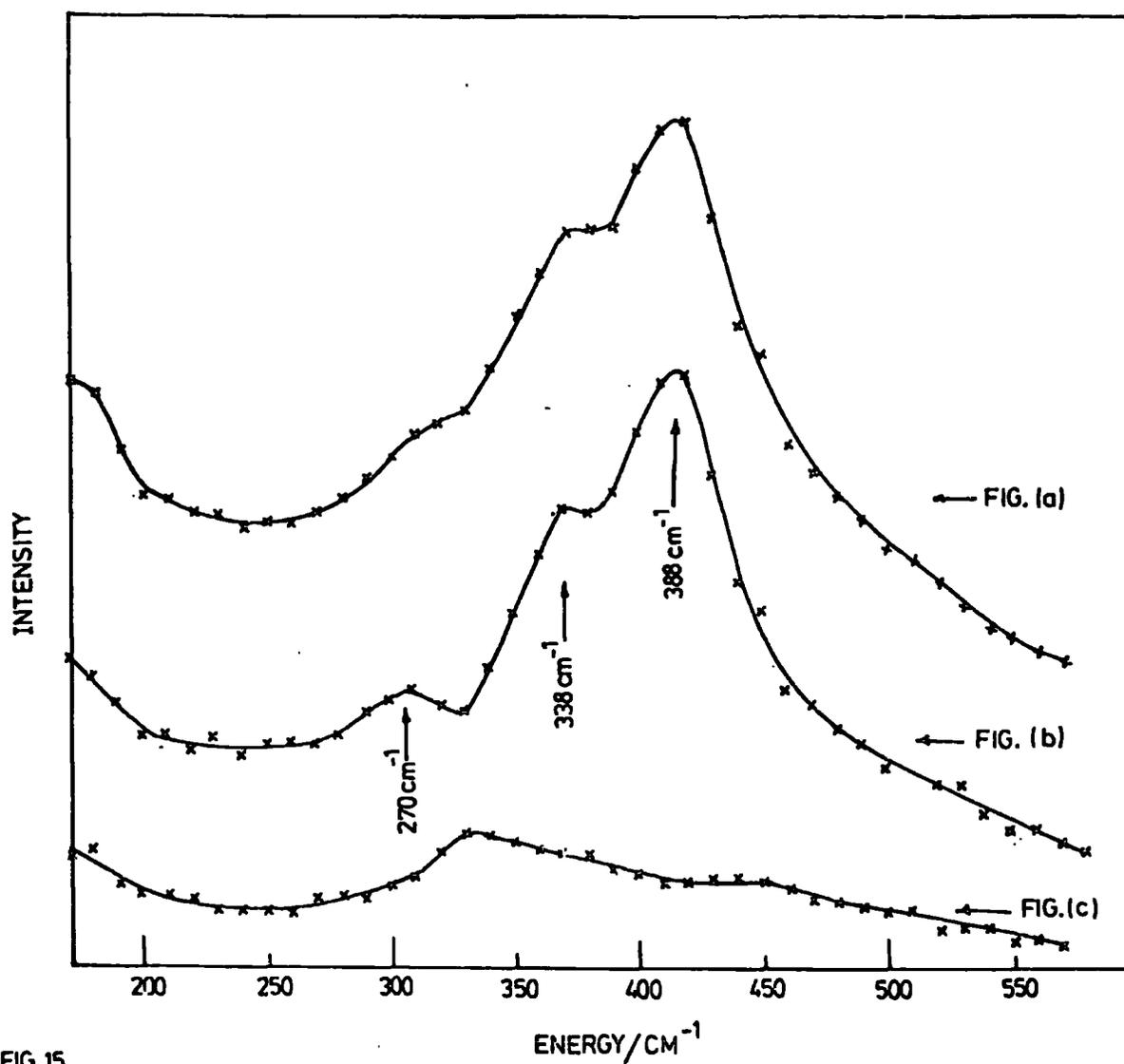
FIG.15.

(a) TRANS $C_2D_2H_2$ + Ag13X, LOW COVERAGE NO BACKGROUND SUBTRACTED

(b) TRANS $C_2D_2H_2$ + Ag 13X, LOW COVERAGE, BACKGROUND SUBTRACTED

(c) Ag 13X + SILICA CONTAINER ; BACKGROUND

The i.n.s. spectrum of the degassed zeolite contains a very broad band in this region, possibly corresponding to several unresolved peaks. If the adsorbed ethylene were simply mirroring the motion of the Ag^+ ions this would imply that the force constant between the ethylene and the silver ion was much greater than that between the silver ion and the oxygen ring. This is unlikely. A more probable situation is that we may observe mixing between the zeolite vibrations and the vibrations relative to the surface. A treatment of mixing, however, requires a normal co-ordinate analysis and this is not possible in the present case.

As with adsorbed C_2H_4 there is little difference between the 4:1 and 8:1 spectra of adsorbed C_2D_4 except that perhaps the existence of two unresolved peaks is more evident in the higher coverage case. Although the incoherent cross section of D is small (2.0) the incoherent cross section of carbon is zero so that extra scattering, above background, must be due to the D atoms in C_2D_4. The observed scattering from the C_2D_4 was in accord with that predicted from its cross section and the known scattering from adsorbed C_2H_4.

The most striking feature of the higher energy (figs. 13,14,15) spectra is the shift of the intense peak in the C_2H_4 spectrum (418 cm^{-1}) to $\sim$ 266 cm^{-1} (C_2D_4) and $\sim$ 380 cm^{-1} ($C_2D_2H_2$). The band at 266 $\pm$ 14 cm^{-1} in the spectrum of C_2D_4 adsorbed at low coverage is composed of two incompletely resolved peaks. We have resolved these using gaussian bandshapes. The components were constrained to have equal F.W.H.H. and intensity ratio of 2:1 (see later discussion). The result is shown in fig. 16 and the F.W.H.H. is 95 cm^{-1}. The peak positions are 199 cm^{-1} and 276 cm^{-1}. The observed shift for C_2D_4 was thus 0.66, calculated assuming the most intense peak (418 cm^{-1}) in

Fig. 16   Results of the Curve Fitting to the Spectrum of C_2D_4 + Ag13X
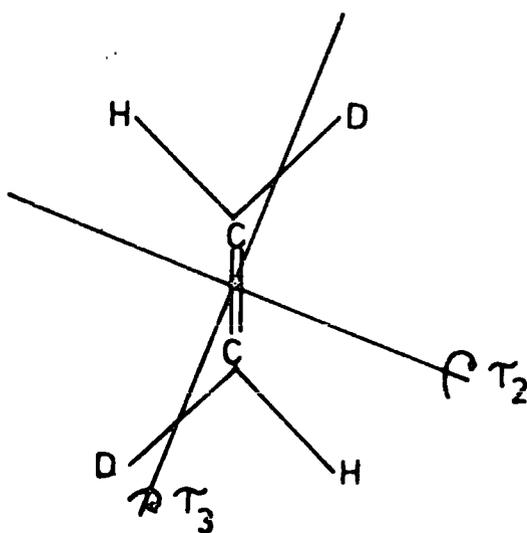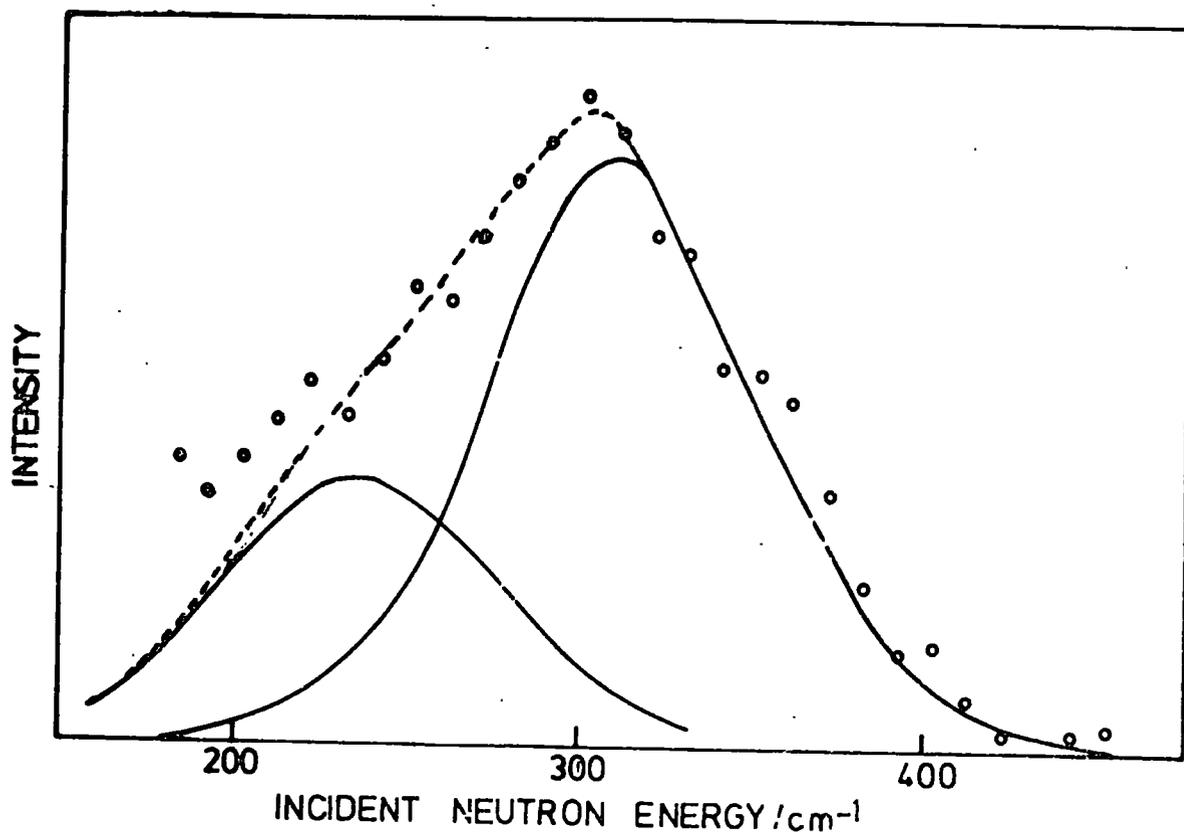
Fig. 17   Principal Axes of Trans-$C_2D_2H_2$

the C_2H_4 spectrum has shifted to 276 cm^{-1} for adsorbed C_2D_4. This large shift can only be explained if it corresponds to a mode in which the carbon atoms are stationary. The only mode which could occur at low enough frequency is τ_3. This mode occurs at 1180 cm^{-1} in Zeises' Salt.[30]

It is difficult to predict shifts for trans - $C_2D_2H_2$ because two of the torsions are taking place about different axes compared with C_2H_4. Because of this the carbon atoms are not on a principal axis so that τ_3, for trans $C_2D_2H_2$, involves the motion of the carbon atoms relative to the surface i.e. it involves τ_2 and vice versa (fig. 17).

We can obtain approximate values for the intensities of the normal modes by noting that for a wagging mode the square of the amplitude of vibration is approximately proportional to $\frac{n}{M}$ where n is the number of scattering atoms and M is the mass of the ligand. The squared amplitude of a torsional mode is approximately proportional to $\frac{nr^2}{I_r}$ where r is the perpendicular distance of the scattering atoms from the axis of rotation and I_r is the reduced moment of inertia for the ligand about that axis. These relative intensities are shown in Table 5. The calculations were performed for both cases noted earlier i.e. A) the ethylene is planar and B) the ethylene has the geometry found for the ligand in Zeises' Salt. It is apparent that the most intense vibration is always τ_3. The increase in intensity of τ_3 relative to the antisymmetric stretch (τ_2) in trans $C_2D_2H_2$ as compared with C_2H_4 occurs as a result of the different principal axes of inertia. The hydrogen atoms are closer to the axis of rotation for the antisymmetric stretch in trans - $C_2D_2H_2$ than in C_2H_4 and further away in the case of τ_3.

Therefore on the grounds of intensity and shifts on deuteration we assign the most intense peak, in each B.F.D. spectrum, to τ_3.

If we consider only the low-coverage case for adsorbed C_2H_4 and C_2D_4 then we have assigned bands to τ_1 and τ_3. We are constrained therefore to assigning the remaining peaks to the symmetric and antisymmetric stretches by comparison with the spectra of the model compounds. The symmetric stretch is expected to be the lower energy vibration.[30] Our calculations indicate that these bands should be more intense than the hindered translations. The assignments for the higher coverage case are identical. Further confirmation of these assignments is gained by comparing the integrated intensities of the bands at 258 and 418 cm^{-1} in the spectrum of adsorbed C_2H_4 (Fig. 13). The actual baseline is unknown so two extremes were considered (shown -·-·- and ----- on fig. 13). The ratios of the integrated intensities in these two cases were 2.2 and 3.7. The predicted ratio for τ_3 and τ_2 (table 5) is 2.69. This is in good agreement with the experimental results.

The assignment of the spectrum of adsorbed trans $C_2D_2H_2$ (low coverage) is more difficult. We do not have any low frequency data, however, in the higher energy region there are three bands as compared to the two found for C_2H_4. There are three new factors to consider for this system.

a) the lower symmetry of trans $C_2D_2H_2$ compared with C_2D_4 or C_2H_4.

b) the change in principal axes of inertia, which leads to τ_2 and τ_3 not being pure modes.

c) the predicted shift for τ_3 from the C_2H_4 data places this mode closer to the centre of the broad background peak. This increases the probability of mixing between this mode and the zeolite modes.

It is difficult to predict the sum of these effects or to decide which, if any, is dominant. The single most significant feature is the absence of any band close to the predicted frequency (~ 235 cm^{-1}) for the τ_2 mode. Both medium intensity bands in the spectrum of trans-$C_2D_2H_2$ are at <u>higher</u> frequency than the τ_2 mode for adsorbed C_2H_4. This could possibly be rationalised by suggesting that as a result of the mixing between τ_2 and the higher frequency mode τ_3 the frequency of τ_2 is increased. However, if this were the case it would suggest that the frequency of τ_3 should be lowered. This does not seem to be the case. Two further observations are:

1. the peak at ~ 270 cm^{-1} is evident only after the background subtraction. Its position and intensity are therefore not very well defined (fig. 15).

2. If the shoulder at 338 cm^{-1} represents a peak of reasonable intensity then the F.W.H.H. of the peak at 380 cm^{-1} is very much less than that of corresponding modes in adsorbed C_2D_4 and C_2H_4. This seems unlikely and so this mode is probably weaker than it appears.

Infrared evidence would be useful in assigning these vibrations, however, so far our attempts to obtain far infrared spectra have been unsuccessful.

A further indication that there is no significant mixing between the C_2X_4(X = H,D) and the zeolite is that the spectrum of C_2H_2 adsorbed on Ag-13X is rather different from adsorbed C_2X_4(X = H,D) in the

region 200 to 500 cm^{-1}. If the C_2H_4 were simply mirroring surface modes then because the mass difference between C_2H_4 and C_2H_2 is small it is reasonable to assume that the spectra would be fairly similar. In fact for adsorbed C_2H_2 there is no vibration in the region mentioned.

Finally because the C_2H_4 is non-planar in Zeises' Salt and the same is almost certainly true of the adsorbed gas then τ_3 must involve motion of the carbon atoms (i.e. in this case t_1). This effect is not as significant as the involvement of τ_3 and τ_2 for trans $C_2D_2H_2$ because the distance of the carbon atoms, from the principal axis of τ_3, is very much smaller.

Finally as we noted earlier Yates et al.[20] were not able to reach any conclusion concerning the rotational freedom of the C_2H_4 molecules on site II because the infrared bands were incompletely resolved. If the C_2H_4 were freely rotating we would expect to observe broadening of the quasi-elastic peak (chapter 2) in our experiments. In fact the F.W.H.H. of the quasi-elastic peak is equal to the instrumental resolution. Although these were only medium resolution measurements they do indicate that free rotation is not taking place for C_2H_4 on either adsorption site.

Section VI <u>A Neutron Scattering Study of C_2H_4 + Na13X</u>

Infrared studies have shown that there are differences in the interaction of C_2H_4 with Na and Ag zeolites. It was therefore expected that there should be significant differences between the neutron spectra of the two systems. In the absence of isotherm data for C_2H_4 + Na13X we decided to investigate just one coverage, corresponding to 40 cms. Hg pressure of C_2H_4 over the zeolite.

<u>Experimental</u>

The experimental procedures were identical to those used for Ag13X (chapter III and V). Spectra were obtained at several temperatures on the 6H and 4H5 time-of-flight spectrometers. For these experiments the 4H5 spectrometer was fitted with one six and one twelve slot rotor. The B.F.D. spectra were obtained at c.a. 90K. Coherent scattering experiments were carried out at ambient temperature on Na13X and Na13X + C_2D_4 using the Curran spectrometer[40] at A.E.R.E. Harwell. The deuterated form of the gas was used because of its very low incoherent cross section.

<u>Results and Discussion</u>
<u>Quasi-elastic region</u>

Figs. 18 and 19 show the time-of-flight spectra of C_2H_4 + Na13X obtained at two different temperatures on the 6H spectrometer. At ambient temperature there is a very dramatic decrease in the intensity of the quasi-elastic peak, relative to the inelastic region, with increasing momentum transfer (Q). Recalling eqn. 22a of chapter II

$$\text{Intensity} \ \alpha \ \exp(-\tfrac{1}{6} Q^2 <u^2>)$$
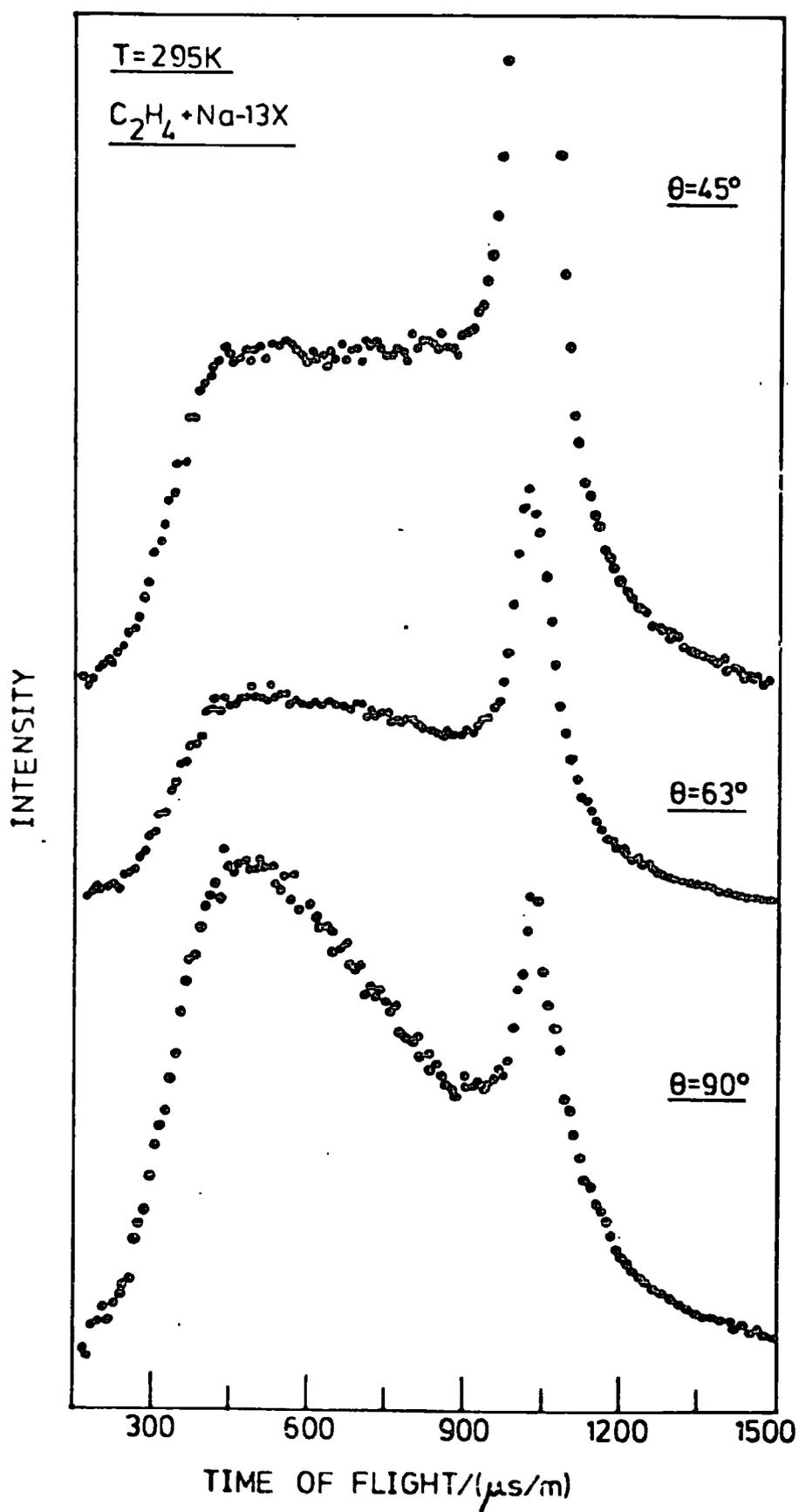
Fig. 18 T.of.F. Spectrum of C_2H_4 + Na13X (295K)
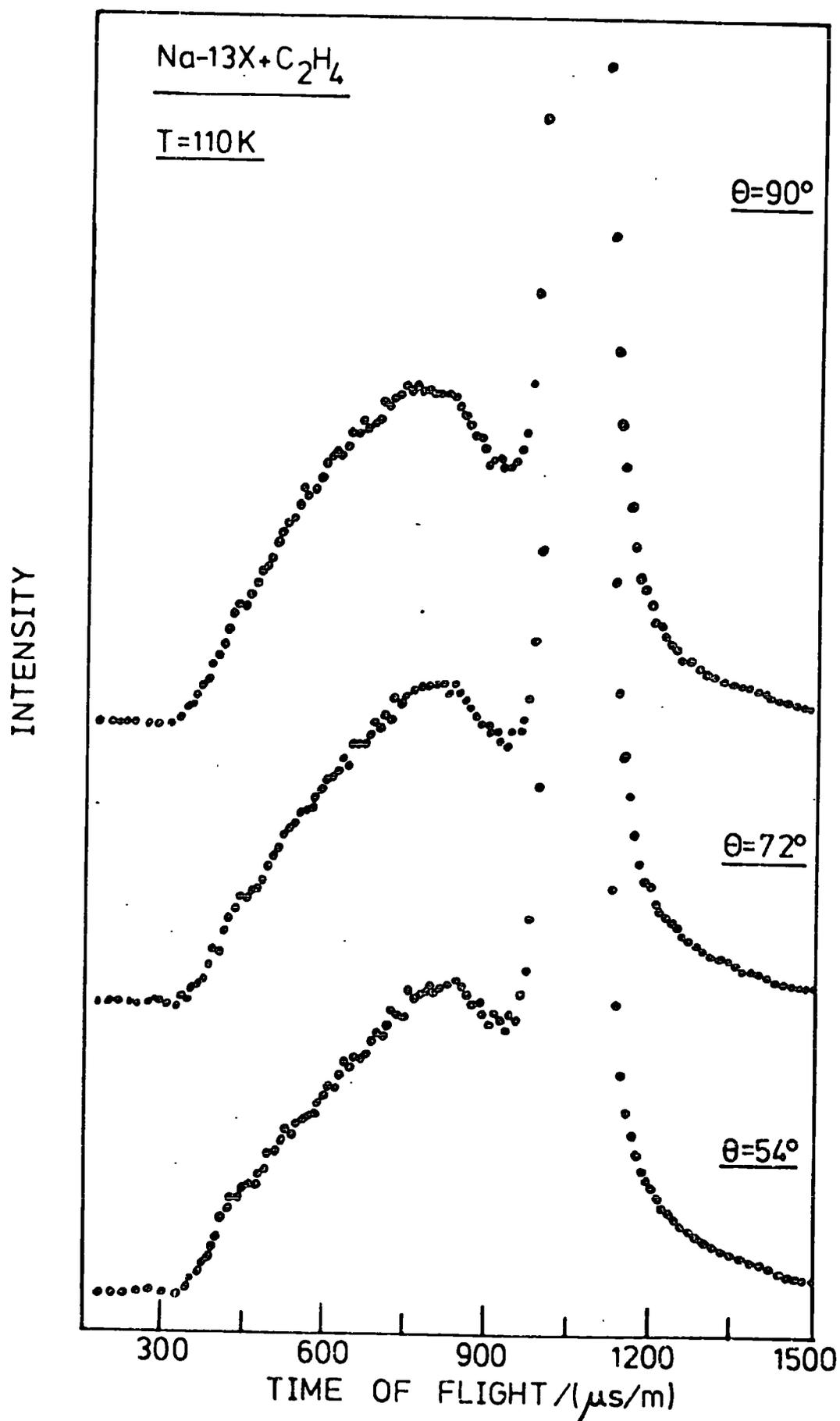
Fig. 19 T.of.F. Spectra of C_2H_4 + Na13X (110K)

we can see that the intensity of the elastic peak is expressed in terms of the Debye Waller factor and this is a function of Q^2. Thus if $<u^2>$ is large the quasi-elastic intensity decays rapidly. Such behaviour is characteristic of the i.n.s. spectra of liquids and gases. It would appear therefore that the value of $<u^2>$ is large for the C_2H_4 + Na13X system. The decrease in the intensity of the quasi-elastic peak with Q is much less marked at lower temperatures (fig. 19).

By comparing the half width of the quasi-elastic peaks of the sample spectrum, with the resolution function of the instrument we can see that there is significant broadening of the quasi-elastic peak. Analysis of the shape of this peak yields information on the processes leading to the broadening.

We have obtained the coherent neutron spectrum of C_2D_4 + Na13X and of Na13X in order to determine the positions of any Bragg peaks which change in intensity or position on adsorbing the C_2H_4. It is possible that the Q value at zero energy transfer for some scattering angle in the spectrum of C_2H_4 + Ag13X, corresponds to such a peak. If this is the case then the subtraction of the background from the sample spectrum will lead to a quasi-elastic peak which is not due entirely to incoherent scattering from the C_2H_4. It would then be incorrect to include that angle in the analysis of the quasi-elastic data. The results of the coherent scattering experiment are shown in fig. 20 together with the Q values for the incoherent scattering experiment (arrowed). There are in fact only two angles of detection, 74° and 45°, which we can say uniquivocably are not effected by Bragg scattering.

As a result of this a full analysis of the quasi-elastic region is not possible but we thought it might be possible to exclude some of the
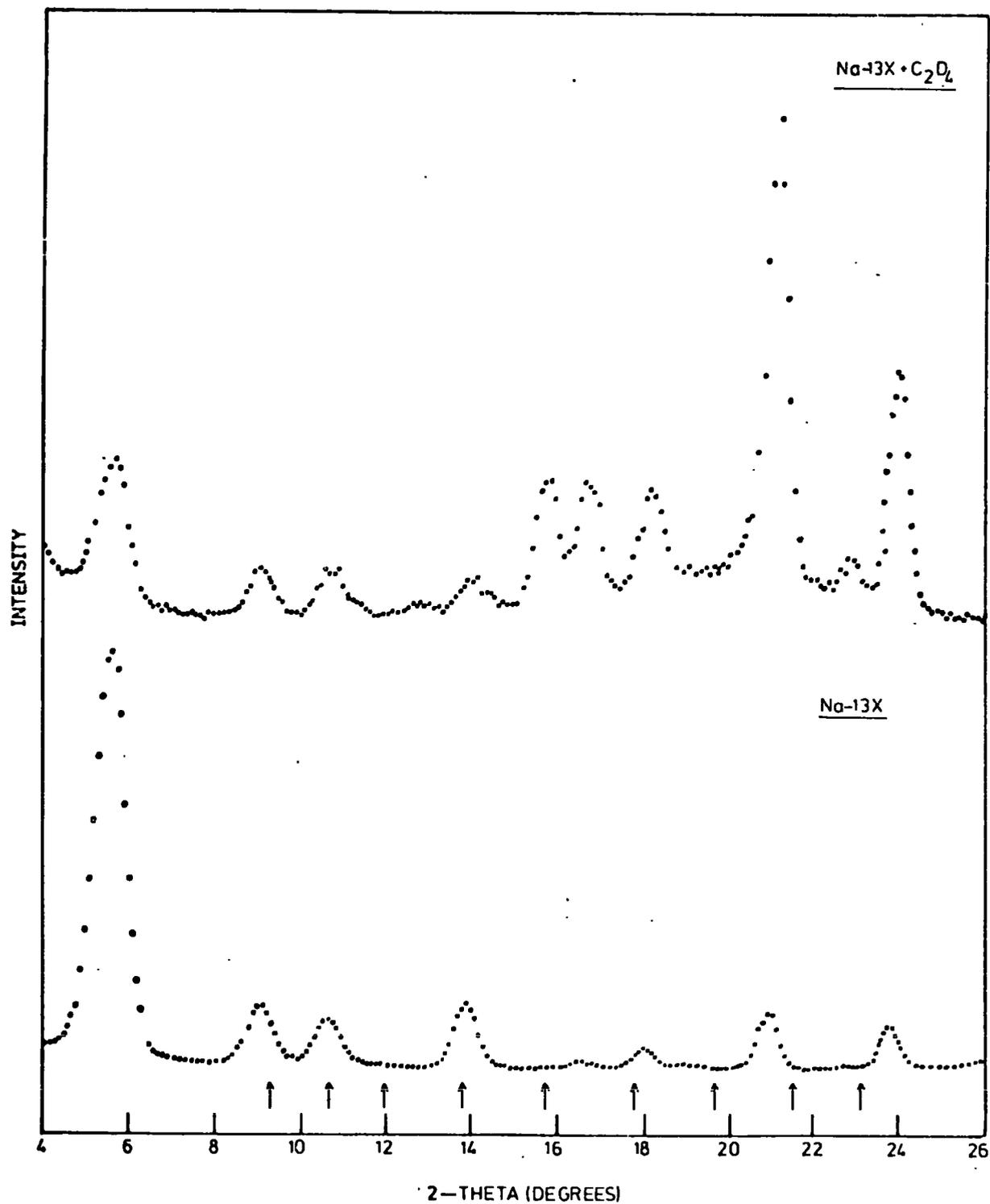
Fig. 20 Results of 2θ Scan for Na-13X and Na-13X + C_2D_4

possible processes which could lead to the broadening.

Curve Fitting

Using the random walk model described in chapter II we have obtained jump times (τ) corresponding to the best fits to the data at angles $74°$ and $43°$, with a sample temperature of $-56°C$. We assumed that the random walk took place about an axis joining the centre of the double bond to the Na^+. The radius of gyration used was 1.559Å which was calculated from the gas phase structure of C_2H_4. We chose jumps (N) involving 2, 4, 6 and 10 sites and the results are shown in table 6.

Table 6   Results of the Curve Fitting to the Quasi-Elastic Peaks for C_2H_4 + Na13X at $-56°C$

N	$74°$		$43°$	
	τ^*	Dr^a	τ^*	Dr^a
2	2.9	.68	4.4	.46
4	3.25	.31	2.45	.41
6	1.75	.29	1.17	.43
10	0.70	.27	0.45	.42

*) in picoseconds   a) in units of 10^{12} secs.

Good fits to the data (see figs. 21,22 for some results) were obtained with N equal to 4, 6 or 10. The reason for this is evident if we calculate the corresponding values of the diffusion coefficients by using equation30 of chapter II. These are also shown in table 6 and it can be seen that for either angle the calculated values are in reasonable agreement, but that the calculated diffusion coefficient varies with angle.
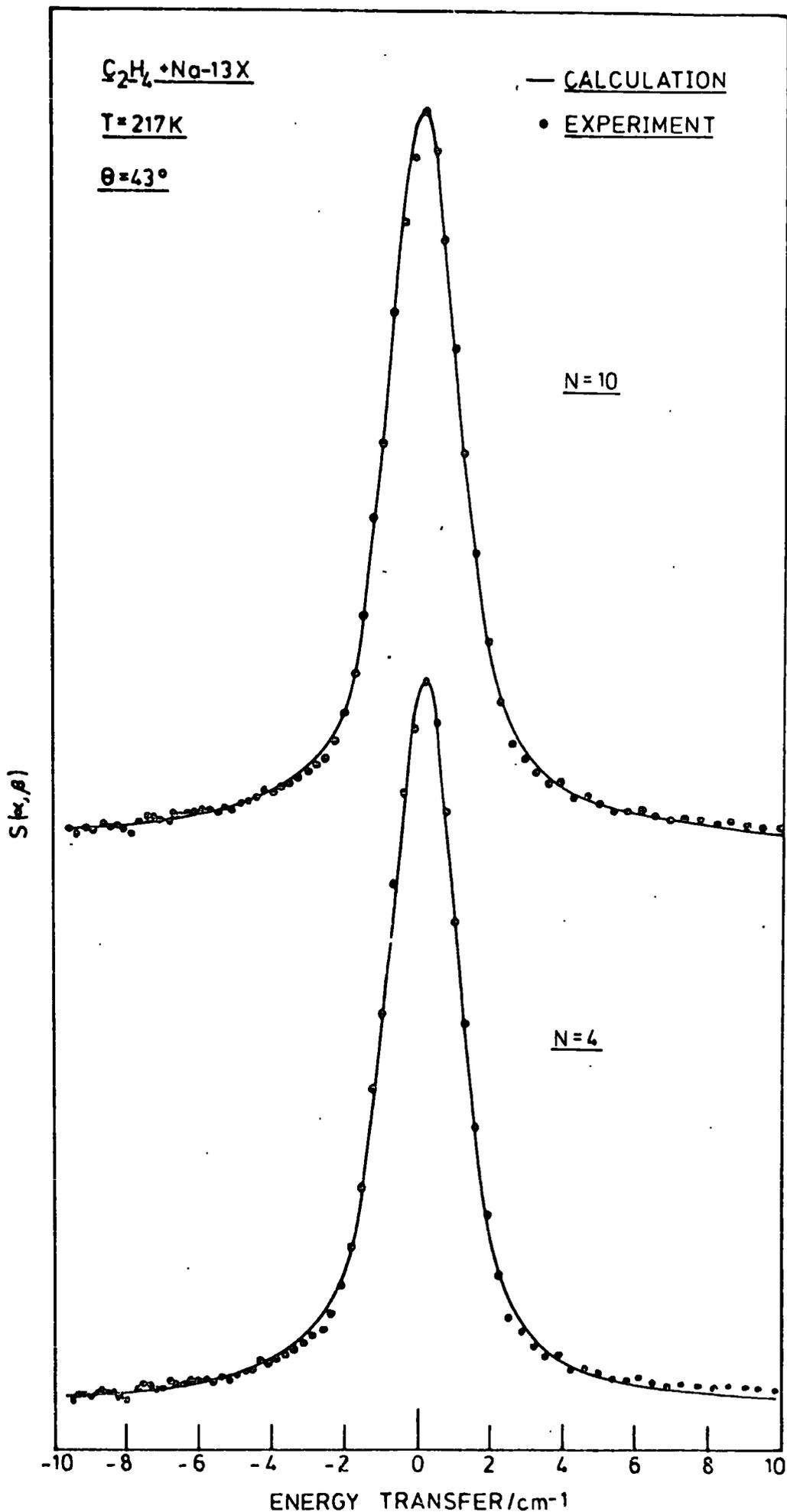
Fig. 21   Theoretical and Observed Quasi-Elastic Lineshapes for

C_2H_4 + Na-13X (43°)
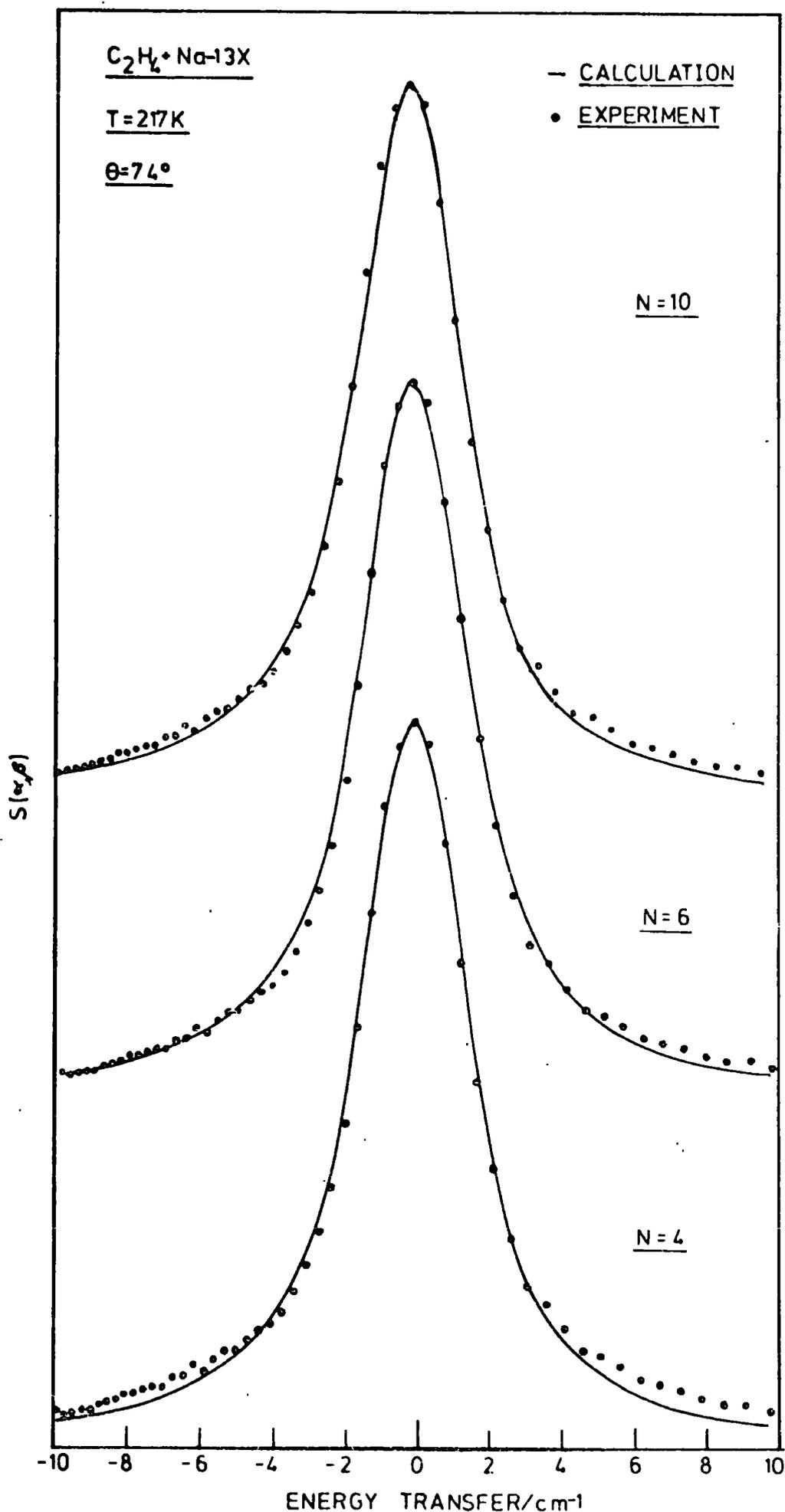
Fig. 22   Theoretical and Observed Quasi-Elastic Lineshapes for
C_2H_4 + Na13X (74°)

There are at least two possible reasons for this variation

1.   Incorrect background subtraction. The subtraction of the correct
background is a notoriously difficult problem in quasi-elastic neutron
scattering. We have plotted values of $S(\alpha, \beta)$ to the smallest (negative)
energy available and to $+20$ cm^{-1} and then simply drawn a straight line
through the wings and taken this to be the background (fig.23). The
difficulty here of course is that there may be some very low energy
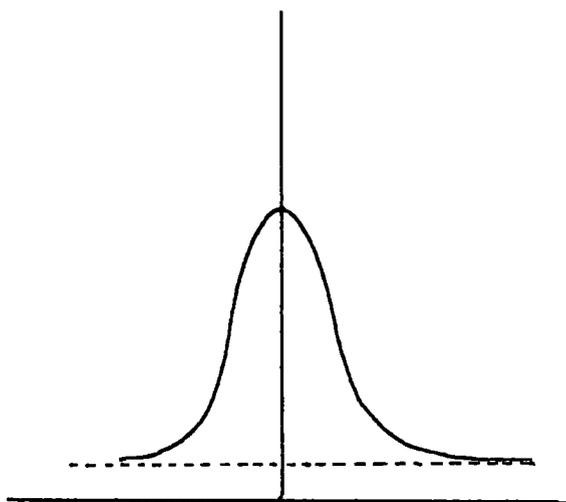
inelastic feature contribut-
ing to the so called back-
ground. In this case we
would be subtracting too high
a value. Although accurate
background subtractions are
vital the correct level of
background is in fact very
difficult to determine.

Fig. 23 Background Subtraction

Changes in the background
level will obviously change the values of τ corresponding to the best
fit.

2.   There may be more than one process contributing to the broadening
of the quasi-elastic peak e.g.

a)   rotation about a different axis

b)   translational diffusion,

and these would have a different Q dependence so that a value of τ
corresponding to a good fit at one angle would not necessarily lead to
a good fit at another angle. We have found it impossible to obtain a
reasonable fit to the data using a model involving rotational diffusion
about the axis joining the carbon atoms.$(N = 2)$. A poor fit was also

obtained with N = 2 for rotation about the C_2 axis. Clearly then rotational diffusion about the C=C axis cannot be the major cause of the broadening though it could contribute to it. Translational diffusion is a very likely possibility in view of the rapid and easy desorption of the gas. A model involving translational diffusion has been used by Egelstaff et al.[41] to analyse the quasi-elastic broadening of CH_3CN, CH_3OH and NH_3 adsorbed on zeolite 3A. Their analysis did, however, involve only measurements of the peak half widths and this is now known to be too insensitive a measure of the peak shape to allow a reasonable test of a model.

Clearly with the data available there is no point in attempting a more sophisticated analysis because for the increasing number of parameters involved we simply do not have enough data. Furthermore it is necessary to stress that we have not made any multiple scattering corrections and that we have used a value of $<u^2>$ calculated from a plot of log (Intensity of quasi-elastic peak) against Q^2 (chapter II). This latter procedure is not strictly valid because as we showed in chapter II, if there is rotational motion present then (ignoring the translational motion)

$$\text{Intensity} = \exp(-Q^2 < u^2 >) \times S_r(Q, \omega)$$

In order to obtain a meaningful straight line it would be necessary to plot $\log_e\left(\dfrac{\text{Intensity}}{S_r(Q, \omega)}\right)$ v.s. Q^2 but of course we do not know $S_r(Q, \omega)$! In a more sophisticated teeatment it would be possible to include $<u^2>$ as a fitting parameter. Also of course we have the difficulty of the Bragg scattering contributing to the quasi-elastic intensity at most of the angles of detection. In fact experience has shown that changing $<u^2>$ by as much as 100% has very little effect on the fitted spectra

provided that $<u^2>$ is not too large (c.a. $> .8\overset{\circ}{A}{}^2$). We used a value for $<u^2>$ of $0.45\overset{\circ}{A}{}^2$.

Conclusions

We can conclude therefore that neither jump nor rotational diffusion about the C=C axis (1) can produce the observed broadening. Rotational diffusion about the axis (2) joining the centre of the C=C bond to the Na^+ ion can account for the broadening as also can several different jump models but there is likely to be a contribution from translational diffusion and perhaps also from motion about the axis (1).

The results therefore support, in some measure, the results from the infra-red study of Yates i.e. for the C_2H_4 - Ag13X system there is hindered rotation about axis 2 but that the rotation about the same axis is much less strongly hindered for the C_2H_4 + Na13X system.

Inelastic Region

As we showed in chapter II the intensity $\left(\dfrac{d^2\sigma}{d_{\Lambda}dE}\right)$ can be expressed as

$$\text{Intensity} \ \alpha \ \frac{k'}{k} \ S_v(\underline{Q}, \ \omega)^* S_r(\underline{Q}, \ \omega)^* S_t(\underline{Q}, \ \omega)$$

where * denotes convolution. As a result the inelastic vibrational components are broadened because of the overall rotational and translational molecular motion. Figs. 18, 19 shows the time-of-flight spectra for Na13X + C_2H_4 at two temperatures and it can be seen that the bands are poorly resolved. Fig. 24 shows the P(α, β) data at 110K for several angles and there are some indications of three features, at $\sim$70, $\sim$110 and $\sim$170 cm^{-1}, with the possibility of a shoulder at $\sim$40 cm^{-1}. The B.F.D. spectrum is shown in fig. 25a and just two bands were observed, at 190 ± 14 cm^{-1} and 98 ± 14 cm^{-1}. There are no further features until above
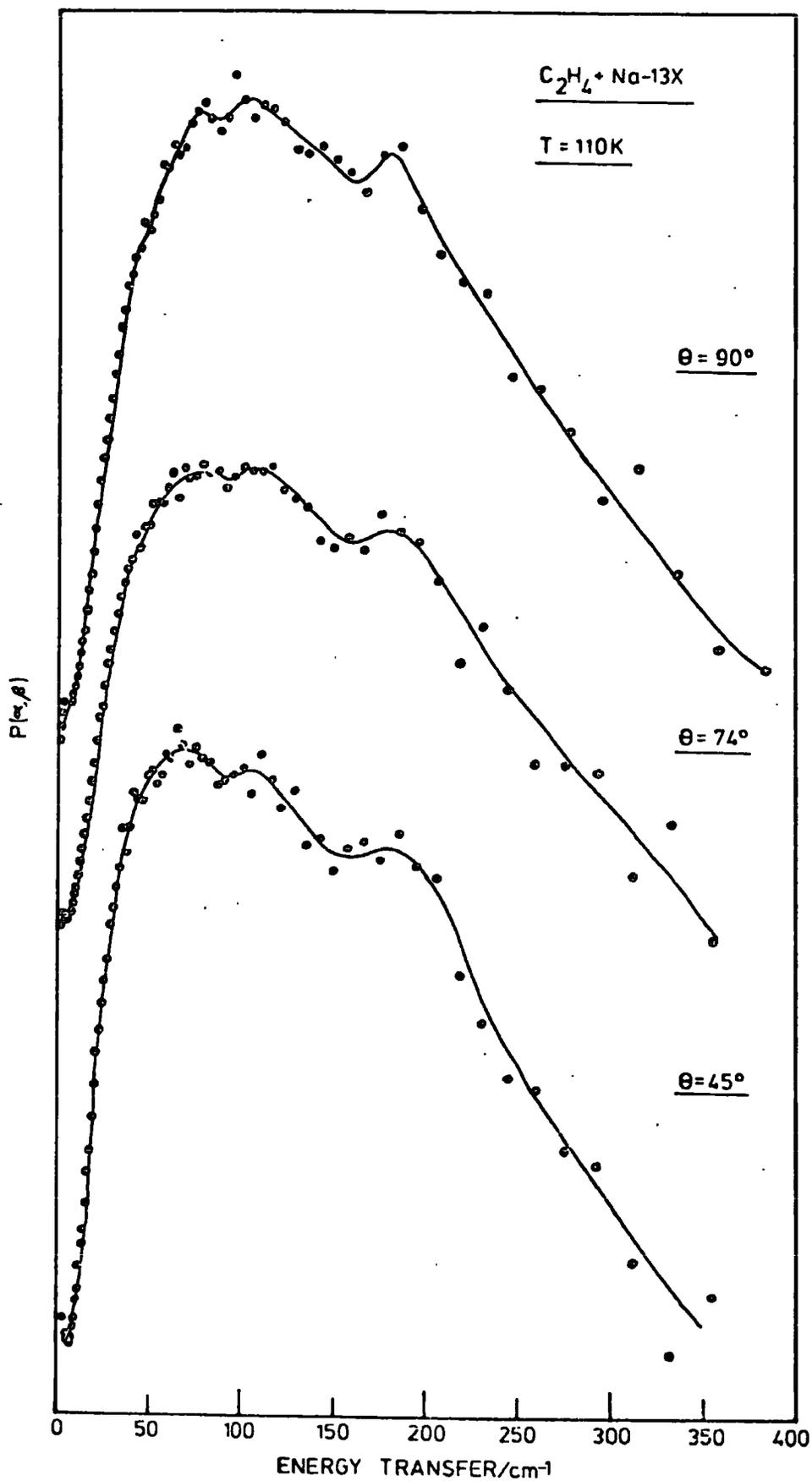
Fig. 24 P(α, β) Data for C_2H_4 + Na13X (110K)
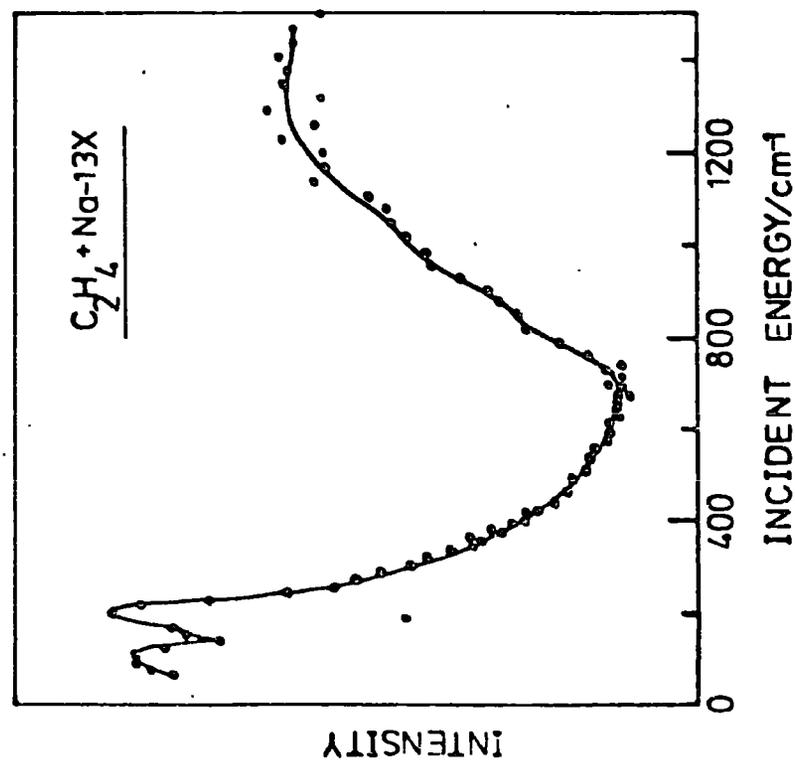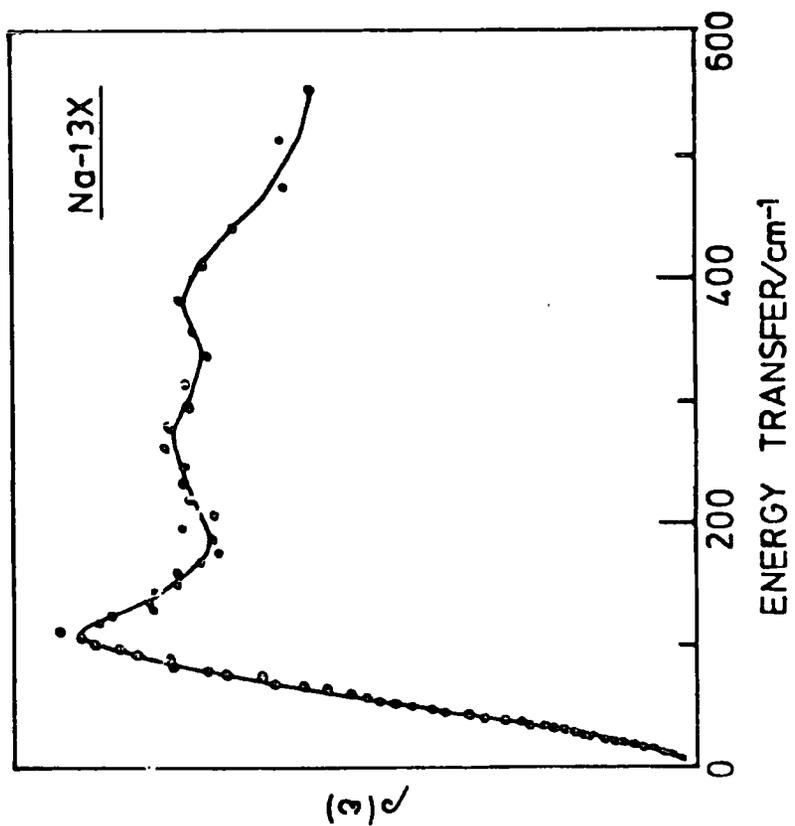
Fig. 25   a)   B.F.D. Spectrum of C_2H_4 + Na-13X

b)   Density of States of Na-13X

800 cm^{-1} where the intramolecular ethylene modes occur. By comparison

with our results for C_2H_4 + Ag13X (table 4) it immediately appears that

τ_3 and τ_2 (fig. 4) have shifted to much lower frequencies.

From the $P(\alpha, \beta)$ data it can be seen that the relative intensities

of the bands at ~ 70 and 110 cm^{-1} vary with angle. At low angles the

70 cm^{-1} band is the more intense and at higher angles the order reverses.

The i.n.s. spectrum of Na13X is shown in fig. 25b, and the most intense

peak occurs at 100 cm^{-1}. It is most prominent at high angles and at low

angles it merges with the remainder of the spectrum which then consists

simply of a broad hump. At least some of this variation in intensity of

the peaks in the sample spectrum can be accounted for by the increasing

intensity of overtones with increasing Q values (see equations 3 and 4).

Significant amplification of the zeolite modes by the adsorbed gas seems

unlikely as this was not observed for the C_2H_4 and C_2H_2 (chapter V and Vl)

+ Ag13X systems where the ligand -zeolite interaction is stronger.

The observed bands are badly resolved and we are not able to obtain

accurate values for the peak positions or the intensities. Without

further data the spectra obtained are not amenable to detailed analysis.

By comparison with our results for C_2H_4 + Ag13X we can perhaps make

some general deductions. We know that we expect intense modes due to

τ_1, τ_2 and τ_3 (fig. 4). The most intense mode in the C_2H_4 + Na13X

spectrum depends on the angle of detection as stated earlier. We can,

however, note that we do not expect any mode in the C_2H_4-Na13X system.
to be of higher frequency than the corresponding mode in the $C_2H_4-Ag13X$ system.
This is borne out by the absence of any band in the region 300 - 450

cm^{-1} (fig. 25a) where τ_3 was found for C_2H_4 + Ag13X. With regard to our

conclusions from the analysis of the quasi-elastic peak we stated in

chapter II that under certain conditions identical results would be

obtained from both random walk and rotational diffusion models. If

we have true rotational diffusion then the rotational levels are completely blurred by interactions between the rotations and the thermal vibrations. In this case we would not expect to see an inelastic feature corresponding to the torsion τ_1. If, however, we have jump diffusion then an inelastic feature can be expected corresponding to transitions (τ) during the librational period (see chapter II). This could be the case in the lowest temperature experiment (110K) where there is a shoulder at c.a. 40 cm^{-1} (90° angle see fig. 24), however, this shoulder could also be a hindered translation and there is no way for us to make a definite assignment. Bands at 70 cm^{-1} and higher frequency cannot be assigned to τ_1 because τ_1 occurs at lower frequency than this in the i.n.s. spectrum of C_2H_4 + Ag13X.

Conclusion

The observed spectra are too badly resolved for definite assignments to be made, however, the 6H spectra do indicate that good spectra could probably be obtained for this system using the IN4 downscattering spectrometer with the samples at liquid helium temperatures.

References

1. J.V. Smith, Minerological Society of America, Special Paper No. 1. (1963).

2. D.W. Breck, Zeolite Molecular Sieves. Wiley Interscience, 1973.

3. Molecular Sieve Zeolites, Advances in Chemistry Series 101, American Chemical Society, Washington, D.C., 1971.

4. Molecular Sieves, Advances in Chemistry Series, 121, American Chemical Society, Washington, D.C., 1973.

5. D.H. Olson, G.T. Kokatailo and J.F. Charnell, Nature; 215, 270, (1967).

6. D.W. Breck, J. Chem. Educ., 41, 678, (1964).

7. J.V. Smith, Reference 3, page 171.

8. W.J. Mortier, H.J. Bosmans and J.B. Uttherhoeven, J. Phys. Chem., 76, 650, (1972).

9. D.J.C. Yates, J. Phys. Chem., 70(11), 3693, (1966).

10. D.W. Breck and E.M. Flanigan, Molecular Sieves, Society of Chemical Industry, London, 1968, p.47.

11. H.S. Sherry, J. Phys. Chem., 70, 1158, (1966).

12. Nguyen The Tam, R.P. Cooney and G. Curthoys, Personal Communication.

13. C.L. Angell, J. Phys. Chem., 77(2), 222, (1973).

14. J.J. P.M. De Kanter, I.E. Maxwell and P.J. Trotter, J.C.S. Chem. Comm., 733, (1972).

15. Ref. 2, page 415 and references therin.

16. I.A. Brodskii, S.P. Zhdanov and A.E. Stanevich, Opt. Specktrosk, 30(1), 58, (1971).

17. P.E. Riley, K.B. Kunz and K. Seff, J. Amer. Chem. Soc., 97(3), 537, (1975).

18. P.E. Riley and K. Seff, Inorg. Chem., 14(4), 714, (1975).

19. A.A. Amaro and K. Seff, J. Phys. Chem., 77(7), 908, (1973)

20. J.L. Carter, D.J.C. Yates, P.J. Lucchesi, J.J. Elliot and

V. Kevorkian, J. Phys. Chem., 70, 1126, (1966).

21. N. Sheppard and D.J.C. Yates, Proc. Roy. Soc. A, 238, 69, (1956).

22. See Ref. 21.

23. G.M. Muha, J.Chem. Phys., 55, 467, (1971).

24. C.M. Muha, D.J.C. Yates, J. Chem. Phys., 49(11), 5073, (1968).

25. J. Chatt, L.A. Duncanson, J. Chem. Soc., 2939, (1953).

26. L.S. Bartell, E.A. Roth, C.D. Hollowell, K. Kuchitsu and J.E. Young Jr,

J. Chem. Phys., 42, 2683, (1965).

27. R.A. Love, T.F. Koetzle, G.J.B. Williams, L.C. Andrews, R. Bau, Inorg.

Chem. 14(11), 2653, (1975).

28. R.E. Ghosh, T.C. Waddington and C.J. Wright, J.C.S. Faraday II, 69,

275, (1973).

29. J. Howard, T.C.Waddington and C.J. Wright, J.C.S. Faraday II, 72,

513, (1976).

30. J. Hiraishi, Spectrochim. Acta., 25A, 749, (1969).

31. J. Chatt and M.L. Searle, Inorg. Synth., 5, 210, (1957).

32. R.M. Barrer and W.M. Meier, Trans. Faraday Soc., 54, 1074, (1958).

33. L.J. Bunce, D.H.C. Harris and G.C. Striling, A.E.R.E. Report

R6246 (H.M.S.O., London, 1970).

34. D.H.C. Harris, S.J. Cocking, P.A. Egelstaff and F.J. Webb, Inelastic

Scattering of Neutrons in Solids and Liquids I, International Atomic

Energy Agency, Vienna, 1963, p.107.

35. P.H. Gamlen, N.F. Hall and A.D. Taylor, A.E.R.E. Harwell, internal

report RRL 74/693.

36. A.H. Baston, A.E.R.E. Report M2570 (H.M.S.O., London, 1972).

37. R.E. Ghosh, A.E.R. E. Harwell, Internal Report RRL 74/552.

38. R.L. Arnett and B.L. Crawford Jr, J. Chem. Phys., 18(1), 118, (1950).

39. M.J. Grogan and K. Nakamote, J. Amer. Chem. Soc., 88, 5456, (1966).

40. N.J. Hance, Unpublished A.E.R.E. Report M2583, 1973.

41. P.A. Egelstaff, J. Stretton Downes and J.W. White, "Molecular Sieves", Society of Chemical Industry Conference, London, 1967.

Chapter VI

<u>I.N.S. Study of C$_2$H$_2$ and C$_2$D$_2$ Adsorbed on Type 13X Zeolites</u>

<u>Introduction</u>

This study follows naturally from our work with ethylene adsorbed on the same zeolites. The present system is rather different, however, because the much more acidic protons on C$_2$H$_2$ compared to C$_2$H$_4$ increases the possibility of direct interaction with the oxide framework.

There are very few simple π-bonded organometallic complexes of C$_2$H$_2$. We have not, so far, obtained the i.n.s. spectrum of any of these. As far as we are aware there has been only one n.m.r. study of a complex containing C$_2$H$_2$.[1] The authors found, from the temperature dependence of the n.m.r. spectrum of (π-C$_5$H$_5$)Cr(CO)(NO)(π-C$_2$H$_2$) in solution, that the C$_2$H$_2$ ligand undergoes a "propeller like motion above room temperature". They derived a value for ΔG of 50-60 kJ mole^{-1}.

Because there is so little I.R. and R. data on simple C$_2$H$_2$ complexes and because we have no i.n.s. data on such complexes we will need to use the results from our study of adsorbed C$_2$H$_4$ to aid in the interpretation of our i.n.s. spectra of adsorbed C$_2$H$_2$ and C$_2$D$_2$.

Section I

Relevant Previous Work

a)   Infrared and Raman Studies

There have been several recent infrared[2,3] and Raman[3] studies of

zeolites containing adsorbed C_2H_2. The observed bands were limited to

intramolecular C_2H_2 modes and in no case was a vibration relative to

the surface observed. Furthermore the zeolites were limited to those

containing alkali or alkaline earth metals.

There are two possible configurations for the adsorbed C_2H_2

involving either

a) "Side-on" interaction with a cation or

b) "end-on" interaction with the oxide framework.

Both configurations have been identified[4] for ethylene adsorbed on

alumina. The hydrogen-bonded form produced an increase in the $C \equiv C$

stretching frequency (2005 cm^{-1}) relative to the gas phase value

(1974 cm^{-1}) while for the "side-on" form this vibration was found at

ca. 1950 cm^{-1}.

From an infrared study of the C-H vibrations of the adsorbed gas

Tsitsishvili et al[2] have proposed the hydrogen-bonded configuration,

for C_2H_2 adsorbed on some A and X type zeolites. However some of their

experiments have been repeated recently[3] and in all cases the

$v_2(C \equiv C$ stretching) vibration has been observed in the infrared and

always at lower frequency than the corresponding mode in the gas phase.

The observed values of v_2 for the adsorbed molecules are in fact close to

the v_2 value for crystalline C_2H_2 (1956 cm^{-1}) (table 1).

Table 1 Spectra[a] of Various Acetylene Phases (cm^{-1})

Mode	Activity	Gas[b]	Liquid[c]	Crystal[d](I)	Adsorbed on NaA	Adsorbed on CaA
ν_1	R	3374	3341	3324	3321	3327
ν_2	R	1974	1961	1956	1953	1957
ν_3	I.R.	3287	-	3226	3205	3214
$\nu_4,\nu_4{}'$	R	612	630	626	642	640
$\nu_5,\nu_5{}'$	I.R.	729	-	760	760	750

a) Ref. 3   c) Ref. 12

b) Ref. 11   d) Ref. 8,9

Gas phase C_2H_2 has $D_{\infty h}$ symmetry and the ν_2 (C $\equiv$ C stretch) vibration is active only in the Raman spectrum. If "side-on" adsorption occurs the symmetry of the system C_2H_2-AgX is at most C_{2v}. The C $\equiv$ C stretch is then an a_1 mode so that is formally both infrared and Raman active.

In the most recent study[3] the authors were able to observe five fundamentals for C_2H_2 on NaA and CaA zeolites but only two were observed on type X. Both the activity, in the I.R. spectrum, of the normally inactive ν_2 and its decrease in frequency on adsorption favour the "side-on" form of interaction with the metal ions. This conclusion is in agreement with the X-ray determinations described in the previous chapter.

The value of v_2 was observed to decrease with increasing cation radius and this is the opposite to what would be predicted from a consideration of polarising power. The authors point out, however, that there are at least three factors influencing the interaction between the C_2H_2 and the zeolite.

1. the degree of shielding of the cation by the framework

2. electrostatic repulsion between the π-electron system of C_2H_2 and the oxide framework

3. electrostatic attraction between the π-system of C_2H_2 and the cation.

The shielding effect of the framework has been found to be important[5] in explaining the significant differences between sites II and III in zeolite X. It has been suggested[6] that while small ions (e.g. Li^+) will probably be stable in the plane of the six-membered oxygen ring (site II) larger ions will probably project into the adsorption cavity. This has been observed for a K-Y and a Tl - A zeolite.[7] Ag^+ is of similar size to K^+ and so similar effects probably occur. This would result in a reduced level of screening for the larger ions and it may compensate for their reduced electrostatic field.

From normal co-ordinate analyses of the systems, values of 46 cm^{-1} (NaA) and 41 cm^{-1} (CaA) were derived for the C_2H_2-cation vibrational frequencies.

The observed values (see table 1) for the intramolecular vibrations of the adsorbed molecules are much closer to those obtained for solid C_2H_2 (phase I) than to the gas phase. The normal

modes are shown in fig. 1.

Fig. 1 Normal Modes of an Isolated linear X_2Y_2 Molecule
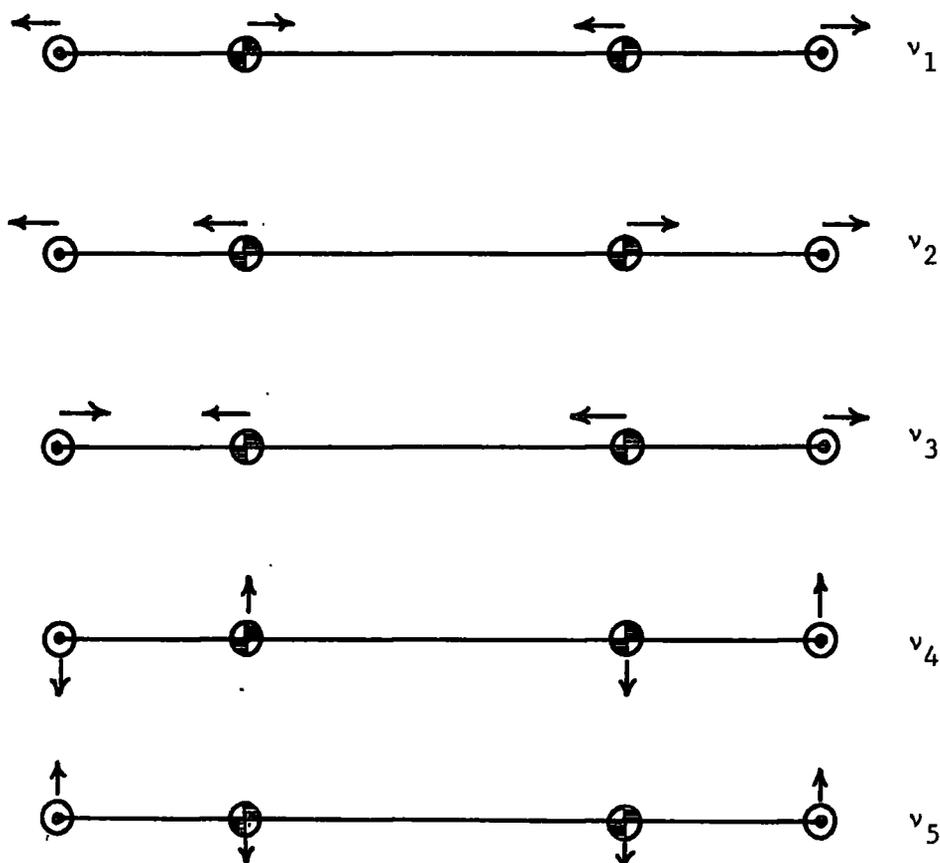
b)   Crystal Structures and Cation Location

These were discussed in chapter V.

Section II

Experimental

The experimental procedures and data analysis were identical to those described for the study of C_2H_4 adsorbed on zeolite 13X (chapter V). Spectra were obtained at only one coverage, corresponding to a pressure of 40 torr of C_2H_2, and at only one temperature on each spectrometer i.e.

a) 136K on the 6H time of flight spectrometer.

b) c.a. 90K on the Beryllium Filter Detector spectrometer (B.F.D.).

Section III

I.N.S. Results for C_2H_2 and C_2D_2 adsorbed on Ag-13X

A summary of the results is given in table 2. Beryllium Filter

Detector Spectra are shown in figs. 2 and 3 and time-of-flight (t.of f.)

spectra in figs. 4 and 5. The t. of f. spectra are more difficult to

interpret than the Beryllium Filter Detector spectra because they

consist of incompletely resolved bands. In order to help in the

problem of locating peak positions with accuracy the spectra from each

of the nine angles of detection were fitted to a smooth curve using

the Harwell routine "DOUGAL", (see chapter III). Some of the results

of this fitting procedure are shown in figs. 6 and 7.

Section IV

Discussion and Assignment

a)   Intramolecular Acetylene Modes

By comparison with the I.R. and Raman results for solid C_2H_2 and

C_2H_2 adsorbed on NaA and CaA (table 1) we can assign the bands at 794

and 673 cm^{-1} in the i.n.s. spectrum of C_2H_2 + Ag13X (fig. 2), to v_4 and

v_5 respectively. The increase in frequency of these bands relative to

solid C_2H_2 is greater than observed on type A zeolites (table 1). Of

the two possible explanations for this, a)   the change of cation and

b)   the change of framework, the former is probably the more important.

Changing from an A to an X type zeolite increases v_2 by only 1 cm^{-1}.[3]

The broad band, with a maximum at 584 cm^{-1}, in the I.N.S. spectrum

of C_2D_2 + Ag13X, is probably unresolved v_4 and v_5. v_5 has been

assigned at 567 cm^{-1} and $2v_4$ at 1057.5 cm^{-1} in the solid phase of

C_2D_2.[8]

Table 2 <u>I.N.S. Results for Acetylene Adsorbed on Ag13X</u> (cm^{-1})

C₂H₂ + Ag13X[†]		C₂D₂ + Ag13X		Assignments	Ratio of frequencies	Predicted Ratio of Frequencies	
B.F.D.[†]	t.of f.	B.F.D.	t.of f.			Non-linear molecule *	Linear molecule
$794^{+}_{-}14$				} Intramolecular modes ν_4 and ν_5			
$673^{+}_{-}14$		$584^{+}_{-}14$			—		
$523^{+}_{-}14$		$380^{+}_{-}14$		τ_3	$.73^{+}_{-}05$	.734	Indeterminate
		(300?)					
$150^{+}_{-}14$		$113^{+}_{-}14$	$102^{+}_{-}6$	τ_2	$.75^{+}_{-}15$	.850	.849
	$53.5^{+}_{-}2.5$		$46^{+}_{-}2.5$	τ_1	$.86^{+}_{-}08$	.850	.849
$86^{+}_{-}14$	$27^{+}_{-}1.5$		$24^{+}_{-}1.5$	τ_1	$.89^{+}_{-}.11$	.850	.849

* C $\equiv$ C as 1.2Å $\widehat{CCH}$ = 170°

  C – H as 1.06Å

† B.F.D. Beryllium Filter Detector

Fig. 2.
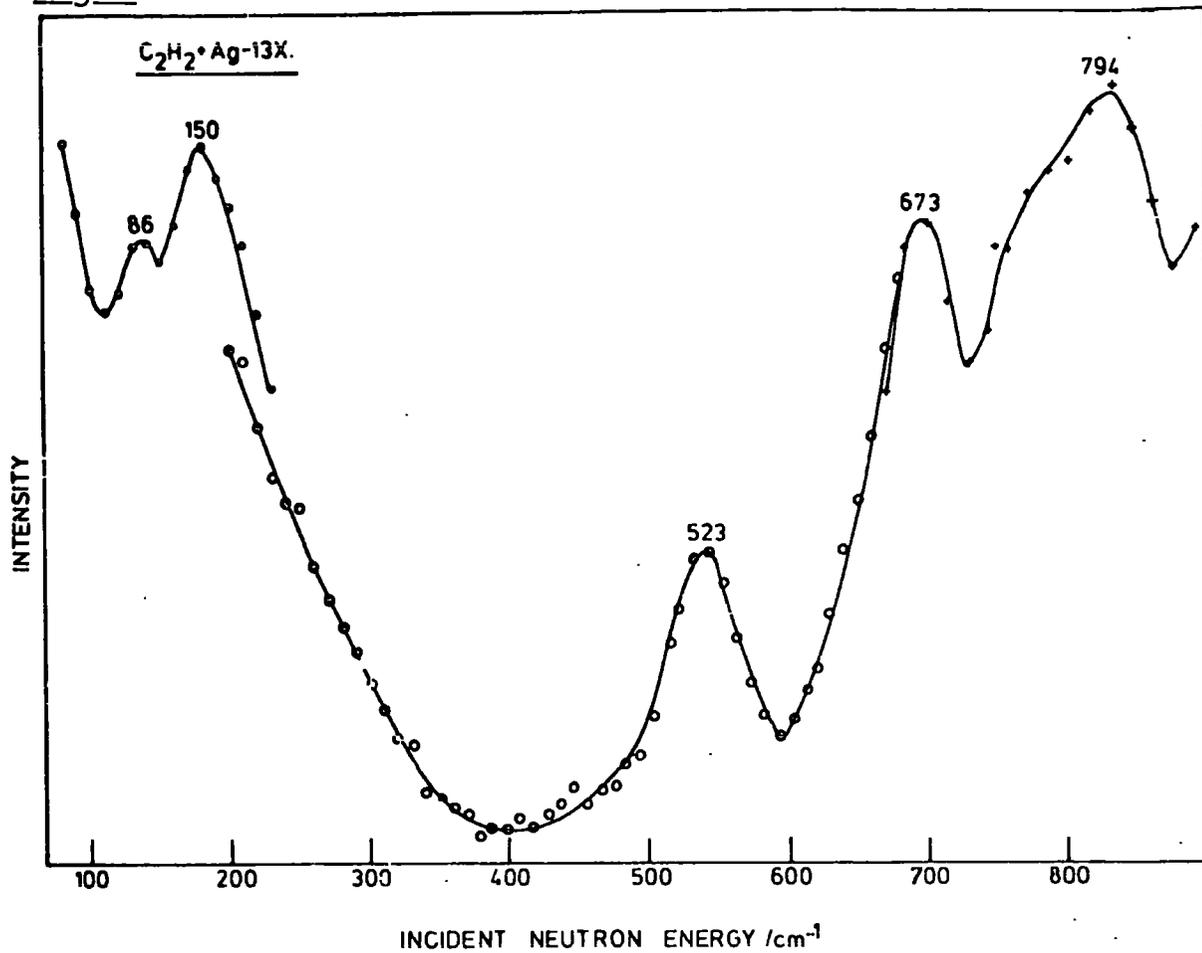
Fig 3.
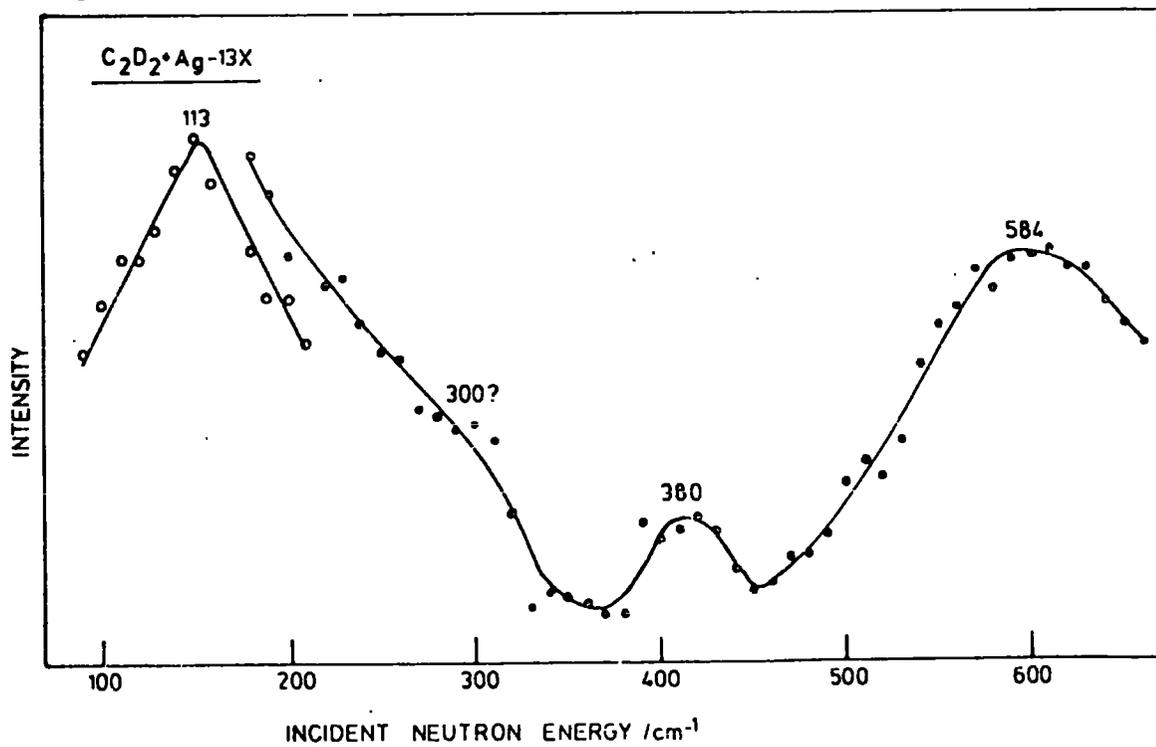
Figs. 2 and 3   B.F.D. Spectra of C_2H_2 and C_2D_2 adsorbed on Ag-13X
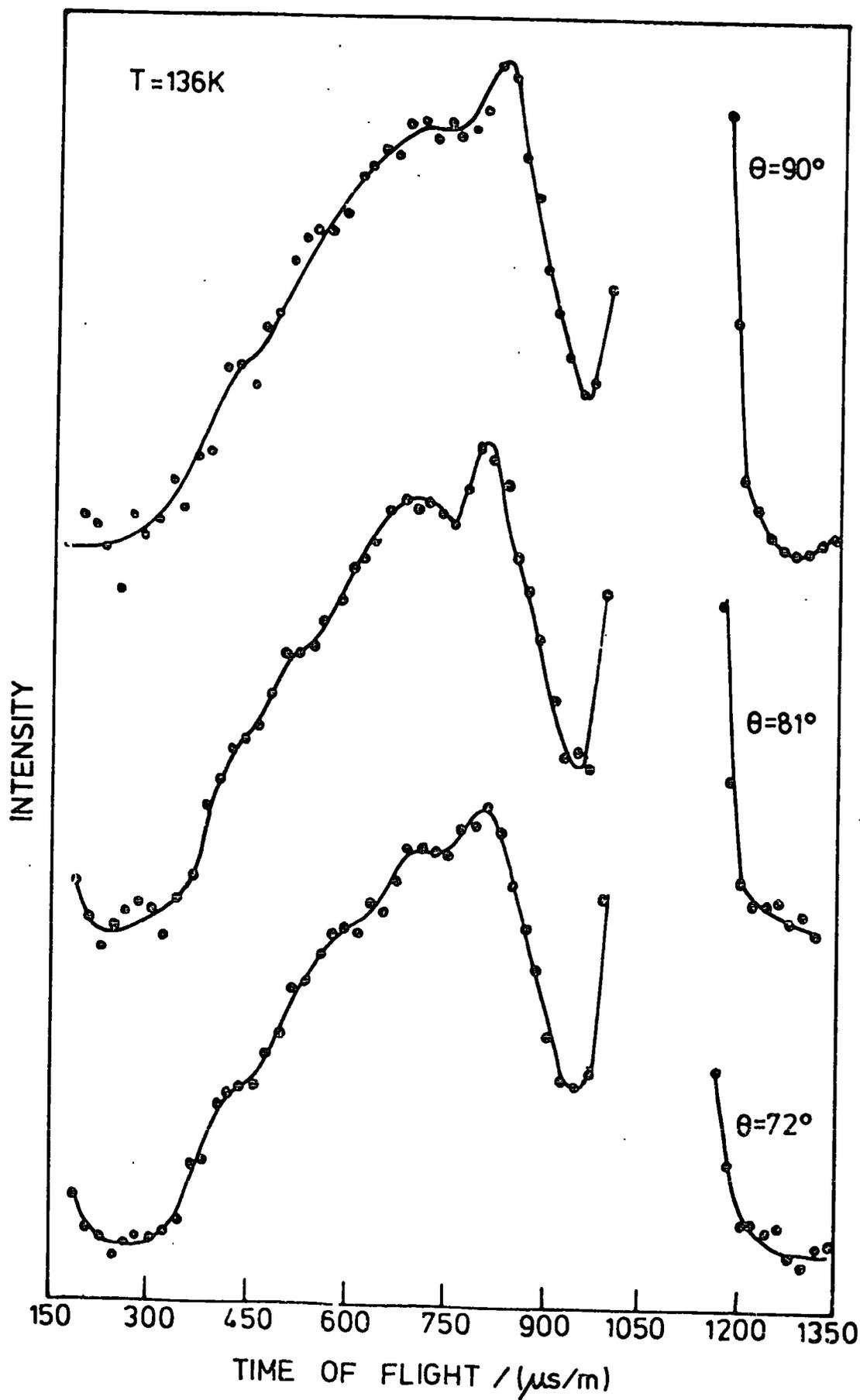
Fig. 4 T.of.F. Data for C_2H_2 + Agl3X
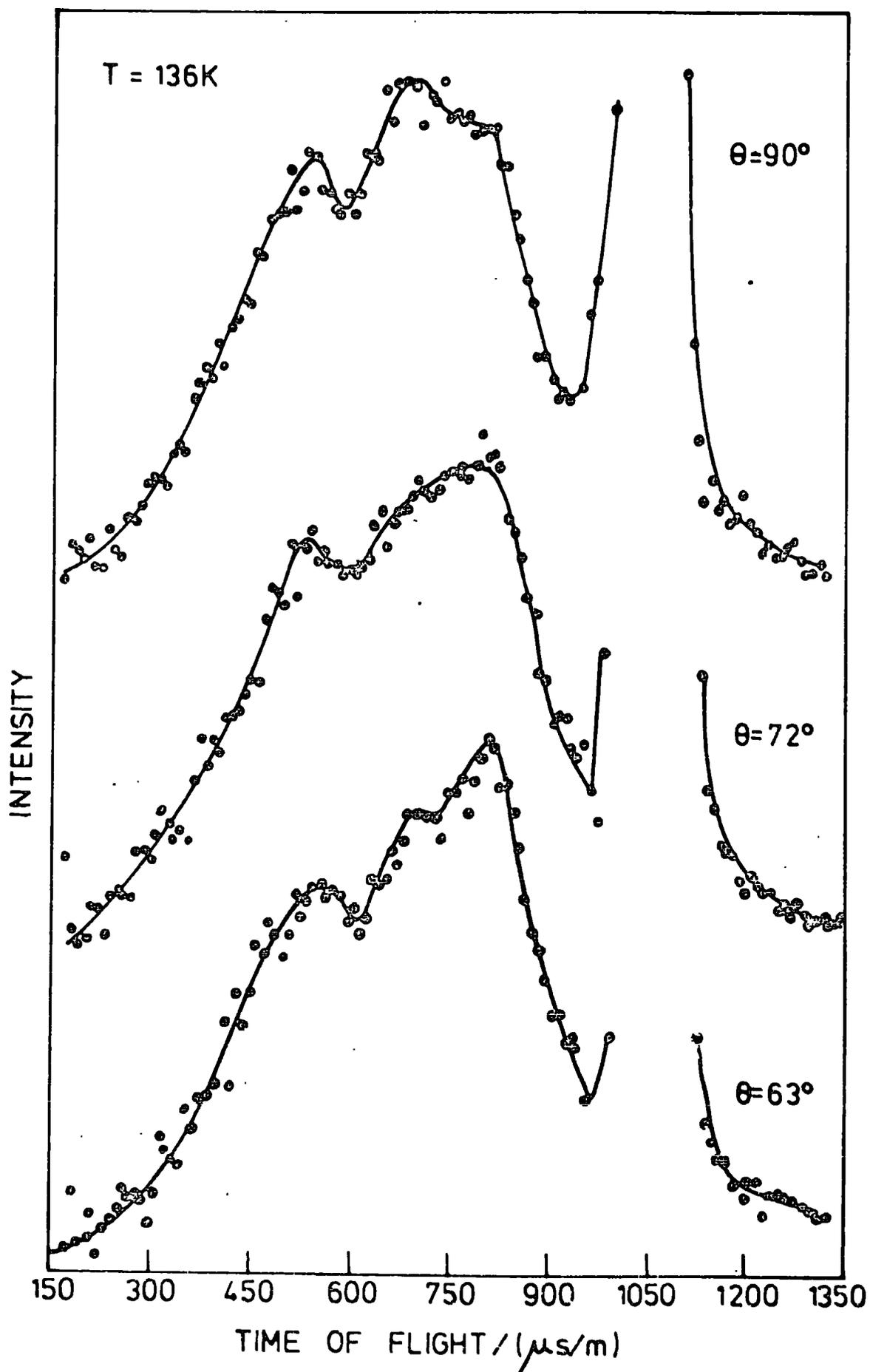
Fig. 5 T.of.F. Data for C_2D_2 + Ag13X

Fig. 7   Computer Fits to the T.of.F. Data for
C_2D_2 + Ag13X

Fig. 6   Computer Fits to the T.of.F. Data for
C_2H_2 + Ag13X
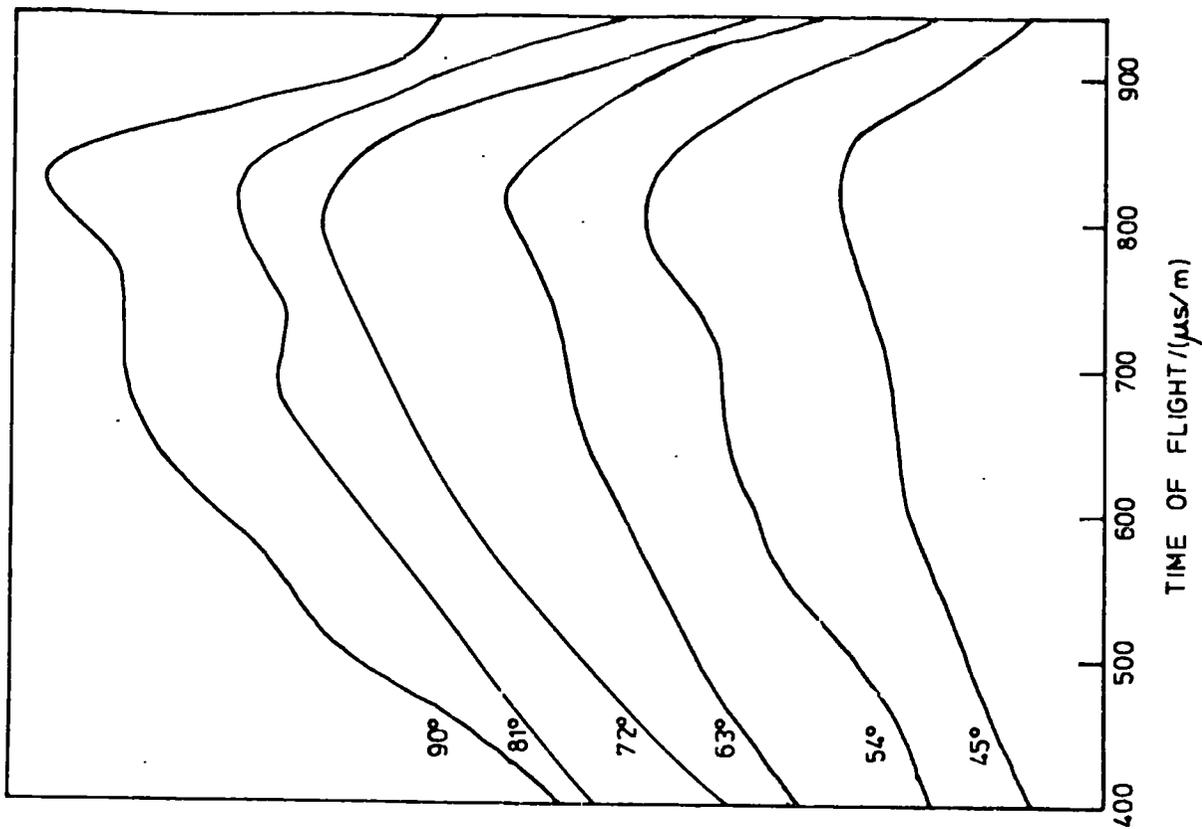
Although each of the bands, ν_4 and ν_5, is degenerate in the gas

phase they should be split into their components in the adsorbed

phase. No actual splittings were observed but the bands were broad.

b)   Acetylene-zeolite modes

There is no adsorption data available for this system but

because the gas pressure is relatively high we would expect all of the

available adsorption sites to be occupied by C_2H_2 molecules, i.e. we

would expect the system to be very similar to C_2H_4 + Ag13X as far as

site occupancy is concerned.

As far as we are aware there are no bands in the region 200 $cm^{-1} \rightarrow$

550 cm^{-1} in the I.R. or Raman spectra of solid C_2H_2 or 200 $\rightarrow$ 400 cm^{-1}

for C_2D_2.[8,9,10,11,12] The peaks at 523 cm^{-1} (C_2H_2 + Ag13X) and 380 cm^{-1}

(C_2D_2 + Ag13X) must therefore be vibrations of the acetylene molecule

relative to the surface. (The six possible vibrations are shown in

fig. 8). It is reasonable to assume that they are the same mode which

has shifted as a result of deuteration. The ratio of their frequencies

is $\left(\dfrac{\nu_{C_2H_2}}{\nu_{C_2D_2}}\right) = .727$. This corresponds very closely to a $1/\sqrt{2}$ shift

(.707) and this is only possible if the carbon atoms contribute very

little (or nothing) to the moment of inertia of the mode. Clearly

there is only one possible C_2H_2-zeolite vibration which can satisfy

this criterion - τ_3 (fig. 8). τ_3 would be of zero frequency if the

adsorbed molecule were linear and hence it appears that the molecule

must be distorted from its gas phase configuration. This is opposed

to the conclusions reached for C_2H_2 on alkali and alkali metal

zeolites,[2,3] however, as pointed out in the previous chapter silver is

able to use its filled "d" orbitals for back donation to acetylene
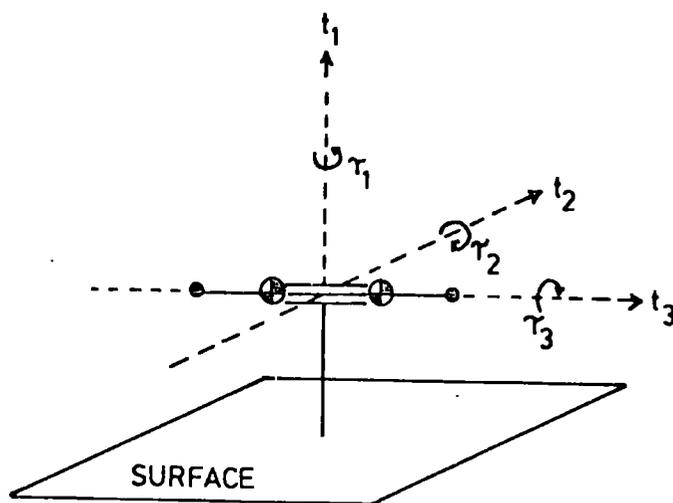
Fig. 8 C_2H_2 to Surface Modes (Notation)
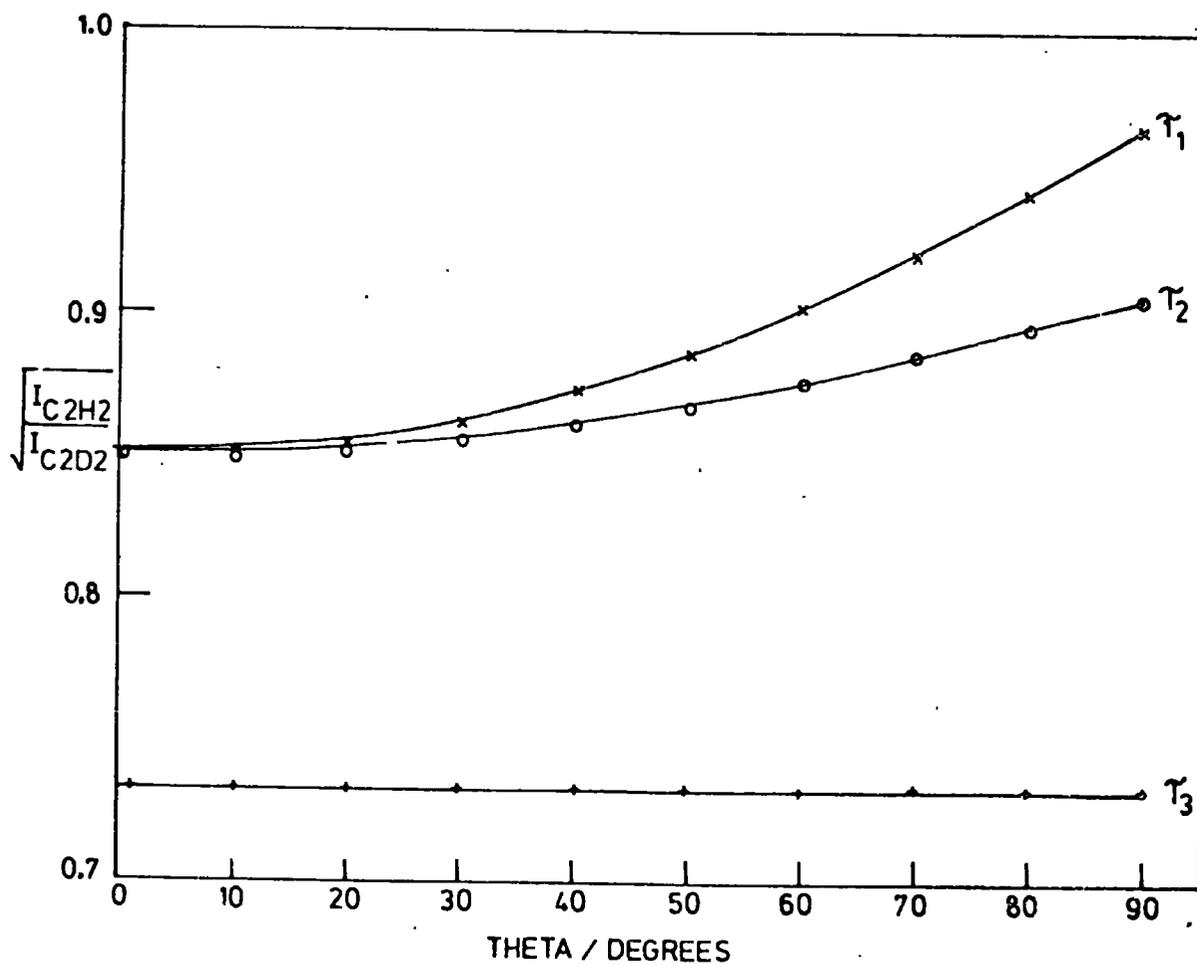
Fig. 9 Variation in Shift on Deuteration with Bond Angle

leading to stronger interactions with the adsorbed gas than are

expected for Na^+ etc. The ratio of the moments of inertia

$$\sqrt{\frac{I_{C_2H_2}}{I_{C_2D_2}}}$$ for mode τ_3 is independent of the angle $\hat{CCH}$ provided it is

non-zero. With C-H as 1.06Å and $C \equiv C$ as 1.2Å the ratio is .7338.

The ratios $\sqrt{\frac{I_{C_2H_2}}{I_{C_2D_2}}}$ for modes τ_1 and τ_2 are shown in table 2 and fig. 9.

Uncertainty in the bond lengths of the adsorbed molecules and the

uncertainty in the positions of the i.n.s. bands makes it impossible

for us to estimate the angle $\hat{CCH}$ from our data.

The observed frequency ratio for the τ_3 mode (.727) is in

excellent agreement with the predicted value (.734). Thus on the basis

of the shifts of deuteration we are able to assign the peaks at 523 cm^{-1}

(C_2H_2 + Ag13X) and 380 cm^{-1} (C_2D_2 + 13X) to τ_3 and to postulate that

the adsorbed molecule is non-linear. The higher frequency of this

mode relative to that observed for adsorbed C_2H_4 (see previous chapter)

may be due to the large difference in their moments of inertia.

The peaks at 150 cm^{-1} (C_2H_2 + Ag13X) and 113 cm^{-1} (C_2D_2 + Ag13X)

may also be assigned to the same mode. Their frequency ratio

$\left(\dfrac{\nu_{C_2H_2}}{\nu_{C_2D_2}}\right)$ is .75 and this is close to the value expected for τ_3, however,

because of the uncertainty of $\pm$ 14 cm^{-1} in the location of the band

centres there is considerable uncertainty ($\pm$ .15) in the value of

this ratio. This is not the case for the higher frequency vibrations

where, because the frequencies themselves are greater, the

uncertainty in the frequency ratio is reduced to .05. The band at

523 cm^{-1} is of higher frequency than all of the C_2H_4 to $PtCl_3$

Although we have no absolute way of distinguishing between modes τ_1 and τ_2, because they have almost identical moments of inertia, the frequency shift on deuteration indicates that the bands at 150 cm^{-1} (C_2H_2 + Ag13X) and 113 cm^{-1} (C_2D_2 + Ag13X) should be assigned to one of them. By comparison with our data for adsorbed C_2H_4 it would appear more reasonable to assign these bands to τ_2 i.e. the antisymmetric stretch is of higher frequency than the C_2 torsion.

The lower frequency bands at 53.5 and 27 cm^{-1} (C_2H_2 + Ag13X) and 46 cm^{-1} and 24 cm^{-1} (C_2D_2 + Ag13X) are more difficult to assign. The frequency shifts are subject to large errors because the centres of the peaks are difficult to determine. Both peaks are, however, definitely shifted to lower frequencies on deuteration. Because the adsorbed molecule is non-linear we would expect six C_2H_2 - zeolite modes i.e. τ_1, τ_2, τ_3 and t_1, t_2, t_3 (fig. 8). Of these our experience with model complexes and C_2H_4 + Ag13X indicates that modes τ_1, τ_2 and τ_3 will be the more intense (table 4). It has also been possible to assign t_1 in previous cases but it has been quite distinct from any other spectral feature. There are then at least three possibilities

a) From the frequency shifts and ratios (tables 2 and 3) we could assign the 53.5 and 46 cm^{-1} peaks to τ_1 and the lower energy peaks to one of the hindered translations (probably t_1).

b) The peaks at c.a. 50 cm^{-1} may be hindered translations and the lower frequency peaks may be τ_1.

c) Because we have no isotherm data for these systems the i.n.s. experiments were carried out at only one coverage (40 torr of C_2H_2). It is possible therefore that we have a situation similar to C_2H_4 + Ag13X i.e. the lower frequency peaks are both τ_1 which has been split by

Table 4   Predicted Relative Intensities for Adsorbed C_2H_2 and C_2D_2

	C_2H_2		C_2H_2	
	Linear molecule	$\hat{CCH} = 170^{\circ}$	Linear molecule	$\hat{CCH} = 170^{\circ}$
τ_1	5.06	5.0	3.97	3.89
τ_2	5.06	5.04	3.97	3.90
τ_3	0.0	12.0	0.0	6.0
t_1, t_2, t_3	1.0	1.0	1.0	1.0

steric hinderance within the supercage.

We consider alternative "c" to be the correct one for two reasons. Firstly the radius of gyration of the protons in C_2H_4 and C_2H_2 are 1.56 and 1.66 Å respectively (gas-phase geometries)so that interaction is even more probable than for adsorbed C_2H_4. Secondly assignment "c" is more acceptable on intensity grounds. As explained earlier the mass sensitive modes are expected to be considerably less intense than the torsions.

Only one spectral feature remains to be assigned - the band at 86 cm^{-1} in the C_2H_2 + Ag13X spectrum. There is no band corresponding to this in the spectrum of adsorbed C_2D_2. If our previous assignments are correct then this must be a mode arising from a hindered translation. Its intensity relative to the τ_2 mode (at 150 cm^{-1}) appears to be of the correct order (table 4), however, because we do not have any indication of the true background level we cannot make accurate quantitative measurements. The corresponding feature for C_2D_2 + Ag13X is perhaps not resolved from the peak at 113 cm^{-1}.

Section V: I.N.S. Results for C_2H_2 adsorbed on Na13X

We have obtained only time-of-flight data for this system (120K).
The frequency distribution and t.of.f. spectra are shown in fig. 10 and
it can be seen that the spectrum is shifted to lower energies compared
to the C_2H_2 + Ag13X system. It is also very poorly resolved. There is
in fact just a single broad band which is peaked at c.a. 130 cm^{-1}. There
are no distinct bands below 600 cm^{-1} and above this the intermolecular
acetylene modes occur. This indicates that either τ_3 has shifted (from
523 cm^{-1} in Ag13X + C_2H_2) to less than 250 cm^{-1} or else the adsorbed
molecule is linear. Because of the expected weaker interaction between
C_2H_2 and Na$^+$ compared to Ag$^+$ we are inclined to the latter view.

In the quasi-elastic region the variation in intensity of the
elastic peak with $\underline{Q}$, relative to the inelastic region is far less
marked than was found for C_2H_4 + Na13X. The elastic peak is broadened
relative to the resolution function of the instrument and once again
this indicates that some diffusive motion is present. We do not have any
structural data for Na13X + C_2D_2 so that further analysis of the broad-
ening is not really justified.

Conclusion

We have assigned the low frequency vibrations of C_2H_2 and C_2D_2 on
Ag13X zeolite. The molecules on the two different adsorption sites
interact and two hindered torsions (τ_1) are observed as a result. From
the observed deuteration shifts we have shown that the adsorbed molecule
is non-linear. Low frequency intermolecular modes of the adsorbed
acetylene molecule have also been assigned.

For the system Na-13X + C_2H_2 no assignments could be made because
the spectrum was poorly resolved.

204.

Fig. 10 T.of.F. and Density of States for C_2H_2 + Na-13X

$\underline{\underline{C_2H_2^+ Na\text{-}13X}}$
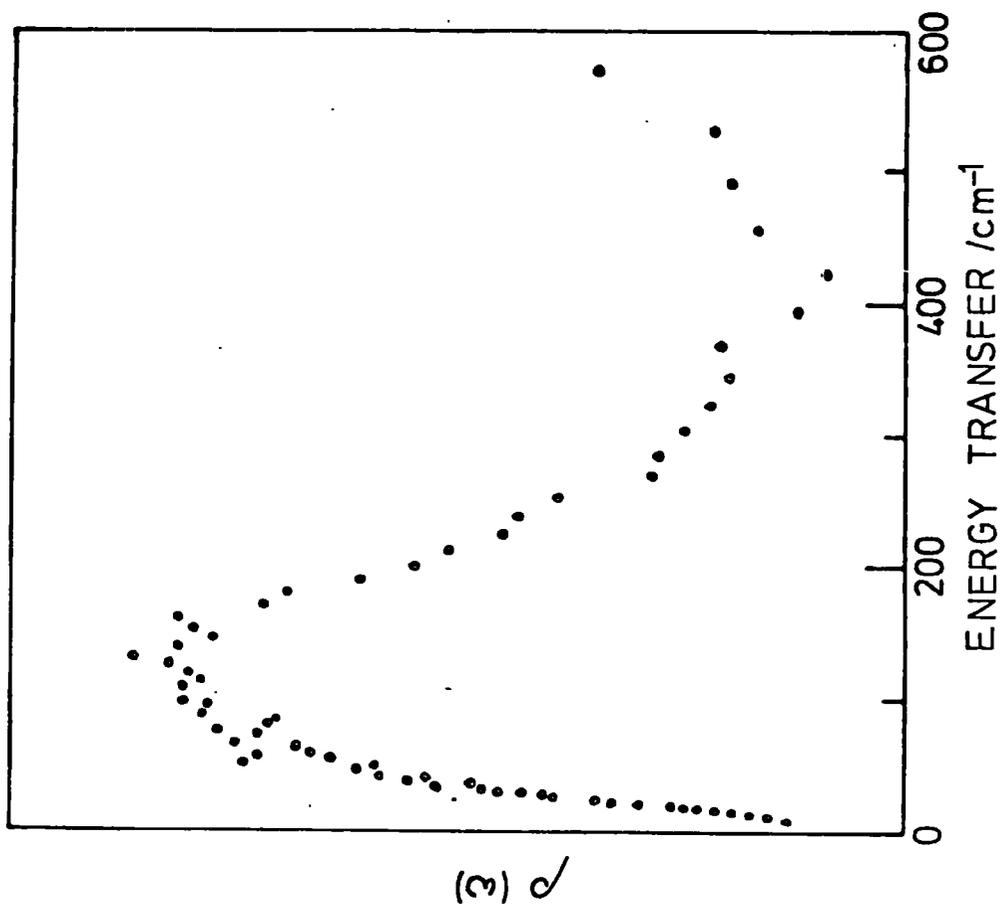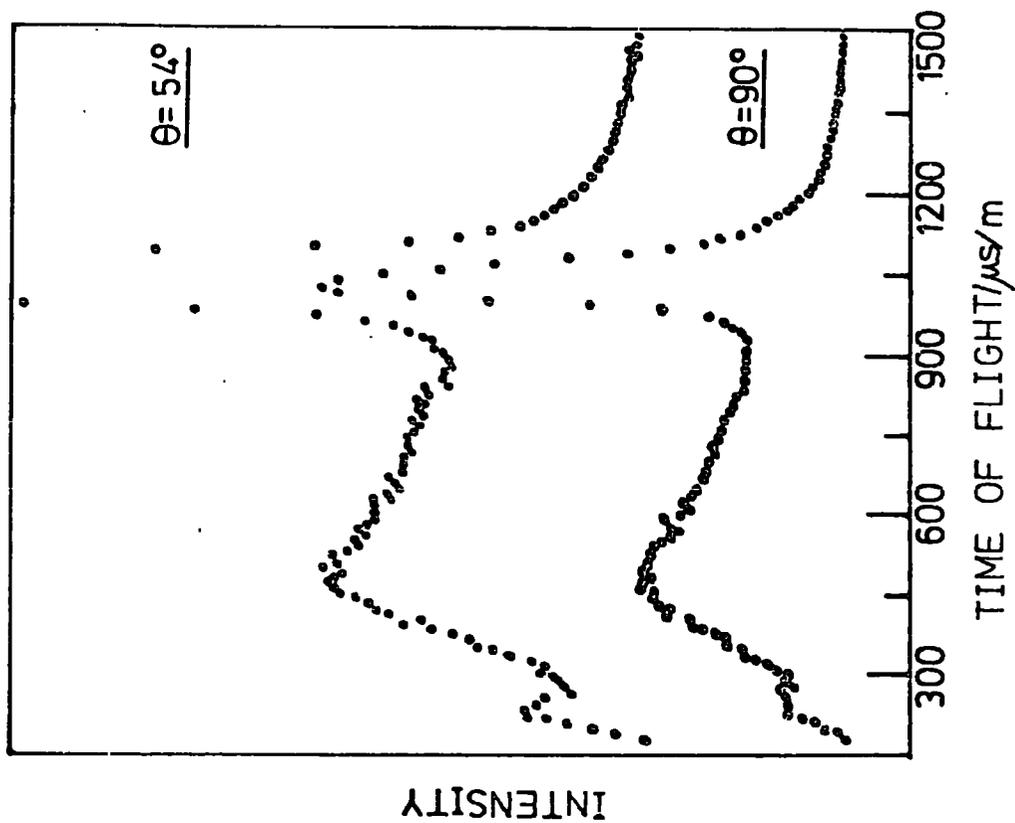
References

1. M. Herberhold, A. Alt and C.G. Kreiter, J. Organometal. Chem.,
   (1972), <u>42</u>, 413.

2. G.V. Tsitsishvili, G.D. Bagratishvili and N.I. Oniashvili, Zh. Fiz.
   Khim., (1969), <u>43(4)</u>, 950.

3. Nguyen The Tam, R.P. Cooney and G. Curthoys, Personal communications.

4. D.J.C. Yates and P.J. Lucchesi, J. Chem. Phys. (1961), <u>35</u>, 243.

5. J.A. Rabo, C.L. Angell, P.H. Kasai and V. Schomaker, Disc. Faraday
   Soc., (1966), <u>41</u>, 328.

6. H.W. Hapgood, Canad. J. Chem., (1964), <u>42</u>, 2340.

7. T.B. Reed and D.W. Breck, J. Amer. Chem. Soc., (1956), <u>78</u>, 5972.

8. G.L. Bottger and D.F. Eggers, J. Chem. Phys., (1964), <u>40</u>, 2010.

9. M. Ito, T. Yokoyama and M. Suzuki, Spectrochim. Acta., (1970), <u>26A</u>,
   695.

10. A. Anderson and W. Hayden Smith, J. Chem. Phys., (1965), <u>44</u>, 4216.

11. G.Hertzberg, Infrared and Raman Spectra of Polyatomic Molecules,
    Von Nostrand, New York, (1945), p.288-290.

12. G. Glocke and M.M. Renfrew, J. Chem. Phys., (1938), <u>6</u>, 340.

Chapter VII : Organometallic Complexes Containing π-bonded Ligands

Introduction

There is considerable interest in the dynamic complexes now known to

be so common in organometallic chemistry. We have studied three types

of complex, two of which continue our work on olefin systems and we have

also studied some π-allyls. As explained earlier (chapter 1) it has been

suggested that π-allyl groups are formed on adsorbing many materials onto

metal surfaces. The experience and results gained as a consequence of

our study of these complexes should then be helpful when we come to study

more complex adsorbed species.

The i.n.s. method is not subject to electromagnetic selection rules

so that all modes involving hydrogen motion are "active". This can have

its disadvantages if the modes of vibration occur close together

because the resolution of i.n.s. spectrometers is poor by the standards

of i.r. and Raman spectroscopy (however, see chapter III). There are

cases, however, where optical spectra (particularly Raman) are difficult

or impossible to obtain because of sample decomposition in the beam e.g.

$[C_3H_5NiBr]_2$.[1] Also, selective deuteration can be difficult e.g. π-allyls,

C_7H_8 complexes, so that full assignments using i.r. and Raman are

difficult to make. Finally, of course, some normal modes are formally

i.r. and Raman inactive and others only weakly so e.g. hydrocarbon-

metal torsions and deformations. These modes are often associated with

intense i.n.s. bands.

One cannot decide the symmetry of a mode from an i.n.s. spectrum

unless there are very different intensities i.e. very different

amplitudes of vibration of the protons in the different modes. Basically

this means that assignments based solely on i.n.s. spectra can be

difficult even with the help of deuteration experiments. It is very rarely the case, however, that only i.n.s. data is available and so from a combination of i.n.s. and other spectroscopic data, as available, it is usually possible to obtain reasonably complete assignments for the lower energy vibrations.

Section I: $C_4H_4Fe(CO)_3$

Electron diffraction investigations of cyclobutadiene iron tricarbonyl have shown that the C_4 ring is square[2,3] and this indicates that there is extensive delocalisation around the ring. We have found that, unlike $(\pi-C_5H_5)_2Fe$,[4] there is no diffusive motion in the solid state and this implies that the barrier to rotation is higher than in ferrocene.

The vibrational spectra of $C_4H_4Fe(CO)_4$ has been studied using both Raman and i.r.[5,6] spectroscopy. The assignments were made on the basis of the local symmetry of the (C_4H_4)-$Fe(C_{4v})$ and $Fe(CO)_3(C_{3v})$ units. Table 1 lists the formal infrared and Raman activities of these fragments.

Table 1   I.R. and R. Activities of the Species of the C_{4v} and C_{3v} Groups

Activity	C_{4v}	C_{3v}
i.r. active	A_1, E	A_1, A_2, E
Raman active	A_1, B_1, B_2, E	A_1, A_2, E
Inactive	A_2	A_2

A normal co-ordinate analysis (N.C.A.) has also been carried out[7] and there appears to be good agreement between the predicted and observed

frequencies. We have also obtained the solid phase far-i.r. and Raman

spectra (table 2). The far infrared spectrum has not previously been

published and our solid-phase Raman agrees reasonably well with the

published data.

Experimental

Inelastic neutron scattering spectra were obtained using the 6H

time-of-flight[8] (sample temperature -140°C and 1°C) and Beryllium

Filter Detector (sample temperature c.a. 90K) spectrometers.[8] The far-

infrared spectra were obtained at Liq. N_2 temperature using a Beckman-

RIIC FS720 Fourier Transform spectrophotometer.[8] The sample was

sublimed onto a polythene disc in the i.r. cell. The Raman spectrum

was obtained using a Cary 82 Laser Raman Spectrophotometer[8] and a wave-

length of 632.8 nm with 6mW power at the sample. In this case the

sample was sublimed onto a copper block.

Results and Discussion

The i.n.s., Raman and i.r. results are listed in table 2 and the

neutron spectra are shown in figs. 1 and 2. Fig. 3 is a plot of the

vanadium and $C_4H_4Fe(CO)_3$ quasi-elastic peaks at a scattering angle of

90°, for the spectrum obtained at 1°C. The other eight angles of

detection show identical results i.e. there is no significant broadening

of the quasi-elastic peak in the sample spectrum. This is very different

from the results found for ferrocene where significant broadening was

observed.[4] The absence of broadening indicates the absence of

diffusive motion (chapter II) and so we would therefore expect to find

a mode in the i.n.s. spectrum which corresponds to the A_2 torsion about

the C_4 axis. The spectra obtained using the t. of f. spectrometer

Table 2 Spectroscopic Data for $C_4H_4Fe(CO)_3$ [a]

Raman	I.R.	I.N.S.	Assignment
7			
16			
34			
54			
59	63	60 ± 3	C_4H_4 torsion (A_2)
70	71		
	77		
93	84	85 ± 5	$\delta(C-Fe-C)$ (E)
104	102vw		$\delta(C_4H_4-Fe-(CO)_3)$ (E)
	115		
126	119		
	142		
148	147	145 ± 10	$\delta(C-Fe-C)$ (A_1)
406			
429		422 ± 14	$\nu(C_4H_4-Fe)$
441			
475		514 ± 14	Ring tilt
517			
608		595 ± 14	
645			
776			
798			
831			
838			
936			
956			
1228			
1238			
1288			
1323			
1381			
1912			
1928			
1935			
1942			
1956			
1988			
2034			
3107			
3122			
3125			
3156			

a) Solid phase - this work
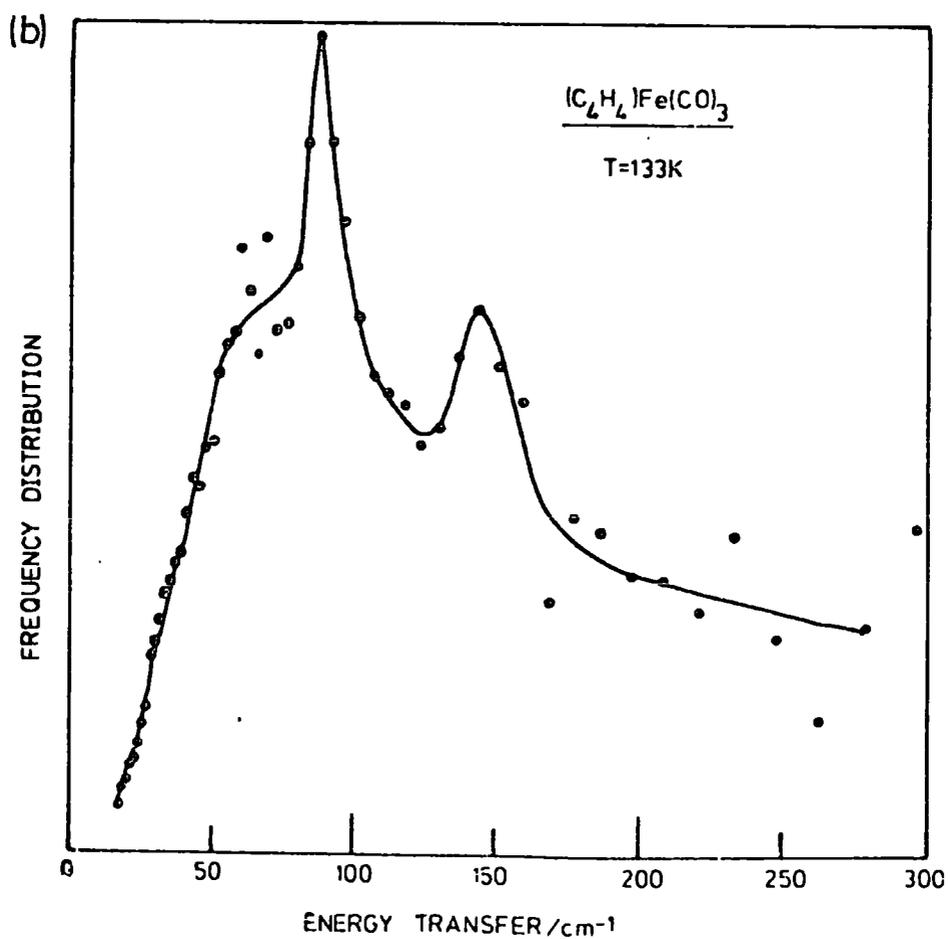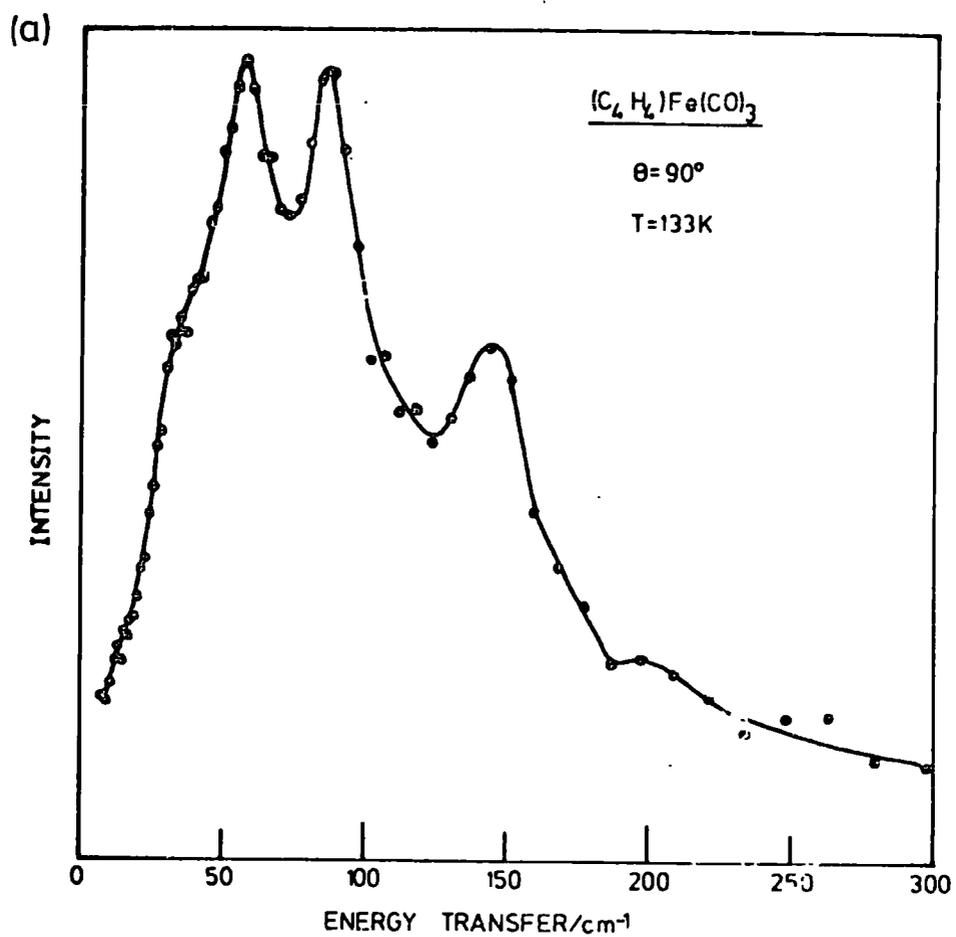
Fig. 1 Time of Flight Spectra of $C_4H_4Fe(CO)_3$

Fig. 2 B.F.D. Spectrum of $C_4H_4Fe(CO)_3$

$(C_4H_4)Fe(CO)_3$

INCIDENT NEUTRON ENERGY/cm^{-1}

INTENSITY
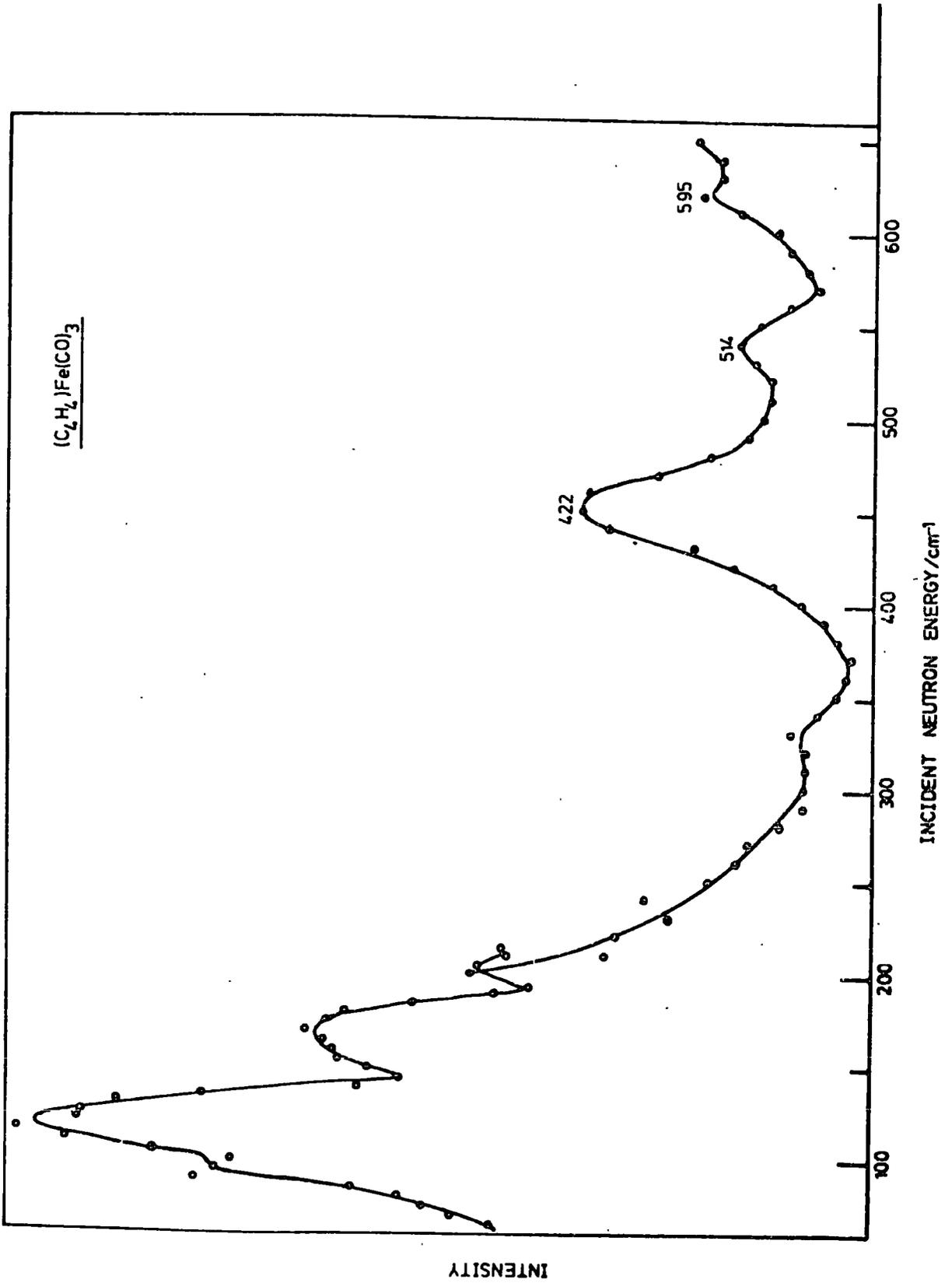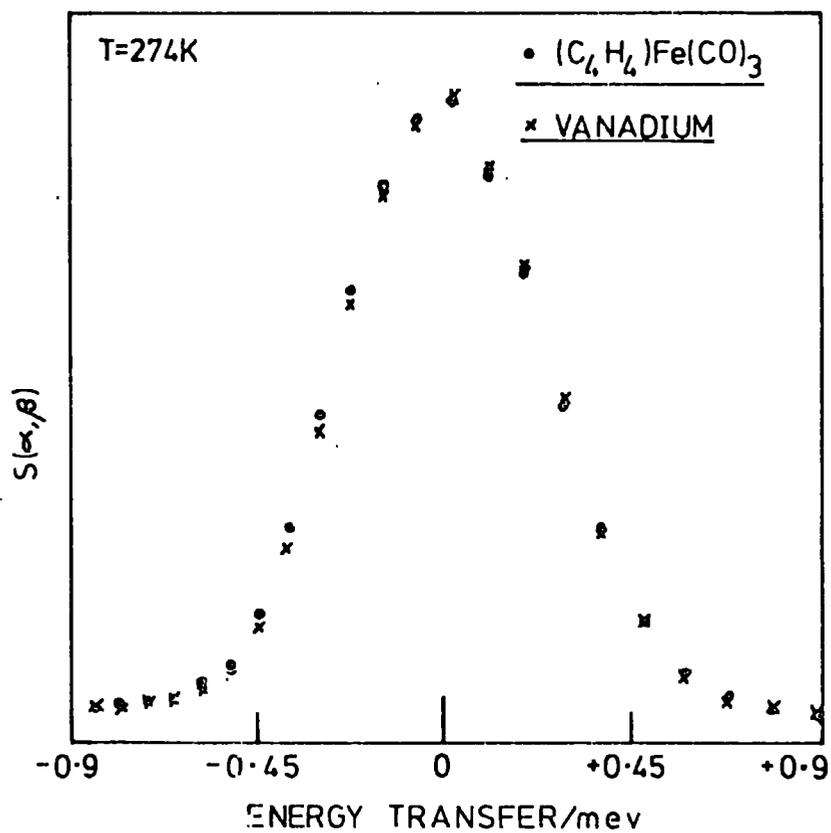
Fig. 3 Quasi-Elastic Peak for $C_4H_4Fe(CO)_3$ and V (90°)

Torsion   Tilt   Stretch   Deformation
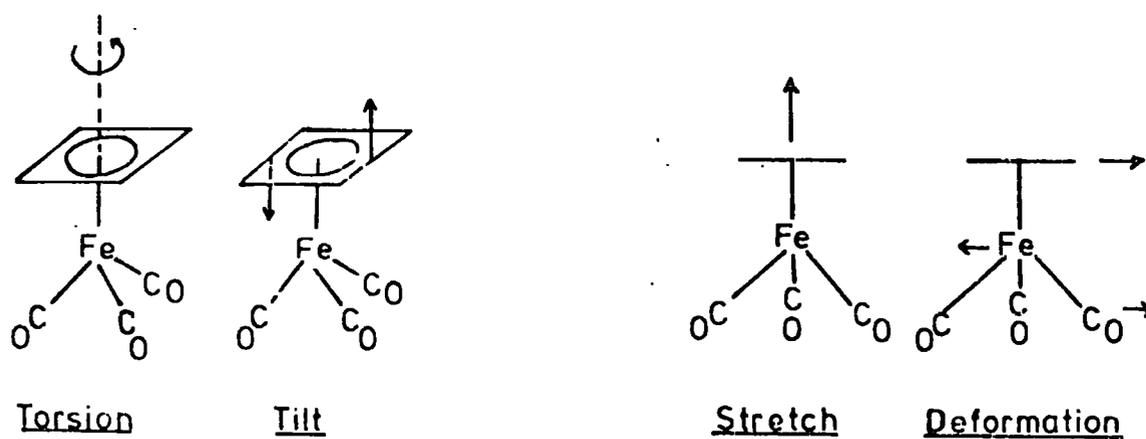
Fig. 4 Some normal modes of $C_4H_4Fe(CO)_3$

(fig. 1a,b) contain three peaks, at 60 ± 3, 85 ± 5 and 145 ± 10 cm^{-1}. A polarised band at 135 cm^{-1} in the Raman spectrum of the liquid has been assigned to the A_1 C-Fe-C deformation.[5] We have found infrared and Raman bands in the solid at 147 and 148 cm^{-1} respectively and so we assign these bands and the i.n.s. band at 145 cm^{-1} to this A_1 mode in the solid state. Some of the normal modes of $C_4H_4Fe(CO)_3$ are shown in fig. 4. Two further bands have been assigned in the low energy region viz. the C-Fe-C and C_4H_4-Fe-(CO)$_3$ deformations at 104 and 94 cm^{-1} respectively in the Raman spectrum of the liquid.[5] However, the N.C.A. indicates that these assignments should be reversed.[7] Both are E modes. We have observed i.r. bands at 84 and 102 cm^{-1} and Raman bands at 93 and 104 cm^{-1}. There is a strong band in the i.n.s. spectrum at 85 cm^{-1}, however, there is no indication of a band at 104 cm^{-1}. It is possible that the C-Fe-C deformation mode is not resolved from the peak at 85 cm^{-1} particularly if this mode is of low intensity.

We are left therefore with a band at 60 cm^{-1} in the i.n.s. and corresponding bands at 59 and 63 cm^{-1} in the Raman and i.r. spectra. We assign these to the torsion about the C_{4v} axis. This assignment is compatible with the expected intensity of the i.n.s. band and because the band shows no momentum transfer dependence it is unlikely to be a lattice mode. Furthermore, there are no bands below 94 cm^{-1} in the Raman spectrum of the liquid. It therefore appears that there may be free rotation in the liquid phase and an i.n.s. spectrum of the liquid phase would establish whether or not this were true. A nematic phase n.m.r. study of $C_4H_4Fe(CO)_3$[9] has shown that the C_4H_4 ring is rotating relative to the carbonyl framework. The ratio of the moment of inertia of the C_4H_4 unit about the axis through the iron atom to that of the (CO)$_3$ unit about the same axis is c.a. 1:4.5.

The remaining bands in the i.n.s. spectrum are at 422 ± 14, 514 ± 14 and 595 ± 14 cm^{-1}. The C_4H_4-Fe stretch has been assigned at 399 cm^{-1} and the ring tilt at 472 cm^{-1}. These most probably correspond to the two i.n.s. bands at 422 and 514 cm^{-1} respectively. A Raman band at 606 cm^{-1} has been assigned either as a formally forbidden A_2(Fe-C-O deformation) or as a combination band (514 + 94 cm^{-1}).[5] The N.C.A.[7] places the A_2(Fe-C-O) mode at 531 cm^{-1} (Aleksanyon and Nefedova observed a weak band at 524 cm^{-1} at -180°C) and in view of the intensity present at 595 cm^{-1}, in the i.n.s. spectrum, it appears that there is some proton motion associated with this mode and so this indicates that it may be a combination band.

More bands are observed in the Raman spectrum of solid C_4H_4Fe(CO)$_3$ than for the liquid phase. In particular only one ν(C-H) mode was found for the liquid whereas there are four in the solid (predicted A_1+B_1+E). There are also additional modes in the 1200-2000 cm^{-1} region (table 2) and some lattice modes below 50 cm^{-1}.

The description of the vibrational modes of C_4H_4Fe(CO)$_3$ in terms of the local symmetries C_{4v} and C_{3v} is very useful. However, in practice the torsion of the C_4H_4 ligand about the axis through the iron atom is hindered and this means that the maximum symmetry of the molecule is C_s. Therefore all modes should be both i.r. and Raman active. If, as it appears, the C_4H_4 rotates in the liquid phase then it appears likely that intermolecular forces contribute more to the barrier to the C_4 torsion than do intramolecular forces.

Barrier Calculations

We can use the observed torsional frequency to calculate the external barrier to the torsion. The moment of inertia of the C_4H_4

ligand about the axis through the metal atom was calculated to be
114×10^{-40} g cm^2. If we assume the barrier multiplicity to be four
then using the approximation due to Das (with three terms) (chapter II)
we obtain 8.8 kJ mole^{-1} (742 cm^{-1}) as the barrier height. We can
compare this with an identical calculation for ferrocene using the
assignment of 44 cm^{-1} to the torsional mode[46] and a moment of inertia
of one ring about an axis through the metal atom of 193.7×10^{-40} g cm^2.[47]
In this case the barrier multiplicity was taken as five and the result
was 6.7 kJ mole^{-1} (559 cm^{-1}). As we suggested earlier the torsional
barrier is somewhat higher for $C_4H_4Fe(CO)_3$ than for $(\pi-C_5H_5)_2Fe$.

Section II: 2.2.1.   Bicyclohepta 2,5 diene (norbornadiene) Complexes

of some Transition Metals

Introduction

We have obtained i.n.s., Raman and i.r. spectra of the norbornadiene

complexes, $C_7H_8X(CO)_4$ (X = Cr, Mo, W), $C_7H_8YCl_2$ (Y = Pd or Pt) and

$Cs(Ru CO Cl_3 C_7H_8)$. Although some of these have been studied previously

by optical spectroscopy, their spectra are very complex and the assign-

ments are incomplete. This is perhaps partly due to the lack of

availability of partially deuterated C_7H_8. In particular the low

frequency modes associated with the C_7H_8 ligand have, except for the two

stretches, not been assigned or are tentative. The low frequency region

is the region of particular interest to us.

Butler and Barna[10] have reported i.r. (4000 → 250 cm^{-1}) and complete

Raman data for the carbonyl complexes. They have assigned the symmetric

and antisymmetric C_7H_8-Metal stretches in the region of 250 cm^{-1} and it

is interesting that for the chromium complex polarised Raman data

indicates that the frequencies of these modes are in the reverse order

from that usually found. These complexes have also been studied by

Carbuzova et al.[11] and their results are in agreement with those of

Butler and Barna. The Cr and Pd complexes have been investigated (i.r.

and Raman) by Fernando and Adams[12] who have assigned the two M-olefin

stretches and tentatively assigned several of the low frequency

vibrations associated with the C_7H_8 ligand. The spectra (i.r. and

Raman) of C_7H_8 have been studied by Butler and Barna and Fernando and

Adams and by several other authors.[13,14]

The new data that we are presenting is

1. i.n.s. spectra of all of the complexes.

2. Far infrared spectra of the Mo, W, Ru and Pt compounds.

3. Near infrared and Raman spectra for the Ru complex.

4. i.n.s. spectra of C_7H_8.

Vapour phase electron diffraction studies[15,16] of C_7H_8 have shown that is has approximately C_{2v} symmetry. The crystal structures of $[(C_7H_8)Cu\ Cl]_4$[17] and $[(C_7H_8)Pd\ Cl_2]$[18] have been determined and they confirm that the ligand retains approximately C_{2v} symmetry on co-ordination. The assignments have all been based on the reasonable assumption that the ligand, in all of the complexes, is bonded to the metal atom via the two C=C double bonds (fig. 5).
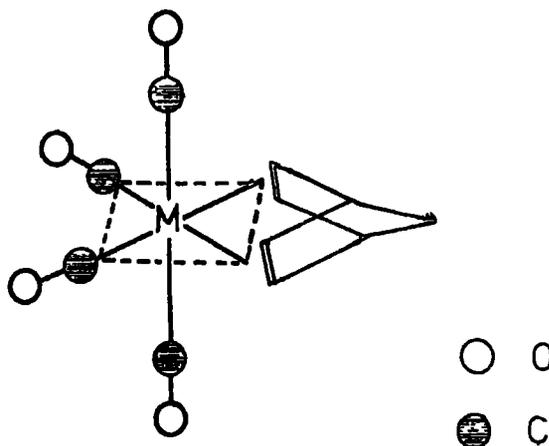
Fig. 5. Molecular Structure of Norbornadiene Complexes.

All of the complexes, except the Ru compound, are assumed to have C_{2v} symmetry (fig. 5) and for the isolated $C_7H_8M(CO)_4$ molecules the symmetries of the modes are given in table 3. The Ru complex has C_s symmetry.

Table 3 Symmetries of the fundamental modes of the $C_7H_8M(CO)_4$ complexes[10]

Fundamental	Symmetry	Number of IR/R bands
$\nu(C-O)$	$2a_1+b_1+b_2$	4/4
$\nu(M-C)$	$2a_1+b_1+b_2$	4/4
$\nu(M-olefin)$	a_1+b_1	2/2
$\nu(C=C)$	a_1+b_1	2/2
$\delta(M-C-O)$	$2a_1+2a_2+2b_1+2b_2$	6/8
$\delta(C-M-C)$	$2a_1+a_2+b_1+b_2$	4/5
$\delta(C-M-olefin)$	$a_2+b_1+b_2$	2/3
$\delta(olefin-M-olefin)$	a_1	1/1

With C_{2v} symmetry all of the normal modes should be Raman active and all except a_2 should be i.r. active.

Co-ordination of C_7H_8 to MCl_2 or $M(CO)_4$ results in several new modes, these are shown in fig. 6.

Experimental

The carbonyl complexes were kindly donated by Dr. M. Harris and the Ru complex by Dr. T. Stephenson. $C_7H_8PtCl_2$ and $C_7H_8PdCl_2$ were prepared by literature methods.[19] The time-of-flight (6H spectrometer) spectra were obtained at room temperature and the Beryllium Filter Detector spectra[8] were obtained at c.a. 90K. All samples were contained in thin-walled silica cells.

Far i.r. spectra were obtained using a Beckman-RIIC FS 700 Fourier Transform spectrophotometer. Samples were run as nujol mulls supported on a polythene disc. The near i.r. spectra were obtained, using nujol

a_1

$\nu(M-C_7H_8)_s$

b_1

$\nu(M-C_7H_8)_{as}$

b_2

TILT 1

a_2

TORSION.
TILT 2

a_1

BUTTERFLY BEND

a_2
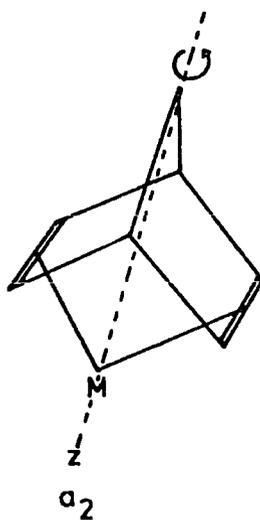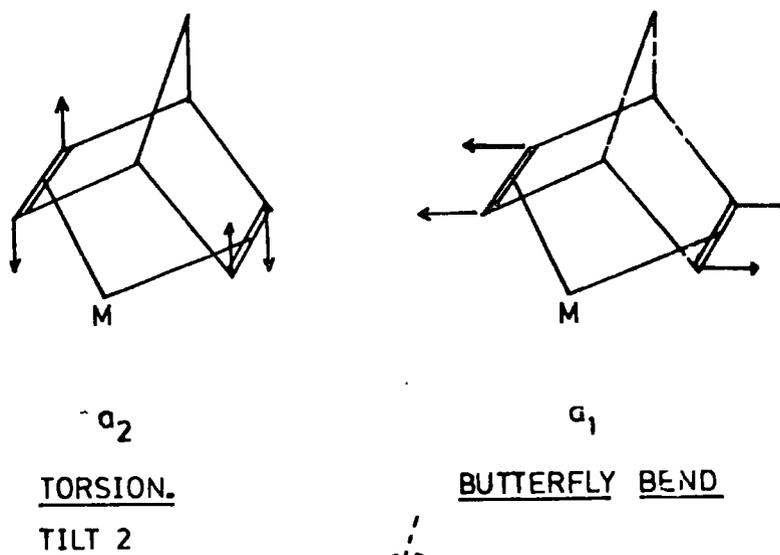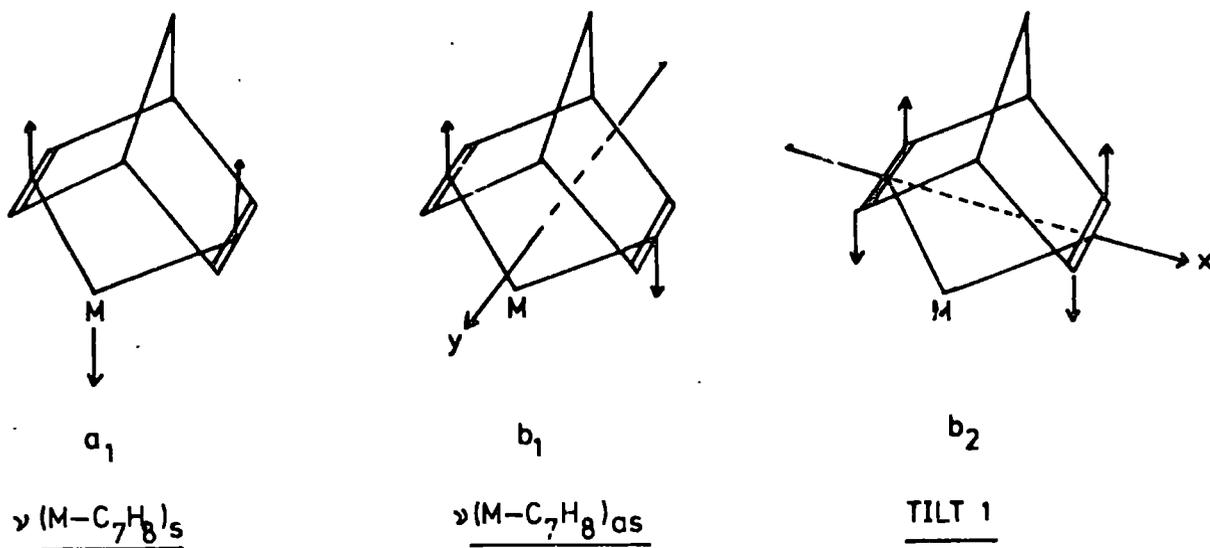
TORSION

Fig. 6 Some Normal Modes
of Norbornadiene
Complexes

mulls, on a Perkin Elmer 457 grating spectrometer. The Raman measurements we made on a Cary 82 Laser Raman spectrophotometer using a wavelength of 632.8 n.m. with 6mW power at the sample.

Results and Discussion

a) Vibrations > 200 cm^{-1}

The i.n.s. spectra are very similar (figs. 7 and 8) (tables 4 and 5) as one would expect. A strong band in the region 200 → 270 cm^{-1} corresponds to the assignments of symmetric and antisymmetric stretches (fig. 6) based on the infrared and Raman studies (tables 4 and 5). Only one band is in general observed in the i.n.s. spectrum. The two stretches would have i.n.s. bands of different intensities and as they have been assigned fairly close together it is perhaps not surprising that they have not been resolved in the i.n.s. spectra. The i.n.s. band in the Pt complex is at higher frequency than that in the Pd complex and this probably reflects a stronger metal-ligand bond.

In the far-i.r. spectrum of the platinum complex (fig. 9 and table 5) there are strong bands at 264.5 and 290.5 cm^{-1} and these we assign to the symmetric and antisymmetric stretches by analogy with the results for the Pd complex (table 5). There are no other bands in the region 170 → 300 cm^{-1} in the i.r. of $C_7H_8PtCl_2$ so that no alternative assignment is possible. We find only one Raman band, at 292 cm^{-1}, which we also assign to the antisymmetric stretch. Fernando and Adams[12] found only a very weak Raman band corresponding to the symmetric stretch for the Pd complex and our results agree with theirs in this respect. The i.n.s. band at 297 cm^{-1} in the spectrum of $C_7H_8PtCl_2$ must be the antisymmetric stretch. This is the only complex for which the two stretches were resolved in the i.n.s. spectrum.
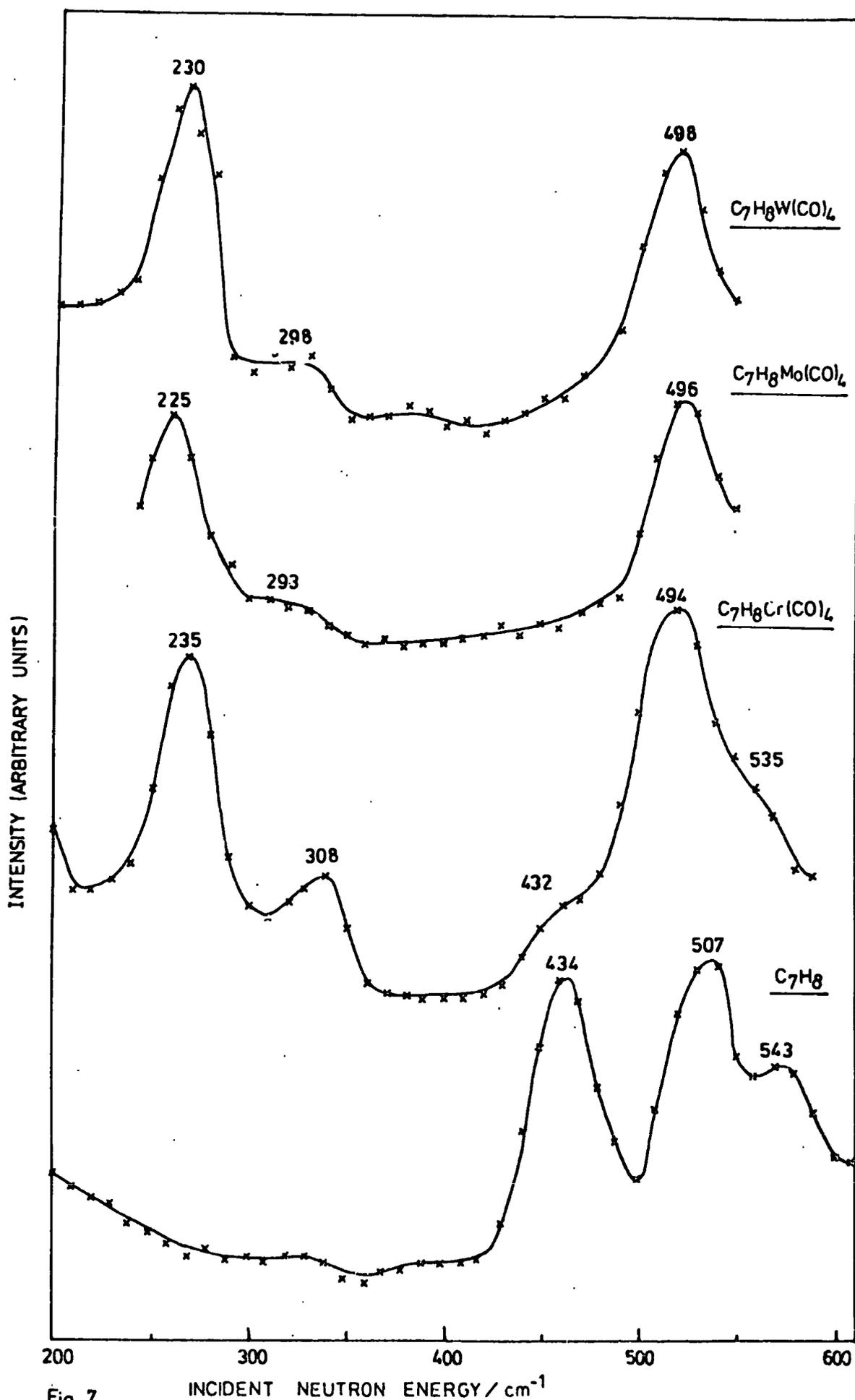
Fig. 7.
INCIDENT NEUTRON ENERGY / cm⁻¹
Neutron Energy Loss Spectra of the Norbornadiene Complexes of Cr, Mo and W.
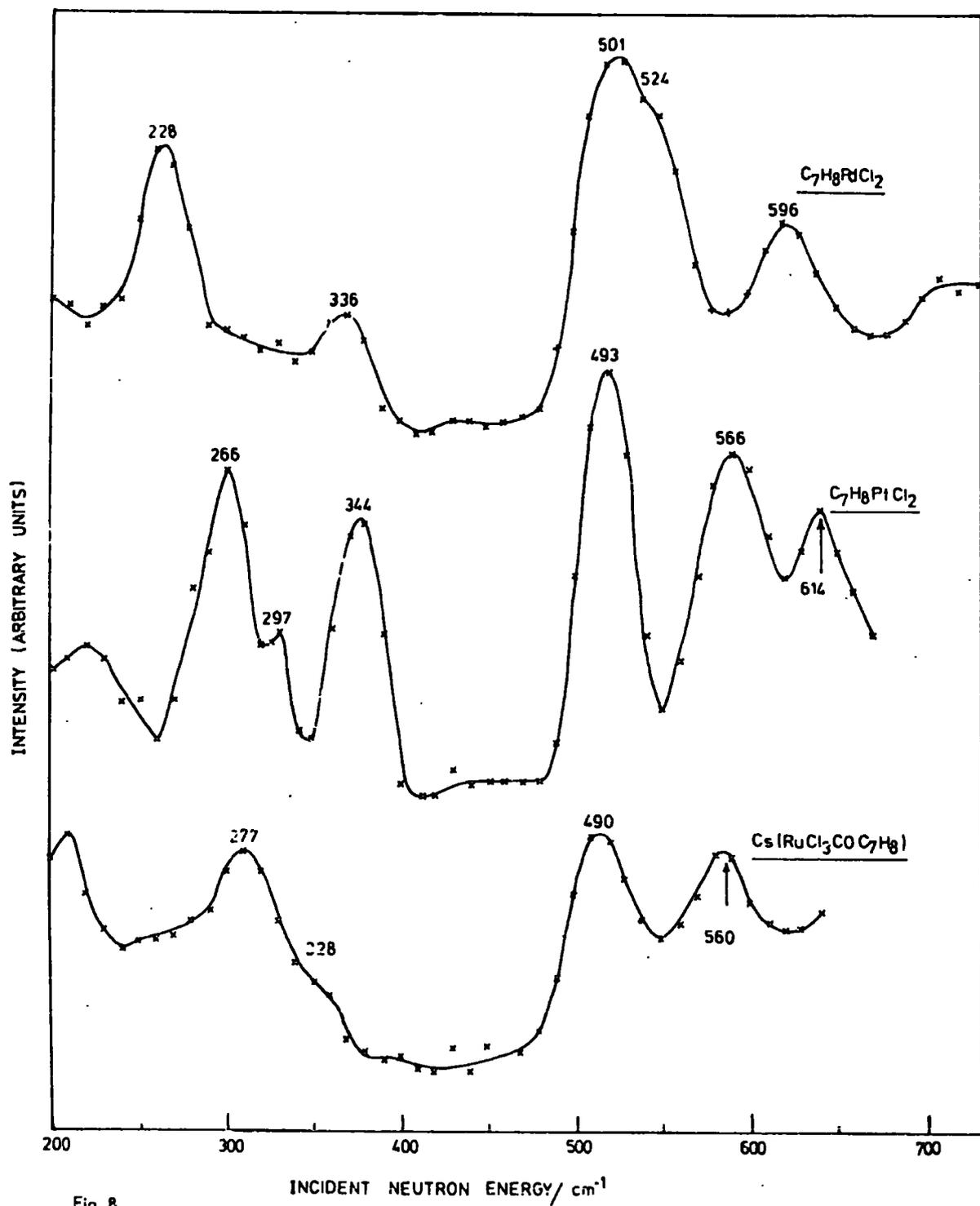
Fig. 8.

Neutron Energy Loss Spectra of the Norbornadiene Complexes
of Pd, Pt and Ru.

Fig. 9 Far-i.r. Spectrum of $C_7H_8PtCl_2$ and the Relevant Background

$C_7H_8PtCl_2$

BACKGROUND

ABSORBANCE

WAVENUMBER/cm⁻¹
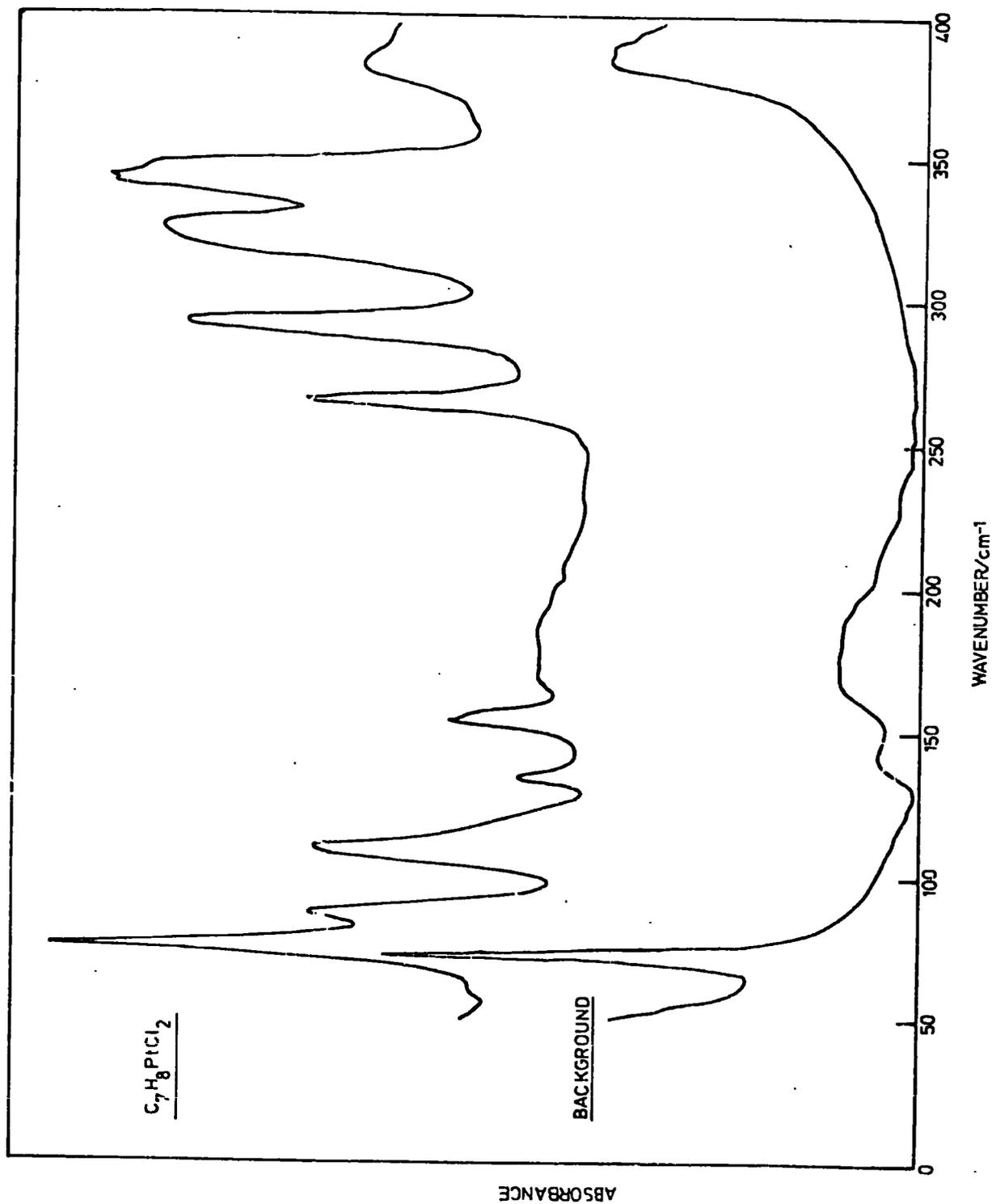
Table 4 Vibrational Modes (cm^{-1}) for the Carbonyl Complexes (> 200 cm^{-1})

C$_7$H$_8$Cr(CO)$_4$			C$_7$H$_8$Mo(CO)$_4$			C$_7$H$_8$W(CO)$_4$		
R.[a]	I.R.[a]	I.N.S.	R.[a]	I.R.[a]	I.N.S.	R.[a]	I.R.[a]	I.N.S.
251	257[b]	235±14	220		225±14	217		230±14
239	244[b]		241		293±20	237	326	296±20
	296[b]	308±14	387	391		394	391	
433	411	432±14	405			414		
						431		
454	448		423	437		444	446	
469	466		464	462				
		494±14					482	
				496	496±14		492	498±14
	515		506	503		511	511	
539		535±14	543	549		551	547	
552			554			556		
			570	570		569	570	
606	602		609	592		604	606	
621	621		625	616			616	
	635							
	643							
	667			655				
674			682					

a) From Ref. 10   b) From Ref. 12

Table 5 Vibrational Modes (cm^{-1}) for the Pd, Pt and Ru complexes and solid C$_7$H$_8$ (> 200 cm^{-1})

C$_7$H$_8$PdCl$_2$			C$_7$H$_8$PtCl$_2$			Cs[RuCl$_3$COC$_7$H$_8$]			C$_7$H$_8$ (solid)			
R.	I.R.	I.N.S.	R.	I.R.	I.N.S.	R.	I.R.	I.N.S.	R.	I.R.	I.N.S.	
233	238			264	266±14	262	265					v(M-Olefin)sy
265	268	228±14	292	291	297±14	284	284	277±14				v(M-Olefin)an
305	304											
			321	321		322	332					
337	338	336±14	325					328±14				
			339	340	344±14							
			348									
									430	421		
487	491	501±14	485			481	486	490±14	446		434±14	
518	516	524±14	492	494	493±14		497			501	507±14	
			549			520	528		543	541	543±14	
595	589	596±14	566	566	566±14	554	565	560±14				
			616	618	614±14							
	687								667	665		
									710	726		
772	770											

Table 6 Low Frequency I.N.S., Raman and Infrared Data for $C_7H_8MCl_2$, $Cs[RuCl_3COC_7H_8]$ and C_7H_8 (cm^{-1})

$C_7H_8PdCl_2$			$C_7H_8PtCl_2$			$Cs[RuCl_3COC_7H_8]$			C_7H_8 (solid)		
R.	I.R.*	I.N.S.	R.	I.R.*	I.N.S.	R.$^+$	I.R.	I.N.S.	R.	I.R.*	I.N.S.
54$^+$		35$\pm$25	33	30	40$\pm$25	17		30$\pm$25	42		45$\pm$25
67	55		39			28					
		65$\pm$3	44			45		48$\pm$3			
			55	62sh	65$\pm$3	63	55		58		
82	78		60	73			72		74		80$\pm$3
	92		73	87			84				
117	110	120$\pm$6	110	109	115$\pm$6	103	106		101		
129	120			116			123				120$\pm$6
			129	133							
145	144					143	144	135$\pm$6			
			154	154							
167											
181	178					174	176				

* This work; Liquid Nitrogen Temperature

+ This work

Tilt 2 (fig. 6) is a mode of the free ligand and it has been assigned at 446 cm^{-1} in its Raman spectrum.[12] There is a band at 434 cm^{-1} in the i.n.s. spectrum of C_7H_8. We would expect the frequency of tilt 2 to change on co-ordination of C_7H_8 to a metal, however, the frequency should be relatively independent of the particular metal. Tilt 2 has been tentatively assigned at 487 (R) and 491 cm^{-1} (I.R.) for $C_7H_8PdCl_2$.[12] This assignment seems reasonable because there is an intense band in this region of the i.n.s. spectra for all of the complexes (figs. 7,8). Tilt 2 is an a_2 mode so that formally it should be associated with a Raman band which has no i.r. equivalent. This is not found to be the case for the Pd and Pt complexes because i.r. bands are found at 491 cm^{-1} and 494 cm^{-1} respectively and these are very close in frequency to the Raman band which has been assigned to tilt 2 in the Pd complex (487 cm^{-1}). It is difficult to say whether the same is true of the carbonyl compounds because this region is one in which several carbonyl modes occur so that the i.r. is expected to be fairly complicated. The detailed assignments of tilt 2 are given in table 8. The corresponding mode has been assigned at c.a. 575 cm^{-1} in the 1,5 cyclooctadiene (COD) complexes of Rh, Pd and Pt[20] (table 7).

Table 7   Metal-ligand Modes for some 1,5 Cyclooctadiene Complexes[20]

		COD PtCl$_2$*	COD PdCl$_2$	[COD RhCl]$_2$
TILT 2	I.R.	570	588	583
	R.	569	587	586
TILT 1	I.R.	464	480	490
	R.	464	482	480
antisymmetric ν(M-olefin)	I.R.	415	461	476
	R.	413	461	480
symmetric ν(M-olefin)	I.R.	350	378	388
	R.	352	385	383

* COD = cyclooctadiene

Table 8   Summary of I.N.S. Bands and their Assignments (cm^{-1})

$C_7H_8PdCl_2$	$C_7H_8PtCl_2$	$C_7H_8Cr(CO)_4$	$C_7H_8Mo(CO)_4$	$C_7H_8W(CO)_4$	$Cs[RuCl_3COC_7H_8]$	Assignments
35	40	30	30	30	30	
65	65	55	55	55	48	C_2 torsion
120	115	115	110	105	135	δ(olefin-M-olefin)
228	266 ⎱ 297 ⎰	235	225	230	277	ν(M-olefin)sym ν(M-olefin)asy
336	344	308 432	293	298	328	TILT 1
501	493	494	496	498	490	TILT 2
524	566	535			560	"Butterfly Bend"
596	614					

Table 9   Low frequency I.N.S., Raman and Infrared Data for $C_7H_8M(CO)_4$ (cm^{-1})

$C_7H_8Cr(CO)_4$			$C_7H_8Mo(CO)_4$			$C_7H_8W(CO)_4$		
R^+	I.R.*	I.N.S.	R^+	I.R.*	I.N.S.	R^+	I.R.*	I.N.S.
31	34	30±2.5	28	30	30±2.5	25	29	30±2.5
41	41					43	44	
52	52	55±3	48	48	55±3	49	51	55±3
68	62		63	65			67	
			77			77		
82	84			85			87	
	95		95	95				
				102				
105	105	115±6	104	110	110±6	99	96 113	105±6
120	118			120			127	
142	132		136			137		

+   Data from ref. 10

*   This work; Liquid Nitrogen Temperature

In the i.n.s. spectrum (fig. 8) of the Pd compound the band at 501 cm^{-1} (tilt 2) has a strong shoulder at 524 cm^{-1}. This corresponds to a polarised Raman band (518 cm^{-1}) and an i.r. band (516 cm^{-1}) which have been assigned[12] as the "butterfly bend" (fig. 6). This mode is also a mode of C_7H_8 and it has been assigned at 424 cm^{-1} (R) and 420 cm^{-1} (i.r.) in the spectra of the ligand.[12] As there is only 20 cm^{-1} difference between tilt 2 and the "butterfly bend" for C_7H_8 (table 5), it is not surprising that only a single unresolved band is found (at 434 cm^{-1}) in the i.n.s. spectrum of the ligand (fig. 7). The "butterfly bend" is assigned, by comparison with the i.n.s. spectrum of $C_7H_8PdCl_2$, to the intense (i.n.s.) band at 566 cm^{-1} in the spectrum of $C_7H_8PdCl_2$ and hence to the bands at 566 (Raman) and 568 cm^{-1} (i.r.). The only i.n.s. data we have for the carbonyl complexes, in this region, is a shoulder at 535 cm^{-1} for the Cr complex (fig. 7). There is a very weak Raman band at 539 cm^{-1}. These we also assign to the "butterfly bend".

The assignment of Tilt 1 (fig. 6) is rather more problematic. It has been assigned, from optical spectra, at 305 cm^{-1} for $C_7H_8PdBr_2$ and 304 cm^{-1} for $C_7H_8PdCl_2$[12] on the basis that

1. tilt modes have always been assigned at higher frequency than stretching modes.

2. No C_7H_8 vibrations are expected below 400 cm^{-1} and the Pd-Br stretching modes occur at c.a. 250 cm^{-1}. It therefore appears that for $C_7H_8PdCl_2$ the tilt 1 and v(Pd-Cl) may be coincident at 304 cm^{-1}.

3. The symmetry of the band at 304 cm^{-1} must be different from that of the neighbouring a_1(308 cm^{-1}) and b_1(337 cm^{-1}) bands.

The tilt 1 mode has been assigned at 460-500 cm^{-1} in the 1,5-cyclooctadiene complexes (table 7) and is of higher frequency than the stretching modes.

The same order is found for $C_4H_4Fe(CO)_3$ (table 2).

We would expect Tilt 1 to be associated with a fairly intense band in the i.n.s. spectrum because it should be associated with some large amplitude vibrations of the protons (particularly of those on the central bridging carbon). Reference to figs. 7 and 8 shows that in the appropriate region (300-350 cm^{-1}) there is a very strong band in the i.n.s. spectrum of the Pt complex, moderate intensity in the spectra of the Pd and Cr complexes and very weak intensity for the Mo and W compounds. If the assignment of tilt 1 to this region is correct then we cannot explain the low intensity, particularly for the Mo and W complexes. Conversely if the assignment is incorrect then we must look elsewhere in the i.n.s. spectra for this mode and also explain the bands observed in the 300-350 cm^{-1} region.

It would be unacceptable to place tilt 1 at higher frequency than tilt 2 and so because there are no peaks in any of the i.n.s. spectra in the region 350 → 480 cm^{-1} we must look to lower frequencies. The assignment of the M-olefin stretches is unequivocal so that the only possible assignment we could make is to the bands below 140 cm^{-1}. This seems very low compared to the results for the COD complexes and for $C_4H_4Fe(CO)_3$ (tables 2 and 7). We will also present alternative assignments for these low energy modes (< 150 cm^{-1}) and so in the absence of more data we must tentatively agree with the assignment of tilt 1 given by Fernando and Adams[12] and by analogy assign the bands, which occur between 300 and 350 cm^{-1} in the i.n.s. spectra of each of the compounds, to tilt 1. It is interesting to note in this connection, however, that on the basis of polarisation measurements on $C_7H_8Cr(CO)_4$ the symmetric stretch (a_1) has been placed at higher frequency than the antisymmetric stretch (b_1).[10]

The remaining bands in the i.n.s. spectra in this energy range are

a) at 596 and 614 cm^{-1} in the spectra of the Pd and Pt complexes

   respectively. These we assign to ligand modes (possibly the mode

   at 543 cm^{-1} in the i.n.s. spectra of C_7H_8 fig. 7) which has been

   increased in energy on co-ordination.

b) There is possibly a shoulder in the spectrum of $C_7H_8Cr(CO)_4$ at

   432 cm^{-1}. There is no corresponding band in any of the other

   spectra nor in the i.r. or Raman.

c) There is a peak in the Beryllium Filter Detector Spectrum of

   $C_7H_8PtCl_2$ at 183 cm^{-1}. This does not occur for any of the other

   complexes and we are not able to assign, or explain it.

We have not discussed the spectrum of the Ru complex, however, its

i.n.s. spectrum is so similar to that of the other complexes that by

analogy with them we make the assignments shown in table 8.

b) <u>Vibrations < 200 cm^{-1}</u>

The i.n.s., Raman and i.r. data for this region are summarised in

tables 8 and 9, and examples of the spectra are shown in figures 10 and

11. The i.n.s. spectra are remarkably similar. They all show three

bands, one of which is c.a. 35 cm^{-1} and of much lower intensity than the

other two. The lower of the two more intense bands occurs at 55 cm^{-1} in

the spectra of all of the carbonyl complexes and at 65 and 68 cm^{-1} in

the Pd and Pt complexes respectively. The higher energy band occurs

between 105 and 120 cm^{-1} with carbonyl complexes generally of lower

frequency than the halogen complexes. The i.n.s. spectrum of

$Cs(RuCl(CO)_3C_7H_8)$ makes an interesting comparison. It also has a very

low energy band c.a. 30 cm^{-1} and a more intense mode at c.a. 50 cm^{-1},

however, the higher energy mode is now at 135 cm^{-1}. In every case,

Fig. 10   6H Spectra of Some Norbornadiene Complexes
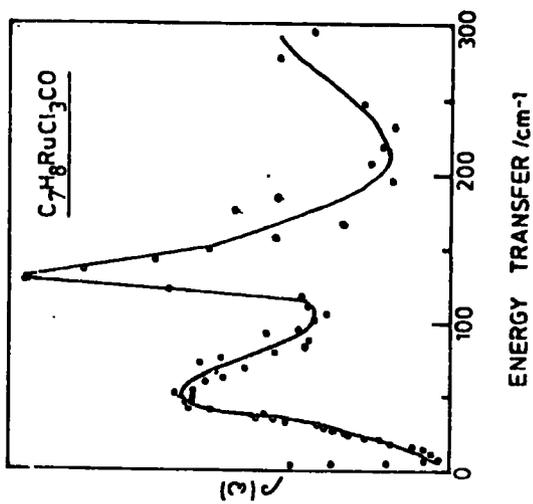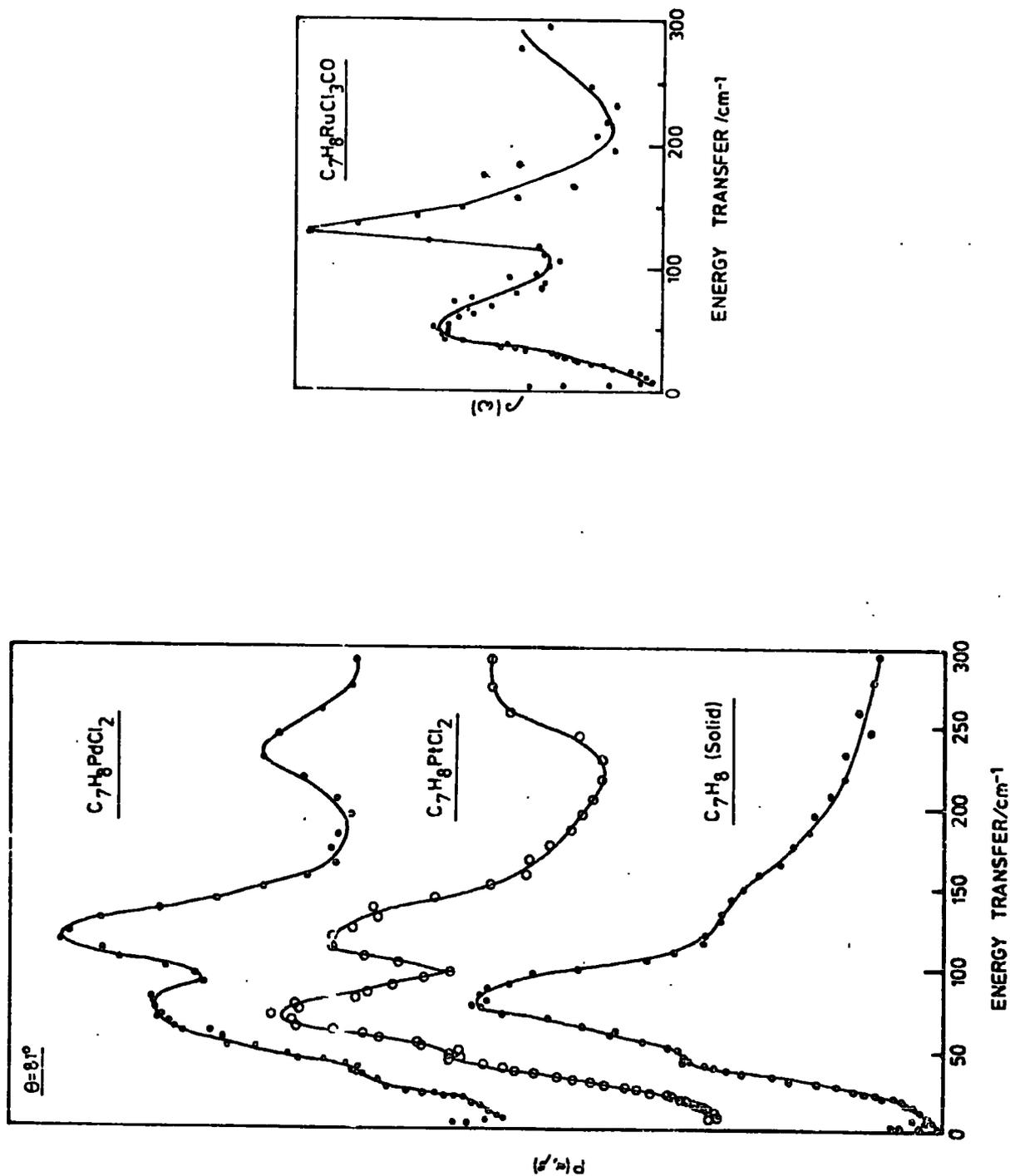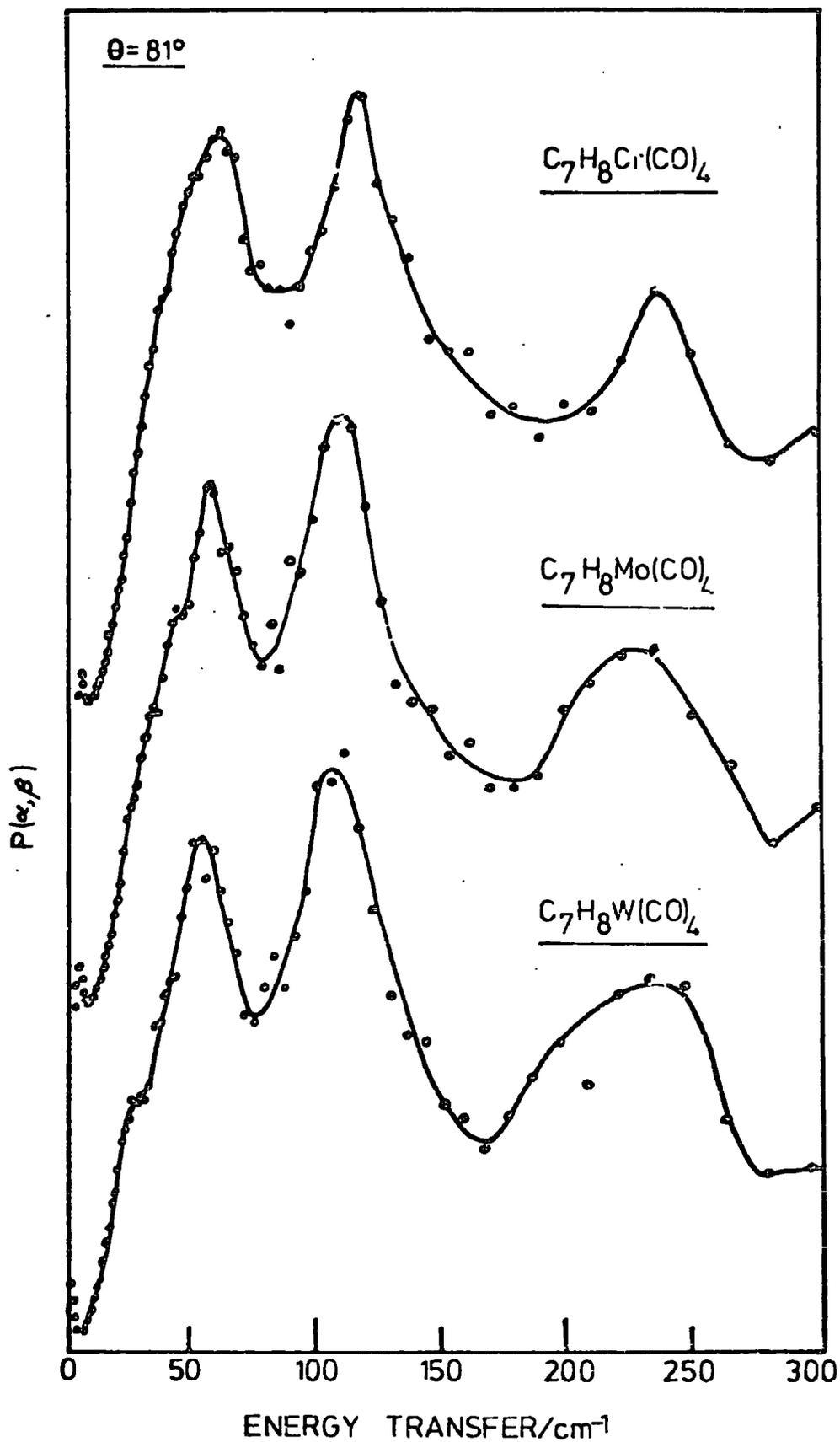
Fig. 11 6H Spectra of Some Norbornadiene Complexes

except for the Pt complex, the Boltzmann corrected scattering is more intense for the mode c.a. 120 cm^{-1} than for the mode at c.a. 50-60 cm^{-1}. Infrared and Raman bands occur close to these frequencies for all of the complexes. In the i.n.s. spectrum of C_7H_8 (fig. 10) there are two bands, at 42 cm^{-1} and 80 cm^{-1}. These correspond to lattice modes which have been assigned[10] at 42 and 74 cm^{-1}.

According to Butler and Barna[10] the region below 150 cm^{-1}, for the carbonyl complexes, should display nine C-M-C, C-M-olefin and olefin-M-olefin bands as well as various lattice modes. In particular we would expect to observe an intense band due to the torsion about the C_2 axis, as found for instance in $C_4H_4Fe(CO)_3$ (fig. 1) and several C_2H_4 complexes.[21] By comparison with the i.n.s. spectrum of $C_4H_4Fe(CO)_3$ we also know that the δ(olefin-M-olefin) (figs. 1 and 4) modes can be very intense. Therefore by comparison with the results for $C_4H_4Fe(CO)_3$ and the C_2H_4 complexes we could assign the bands at 50-70 cm^{-1} and 105-135 cm^{-1} to the C_2 torsion and the deformation in each complex.

The decision as to which i.n.s. band is associated with which mode is not straightforward. Further comparison with the assignments for π-$C_4H_4Fe(CO)_3$ is not necessarily valid because in that case the C_4H_4 ligand would appear to be symmetrically bonded to the metal atom. This is not the case for the C_7H_8 ligand. Calculation of the potential barriers, using both frequencies, may help in the assignment.

Potential Barriers

In order to calculate the barriers to rotation from our values of the torsional frequencies we need to know the barrier periodicities and the crystal structures so that the reduced moments of inertia can be

calculated. The crystal structure of only one of the complexes is known so we have made the following assumptions concerning the geometries of the molecules:

1. In all of the complexes the geometry of the C_7H_8 ligand is the same as that found in $C_7H_8PdCl_2$

2. there is a C_2 axis passing through the bridge-head carbon and the metal atom ,

3. for the carbonyl complexes we have taken M-CO to be $1.94\overset{\circ}{A}$ (found $1.94\overset{\circ}{A}$ in cis (diethylenetetramine) molybdenum tricarbonyl(I)[22] and $1.92\overset{\circ}{A}$ in $Cr(CO)_6$) and C-O to be $1.15\overset{\circ}{A}$ as found in I. The angle between the C_2 axis and the axis joining the metal atom to CO was taken at 45° - again as found in (I).

4. Pt-Cl was taken as the same as Pd-Cl[18,23]

If we use the high barrier approximation (chapter II)

$$V = \frac{8\pi^2 Ic}{n^2} \; v^2$$

thus $\qquad n^2 V = 8\pi^2 Icv^2$

The values of n^2V, the effective force constants, are listed in table 10.

It is reasonable to assume that the barrier periodicity is 2, at least for the square planar complexes. The values of V calculated with n = 2 are also shown in table 10. The corresponding values of n^2V and V(n = 2) for Zeise's Salt are included for comparison.

It has been shown[24] that for Zeise's Salt it is necessary to use a potential of the form

$$V = \frac{V_o}{2}(1 - \cos 2\theta) + \frac{V_4}{2}(1 - \cos 4\theta)$$

in order to reconcile the barriers to the torsion calculated from i.n.s. and n.m.r. data. We have no n.m.r. data for the norbornadiene complexes, however, by putting $V_4 = V_o$ we can calculate the values of V_o for this one parameter model. These values are shown in table 10.

It is apparent that for the norbornadiene complexes all of the parameters, $n^2 V$, V and V_o are smaller than the corresponding parameters for Zeise's Salt if we use the band at c.a. 60 cm^{-1} as the torsional frequency and larger if we use the band at c.a. 115 cm^{-1}. We can certainly deduce from this that the change in frequency of the C_2 torsion, relative to Zeise's Salt, is due to other factors as well as to the moment of inertia change. Because the bonding in the two sets of complexes (C_2H_4 and C_7H_8) is rather different it is not possible to say absolutely which will have the higher barrier, however, as we mentioned earlier in the case e.g. of $C_7H_8PtCl_2$ the torsion involves a tendency towards tetrahedrally co-ordinated Pt and the barrier to this is expected to be high. Perhaps therefore the potential calculations indicate that the torsion is in fact the higher frequency mode. If this is so then the i.n.s. band at c.a. 55 cm^{-1} is the deformation mode.

One further possibility is that we are observing the in-phase (i.p.) and out-of-phase (o.p.) torsions of the molecule (about the C_2 axis). Ratcliffe[25] has shown that two well separated peaks will be obtained only if both the internal and external fields are high. The in-phase motion is of course a whole body rotation. This assignment seems unlikely in view of the large moment of inertia of the whole molecule ($> 840 \times 10^{-40}$ g cm^2 for the carbonyl complexes). From our work on

Table 10   Effective Force Constants and Potential Barriers for Some Olefin Complexes

	n^2V				V (n = 2)				$5V_o$			
	a		b		a		b		a		b	
	kJ mol^{-1}	cm^{-1}	kJ mol^{-1}	cm^{-1}	kJ mol^{-1}	cm^{-1}	kJ mol^{-1}	cm^{-1}	kJ mol^{-1}	cm^{-1}	kJ mol^{-1}	cm^{-1}
$C_7H_8PdCl_2$	261.4	21,881	890.9	74,575	65.4	5,474	222.7	18,642	65.3	5,466	222.6	18,633
$C_7H_8PtCl_2$	261.4	21,881	818.2	68,489	65.4	5,474	204.6	17,126	65.3	5,466	204.4	17,120
$C_7H_8Cr(CO)_4$	228.6	19,135	999.5	83,665	57.2	4,788	249.9	20,918	57.1	4,780	249.6	20,893
$C_7H_8Mo(CO)_4$	228.6	19,135	914.5	76,550	57.2	4,788	228.6	19,135	57.1	4,780	228.4	19,119
$C_7H_8W(CO)_4$	228.6	19,135	833.2	69,745	57.2	4,788	208.3	17,436	57.1	4,780	208.1	17,419
Zeises' Salt	444.5 (37,208 cm^{-1})				111.1 (92,998 cm^{-1})				118.0 (98,774 cm^{-1})			
Zeises' Dimer	422.3 (35,349 cm^{-1})				105.6 (88,394 cm^{-1})				106.0 (88,729 cm^{-1})			

a) Calculated using band at c.a. 60 cm^{-1}

b) Calculated using band at c.a. 115 cm^{-1}

$(C_3H_5)_2M$ compounds we have assigned the i.p. and o.p. modes at c.a. 70 and 150 cm^{-1} respectively. The moment of inertia of C_7H_8 and C_3H_5 about the axis through the metal atom are in the ratio of c.a. 4:1 and similarly the moments of inertia of the whole molecules about the same axes are in the ratio c.a. 6:1 (for $C_7H_8M(CO)_4$). If the force fields were the same we would therefore expect the i.p. and o.p. frequencies to be very different. This would appear to be the case for the proposed o.p. modes (150 and 115 cm^{-1}) but the proposed i.p. modes are very similar in frequency (70 and 60 cm^{-1}). We consider this assignment to be unlikely compared to the assignment to the C_2 torsion and a deformation mode. Furthermore the norbornadiene complexes are soft crystals and there is no indication of strong hydrogen bonding. We have made the assumption that the external barrier is zero for the barrier calculations.

Conclusion

Many of the M-olefin modes have been assigned though there is an anomoly in the intensities associated with the i.n.s. bands assigned to tilt 1. The low frequency i.n.s. spectra are very simple but we are unable to decide unequivocally which of the two intense bands should be assigned to the C_2 torsion and which to the deformation mode.

Section III: π-Allyl Complexes of Nickel, Palladium and Platinum

π-Allyl complexes are of great importance in organometallic chemistry and with this in mind it is strange that the first spectroscopic studies of "pure" π-allyls i.e. those containing no other ligands, were not reported until 1973.

The π-allyls are relatively complex molecules for i.n.s. study in so far as

a) nearly all of the normal modes involve significant proton motion so that they should all produce bands in the i.n.s. spectrum.

b) Many of the normal modes occur within e.g. 20 cm^{-1} of one another. This means that they cannot be resolved on many i.n.s. spectrometers (however see chapter III).

What we have been able to do in our study of some allyls is

1. to show that we can observe the low frequency (<800 cm^{-1}) metal-allyl vibrations and to assign some modes in a less stable complex by comparison with previous assignments from the optical spectra of a more stable material.

2. Detect modes which have proven too weak to be observed in the i.r. or Raman of stable complexes.

Experimental

$(\pi\text{-}C_3H_5PdCl)_2$ was purchased from Strem Chemicals Inc., $(\pi\text{-}C_3H_5)_2Ni$,[26] $(\pi\text{-}C_3H_5)_2Pd$[27] and $(\pi\text{-}C_3H_5NiBr)$[28] were prepared by literature methods. All samples were sealed into silica cells for the i.n.s. experiments. I.n.s. spectra were obtained at -37°C for $(\pi\text{-}C_3H_5)_2Pd$, -3°C for $(\pi\text{-}C_3H_5\text{-}NiBr)_2$

and $20^{\circ}C$ for $(\pi\text{-}C_3H_5PdCl)_2$ (time-of-flight experiments[8]) and c.a. 90K (Beryllium Filter Detector[8] experiments for all four samples). We did not obtain the t. of f. spectrum of $(\pi\text{-}C_3H_5)_2Ni$ although we were able to obtain data down to 60 cm^{-1} using the B.F.D. spectrometer.

The far-infrared spectrum of $(\pi\text{-}C_3H_5)_2Ni$ was obtained by subliming the sample onto a polythene disc in a cold cell (chapter III). Spectra were obtained on a Beckman-RIIC FS720 Fourier Transform spectrophotometer. Raman data was obtained using a Cary 82 Laser Raman spectrophotometer and a wavelength of 632.8 mm with c.a. 10 mW power at the sample.

a) $(\pi\text{-}C_3H_5PdCl)_2$ and $(\pi\text{-}C_3H_5NiBr)_2$

$(\pi\text{-}C_3H_5PdCl)_2$ has been studied, using i.r. and R. spectroscopy, by several authors.[29-35] Complete assignments have been proposed and both deuteration[32] and metal-isotope studies[33] have been published together with force-constant calculations.[30,31,36] The crystal structure has been determined[37,38] and it was found that the $PdCl_2Pd$ skeleton is planar with the planes of the allyl groups at an angle of $111.5 \pm 9^{\circ}$ to the plane of the skeleton. Although the molecular symmetry is C_{2h} the spectra have been assigned by considering the local symmetries of the components C_3H_5 (C_s), $PdCl_2Pd$ (C_{2h}) and $C_3H_5\text{-}Pd$ (C_s). Such an approach has not always been successful e.g. it was necessary to assign the spectra of $\pi\text{-}C_5H_5Mn(CO)_4$ using C_s symmetry rather than the C_{4V} local symmetry of the $Mn(CO)_4$ group.[39]

Some assignments are also available for $(\pi\text{-}C_3H_5PdBr)_2$[29,32,34] and reasonably complete assignments for $(\pi\text{-}C_3H_5PdOCOCH_3)_2$ and $(\pi\text{-}C_3H_5PdOCOCF_3)_2$.[35] Fig. 12 shows the forms of the six allyl-metal vibrations.[32]

$\nu_s(M-C_3H_5)(T_x)$ twist (R_y) wag (R_z)

$\delta(C_3H_5)(T_z)$ $\gamma(C_3H_5)(T_y)$ torsion (R_z)
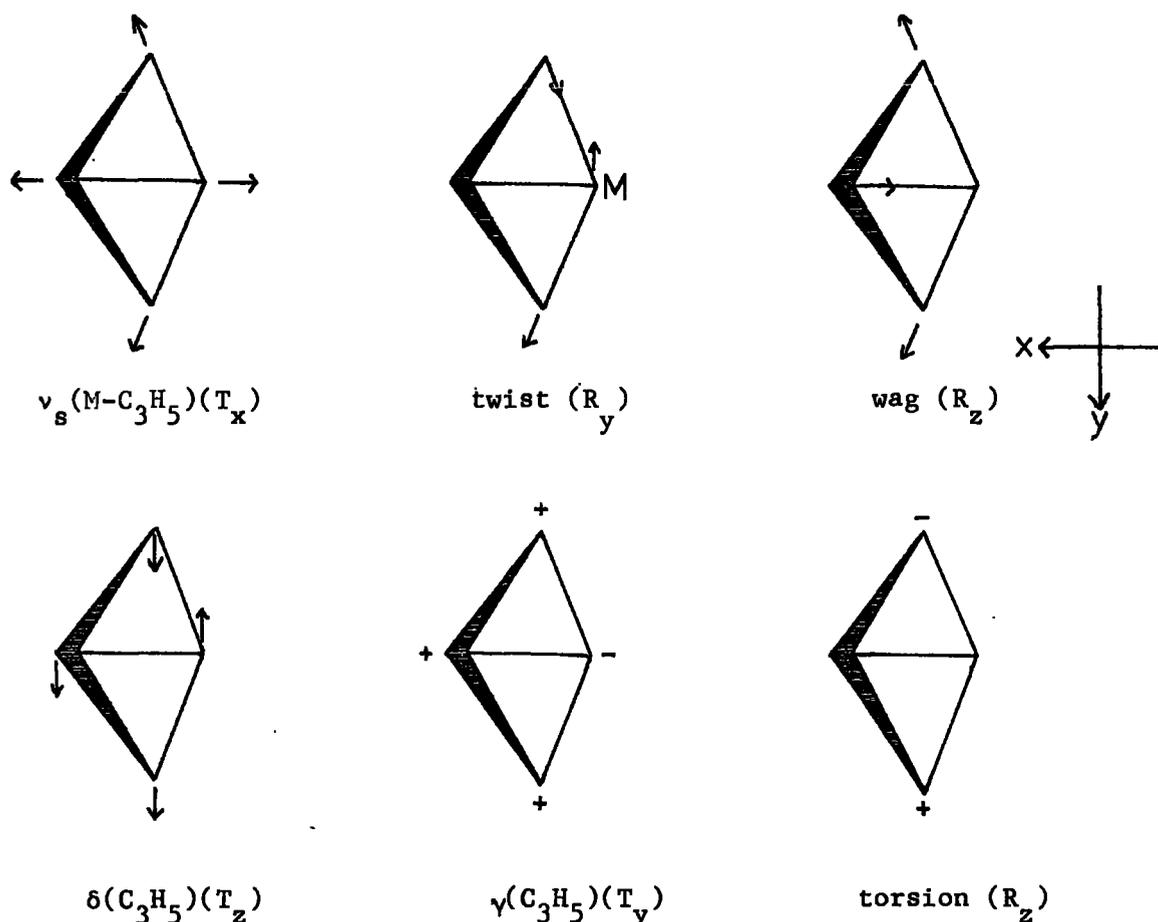
Fig. 12 Allyl-Metal Vibrations. (allyl group pivoting about O-Z)

The data for $(\pi-C_3H_5NiX)_2$ X = Cl, Br, I is less complete. No crystal structure is available. The i.r. spectrum has been obtained[35,40] and in particular Chenskaya et al.[1] have obtained data down to 60 cm^{-1}. Raman data was not obtained because the sample was found to decompose rapidly in the laser beam.[1]

Our i.n.s. data is shown in tables 11 and 12, together with the available i.r. and Raman data and assignments (<600 cm^{-1}). The i.n.s. spectra are shown in figs. 13 and 14. Although there are differences in the characters assigned to some of the modes the assignments do agree in outline. Considering firstly the region 200 → 600 cm^{-1} it can be seen that the i.n.s. spectra correspond with what would be expected from the i.r. and Raman assignments. Three of the metal-allyl modes occur very

Table 11   Spectroscopic Data for $(\pi-C_3H_5NiBr)_2$ (cm^{-1})

I.N.S.	I.R.	Assignment[a]	I.R.	Assignment[b]
25 ± 2.5				
97 ± 6.5	110	Skeletal		
	128	deformation		
139 ± 11			150	
201 ± 14	205⎤ 221⎦	ν_{Ni-Br}	200 224	$\nu(Ni-Br)$
$287\pm14\nu_w$			270	
368 ± 14	370	$\nu_{Ni-C_3H_5}$ A'	380	$\nu(Ni-C)_{sym}$
419 ± 14	413⎤ 425⎦	$\nu_{Ni-C_3H_5}$ A' A''		
			440	$\nu(Ni-C)_{antis}$
505 ± 14		δ_{C-C-C} A'	520	$\delta(C-C-C)$

a) ref. 1

b) ref. 40

Table 12   Spectroscopic Data for $(\pi-C_3H_5PdCl)_2$ (cm^{-1})

I.N.S.	I.R.		R.		Assignment[a]	R.		I.R.		Assignment[b]
	-180°C	25°C	-180°C	25°C		295K	Cold	Solid	Soln.	
30 ± 2.5			32	28	R''	27	32			⎫
			41	40	R'					
	44	42			T'	45	45			
			47	46	R'					Lattice
50?	55	51			T'	57	59			Modes
			60	59	R'					
	67	64			T'		67			
			68	65	R'					
			77	75	R'		74			⎭
	84	82	100	99	δ Pd_2Cl_2	99	99	93		Bridge def.
100 ± 6.5	98	93	105	104	$t-C_3H_5$ "R_x"	103	105			Lattice mode
	118	114	120	121	γ C_3H_5 "T_y"	116	122	113		⎫ Skeleton
140 ± 11	145	141	148	146	δ C_3H_5 "T_z"	142	138	137		⎭ Def^n
	246	243	242	236	⎫ $\nu(Pd-Cl)$	233	238	243		⎫ ν_{13}, ν_{25}
	256	251	259	259	⎭	256	257	254	254	⎭
	351⎤ 369⎦	365	376	372	w, C_3H_5 "R_z"	372	376	366	367	ν_{12}
375 ± 14 (br)s	384	382	404	398	t, C_3H_5 "R_y"		402	381		ν_{24}
	394⎤ 404⎦	400	412	408	$\nu_s Pd-C_3H_5$"T_x"	407	410	402	397	ν_{11}
511 ± 14	513	511	512	511	S_{C-C-C}	509	509	510	510	ν_{10}

a) ref. 32

b) ref. 34 solution data also available (Raman)
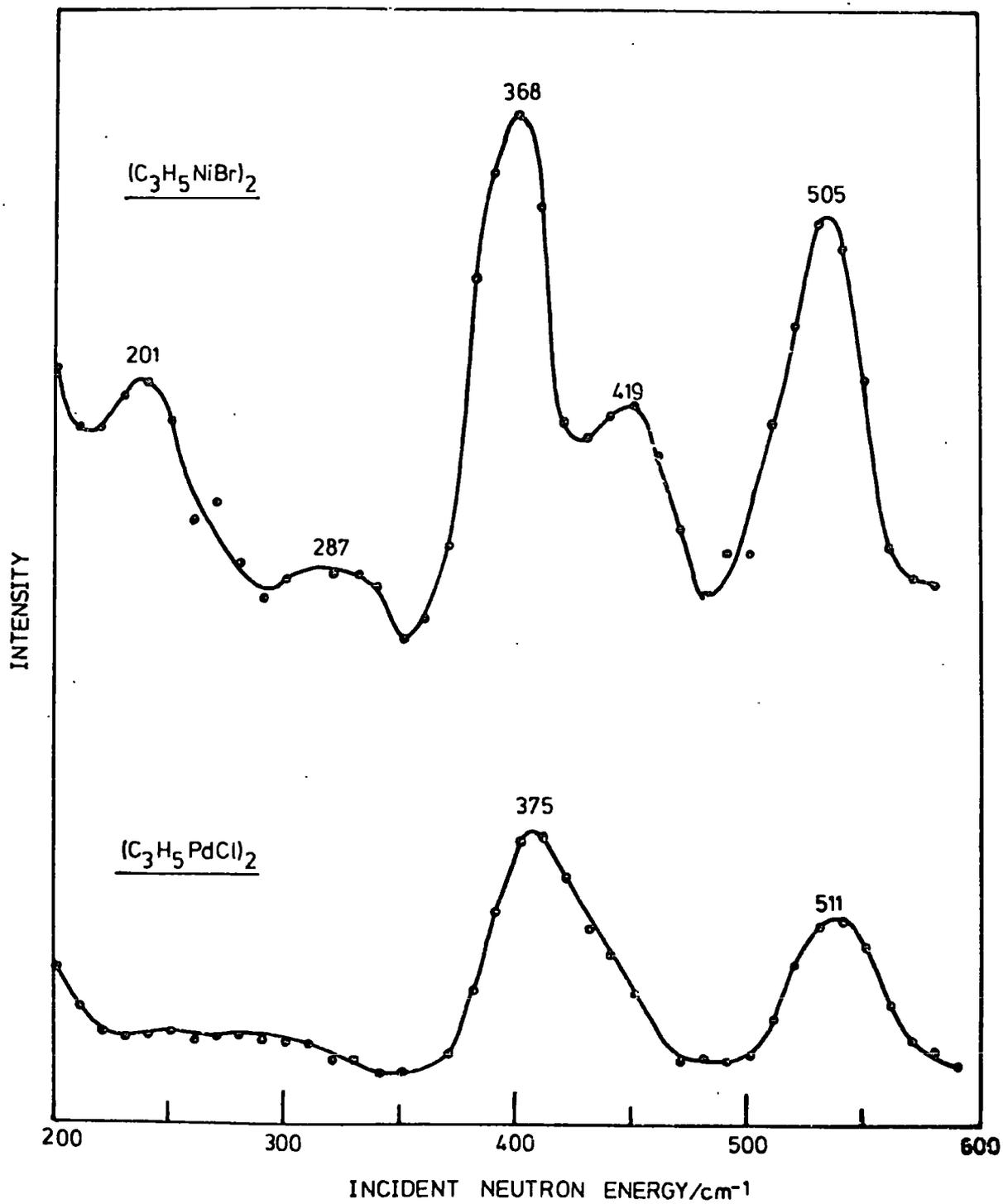
Fig. 13 B.F.D. Spectra of π-allyl metal halides
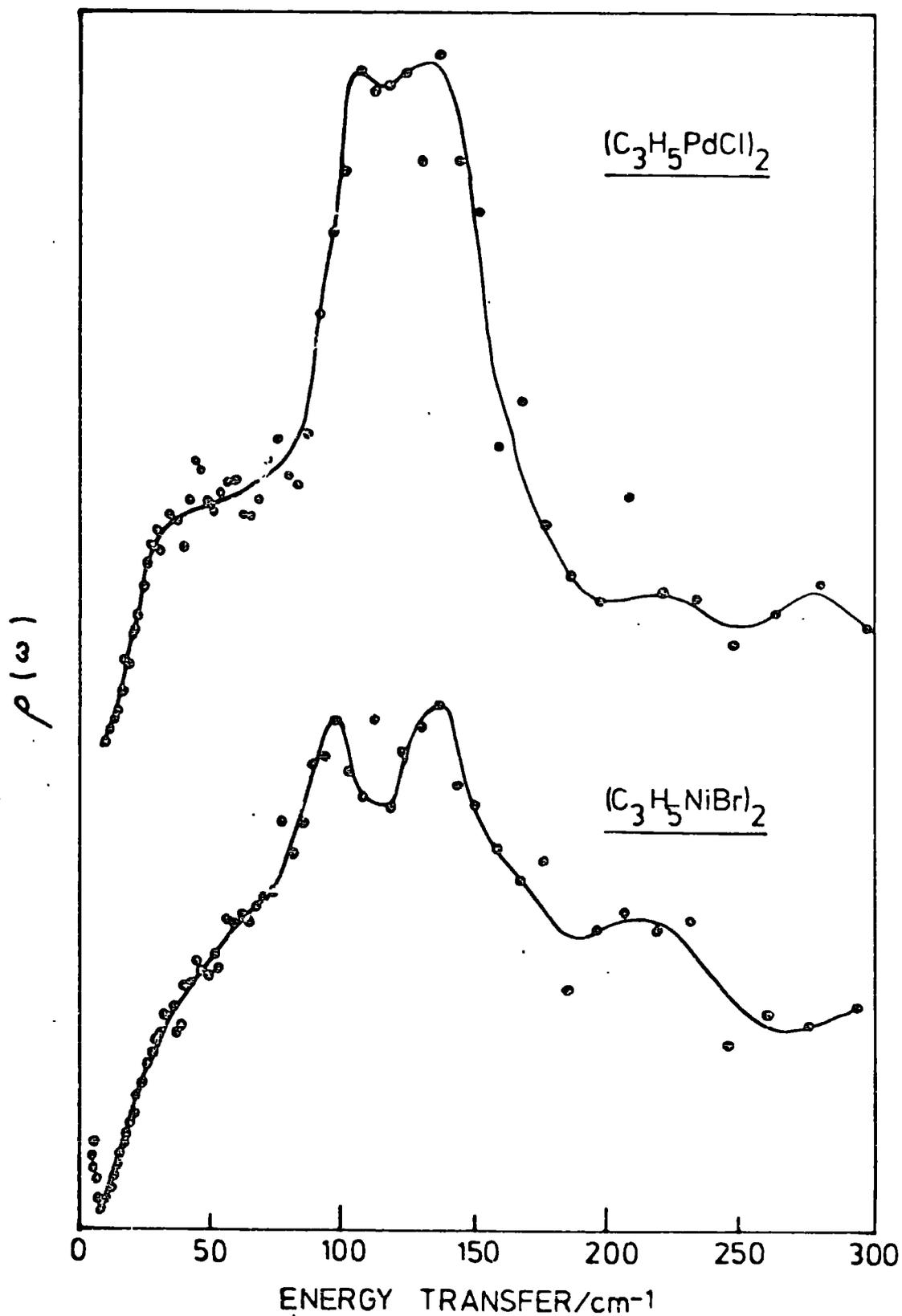
Fig. 14 Density of States of $(C_3H_5PdCl)_2$ and $(C_3H_5NiBr)_2$

close together at c.a. 380 cm^{-1}, and as a result in the i.n.s. spectrum

of the Pd compound (fig. 13) a single broad band is found and for the

Ni complex (fig. 13) where the assigned modes are rather further apart,

two bands.

The three remaining allyl Pd modes have been assigned at 98, 118 and

145 cm^{-1} (table 12) and the torsion is the lowest frequency mode. The

i.n.s. spectrum (fig. 14) contains just two bands in this region, at ~

100 and 140 cm^{-1}. The corresponding modes have been assigned in

$(\pi\text{-}C_3H_5PdBr)$[32] at 98, 114 and 137 cm^{-1} and in $(\pi\text{-}C_3H_5PdOCOCH_3)$[35] at 129,

141 and 158 cm^{-1}. There are no far-i.r. assignments for the nickel

complex although for $(C_3H_5NiOCOCH_3)$[35] the torsion has been assigned at

123 cm^{-1}, γ C_3H_5 at 142 cm^{-1} and δ C_3H_5 at 153 cm^{-1}. In the i.n.s.

spectrum of $(\pi\text{-}C_3H_5NiBr)_2$ there is a broad band c.a. 120 cm^{-1} which peaks

at 97 cm^{-1} and 139 cm^{-1} (fig. 14). By analogy with the previous

results we assign the peak at 97 cm^{-1} to the torsion and the peak at

139 cm^{-1} to δ C_3H_5 with γ C_3H_5 being unresolved but placed somewhere

between these limits. An i.r. band has been reported[1] at 128 cm^{-1}

(table 11). In the far-infrared spectrum (liquid nitrogen temp.) of

$(\pi\text{-}C_3H_5NiBr)_2$ we obtained two weak bands, at 94 cm^{-1} and 116 cm^{-1}. These

results differ from those of Chenskaya et al.[1] (table 11). We assign the

band at 94 cm^{-1} to the torsion and that at 116 cm^{-1} to γ C_3H_5.

The very close correspondence between the vibrational frequencies

for the Pd and Ni allyls, in equivalent compounds, agrees with a

calculation which has shown that the force constant for the metal-allyl

bond has the same value for Ni and Pd compounds but which incidentally

increases sharply for Pt allyls.[41]

There are two remaining features in the i.n.s. spectrum of the

nickel complex, at 201 cm^{-1} and 287 cm^{-1} (fig. 13). The latter band is

very weak and broad and it is probably an overtone of the mode occurring

at 139 cm^{-1}. The band at 201 cm^{-1} coincides with the Ni-Br stretches

assigned in the i.r. There will probably be some proton motion associated

with these stretches although the same should also be true for $(\pi-C_3H_5PtCl)_2$

where in fact very little intensity (fig. 13) is found in its i.n.s.

spectrum in the region of the $\nu(Pt-Cl)$ modes (≈ 250 cm^{-1}). However, the

associated motion of light atoms in a normal mode does increase as the

mass of the heavier atom increases. For instance this type of behaviour

has been found[25] for CH_3CX_3 as X changed from Cl to Br to I. This

probably explains the change in i.n.s. intensity associated with the

halogen modes. On going from $[BrNiC_3H_5]_2$ to $[ClPtC_3H_5]_2$ the mass of the

halogen falls and the mass of the metal atom increases. Both factors will

therefore lead to a decrease in the amplitude of vibration of the C_7H_8

ligand associated with the metal-halogen stretches.

b) $(\pi-C_3H_5)_2Ni$ and $(\pi-C_3H_5)_2Pd$

There are no crystal structures available for these compounds,

however, n.m.r.[42] results have shown that in solution they exist as cis-

trans isomers (fig. 15) with the proportions 1:3 respectively. Bis-π-

2 methallyl nickel has been shown to have the trans configuration in the

solid state.[43]

The two isomers fig. 15 have rather different symmetries (cis is

C_{2v} and trans is C_{2h}) so that an i.r. and Raman study should be able to

distinguish between the two possibilities e.g. the trans form has a
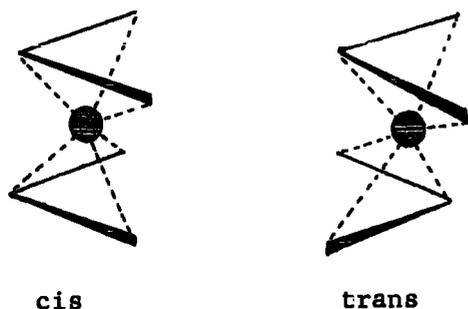
Fig. 15   cis and trans forms of
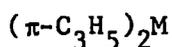
$(\pi-C_3H_5)_2M$

centre of symmetry so that the mutual exclusion (i.r. and Raman) rule applies. The numbers and symmetries of the skeletal vibrations are shown in table 13 and fig. 18.

Table 13: Numbers and Symmetries of Skeletal Vibrations in $(\pi-C_3H_5)_2M$[44]

Vibration Type	C_{2v} (cis)	C_{2h} (Trans)
C_3H_5-M stretch	A_1+A_2	Ag+Bu
C_3H_5-M tilt	$A_1+A_2+B_1+B_2$	Ag+Au+Bg+Bu
C_3H_5-M torsion	A_2+B_1	Au+Bg
C_3H_5-M-C_3H_5 deformation	A_1	Ag

C_{2v}: All modes Raman active, A_1,B_1,B_2 are i.r. active

C_{2L}: Ag and Bg Raman active, Au and Bu are i.r. active

These are more important for distinguishing the configuration than the ligand vibrations, which have been shown to be relatively independent of the configuration and the metal atom.[44]

$(\pi-C_3H_5)_2Ni$[1,44,29] and $(\pi-C_3H_5)_2Pd$[31,44,45] have been studied by optical spectroscopy and the results and assignments (< 600 cm^{-1}) are shown in tables 14 and 15, together with our i.n.s. data. Our i.n.s. spectra are shown in figs. 16,17. The two available assignments for

Table 14 Spectroscopic Data for $(\pi\text{-}C_3H_5)_2Ni$ (cm^{-1})

I.N.S.	I.R.		R.		ASSIGNMENT[a]	I.R.	R.		ASSIGNMENT[b]
	-180°C	20°C	-60°C	10°C		100K	100K	293K	
$68^{\pm}14vs$									
$86(sh)^{\pm}14vs$									
$152^{\pm}14vs$									
$328^{\pm}14(w)$			323⎤ 330⎦	324	Ag	350	331	324	Ag C_3H_5-Ni stretch / Bu C_3H_5-Ni stretch
$388^{\pm}14(br)$ m	380	381			Bu	380			Au C_3H_5-Ni tilt
			385	387	Bg		387	385	Bg C_3H_5-Ni tilt
			406	406	Ag	398			Bu C_3H_5-Ni tilt
	415	410			Au,Bu				
	454	452				454	429	406	Ag C_3H_5-Ni tilt
	483	485			Bu ⎱ δCCC	478			
$498^{\pm}14$			494	500	Ag ⎰	484	507	500	A' δ(C-C-C)
		575				580			

$\nu(Ni\text{-}C_3H_5)$

v.s. very strong; m medium; br broad

a) ref. 1

b) ref. 44

Table 15 Spectroscopic Data for $(\pi\text{-}C_3H_5)_2Pd$ (cm^{-1})

I.N.S.	I.R.[a]		R.	ASSIGNMENT	I.R.[b]		R.		ASSIGNMENT
	215K	293K	100K		c.a. 20°C	Liq N_2	Liq N_2	Soln.	
$50^{\pm}3.5$									
$85^{\pm}6$									
$135^{\pm}10$									
$160^{\pm}11.5sh$									
$318^{\pm}14w$			329	Ag C_3H_5-Pd stretch	314	320			Bu / Ag
	350		373	Bu C_3H_5-Pd stretch	363	369	326	321	Bu / Bg ⎱ νC_3H_5-Pd
							370	365	
$400(br)^{\pm}14s$	402		409	Ag C_3H_5-Pd tilt	393	407			Au / Ag
							408	400	
	460	468		Au/Bu C_3H_5-Pd tilt	472	472			Bu / Ag ⎱ δC-C-C
$483^{\pm}14(br)$		500	493	A' δ(C-C-C)			496	490	
					502				

sh shoulder; br broad; w weak; s strong

a) ref. 44

b) ref. 45

Fig. 16 B.F.D. Spectra of $(C_3H_5)_2Ni$ and $(C_3H_5)_2Pd$
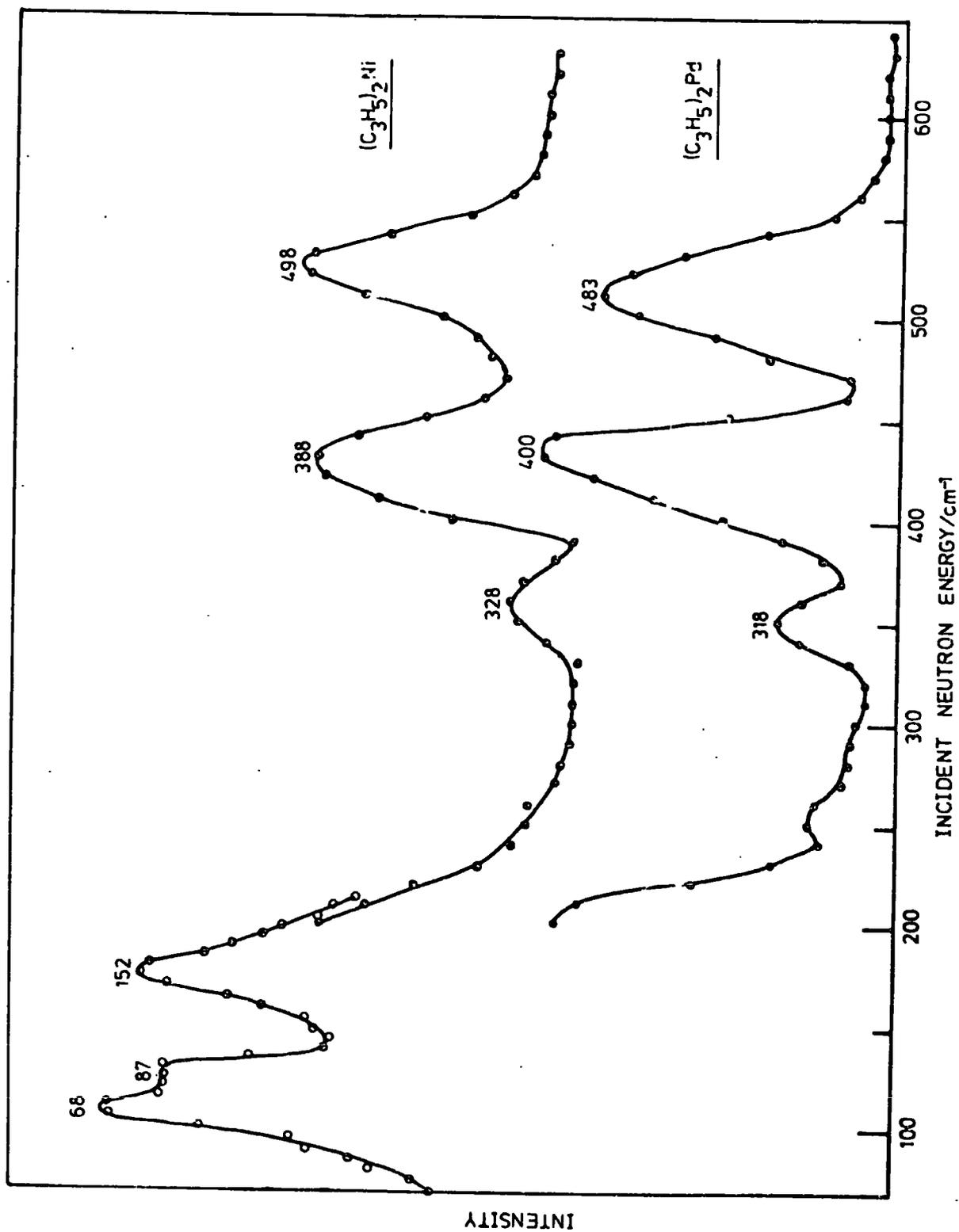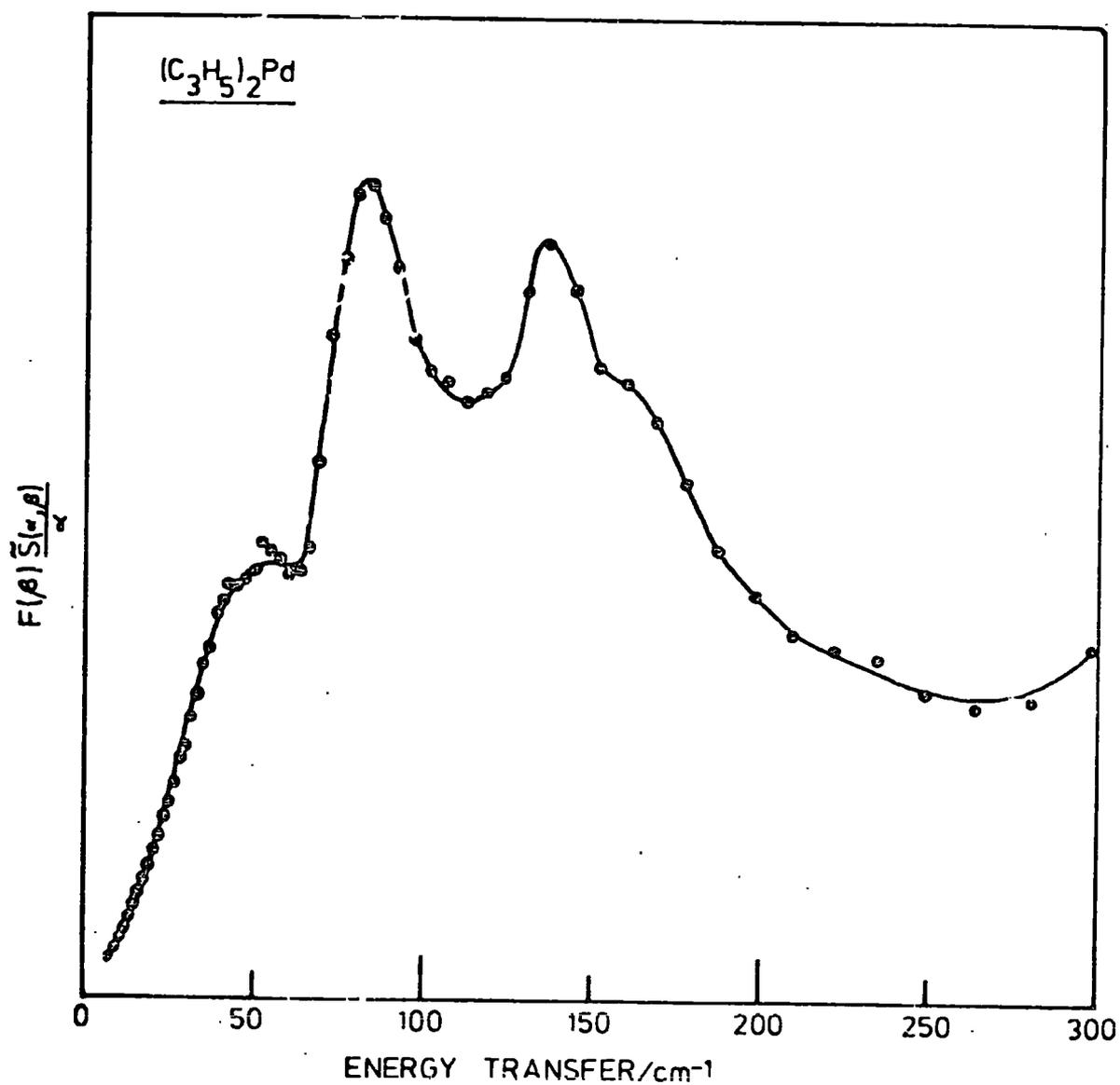
Fig. 17 T.of.F. Data for $(C_3H_5)_2Pd$

STRETCHES

Ag

Bu

TILTS

Ag

Bu

Bg

Au

TORSIONS

Bg

Au
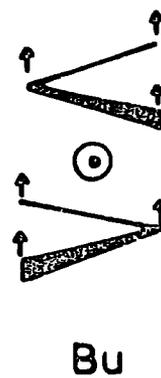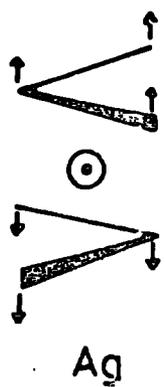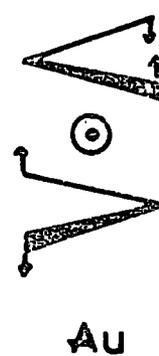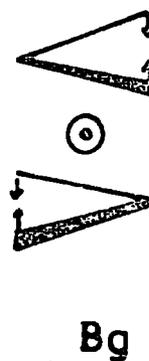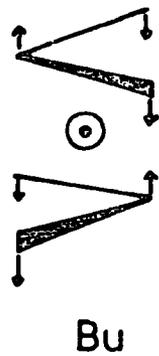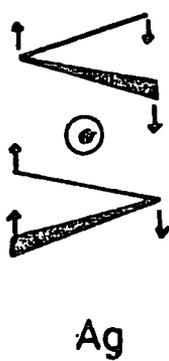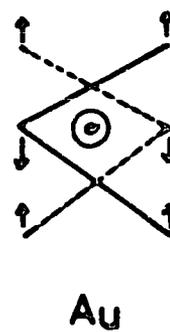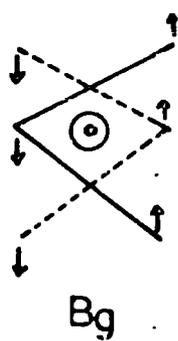
Fig. 18 Some Normal Modes of $(\pi\text{-}C_3H_5)_2M$

$(\pi\text{-}C_3H_5)_2Ni$ do not agree totally (table 14) particularly with regard to the symmetries of the various modes. Both sets of authors do agree, however, that the observed spectra for both complexes are best explained on the basis of a trans configuration of the molecule although it was not possible to completely rule out the cis configuration.

The local symmetry of the C_3H_5 ligand was used successfully to assign the internal vibrations of the allyl group and there was no indication of coupling between the ligands. The full heavy atom skeleton must be considered when assigning the skeletal modes. No vibrations were observed in the optical spectra below 300 cm^{-1} where the allyl-M torsions and (allyl)$_2$M deformation modes should occur.[39]

Consider firstly the region > 200 cm^{-1}. The i.n.s. spectra (fig. 16) once again are what one would expect as a result of the unresolved bands. For $(\pi\text{-}C_3H_5)_2Ni$ Andrews and Davidson[39] assign a weak band at 350 cm^{-1}, occurring only in the i.r. of the solid, to the Bu$_s(\pi\text{-}C_3H_5)_2Ni$ stretch. Chenskaya et al. assign this mode at 380 cm^{-1} and assign the mode that Andrews and Davidson assign at 380 cm^{-1} to c.a. 410 cm^{-1}. As far as we are able to tell there is no band at 350 cm^{-1} in the i.n.s. spectrum. At 350 cm^{-1} the count rate is almost at background and so this indicates that the assignment of Chenskaya is the more correct one, at least in this respect.

In the region below 300 cm^{-1} we have observed the predicted low frequency modes i.e. the two torsions and the deformation mode (tables 14 and 15). Consider firstly the i.n.s. spectrum of $(\pi\text{-}C_3H_5)_2Ni$. There are three intense bands at 68, 87 and 152 cm^{-1} respectively. We have also observed an i.r. band at 150 cm^{-1}. If the trans configuration is

the correct one then this must be the out — of—phase torsion (Au). This also makes good sense as we would expect the out of phase torsion to be of higher frequency than the in-phase torsion. In C_{2h} symmetry Au is the only one of the three very low frequency modes expected to be i.r. active, whereas for the cis configuration two of the three lowest frequency modes should be i.r. active. Although not very decisive, this is further evidence that the trans configuration is the correct one in the solid state.

It remains therefore to assign the i.n.s. bands at 68 and 87 cm^{-1} $((\pi-C_3H_5)_2Ni)$. We have no absolute way of doing this but the in-phase torsion is a whole body rotation. This is expected to be of low frequency so we tentatively assign the band at 68 cm^{-1} to this mode and the band at 87 cm^{-1} to the deformation.

The i.n.s. spectrum of $(\pi-C_3H_5)_2Pd$ shows four bands at ~ 50, 85, 135 and c.a. 160 cm^{-1}. The band at 160 cm^{-1} is a shoulder. The lowest frequency band is considerably less intense than the other three peaks and so we consider that it is probably a lattice mode. The remaining bands we assign by comparison with our assignments for $(\pi-C_3H_5)_2Ni$ to the in-phase torsion, deformation and out-of-phase torsion respectively. These assignments can only be tentative in the absence of further data.

Effective Force Constants

A) $[C_3H_5PdCl]_2$ and $[C_3H_5NiBr]_2$

Because we have only a single rotor we can use the high barrier approximation (chapter II) to calculate the effective force constants for the torsions. Because of the uncertainty in the location of the

peak positions etc. we have made the simplifying assumption that the axis of the rotor is the same as a principle axis of the whole molecule. We therefore obtain for $(C_3H_5PdCl)_2$ (with $\nu = 98$ cm^{-1}) $n^2V = 260$ kJ mole^{-1} and similarly for $(C_3H_5NiBr)_2$ ($\nu = 97$ cm^{-1}) $n^2V = 280$ kJ mole^{-1}. The similarity between these values is expected from the general similarity of the force constants found for Pd and Ni allyl complexes.[45]

B) $\underline{(C_3H_5)_2Ni \text{ and } (C_3H_5)_2Pd}$

In this case we have two identical rotors. If we write the potential energy variation on rotation as

For the external field $\qquad V_i = \dfrac{V_E}{2}(1 - \cos n \ \theta_i)$ $i = 1$ or 2

For the internal field $\qquad V = \dfrac{V_I}{2} (1 - \cos p \ (\theta_1 + \theta_2))$

Then using the methods described in chapter III we can obtain the following formulae for the torsional frequencies.

$$\omega_1^2 = \frac{(n^2V_E + 2p^2V_I)}{2I} \qquad \omega_2^2 = \frac{n^2V_E}{2I}$$

I is the moment of inertia of one rotor about the axis of rotation.

We therefore obtain two modes which are a) ω_1 the out-of-phase torsion and b) ω_2 the whole body rotation against the external field, and have

$$\omega_1^2 - \omega_2^2 = \frac{V_I p^2}{I}$$

Using the above equations we obtain the values for pV_I and n^2V_E shown in table 16.

The values of p^2V_I are very similar as one would expect and this

Table 16   Components of the Effective Force Constants for π-allyl

Complexes

	p^2V_I		n^2V_E		$\omega_1(cm^{-1})$	$\omega_2(cm^{-1})$
	kJ mole^{-1}	cm^{-1}	kJ mole^{-1}	cm^{-1}		
$(\pi-C_3H_5)_2Ni$	297.4	24,894	149	12,477	152	68
$(\pi-C_3H_5)_2Pd$	295.8	24,760	232.4	19,453	160	85
$(\pi-C_3H_5NiBr)_2$	280 (23,438 cm^{-1})		——		97	
$(\pi-C_3H_5PdCl)_2$	260 (21,764 cm^{-1})		——		98	

gives additional support for our tentative assignments for the $(\pi-C_3H_5)_2Pd$ complex.

A similar treatment for the norbornadiene complexes, involving analysis using in-phase and out-of-phase torsions, is not so fruitful because there are two different tops with their own periodicities and external barriers. The number of parameters is so large that with just two observed frequencies it is not possible to achieve a meaningful separation of the parameters for comparison between the complexes. We do, however, point out the very close similarity between the values of n^2V obtained for the π-allyls (table 16) and those obtained for the norbornadiene complexes with the assumption that the lower frequency is the torsional mode.

References

1. T.B. Chenskaya, L.A. Leites, V.T. Aleksanyan, L.S. Isaeva and L.N. Lorens, Zh.Strukt.Khim., 15(1), 31, (1974).

2. M.I. Davis and C.S. Speed, J. Organometal. Chem., 21, 401, (1970).

3. H. Oberhanner and H.A. Brune, Z. Naturforsch.A, 24(4), 607, (1969).

4. A.B. Gardner and T.C. Waddington, unpublished work.

5. D.C. Andrews and G. Davidson, J. Organometal. Chem., 36, 349, (1972).

6. V.T. Aleksanyan and M.N. Nefedova, Zh.Strukt.Khim., 14(5), 839, (1973).

7. D.C. Andrews and G. Davidson, J. Organometal. Chem., 76, 373, (1974).

8. See chapter III.

9. D. Bailey, A.D. Buckingham and A.J. Rest, Mol. Phys., 26(1), 233, (1973).

10. I.S. Butler and G.G. Barna, J. Raman Spectrosc., 1, 141, (1973).

11. I.A. Carbuzova, V.T. Aleksanyan and M.A. Pryanishnikova, Izv.Akad.Nauk. SSSR Ser.Khim., 8, 1722, (1973).

12. D.M. Adams and W.S. Fernando, Inorg. Chemica Acta, 7, 277, (1973).

13. I.W. Levin and W.C. Harris, Spectrochim. Acta, 29A(10), 1815, (1973).

14. V.T. Aleksanyan, I.A. Carbuzova and M.A. Pryanishnikova, Izv.Akad. Nauk. SSSR. Ser.Khim., 4, 777, (1973).

15. T.W. Muecke and I.M. Davis, Trans. Amer. Cryst. Assoc., 2, 173, (1966).

16. A. Yokozeki and K. Kuchitsu, Bull. Chem. Soc. Jap., 44, 2356, (1971).

17. N.C. Baenziger, H.L. Haight and J.R. Doyle, Inorg. Chem., 3, 1535, (1964).

18. N.C. Baenziger, G.F. Richards and J.R. Doyle, Acta. Cryst., 18, 924, (1965).

19. E.W. Abel, M.A. Bennett and G. Wilkinson, J. Chem. Soc., 3179, (1959).

20. D.B. Powell and T.J. Leedham, Spectrochim. Acta, 28A, 337, (1972).

21. See chapter IV.

22. F.A. Cotton and R.M. Wing, Inorg. Chem., 4, 314, (1965).

23. R.A. Love, T.F. Koetzle, G.J.B. Williams, L.C. Andrews and R. Bau,
     Inorg. Chem., 14, 2653, (1975).

24. R.E. Ghosh, T.C. Waddington and C.J. Wright, J.C.S. Faraday II, 69,
     275, (1973).

25. C.I. Ratcliffe, Ph.D. Thesis, University of Durham, 1975.

26. G. Wilke and B. Bogdanovic, Angew. Chem. Int. Ed., 73, 756, (1961).

27. J.K. Brecconsall, B.E. Job and S. O'Brien, J. Chem. Soc. A, 423,
     (1967).

28. E.J. Corey and M.F. Semmelhack, J. Amer. Chem. Soc., 89(11), 2755,
     (1967).

29. L.A. Leites, V.T. Aleksanyan and T.B. Chenskaya, Akad. Nank, SSSR.,
     215, 634, (1974).

30. E.N. Yurchenko and L.I. Kozhevina, Zh. Strukt, Khim.,.16(4), 688,
     (1975).

31. L.I. Kozhevina and E.N. Yurchenko, Zh. Prikl. Spektrosk., 21, 291,
     (1974).

32. C. Sourisseau and B. Pasquier, Can. Jnl. Spectrosc., 18(4), 91, (1973).

33. K. Shabotake and K. Nakamoto, J. Amer. Chem. Soc., 92, 3339, (1970).

34. D.M. Adams and A. Squire, J. Chem. Soc. (A), 1808, (1970).

35. C. Sourisseau and B. Pasquier, Can. Jnl. Spectrosc., 19(1), 11, (1974).

36. E.N. Yurchenko, L.I. Kozhevina and V.I. Smirnov, Zh. Prikl, Spectrosk.,
     23(3), 475, (1975).

37. W.E. Oberhansli and L.F. Dahl, J. Organometal. Chem., 43, 3, (1965).

38. D.R. Russell and P.A. Tucker, S.R.C. Neutron Beam Research Committee,
     Appendix to the Annual Report, 8, (1975).

39. G. Davidson and D.C. Andrews, J.C.S. Dalton, 126, (1972).

40. G.N. Bondarenko and M.P. Teterina, Dokl. Akad. Nauk. SSSR., 211, 95,
     (1973).

41. D.A. Brown and A. Owen, Inorgan. Chim. Acta., 5, 675, (1971).

42. H. Bönnemann, B. Bogdanovic and G. Wilke, Angew. Chem. Int. Ed.,
    6, 804, (1967).

43. R. Uttech and H. Dietrich, Z. Krist, 122, 60, (1965).

44. D.C. Andrews and G. Davidson, J. Organometal. Chem., 55, 383, (1973).

45. T.B. Chenskaya, L.A. Leites, V.T. Aleksanyan, L.S. Isaeva and L.N.
    Lorens, Izv. Akad. Nank. SSSR. Ser. Khim, 12, 2716, (1974).

46. F. Rocquet, L. Berreby and J.P. Marsault, Spectrochim. Acta., 29A,
    1101, (1973).

47. a) J.D. Dunitz, L.E. Orgel and A. Rich, Acta. Cryst., 9, 373, (1956).

    b) B.T.M. Willis, Harwell Report A.E.R.E. R.3708.

Chapter VIII: Ammines and Amides

We have obtained the i.n.s. spectra of some transition   metal

ammines and from the observed torsional frequencies, barriers to the NH_3

torsions have been calculated. As expected these are low and they are

in general agreement with values calculated from other techniques. We

have not observed any interaction between NH_3 rotors in molecules with

more than one rotor and this conflicts with some previously published

calculations and assignments. Evidence for significant metal-metal

interactions in some Pt complexes has also been obtained. Finally we

have studied some sulfur-nitrogen complexes and assigned some low

frequency modes as well as showing that the disilver salt of sulfamide

does not contain an NH_2 group.

Section I: Square Planar Palladium and Platinum Ammines

Introduction

We have obtained i.n.s. data on the complexes shown in table 1 and
this table also summarises on which spectrometers the data was obtained.
It is important to notice the large temperature range over which the
data was collected (table 1).

Table 1   Summary of I.N.S. data available for Pt and Pd ammines

	IN4* (4.5K)	6H* (295K)	BeF* (90K)
cis-Pt(NH$_3$)$_2$Cl$_2$	✓	✓	✓
trans-Pt(NH$_3$)$_2$Cl$_2$	✓	✓	✓
Pt(NH$_3$)$_4$Cl$_2$.H$_2$O		✓	✓
[Pt(NH$_3$)$_4$][PtCl$_4$]		✓	✓
cis-Pd(NH$_3$)$_2$Cl$_2$	✓	✓	✓
trans-Pt(NH$_3$)$_2$Cl$_2$	✓	✓	✓
Pd(NH$_3$)$_4$Cl$_2$.H$_2$O		✓	✓

*   See chapter III; BeF Beryllium Filter Detector

There are two main aspects of this work

a)   the observation of torsional and metal-nitrogen skeletal modes
which are absent or weak in the i.r. and Raman spectra of these complexes.

b)   investigation of the possibility of coupling between NH$_3$ groups on
the same metal atom.

The barriers to rotation of the NH$_3$ ligands in several complexes
e.g. trans-Pd(NH$_3$)$_2$Cl$_2$,[1] trans-Pd(NH$_3$)$_2$I$_2$,[1] [Pd(NH$_3$)$_4$Cl$_2$]Cl,[2]
Co(NH$_3$)$_6$I$_2$,[3] and Ni(NH$_3$)$_6$I$_2$[3] have been determined by a variety of
methods e.g. i.n.s., i.r. bandshape analysis and thermodynamic and

n.m.r. measurements. In every case the barrier has been found to be very low c.a. 2-8 kJ mol^{-1} (table 2). Even with a barrier as low as this the torsional frequency will be comparatively high because the moment of inertia of the ligand, about the axis joining the nitrogen atom to the metal atom, is very small (c.a. 2.816 x 10^{-40}gm cm^2).[4]

Table 2   Potential Barriers to the Internal Rotation of NH_3 Ligands

COMPLEX	BARRIER		Frequency of $\tau(NH_3)$ cm^{-1}	Ref.
	kJ mole^{-1}	cm^{-1}		
trans-Pd(NH$_3$)$_2$Cl$_2$	7.9	661	-	5
trans-Pd(NH$_3$)$_2$Cl$_2$	5.1	430	-	1
trans-Pd(NH$_3$)$_2$Cl$_2$	6.4	532	193	a
trans-Pd(NH$_3$)$_2$I$_2$	2.7	225	-	1
cis-Pd(NH$_3$)$_2$Cl$_2$	5.1	430	-	5
cis-Pd(NH$_3$)$_2$Cl$_2$	6.4	532	192	a
cis-Pt(NH$_3$)$_2$Cl$_2$	5.4	532	177	a
trans-Pt(NH$_3$)$_2$Cl$_2$	4.6	381	162	a
Pd(NH$_3$)$_4$Cl$_2$.H$_2$O	5.4	532	176	a
Pd(NH$_3$)$_4$Cl$_2$	4.2	350	-	6
Pt(NH$_3$)$_4$Cl$_2$.H$_2$O	5.4	532	178	a
(Pt(NH$_3$)$_4$)(PtCl$_4$)	6.8	566	201	a, 15

a)   this work

An n.m.r. study of cis and trans-Pd(NH$_3$)$_2$Cl$_2$[5] has been interpreted on the basis that there are two inequivalent ammine ligands in the trans form and the second moments for both complexes are consistent with ammine reorientation which is occurring at a sufficient rate (above 77K) to narrow the n.m.r. line. It was also concluded that whole-molecule rotation does not take place in either complex but that libration probably does. The presence of the two inequivalent groups in the trans complex can be explained because this complex exists in two

crystalline forms which occur together unless special care is taken during the preparation.[7] It was also found that the activation energy for the cis is lower than for the trans complex and the authors ascribed this to the presence of greater intermolecular interactions[5] in the trans form. From measurements of the band contours of the perpendicular (E) vibration in the i.r. Leech et al.[1] have determined the barriers in trans-$Pd(NH_3)_2Cl_2$ and trans-$Pd(NH_3)_2I_2$ (see table 2).

The possibility of coupling of the NH_3 torsions, in the platinum complexes, via the metal "d" orbitals, has been considered by Nakamoto et al.[8] in order to explain the presence of splitting of i.r. bands in the NH_3 deformation region (c.a. 1580 cm^{-1}). This splitting is characteristic of square-planar platinum complexes which contain at least two ammine ligands and it is of greater magnitude in trans complexes than in cis. They were able to eliminate other possible causes for this splitting and by including the ligand-ligand interaction into a normal co-ordinate analysis they were able to reproduce the observed number of bands and obtain good agreement between the calculated and observed frequencies. The smaller effect in cis complexes compared to trans was explained (see fig. 1) as a consequence of the
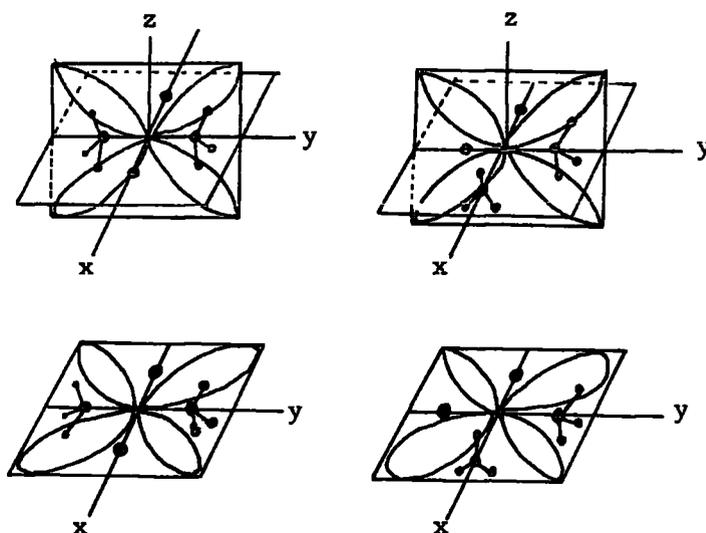
Fig. 1. Possible interactions through "d" orbitals for cis and trans rotors.

ligands having only one "d" orbital in common in the cis form compared to two in the trans configuration. The effect is expected to be smaller for Pd ammines because of the smaller spatial extent of the metals' "d" orbitals (fig. 1).

Experimental

Cis and trans-$Pt(NH_3)_2Cl_2$[9] and cis and trans-$Pd(NH_3)_2Cl_2$[7] were prepared by literature methods. $[Pt(NH_3)_4][PtCl_4]$, $Pt(NH_3)_4Cl_2.H_2O$ and $Pd(NH_3)_4Cl_2.H_2O$ were purchased from Johnson Matthey.

The purity of the complexes was checked by i.r. spectroscopy and in the case of the Pd complexes by comparison of their i.r. spectra and x-ray powder photographs with literature data.[7] The low-temperature monoclinic form of the trans Pd complex was prepared. I.N.S. spectra were obtained with the samples held in thin aluminium sachets. See table 1 for further experimental conditions.

Barrier Calculations

Barrier heights have been calculated using the tables of solutions of the Mathieu Equation produced by Herschbach (chapter II). Because the crystal structures of some of the complexes are not known and in any case no proton positions have been determined, we have used the minimum moment of inertia (I) of gaseous NH_3 (calculated from spectroscopic data[4]) for the barrier calculations. Furthermore because the moment of inertia of NH_3 is so small we have made the approximation $I_r \approx I$ [for example $I = 2.816 \times 10^{-40}$g cm^2;[4] I_r for $Pt(NH_3)_4Cl_2$ is 2.783×10^{-40}g cm^2 assuming NH_3 is a point mass for calculating the moment of inertia of the whole molecule]. I_r is the reduced moment of inertia of a single NH_3 ligand (chapter II).

a) **I.N.S. Results**

Figs. 2a,b,c show our i.n.s. data for the complexes listed in table 1. Some 6H spectra (chapter III) are shown for comparison with the data obtained using IN4 (chapter III). The IN4 data is obviously far better resolved than that from 6H, however, it must be noted that the IN4 results (neutron downscattering) were obtained with the samples at 4.5K and the 6H (neutron upscattering) results with the samples at ambient (c.a. 295K) temperatures. Narrower bands would be expected at lower temperatures.

b) **Ligand-Ligand Interactions**

If the NH_3 ligands in the cis and or trans complexes are coupled then it is easily shown that two torsional modes are expected. These are the in-phase (i.p.) and out-of-phase (o.p.) modes (fig. 3). The dynamical equations for this system can be solved and the results are
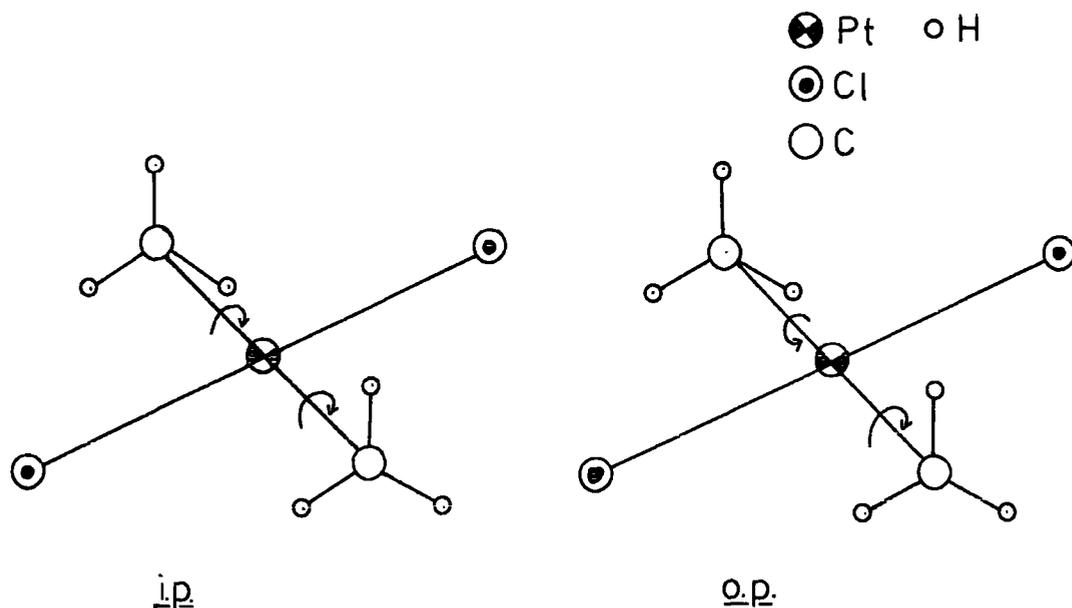
Fig. 3   In and Out-of-Phase Torsions of $M(NH_3)_2X_2$ complexes.
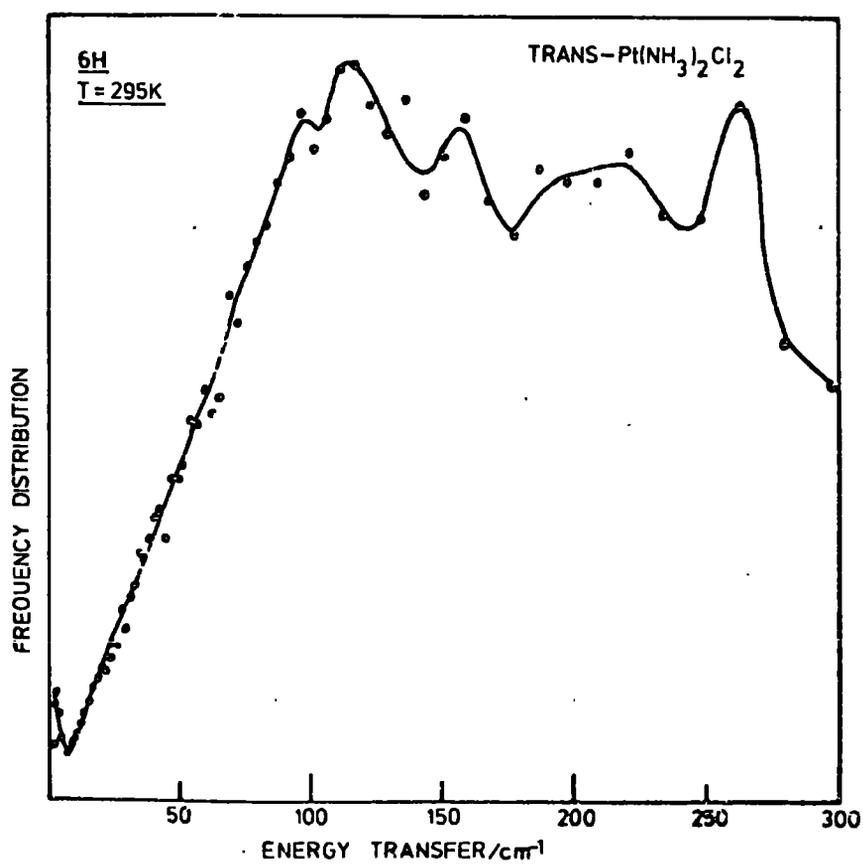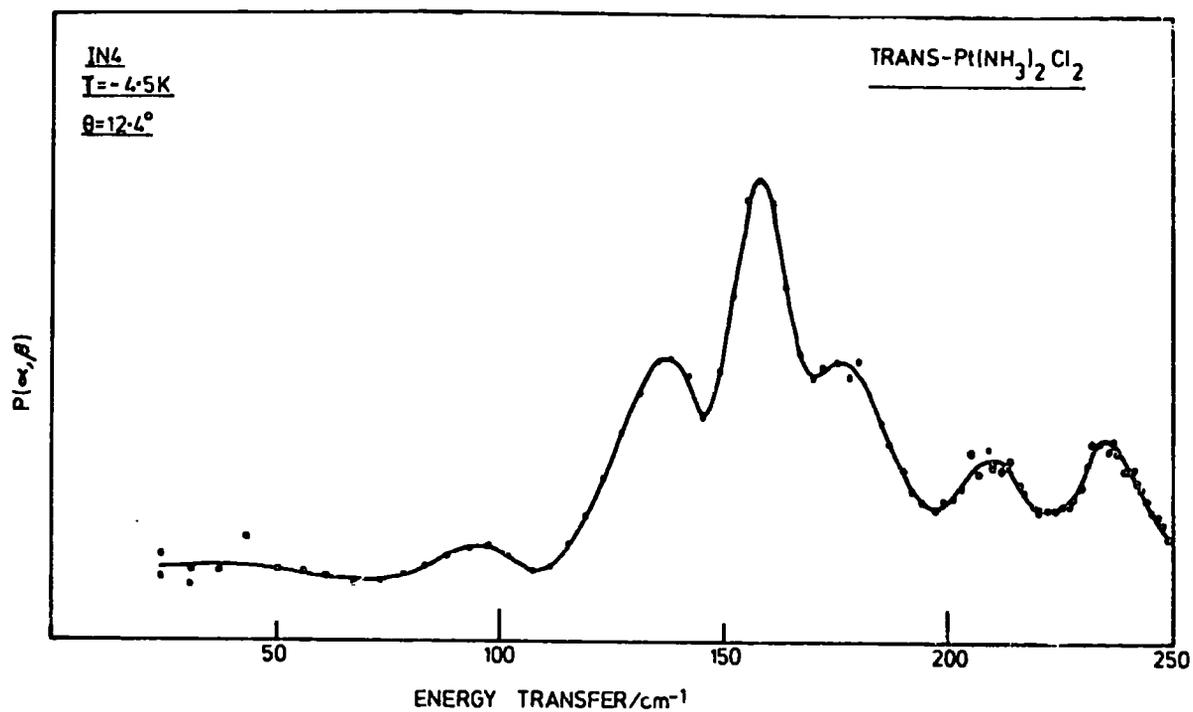
Fig. 2a Time of Flight Data for Trans-Pt(NH$_3$)$_2$Cl$_2$
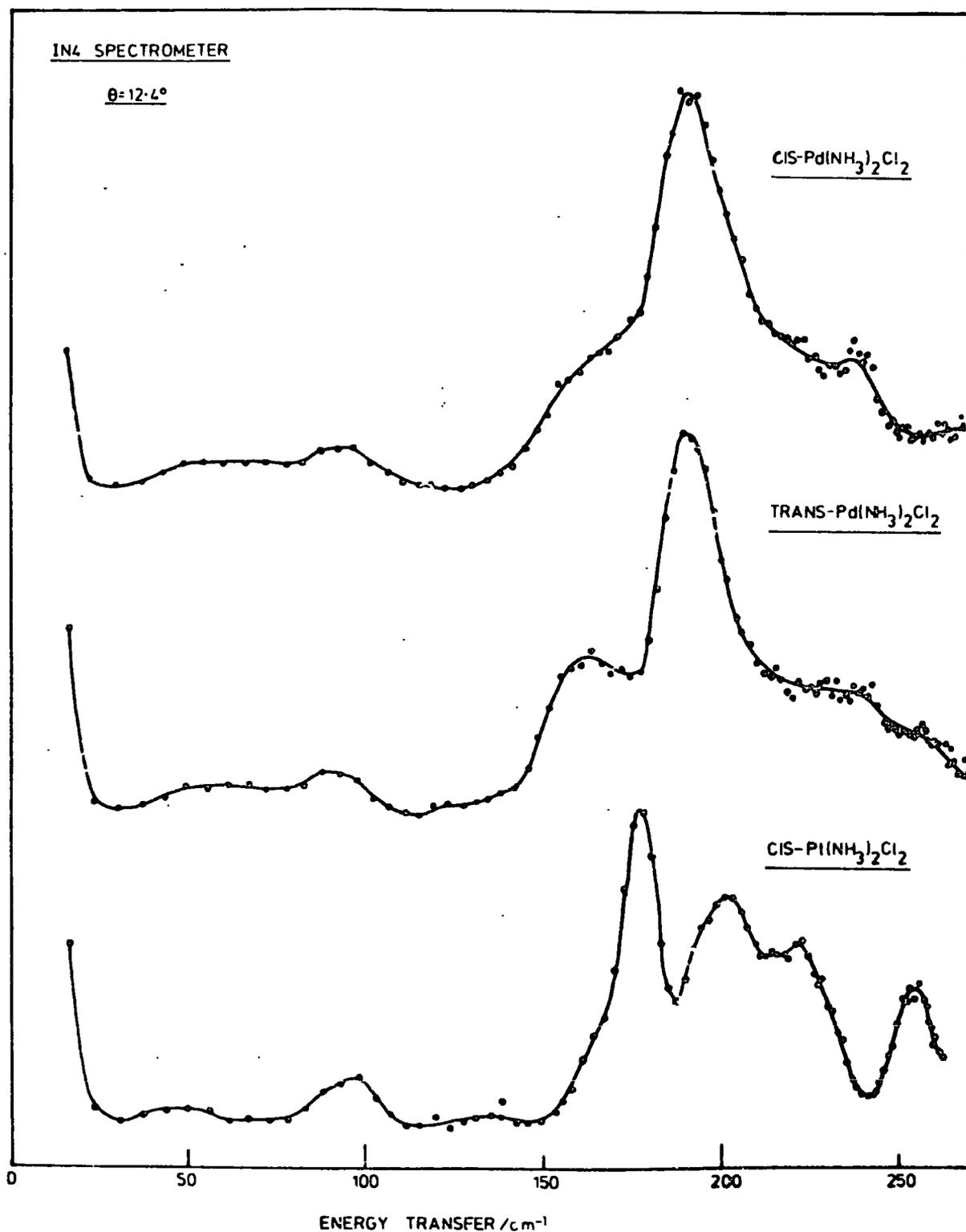
Fig. 2b IN4 Results for Square Planar Pd and Pt Ammines

$\rho(\omega)$

$\underline{Pt(NH_3)_4 \, Cl_2 H_2O}$

$\underline{Pd(NH_3)_4 \, Cl_2 H_2O}$

$\underline{[Pt(NH_3)_4 \,][PtCl_4]}$

ENERGY TRANSFER /cm^{-1}
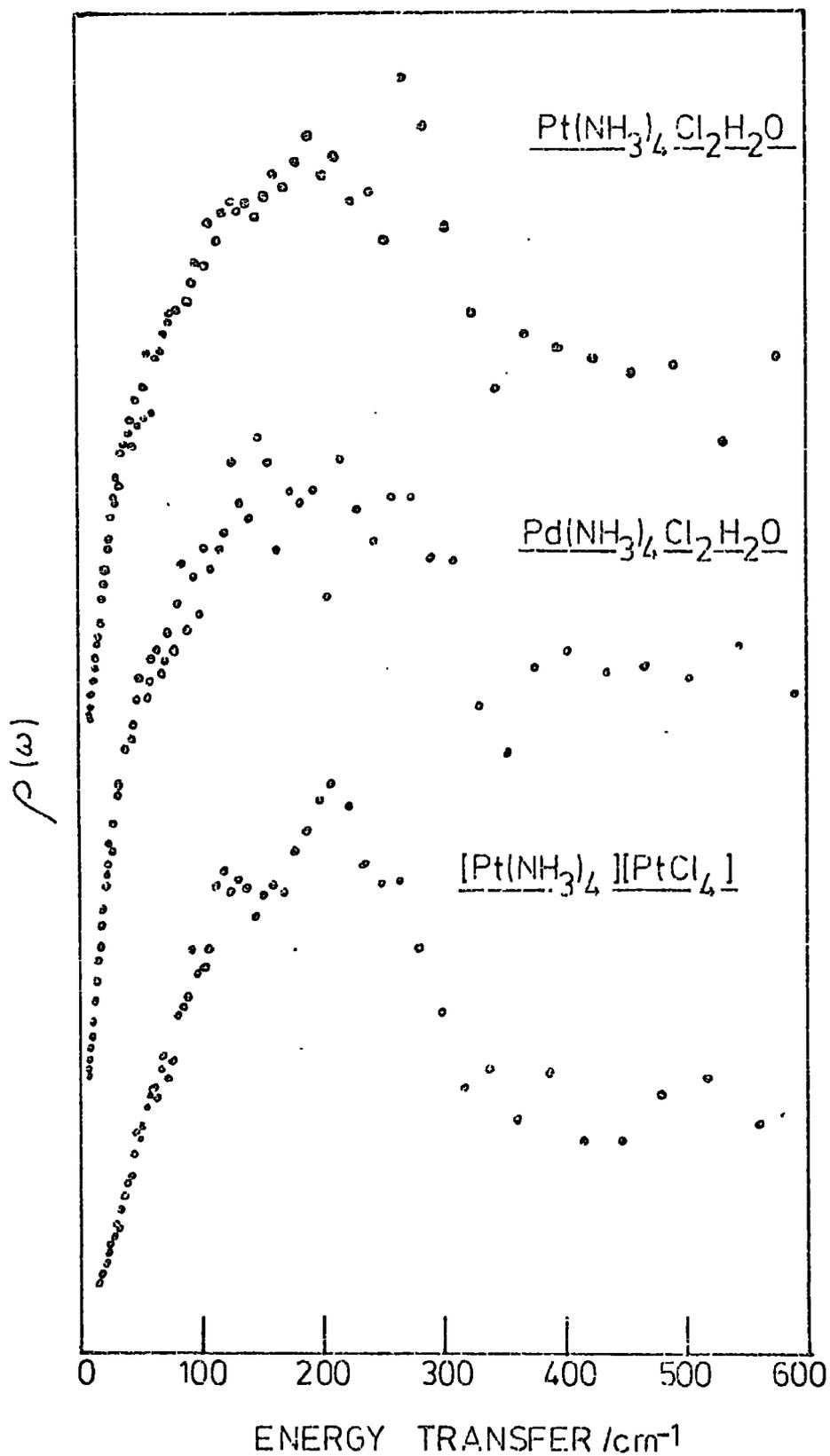
FIG. 2c.

identical to those obtained for the bis-π-allyls (see chapter VII) and for the hydrazinium salts[10] i.e.

$$\omega_{i.p.}^2 = \frac{V_o n^2}{2I} \qquad\qquad \omega_{o.p.}^2 = \frac{V_o n^2 + 2V_{1,2} p^2}{2I}$$

where V_o is the barrier height for a single NH_3 torsion and n is the

barrier multiplicity

$V_{1,2}$ is the barrier height for the interaction between the ligands

and p is the barrier multiplicity. (See chapters II and VII).

These two modes are expected to be of equal intensity in the i.n.s.

spectra and because the moment of inertia is so small we would expect

the torsions to be the most intense bands. Therefore, if significant

ligand-ligand interaction takes place we expect to see two equally

intense features in the i.n.s. spectrum of trans-$Pt(NH_3)_2Cl_2$ with

perhaps two similar bands in the spectrum of the cis complex but being

closer together in this case. The i.n.s. spectra of the Pd complexes

should show little or probably no splitting i.e. contain a single intense

band. Figs. 2a,b, show the relevant i.n.s. spectra and it can be seen

that only a single intense band is found in each case. On the basis of

its intensity we assign this band (150-200 cm^{-1}) in each spectrum

(figs. 2a,b,) to the NH_3 torsion and we conclude that the NH_3 rotors are

at most coupled very weakly.

If the splitting is so small that it has not been resolved we can

at least put a limit on it. The full width at half height of the

torsional band in trans-$Pt(NH_3)_2Cl_2$ cannot be more than 15 cm^{-1} and so

the splitting must be less than this. If there are two unresolved

bands they must be very narrow or very close together. This does not

seem likely because the bands corresponding to the torsional mode in all

of the complexes appear to have approximately the same half widths, though this is difficult to measure because of the incomplete resolution of the spectra.

The i.n.s. data for the cis and trans complexes together with i.r. and Raman assignments is given in tables 3a,b. Nakamoto[8] et al. have predicted a band at 181 cm^{-1} (δ(N-Pt-Cl)) for trans-$Pt(NH_3)_2Cl_2$ and we are able to confirm (fig. 2a) that an i.n.s. band occurs in this region.

If our interpretation of the i.n.s. spectra of these complexes is correct then the reason for the splitting of the i.r. bands in square planar Pt complexes is not yet clear.

c) Metal-Metal Interactions

There have been two detailed assignments of Magnus' Green Salt (M.G.S.), $[Pt(NH_3)_4][PtCl_4]$. Hiraishi et al.[11] assigned a temperature dependent i.r. band at c.a. 200 cm^{-1} to the A_{2u} (In D_{4h} symmetry) translational lattice mode (involving anti-phase motion of anion and cation) which, although it would normally be expected to occur below 100 cm^{-1}, had been increased in frequency as a result of metal/metal interactions. Such interactions have been indicated by some spectral properties[12] and the anisotropic electrical conductivity[13] of M.G.S. Magnus' Green Salt consists of columnar stacks in which anions and cations alternate. The Pt-Pt distance is 3.25Å.[14] Adams et al.[15] obtained single crystal i.r. and Raman spectra of $[Pt(NH_3)_4][PtCl_4]$ and although they agreed that the mode at 200 cm^{-1} had A_{2u} symmetry they assigned it to the NH_3 torsion. They have eliminated the possibility of a phase change (to -100°C) by showing that there was no specific heat anomaly. By comparing the force constant for the metal/metal interaction, implied by the assignment of 200 cm^{-1} to the lattice mode, with known

Table 3a Summary of Spectroscopic Data and Assignments for cis and trans-Pt(NH$_3$)$_2$Cl$_2$(cm^{-1})

cis-Pt(NH$_3$)$_2$Cl$_2$			trans-Pt(NH$_3$)$_2$Cl$_2$		
I.R. + R.[a]	I.N.S.	ASSIGNMENTS	I.R. + R.[a]	I.N.S.	ASSIGNMENTS
248	254	δ(N-Pt-N)	248		δ(N-Pt-N)
210	221	δ(N-Pt-Cl)	235	239	out-of-plane Pt-N bend
			207[a]	213	
198	201	Pt-N out-of-plane bend		181[b]	δ(N-Pt-Cl)
	177	Torsion		162	Torsion
156	165	δ(Cl-Pt-Cl)	156		δ(Cl-Pt-Cl)
127		} Lattice vibrations	136	140	out-of-plane Pt-Cl bend
85	97			95	
	50			50	

a) from ref. 36   b) Predicted in ref. 8

Table 3b Summary of Spectroscopic Data and Assignments for cis and trans Pd(NH$_3$)$_2$Cl$_2$(cm^{-1})

cis - Pd(NH$_3$)$_2$Cl$_2$			trans-Pd(NH$_3$)$_2$Cl$_2$		
I.R.[c]	I.N.S.	ASSIGNMENTS	I.R.[c]	I.N.S.	ASSIGNMENTS
	270			255?	
245	238	Pd-N bend	245	240	Pd-N bend
218	220?	Pd-N bend	220		Pd-N bend
	192	Torsion		193	Torsion
160	165	Pd-Cl bend	162	165	Pd-Cl bend
135		Pd-Cl bend	137		} Lattice modes
109	97	} Lattice modes		93	
	57			60	

c) from ref. 38

metal-metal force constants they deduced that the frequency was too high

for it to be attributed to this mode. Instead the lattice mode was

assigned to a band at 81 cm^{-1}. Our i.n.s. spectra (fig. 4) show that

the most intense band occurs at 200 cm^{-1}. From our previous discussion

we assign this to the $\tau(NH_3)$ mode thereby agreeing, thus far, with the

assignments of Adams et al. The remaining i.n.s. bands coincide with

the i.r. and Raman assignments. In support of their assignment of the

200 cm^{-1} band to $\tau(NH_3)$, Adams et al. point out that there is no

temperature dependent band in the i.r. spectrum of trans-$Pt(NH_3)_2Cl_2$.

If the band at 200 cm^{-1} (in M.G.S.) were the A_{2u} lattice mode

raised in energy as a result of Pt-Pt interaction then this is just what

one would expect because the Pt-Pt distance[16] in the trans Pt complex is

c.a. 5Å compared to 3.25 in M.G.S. We have, however, observed a

temperature dependent i.r. band (fig. 5) at 195-210 cm^{-1} for cis-

$Pt(NH_3)_2Cl_2$ and in this complex the Pt-Pt distance[16] is 3.37Å i.e.

comparable with that found for M.G.S. Furthermore in this case the

torsion occurs at lower frequency than in M.G.S. (162 cm^{-1} (i.n.s.)

fig. 2b) therefore the temperature dependent band cannot be the torsion.

The reduced mass of two $Pt(NH_3)_2Cl_2$ molecules is almost identical to

that of the $Pt(NH_3)_4^{2+}$ $PtCl_4^{2-}$ ions so perhaps it is not too surprising

that the lattice mode should occur at a similar frequency if the Pt-Pt

distances are very similar.

Further evidence that the i.r. and i.n.s. bands close to 200 cm^{-1},

in the spectra of cis-$Pt(NH_3)_2Cl_2$,are due to a lattice mode is obtained

from the momentum transfer (Q) dependence of the i.n.s. spectrum

(fig. 6). It can be seen that at high angles this mode is as intense

as the torsion. This does not occur for any of the other complexes and

Fig. 4 B.F.D. Spectrum of Magnuss' Green Salt

$[Pt(NH_3)_4][PtCl_4]$

201

252

402

515

INTENSITY

INCIDENT NEUTRON ENERGY/cm^{-1}

200 300 400 500 600
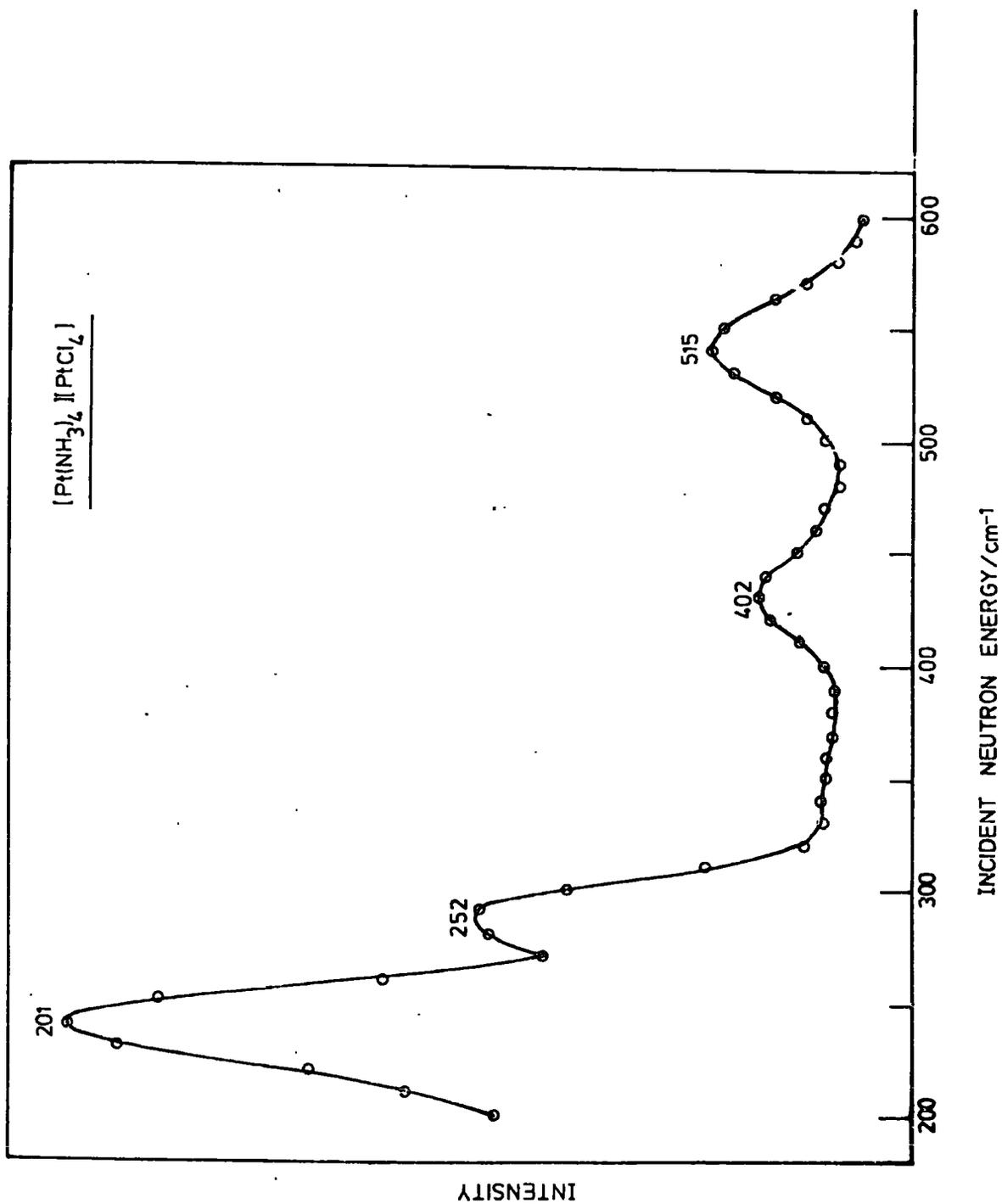
Fig. 5 Temperature Dependence of the I.R. Spectrum of cis-Pt(NH$_3$)$_2$Cl$_2$

266.

INA

CIS-Pt(NH$_3$)$_2$Cl$_2$

$\theta = 12\cdot4°$

$\theta = 87\cdot8°$

$\theta = 123\cdot8°$

INTENSITY

ENERGY TRANSFER/cm^{-1}
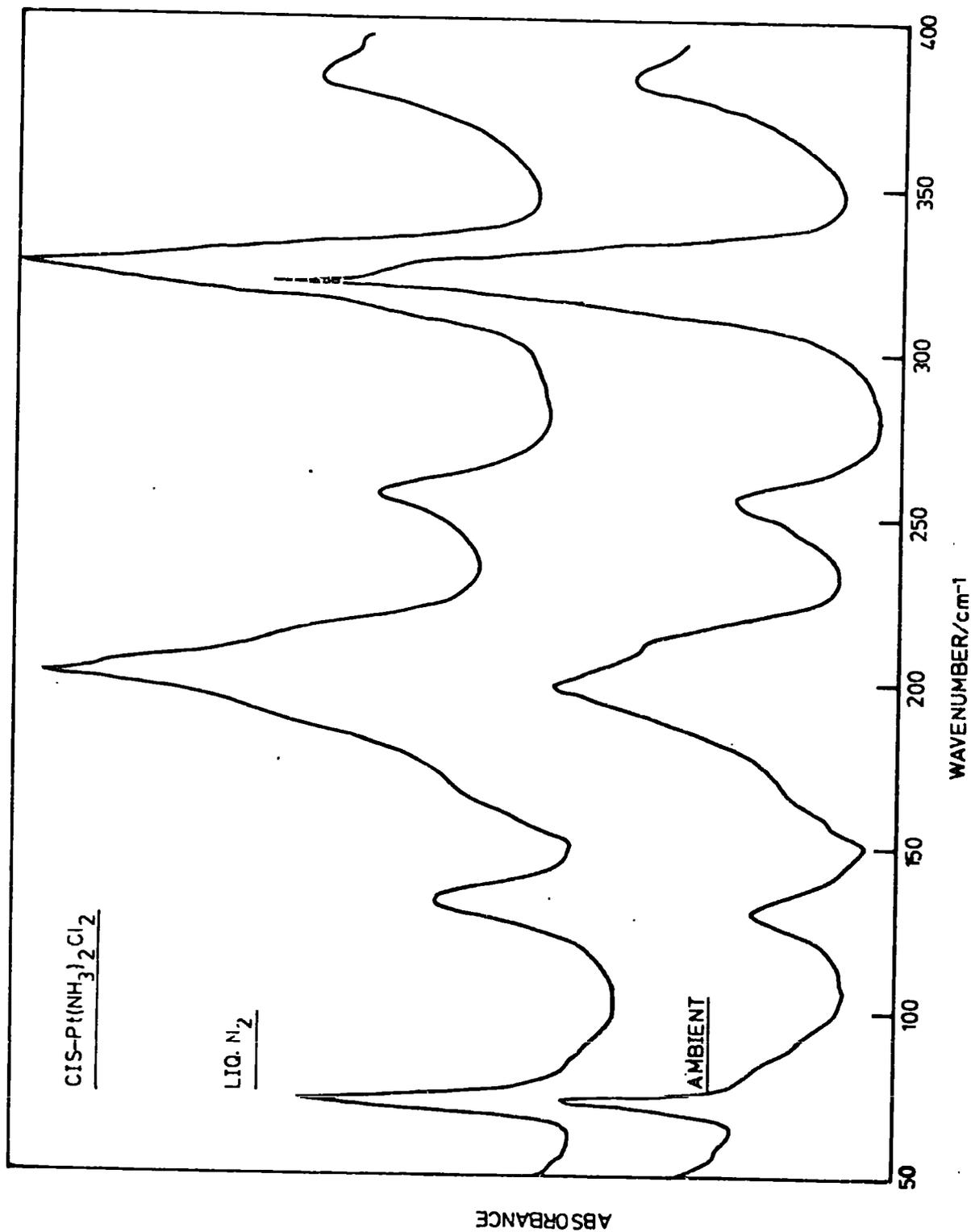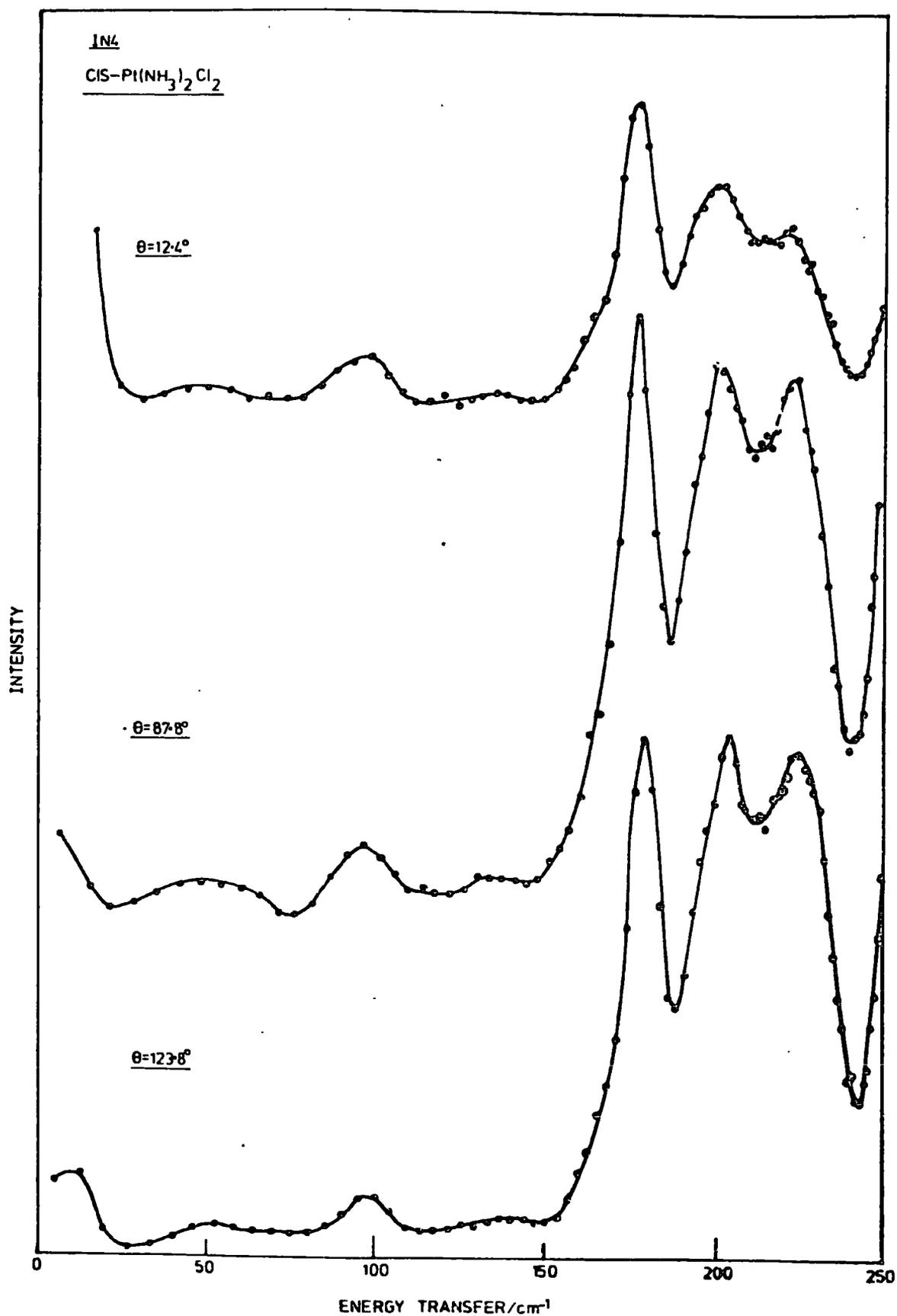
Fig. 6 Momentum Transfer Dependence of i.n.s. Bands of
cis-Pt(NH$_3$)$_2$Cl$_2$

such "$\underline{Q}$" dependence is very difficult to explain on any other basis than that it is associated with a lattice vibration (chapter II).

In view of this data it appears that for M.G.S. the band at 200 cm^{-1} is probably the coincident lattice and torsional modes. These are, however, separated in cis-Pt(NH$_3$)$_2$Cl$_2$. This also explains the very high relative intensity of the torsion in M.G.S. relative to the skeletal modes. The relative intensity is considerably greater than that found in the cis/trans complexes and in Pt(NH$_3$)$_4$Cl$_2$ (see next section).

If the NH$_3$ rotors in Pt(NH$_3$)$_4{}^{2+}$ were coupled, then using the methods described in chapters II and IV, we can show that we would expect three distinct modes (one being doubly degenerate) as a result of this interaction. Unfortunately we do not, as yet, have any high resolution data on M.G.S. or Pt(NH$_3$)$_4$Cl$_2$ but in view of our results for the cis/trans complexes it seems very likely that the interaction is very weak and so we would expect to find just a single torsional mode.

d) $\underline{Pt(NH_3)_4Cl_2}$ and $\underline{Pd(NH_3)_4Cl_2}$

Assignments for the skeletal vibrations of these complexes have been summarised by Schmidt[17] (table 4). In the i.n.s. spectra of both complexes (fig. 7 and table 4) there is once again a band at c.a. 175 cm^{-1}, however, it is not the most intense feature in the spectra. Reference to table 4 shows that three of the skeletal modes occur very close together in each complex and so this explains the high intensity at c.a. 280 cm^{-1} relative to the NH$_3$ torsion, which we assign to the bands at c.a. 175 cm^{-1}. There are no i.r. bands in the region of 175 cm^{-1}.
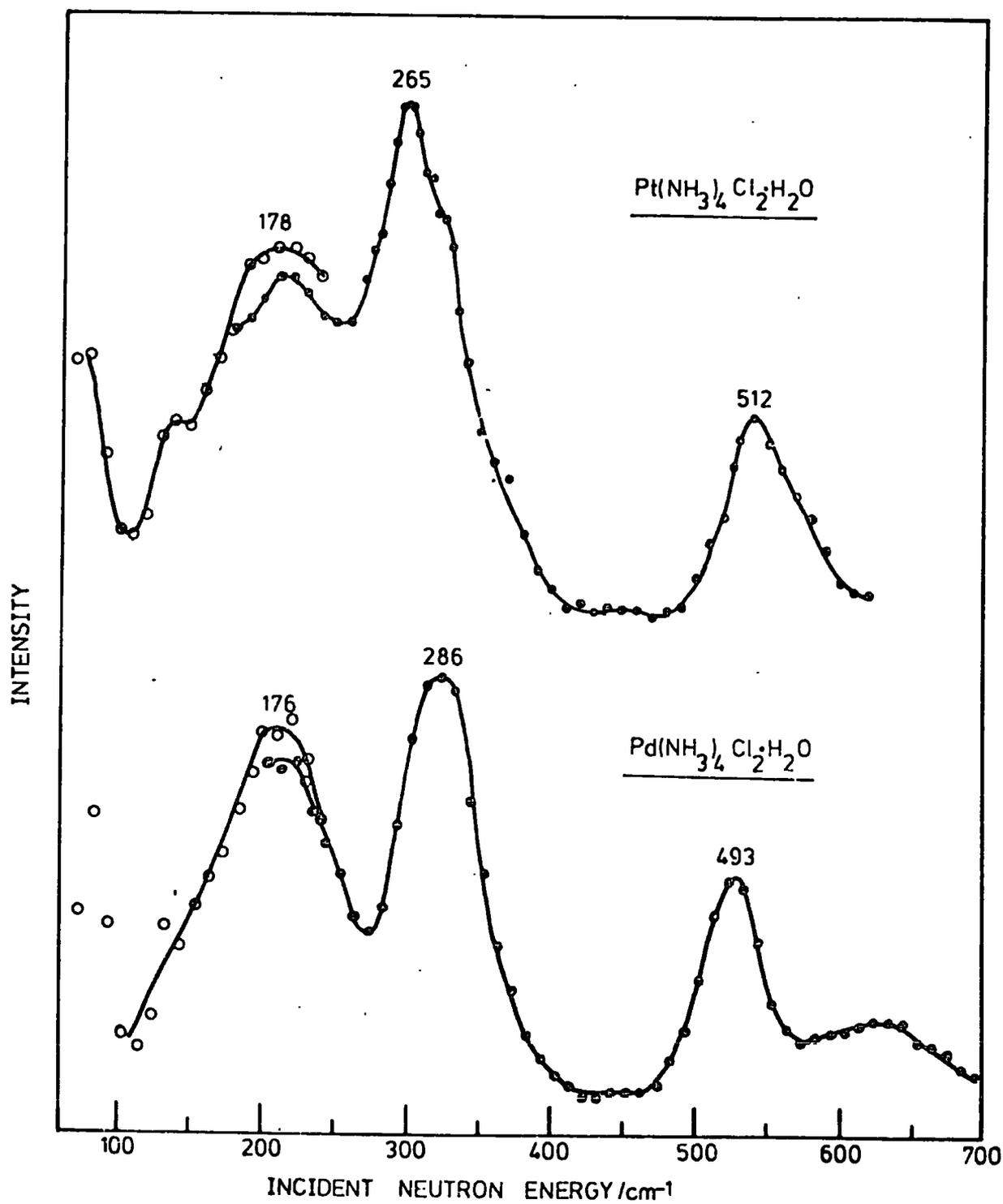
Fig. 7 B.F.D. Spectra of $Pt(NH_3)_4Cl_2.H_2O$ and $Pd(NH_3)_4Cl_2.H_2O$

Table 4 Summary of Spectroscopic data for $M(NH_3)_4Cl_2$ where M = Pd,Pt (cm^{-1})

$Pd(NH_3)_4Cl_2 \cdot H_2O$		Assignment		$Pt(NH_3)_4Cl_2 \cdot H_2O$	
I.R. + R.*	I.N.S.			I.R. + R.*	I.N.S.
105		Latt. vib.		122	
	176	$\tau(NH_3)$			178
237		$\delta(NMN)$ ν_4		235	
291	286	$\delta_a(NMN)$ ν_7		270	265
305		$\delta(NMN)$ ν_3		297	291(sh)
468		$\nu(M-N)$ ν_2		526	
494	493	$\nu_{as}(MN)$ ν_6		510	512
510		$\nu_s(M-N)$ ν_1		538	

* From ref. 17

The barrier to rotation of the NH_3 ligands in $Pd(NH_3)_4Cl_2$ has been calculated[6] from heat-capacity measurements to be 4.2 kJ mol^{-1}. Using the tables due to Herschbach we have obtained the barriers for $Pd(NH_3)_4Cl_2$ and $Pt(NH_3)_4Cl_2$ shown in table 2.

Conclusion

The barrier heights that we have calculated using our i.n.s. data are in general in reasonable agreement with those calculated by other methods (table 2). The barriers for the cis and trans Pd complexes are higher than for the corresponding Pt complexes. From the crystal structures of cis and trans-$Pt(NH_3)_2Cl_2$[16] there appears to be only one possible hydrogen bond in each case. As far as we are aware there are no crystal structures available for cis and trans-$Pd(NH_3)_2Cl_2$. It has

been stated that there is no hydrogen-bonding in M.G.S. and in this case

the barrier height is very close to that found for the cis/trans

palladium compounds.

Section II: Sulfur-Nitrogen Complexes

Experimental

Sulfamic acid was obtained from B.D.H. and used without further purification.   Sodium sulfamate was prepared by neutralisation of sulfamic acid and sulfamide was prepared by a literature method.[37] The disilver salt of sulfamide was kindly donated by E. Nachbaur.

I.N.S. spectra were obtained using the B.F.D. spectrometer (chapter II) with the samples at c.a. 90K.   The samples were run in aluminium sachets except for sulfamic acid which was run in a silica cell.

a)   Sulfamic Acid and Sodium Sulfamate

Sulfamic acid is known to be a Zwitterion.   Its i.n.s. spectrum is shown in fig. 8a.   Detailed infrared[18] and Raman[19] studies have been published and the low frequency assignments $(170 \rightarrow 900 \text{ cm}^{-1})$ together with a summary of the i.n.s. $(160 \rightarrow 550 \text{ cm}^{-1})$ results are shown in table 5.

Table 5   I.N.S. Raman and i.r. Data for Sulphamic Acid

I.N.S.	I.R.	R.	Assignment[a]
162		170	NH ..... O
		240	NH ..... O
267			Torsion[b]
362	352	357 378	SO_3^- rock
520 537	526 540	535 550	SO_3^- def$^{\underline{n}}$
	682	678	S-N stretch
	695	697	
		862	

a) Ref. 19   b) this work

FIG. 8.

(a) $\underline{NH_3SO_3-}$

(b) $\underline{NaSO_3NH_2-}$

162
267
362
520 537
162

344
465
491
574
684
809

INTENSITY

INCIDENT NEUTRON ENERGY /cm⁻¹

FIG. 8.

(c) $SO_2(NH_2)_2^{2-}$

(d) $Ag_2N_2O_2H_2S$

INTENSITY

INCIDENT NEUTRON ENERGY/cm⁻¹
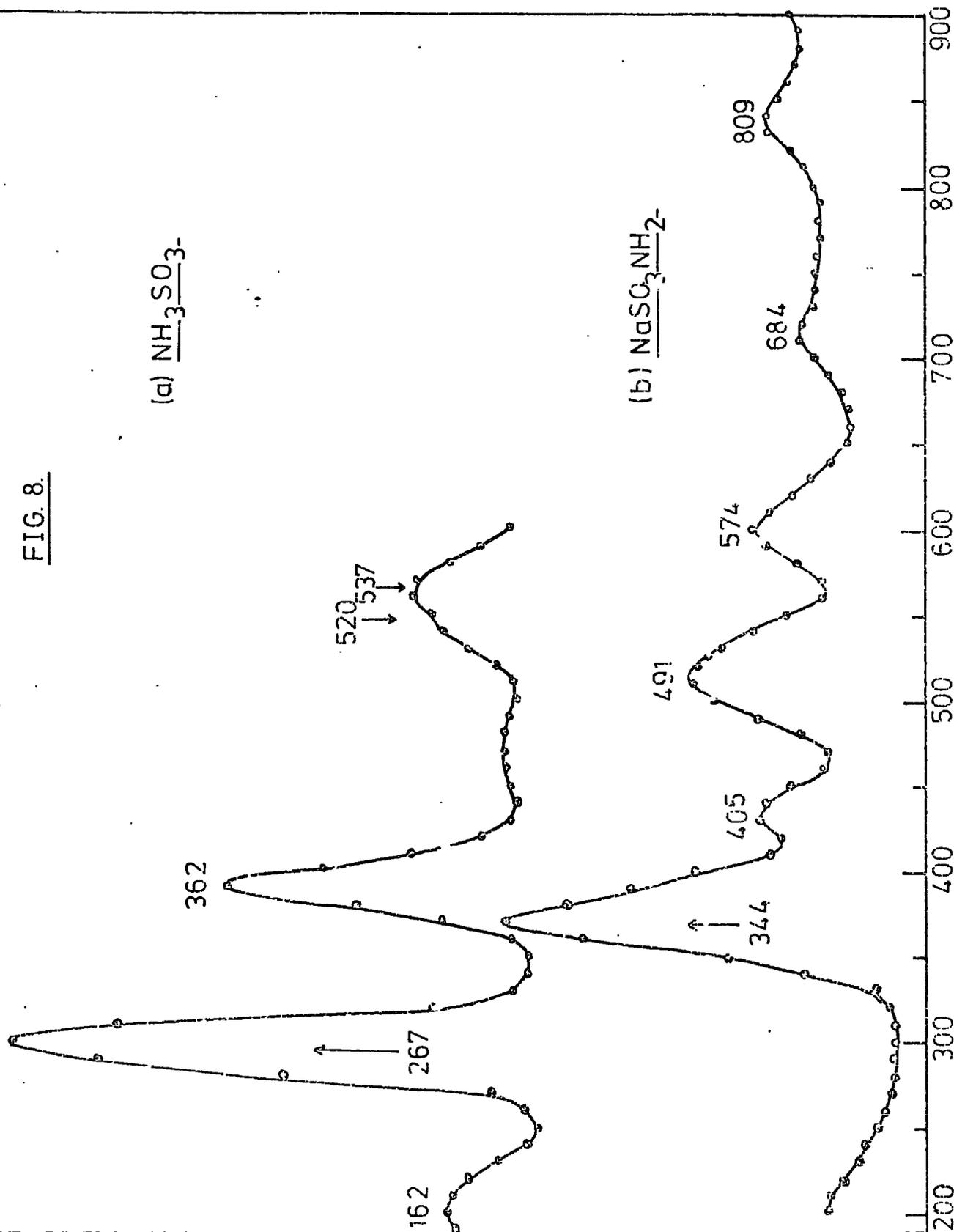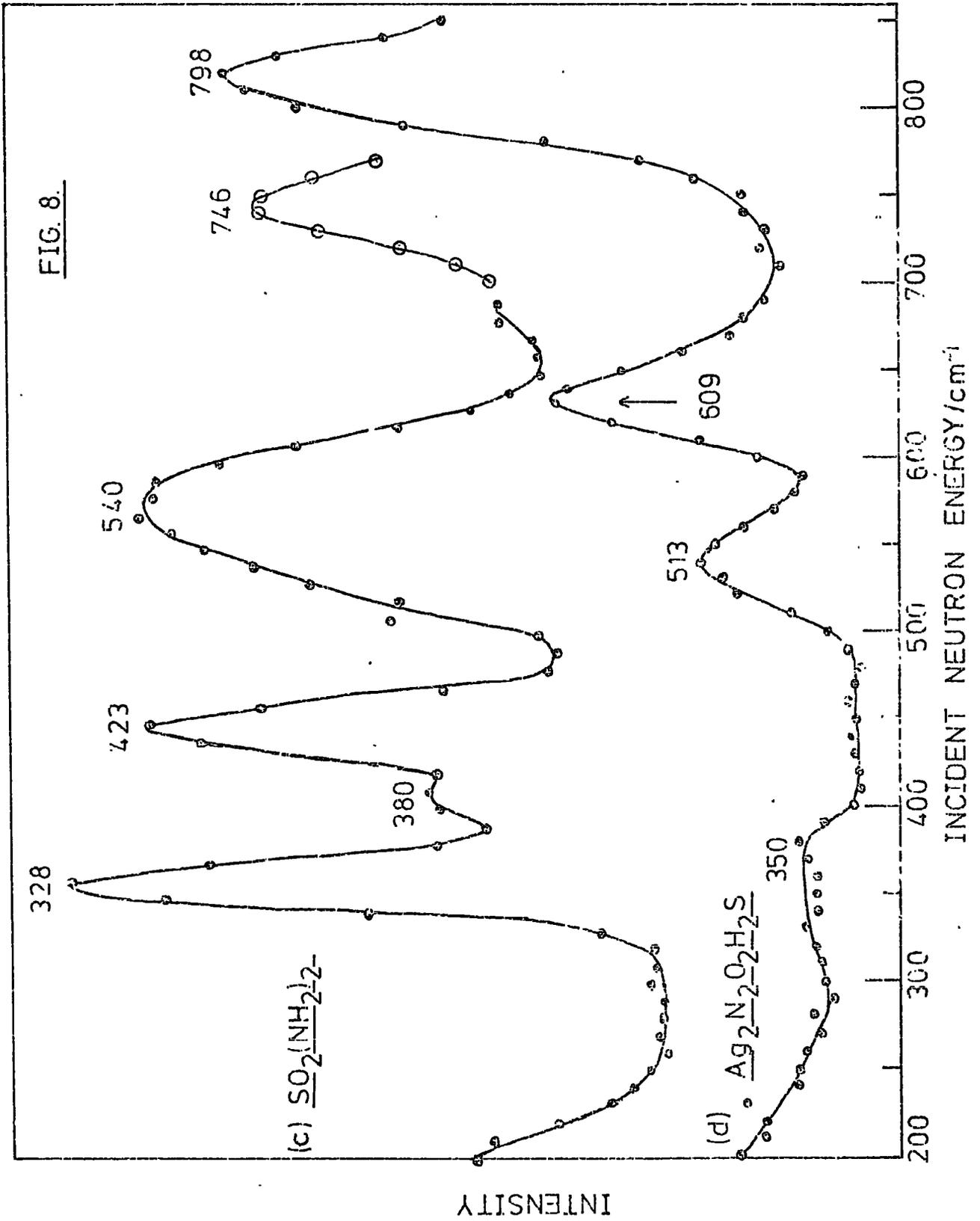
It can be seen from table 5 that the only i.n.s. band which cannot be assigned by direct comparison with the optical data is the very intense band at 267 cm^{-1}. In view of its intensity in the i.n.s. spectrum and its inactivity in the i.r. and Raman spectra we assign this mode to the NH_3 torsion.

From the frequencies of the N-H stretching vibrations and the neutron diffraction data of Sass[20] it has been deduced that extensive hydrogen bonding occurs in the crystal. Fig. 9 shows a projection of the sulfamic acid molecule along the S-N bond.[20] Each hydrogen forms essentially one hydrogen bond as shown. The O-H distances are shown on the diagram. Also the S-N bond length in $NH_3^+ SO_3^-$ is 1.764Å which is very close to the value predicted for a single bond (1.74).[21] The external field, resulting from the hydrogen bonds, probably explains, at least in part, the increase in frequency of the NH_3 torsion in sulfamic acid relative to that found in the ammines of Pd, Pt and Co and Ni (150 → 200 cm^{-1}). If we assume that the barrier multiplicity is three we can use Herschbachs' Tables (chapter II) to calculate the barrier to the torsion. The calculated value is 11.3 kJ $mole^{-1}$ (953 cm^{-1}).

Fig. 9. Hydrogen—Bonding in Sulfamic Acid.

I.R. and R. data and assignments are available for Na^{22}, Ca^{22} and K^{23} sulfamates. The high values (3301 and 3281 cm^{-1}) for the NH_2 stretching modes in the sodium salt indicate that there is no appreciable

hydrogen bonding in the crystal. The structure of the sulfamate ion[24] is shown in fig. 10 and the i.n.s. spectrum in fig. 8b. Table 6 is a summary of the i.r., R. and i.n.s. data with the assignments $(200 \rightarrow 900 \text{ cm}^{-1})$ Because the sulfamate ion has C_s symmetry all of the normal modes are formally both i.r. and Raman active.
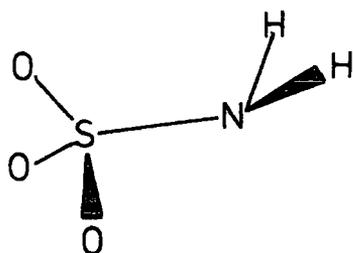
Fig. 10. Structure of sulfamate ion.

Table 6: Summary of i.n.s., i.r. and Raman Data for NH_2SO_3Na

i. n. s.	i. r.[a]	R.[a]	Assignment[a]
		204	
		221	Lattice modes
		244	
		259	
344		374	Sym SO_3 rock
405	402	392	asym SO_3 rock
	433		
	480		
491	498	495	sym SO_3 def^n
	518		
574	515	564	sym SO_3 def^n
	596	580	asym SO_3 def^n
	615		H_2O rock
684	685		
	730		H_2O wag
809	800	796	sym S-N stretch

a) from ref. 22

The only i.n.s. band which does not correspond to bands and assignments in the i.r. and Raman data is the most intense band in the spectrum, at 344 cm^{-1}. We assign this band to the NH_2 torsion. A Raman band at 305 cm^{-1} in the spectrum of KSO_3NH_2 has been assigned to the NH_2 torsion,[23] however, no reasons were given and the author assumed an incorrect structure for his analysis i.e. he assumed the hydrogen atoms to be on a plane of symmetry. No Raman band is found in this region of the spectrum of $NaSO_3NH_2$.

Although there appears to be little hydrogen-bonding in $NaSO_3NH_2$ compared to $NH_3^+SO_3^-$ there are two reasons why the NH_2 torsional frequency should be greater than that of the NH_3^+. Firstly its moment of inertia is smaller (chapter II) and secondly the S-N bond length in $NaSO_3NH_2$ (1.66Å for KSO_3NH_2)[24] is shorter than in $NH_3^+SO_3^-$ (1.764Å) and this is also reflected, for instance, in the increase in frequency of the S-N stretching vibration. We would therefore expect the effective force constant for the NH_2 torsion in $NaSO_3NH_2$ to be greater than that for the NH_3^+ torsion in $NH_3^+SO_3^-$. If we assume that the barrier multiplicity is 6 (internal barrier) then we can calculate the barrier height. The moment of inertia of NH_2 was taken to be $\frac{2}{3}$ x I_{NH_3} and the barrier height obtained was 5.9 kJ mole^{-1} (491 cm^{-1}).

b) Sulfamide and its disilver salt $Ag_2N_2H_2SO_2$

Nearly complete vibrational assignments for $SO_2(NH_2)_2$ have been given by Herrick and Wagner[25] and Uno et al.[26] Their results are in good agreement. The isolated molecule has, at least approximately, C_{2v} symmetry and so we would expect nine skeletal vibrations ($4A_1 + A_2 + 2B_1 + 2B_2$) all of which are i.r. and Raman active except the A_2 mode which is i.r. inactive. X-ray studies have shown the

crystal to be orthorhombic[27] and the site symmetry of the molecule is C_2. In this case all the normal modes are formally both i.r. and Raman active.

The i.n.s. spectrum of sulfamide is shown in fig. 8c and the available i.n.s., i.r. and Raman data and assignments are shown in table 7.

Table 7 <u>Spectroscopic Data and Assignments for $SO_2(NH_2)_2$ and $SO_2(AgNH)_2$</u>

$SO_2(NH_2)_2$				$SO_2(AgNH)_2$		
i.n.s.	i.r.[a]	R.[b]	Assignment	i.n.s.	i.r.[c]	Assignment
328		322				
		335				
380	358	363	NSN bend		300	
				~350		
423	420	422	NH_2 torsion		475	
	440*		SO_2 rock		487	
	450*		SO_2 twist			
	502		SO_2 wag	513	512	
	532	528	SO_2 bend			
540		537)			582	
		546)				
	562	574		609	611	
					622	
746	730		NH_2 wag	798	780	
	904		(N-S)sym stretch		838	(N-S)sym stretch
	931		(N-S)asym stretch			
					875	(N-S)asym stretch

a) ref. 26

b) this work

* estimated from $SO_2(ND_2)_2$ data

c) ref. 32

The assignment of the NH_2 torsion to the mode at 420 cm^{-1} appears
to be in reasonable agreement with the i.n.s. data. We would also
expect the NH_2 torsion in sulfamide to be of higher frequency than in
$NaSO_3NH_2$ because of the shorter S-N distance and the consequent increase
in double bond character (S-N in KSO_3NH_2 is 1.66Å, S-N in $SO_2(NH_2)_2$[27]
is 1.60Å and S=N is predicted[27] at 1.54Å).

A broad band centred at 540 cm^{-1} in the i.n.s. spectrum of
$SO_2(NH_2)_2$ (fig. 8c) can be seen to be due to several unresolved modes
(table 7). We are therefore left with a very intense peak, at 328 cm^{-1}
(fig. 8c). Because there are no reasonable grounds on which to doubt
the majority of the assignments from optical spectra there are only two
possible assignments for this band;

A)   the i.n.s. bands at 328 and 423 cm^{-1} are the in-phase and out-of-
      phase NH_2 torsions.

B)   the band at 328 cm^{-1} is the O_2-S-N_2 twisting mode which has been
      tentatively assigned by Herrick and Wagner at 486 cm^{-1}. Uno et al.
      did not assign this mode nor did they observe a band at 486 cm^{-1}.

All of the fundamentals associated with hydrogen atom motions
should be split because of the in and out-of-phase motions of the two
NH_2 groups. Herrick and Wagner[25] observed some indication of splittings,
particularly at low temperatures, though the resolution of the spectrum
was not good enough to allow separate assignments. If the bands at
328 and 423 cm^{-1} are the in-phase and out-of-phase torsions then this
would indicate very significant interaction between the two groups.
There is little available evidence on this point, however, the n.m.r.
work of Pedersen[28] indicates that the interaction between the two NH_2
groups is certainly less than that found for urea for instance, and the

i.n.s. spectrum of urea does not show any indication of splitting of the NH_2 torsion.[27]

The assignment of the 328 cm^{-1} band to the O_2-S-N_2 twisting mode (A_2) seems the more reasonable because the corresponding mode in crystalline $O_2S(OH)_2$ has been assigned[30] at 392 cm^{-1} and the intensity in the i.n.s. spectrum is compatible with the large mean vibrational amplitude calculated by Copinarth and Rao[31] for the O....N distance (.06488$Å^2$) compared for instance with that found for the S-N distance (.04400$Å^2$). We have also observed Raman bands at 322 and 335 cm^{-1}. The existence of two bands is possibly due to intermolecular coupling which would cause the twisting mode to split into two unit cell modes (two molecules/unit cell) (i.e. Factor Group Splitting).[25]

If we now consider the disilver salt of sulfamide $Ag_2N_2H_2O_2S$ there are several possible molecular structures[32] (fig. 11).
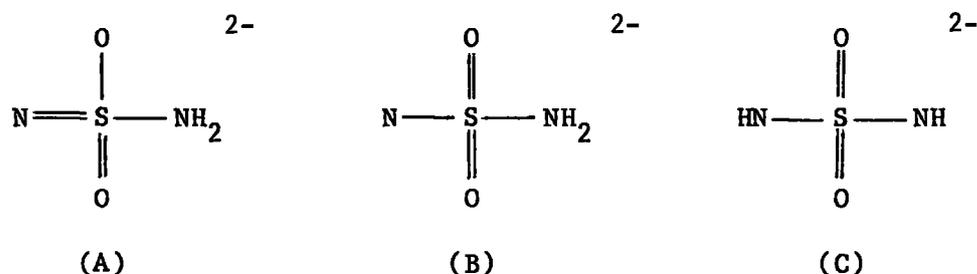
Fig. 11 Possible Structures for $Ag_2N_2H_2O_2S$

In fact, of course, very much more complicated arrangements could exist in the solid state e.g.

$$3Ag^+ \ [NH_2SO_2N \rightarrow Ag \leftarrow NSO_2NH_2]^{3-}$$

or chains involving
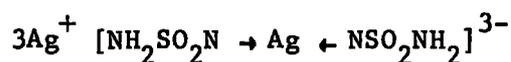
$$\rightarrow Ag \leftarrow [NH-SO_2-NH \rightarrow Ag \leftarrow NH-SO_2-NH \rightarrow]^{3-} Ag \leftarrow NH$$
$$3Ag^+$$
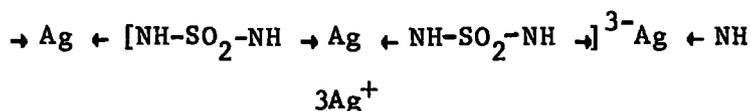
and this might in fact explain the low water solubility of the material. The three structures shown in fig. 10 will, however, serve to illustrate our main arguments.

Very little information can be gained from a knowledge of the number of observed skeletal modes because in each case there is a total of nine possible modes and even for the most symmetrical conformation $\{SO_2(NH_2Ag)_2\}$ eight of these are both i.r. and Raman active and the ninth is Raman active only. Nachbaur et al.[32] have concluded from i.r., broadline proton n.m.r. and chemical (alkylation) evidence that structure (A) is the correct one. The chemical evidence is <u>at most</u> a rather indecisive indication of the structure because of the tendency of sulphur compounds to ionise in solution.

Also, as far as the i.r. evidence[32] is concerned, the bands at 3187 and 3150 cm^{-1}, which are assigned to the in and out-of-phase stretching modes of the NH_2 group, could equally well be the in and out-of-phase stretches of two different NH groups i.e.

Corresponding bands have been assigned for the O-H stretches in sulfuric acid[30] where in fact the difference in frequency between the in and out-of-phase stretches is very much greater (520 cm^{-1}) than for the disilver salt (37 cm^{-1}) of sulphamide. The NH stretches in the silver salt are of significantly lower frequency than those found[22] for NH_2SO_3Na(3240, 3322 cm^{-1}) or $SO_2(NH_2)_2$[26] (3320, 3210 cm^{-1}). The difference in frequency between the N-H stretching modes are $SO_2(NH_2)_2$

(110 cm^{-1}) NaSO$_3$NH$_2$ (82 cm^{-1}) and Ag$_2$H$_2$N$_2$S$_2$O$_2$ (37 cm^{-1}). The splitting is therefore very much smaller in the case of the silver salt than for the two complexes which contain NH$_2$ groups. There are in fact four stretching modes involving the hydrogen motion in the two NH$_2$ groups of SO$_2$(NH$_2$)$_2$ but as we stated earlier very little splitting, as a result of the in and out-of-phase motion of the NH$_2$ groups, was observed. Furthermore in the region 1500 - 1600 cm^{-1}, where the NH$_2$ bending mode should occur, there is only a very weak band in the published i.r. spectrum[32] and in a spectrum recently supplied by Nachbaur et al.[34] there is no indication of a band in this region. Raman data is very difficult to obtain for this complex because of its ready decomposition in the laser beam even with less than 4mW power at the sample.

The strongest evidence that there is in fact an NH$_2$ group present comes from a comparison of the proton n.m.r.[32] of Ag$_2$H$_2$N$_2$O$_2$S$_2$ and Li(NH SO$_2$NH$_2$). These are shown diagramatically in fig. 12.
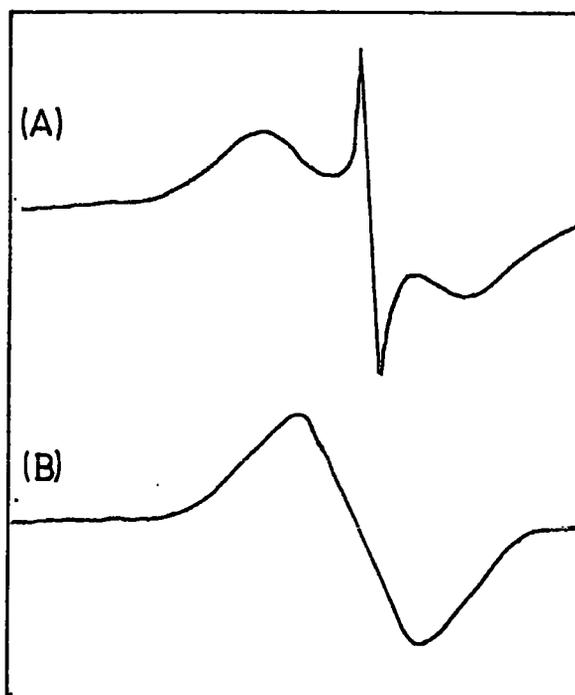
Fig. 12. Proton n.m.r. results for (A) Li(NHSO$_2$NH$_2$) and (B) Ag$_2$H$_2$N$_2$O$_2$S$_2$

Even in this case, however, the maximum in the spectrum B is intermediate

between those of A and the broadening of an N-H band could be due to
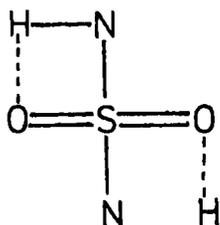
hydrogen bonding (see diagram). The i.r. evidence supports the symmetric structure (C) as regards the positions of the S-N stretching modes. When there is very definite double bond character e.g. $Ag_4N_2O_2S$ the stretches have high frequency[34] (in this case 1080 and 935 cm^{-1}). For $SO_2(NH_2)_2$ these stretches occur at[26] 931 and 904 cm^{-1}. For di-silver sulfamide the stretches occur at[32] 875 and 838 cm^{-1}, and the low value of these is a very strong indication of the absence of a S=N bond i.e. against structure (A).
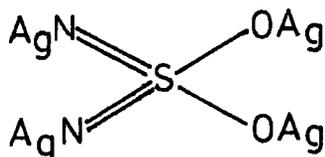
The i.n.s. spectrum of the disilver salt is shown in fig. 8d. It

is obviously very different from that of sulfamide or $NaSO_3NH_2$. There

are no intense bands in the region 200 → 480 cm^{-1} where the NH_2 torsions

were located in the other sulfur complexes. The most intense feature

occurs at 790 cm^{-1}. The S-N stretches are of higher frequency than this

and in any case from our i.n.s. data for $NaSO_3NH_2$ we know that these are

weak in the i.n.s. spectra. Thus the 790 cm^{-1} band is either the

NH_2 torsion,which has been increased in frequency by an enormous amount

(i.e. if we accept structure A or B),or the NH torsion (alternatively

described as a wag) if we accept structure (C). If we consider only

the moment of inertia change on going from NH_2 to NH then the torsional

mode should double in frequency. Thus from our results for $SO_2(NH_2)_2$

and $NaSO_3NH_2$ we would predict the NH torsion to occur between 688 and

846 cm^{-1}. This in fact agrees well with the observed value in the

disilver salt ($790 \ cm^{-1}$). The spectroscopic evidence would seem

therefore to rule out alternative (A) (fig. 11) and structure (C) is

in most agreement with the observed i.n.s. data. It is thought from

previous work on silver amidosulfates and amidoselenates that the

amidosulfates are more salt-like than the selenates.[35] This is

deduced mainly from the existance of v_{AgN} bands in the selenates and

their absence in the sulfur compounds. In practice, of course, we would

expect both an in-phase and an out-of-phase torsion, however, our data

for $SO_2(NH_2)_2$ leads us to expect that these would be degenerate.

If our assignment of the molecular structure to type (C) is

correct then the skeletal modes should be rather similar to those of

$SO_2(NH_2)_2$ and particularly $SO_2(OH)_2$. This in fact leads to some

difficulty because for $SO_2(NH_2)_2$ we observed an intense band at 328 cm^{-1},

which we assigned to the O_2-S-N_2 twist and this mode should also occur

in the spectrum of $SO_2(NHAg)_2$. The mode at 790 cm^{-1} is by far the most

intense mode in the spectrum however. One fairly obvious possible

explanation for this is that as a result of the introduction of the Ag

ions the amplitude of vibration of the oxygen atoms is greater than the

nitrogens (and hence the hydrogen atoms) in this mode. This would then

lead to a reduction of its intensity in the i.n.s. spectrum. This

argument, of course, implies some degree of covalent bonding of the

silver atoms to the nitrogens. The remaining bands in the i.n.s.

spectrum of $SO_2(AgNH)_2$ occur at 609 and 513 cm^{-1} with some very weak

bands in the region of 350 cm^{-1}. The two more intense modes coincide

with observed i.r. bands (table 7). These modes could be the SO_2

wagging and twisting modes which occur in sulfamide in the range

$450 \rightarrow 532$ cm^{-1} and as stated previously one of them could be the O_2-S-N$_2$ twisting mode. As yet we do not have any evidence on which to base further assignments.

Conclusion

The torsional modes in several sulfur-nitrogen complexes have been assigned. These increase in frequency with decreasing S-N bond length. From a consideration of the available spectroscopic data the structure of the disilver salt of sulfamide has been shown not to contain an NH$_2$ group. The SO$_2$ rocking and wagging modes were observed because of their associated proton motion.

References

1. R.C. Leech, D.B. Powell and N. Sheppard, Spectrochim. Acta., 21A, 559, (1964).

2. S.E. Ulrich and B.A. Dunell, J.C.S. Faraday II, 69, 1609, (1973).

3. J.M. Janik, J.A. Janik, A. Migdal and G. Pytasz, Acta. Phys. Pol., A40, 741, (1971).

4. G. Herzberg, Infrared and Raman Spectra of Polyatomic Molecules, D. Van Nostrand Co. Inc., New York, 1945.

5. S.E. Ulrich and B.A. Dunell, Can. J. Chem., 52(19), 3378, (1974).

6. V.A. Sokolov and G.A. Sharpataya, Zh.Fiz.Khim., 44(3), 603, (1970).

7. R. Layton, D.W. Sink and J.R. Durig, J. Inorg. Nucl. Chem., 28, 1965, (1966).

8. K. Nakamoto, P.J. McCarthy, F. Fujita, R.A. Conrate and G.T. Behnke, Inorg. Chem. 4(1), 36, (1965).

9. G.B. Kauffman and D.O. Cowan, Inorganic Syntheses, 7, 239, (1963).

10. C.I. Ratcliffe, Ph.D. Thesis, University of Durham, 1975.

11. J. Hiraishi, I. Nakagawa and T. Shimanouchi, Spectrochim. Acta., 24A, 819, (1968).

12. P. Day, Inorg. Chim. Acta. Rev., 3, 81, (1969).

13. L.V. Interrante, J.C.S. Chem. Comm., 302, (1972).

14. M. Atoji, J.W. Richardson and R.E. Rundle, J. Amer. Chem. Soc., 79, 3017, (1957).

15. D.M. Adams and J.R. Hall, J.C.S. Dalton, 1450, (1973).

16. G.H.W. Milburn and M.R. Truter, J. Chem. Soc. A., 1609, (1966).

17. K.H. Schmidt and A. Muller, Inorg. Chem., 14(9), 2183, (1975).

18. A.M. Vaugnant and E.L. Wagner, J. Chem. Phys., 26, 77, (1957).

19. N. Krishnamurthy, Proc. Ind. Acad. Sci. Sect A., 61(3), 146, (1965).

20. R.L. Sass, Acta. Cryst., 13, 320, (1960).

21. V. Shomaker and D.P. Stevenson, J. Amer. Chem. Soc., 63, 37, (1941).

22. R.S. Katiyar and R.S. Krishnan, Ind. J. Pure Appl. Phys., 6(12), 686, (1968).

23. R.S. Katiyar, Proc. Ind. Acad. Sci. Sect. A., 62(3), 169, (1965).

24. G.W. Cox, Acta. Cryst., 23(4), 578, (1967).

25. I.W. Herrick and E.L. Wagner, Spectrochim. Acta., 21, 1569, (1965).

26. T. Uno, K. Machida and K. Hanai, Spectrochim. Acta., 22, 2065, (1966).

27. K.N. Trueblood and S.W. Mayer, Acta. Cryst., 9, 628, (1956).

28. B. Pedersen, Acta. Chem. Scand., 22(6), 1813, (1968).

29. R.E. Ghosh, Ph.D. Thesis, University of Oxford, 1972.

30. a) P.A. Giguère and R. Savoi, Can. J. Chem., 38, 2467, (1960).

    b) P.A. Giguère and R. Savoi, J. Amer. Chem. Soc., 85, 287, (1963).

31. C.R. Copinath and K.S. Raghavendra Roa., Curr. Sci., 44(4), 107, (1975).

32. E. Nachbaur, A. Popitsch and P. Burkert., Monatshefte für Chemie, 105, 822, (1974).

33. E. Nachbaur, Personal Communication.

34. E. Nachbaur and A. Popitsch, Angew. Chem., 12(4), 339, (1973).

35. R. Paetzold, K. Dostal and A. Ruzicka, Z. Anorg. Allg. Chem., 348(1-2), 1, (1966).

36. P.J. Hendra, Spectrochim. Acta., 23A, 1275, (1967).

37. M. Fearneyhough, Research Assignment Durham 1964.

38. C.H. Perry, D.P. Athans, E.F. Young, J.R. Durig and B.R. Mitchell, Spectrochim. Acta., 23A, 1137, (1967).

Chapter IX: An I.N.S. Study of Hydrogen Adsorbed on Platinum Black

a)   Introduction

A gas atom or molecule experiences an attractive potential on
approaching a surface and the magnitude of this potential determines the
nature of the interaction between the gas and the surface atoms. The
strength of the interaction is reflected in the magnitude of the heat of
adsorption ΔH_{ads} which is the average binding energy per mole between the
interacting gas and the surface atoms and which, for non-dissociative
adsorption, is related to the depth of the potential well. The ratio of
the depth of this well to the thermal energy of the gas atoms ($\Delta H_{ads}/RT$)
determines the residence time τ of those gas atoms on the surface. In
fact[1]

$$\tau = \tau_0 e^{\Delta H_{ads}/RT} \tag{1}$$

where τ_0 is related to the period of a single surface atom vibration.
Typically $\tau_0 \approx 10^{-12}$ sec. For $\Delta H_{ads} = 65$ kJ mole^{-1} and T = 300K
equation 1 implies that $\tau \approx 10^{-2}$ sec. An adsorption process for which
$\Delta H_{ads} > 65$ kJ mole^{-1} is, by convention, called "chemisorption" with
weaker interactions being called "physisorption". While there is
obviously no sharp division between the two processes, chemisorption is
usually associated with actual chemical bonding to the surface, often
accompanied by dissociation of the original molecule. Dissociation
would not be expected to accompany physisorption.

From equation 1 it can be seen that for chemisorption $\tau \gg \tau_0$ so
that even at high temperatures and with moderate gas pressures, large
surface concentrations can occur. For physisorption, however, $\tau \approx \tau_0$ so
that low temperatures are usually used to obtain reasonable surface
coverages.

The existence of two forms of hydrogen chemisorbed on metals has been demonstrated by work function and electrical resistance measurements.[2,3,4,5,6,7] The existence of these two types, called "r" and "s" adatoms, has also been deduced theoretically by Toya.[8] Figure 1

r-type ⟶ ⊕

s-type

r-type ⟶ ⊕

s-type

Metal
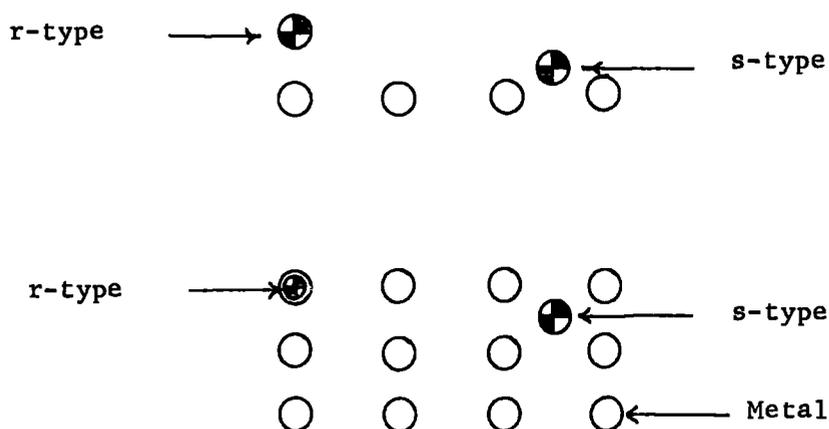
Fig. 1 "r" and "s" type adatoms

illustrates the difference between the two types. Neither adatom is strictly neutral. The "r" adatom is situated c.a. 1Å outside the electronic surface i.e. c.a. 2.5Å from the surface layer.[2] The bond is essentially covalent in character and the adatom is situated directly above a substrate atom. It is therefore expected to have three vibrational modes, one perpendicular to the surface (stretch) and two (bends: probably degenerate) parallel to it. The "r" adatom is slightly negatively polarised.

An "s" adatom may be thought of as dissolved in the metals' surface so that it is embedded in a sea of electrons and is not associated with a particular metal atom. They can be thought of as dissociated into an electron and a proton and they have a stable equilibrium position in a plane parallel to the electronic surface and

c.a. 0.5Å below it. It has been shown that lattice imperfections may produce "s" sites of lower energy[9,10] than exist on perfect planes. Toya's theory does not preclude the existence of molecules on the surface and March et al.[11] have considered what happens when a hydrogen molecule is brought up to a metals' surface with its bond parallel to that surface. At an infinite distance from the surface the molecule is covalently bonded (binding energy 4.7 eV and bond length .74Å). As the molecule enters the region where the conduction electrons spill out from the surface the covalent bond is altered. At less than a critical distance from the surface the protons are ionised and the interaction between the protons becomes oscillatory (fig. 2).
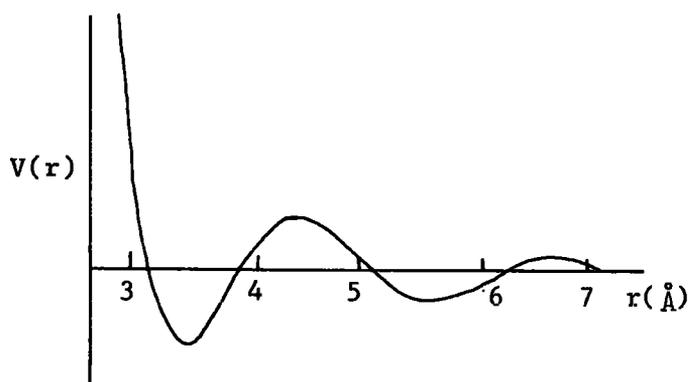
Fig. 2 Interactions between protons near a metal surface.

The bond length is increased from .74Å to 3.5Å (first minimum) and the energy required (parallel to the surface) to separate the protons decreases to .075 eV and therefore ready dissociation is possible.

"s" adatoms occupy interstitial positions and are not bonded to any particular substrate atom; they resemble a two dimensional fluid and conduct two dimensional translations in a plane parallel to the surface while vibrating normal to that surface. A three dimensional analogue is hydrogen dissolved in palladium where n.m.r. experiments have demonstrated that the protons diffuse throughout the bulk material and cannot be regarded as being bonded to any particular metal atoms.[12]

As mentioned earlier, these two types of adsorbed atoms will have different effects on surface properties of the metal. Because an "r" adatom removes electron density from the surface it increases the work function and vice versa for an "s" adatom. Likewise an "r" adatom increases the electrical resistance of the surface and an "s" adatom decreases it. The existence of adsorbed states which have the properties of "r" and "s" adatoms has been verified experimentally,[1,2] and Bond has shown that "s" adatoms should be more strongly bound than "r" adatoms.[13]

b) Previous Work

Many techniques have been applied to investigate the adsorption of hydrogen on platinum e.g. work function measurements,[2] infrared,[14,15,16,17] LEED,[18] electrical resistance measurements, temperature programmed desorption(T.P.D.)[19,20,21] radiotracer studies.[22] These measurements have been made, where appropriate, on supported or unsupported Pt and on films[5,6,7] and filaments[23] and metal in the form of sharpened tips.[6,24] The samples have also been prepared in a variety of ways e.g. degassing at high and at low temperatures and in moderate vacuum or ultra high vacuum (U.H.V.) environments. There seems to have been a vast increase in the number of studies of gases adsorbed at low coverages on single crystal faces in ultra-clean conditions. It must be remembered, however, that this is but one aspect of the general problem, and it may be that a detailed comparison of chemisorption data for perfect crystal faces with that from the polycrystalline form of the metal is not justified.[25]

In general, high surface area polycrystalline materials cannot be outgassed at "very" high temperatures because this will usually lead to sintering and a consequent decrease in surface area. These materials,

therefore, cannot have the same surface cleanliness as can be obtained

for small surface area samples which have been treated using U.H.V.

techniques. Real catalysts are of course not used in single crystal

form and studies on polycrystalline materials under a variety of out-

gassing and cleaning procedures is likely to approximate more nearly

to the conditions obtaining in the real systems.

Number of States of Adsorbed Hydrogen: A recent T.P.D. study (starting

at 150K) concluded that on Pt(111) there exist just two states and that

these are atomic.[18] Another T.P.D. study, starting at 78K, this time

using platinum films,[21] concluded that there were three chemisorbed

states. Tsuchiya et al.[19] have reported four forms of chemisorbed

hydrogen on platinum black from T.P.D. measurements ($-196^{o}C \rightarrow 400^{o}C$).

Five types of hydrogen have been reported on alumina-supported

platinum from measurements of adsorption isotherms.[26] One common

factor running through these experiments is that it is concluded that

there are both weakly and strongly adsorbed forms of hydrogen.

Temperature Programmed Desorption (T.P.D.): The interpretation of

T.P.D. data has been extensively discussed[27,28] Complex desorption

traces have traditionally been analysed in terms of a set of distinct

binding states, however, it has been shown that complex traces may

arise as a result of repulsive interactions between adsorbed species

with the adsorbed layer homogeneous at all coverages.[28] Because

multiple-peak T.P.D. spectra result from changes in activation

energy the problem is to decide whether this change is due to

desorption from different sites or to changes in adatom-adatom

interactions. The interpretation of the data is therefore rarely

unambiguous and complex T.P.D. spectra are expected to be the rule

rather than the exception.

Because our work is primarily based on the T.P.D. studies of
Tsuchiya et al.[19] we will describe their results in a little more
detail. Their method of gas analysis involved thermal conductivity
measurements so that they did not in fact analyse for the constitution
of the desorbed gas, they did however clean their samples at $500^{\circ}C$. As
stated earlier they observed four peaks which they attributed to four
different states of hydrogen on the surface and these were designated
α, β, γ, δ forms. The δ state did not begin to desorb until the
temperature was $175^{\circ}C$ and it was the highest temperature form observed.
Tsuchiya et al. hypothesized that the δ state corresponded to the "s"
state and they further postulated that although the four states could
be illustrated schematically by

```
    H
    ¦
    ¦
    H            H---H           H          H
    ¦           /      \         ¦         / \
    ¦          /        \        ¦        /   \
    Pt        Pt        Pt       Pt      Pt    Pt

   (α)          (β)           (γ)         (δ)
```
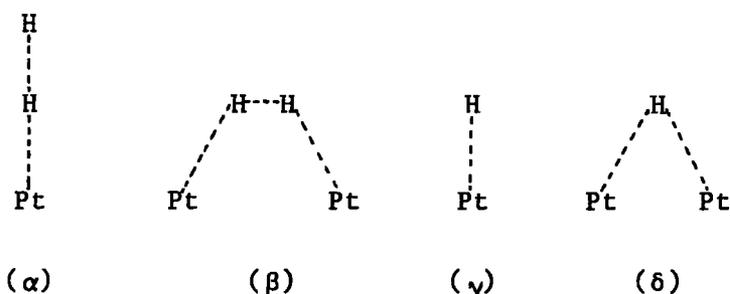
they had no real basis for these assignments and
they were to be regarded as tentative.

In order to study the "simplest" system we have chosen initially
to investigate the δ state which can be obtained as the sole surface
species by adsorbing hydrogen at a sample temperature of $200^{\circ}C$.

Infrared Studies: There have been several infrared studies of hydrogen
adsorbed on supported Pt samples.[14-17] The authors agree that the
chemisorption is dissociative and that a band at 2120 cm^{-1} is due to
the Pt-H stretching vibration while there has been some disagreement

concerning a band observed at 2060 cm^{-1}. This lower frequency band has been assigned by some workers as due to a carbonyl contaminant. A recent study by Dixon et al.[17], however, has shown that

a) although if the surface is not fully clean a carbonyl band does occur at c.a. 2060 cm^{-1}, with a clean surface a weak broad band, due to a Pt-H stretch, also occurs at this frequency.

b) two i.r. active forms of hydrogen exist and at room temperature they are reversibly bound.

c) the higher frequency form is the most easily removed from the surface.

d) only the 2120 cm^{-1} band appears if adsorption is carried out at 77K and then only if the surface has been exposed to hydrogen at 300K i.e. there exists an i.r. inactive form of hydrogen.

e) neither form is necessary for isotopic exchange at 77K.

f) on admitting oxygen to the hydrogen covered surface a band appeared at 1630 cm^{-1}.

It had previously been shown that not all of the adsorbed hydrogen could be accounted for in the i.r.[29] and so the results of Dixon et al. confirm this also.

Although the i.r. results on supported metals are of considerable interest the results are almost certainly not directly transferable to unsupported platinum (see chapter I).

N.M.R.: There have been two n.m.r. studies of the Pt-hydrogen system. Ito et al.[30] studied hydrogen adsorbed at fairly high pressures (> 58 torr) on Pt black. They found two states of hydrogen on the surface and interpreted their results as indicating that below 290K one of the states was mobile on the surface while the other was not. Bonardet

et al.[31] have studied hydrogen adsorbed on silica-supported platinum.
They detected two irreversibly bound forms (25°C) and assigned them as
occurring on the surface and in the interstices. At higher pressures
the hydrogen is adsorbed reversibly and this reversible form exchanges
with the irreversibly bound hydrogen on the interstitial sites. They
have suggested that the i.r. band at 2120 cm^{-1} occurs as a result of the
exchange process; during the exchange an intermediate complex consisting
of several hydrogen atoms is formed. As a result the interstitially bound
hydrogens can be displaced for long enough for them to be interacting
with a reduced number of hydrogens, in a low symmetry site and hence
become i.r. active. After desorption of the reversibly bound hydrogen
the surface hydrogen returns to its interstitial position and an i.r.
band cannot be detected.

Isotope Studies: Chemisorption, at 360°C, of hydrogen labelled with
tritium on Pt black has been studied by Paal and Thompson.[22] The
sample pretreatment involved heating it to 360°C in air followed by
flushing with helium to remove gaseous nitrogen and oxygen after which
hydrogen was passed over the Pt black for 60 minutes before switching
back to helium. Known volumes of gas were then admitted to the sample
area. All operations were carried out at 360°C. They observed that
the surface retained hydrogen long after the initial adsorption and that
exposure to air did not remove this adsorbed phase. It would appear,
therefore, that there are two types of adsorbed hydrogen on the surface,
only one of which is able to react with subsequently adsorbed hydro-
carbons or oxygen. These two forms can interchange.

These results differ from those of Tsuchiya et al.,[19] however, the
experimental conditions differ greatly. In thermal desorption at
10^{-5} torr it may be easier for chemisorbed molecules to leave the
catalyst than in a flow process with helium at one atmosphere. On the

other hand T.P.D. experiments give no information on what is left on

the surface so that the possibility of an extra surface state, stable

at 360°C, does not actually contradict the work of Tsuchiya et al. The

new state is possibly hydrogen dissolved in the surface to a greater

extent than the "s" type. This dissolution may take place during the

initial hydrogen treatment when extensive sintering and recrystallisation

takes place.[32]

I.N.S.: During the course of this work there have been two published

i.n.s. studies of hydrogen adsorbed on metal powders. Renouprez et al.[33]

have studied hydrogen adsorbed on nickel and they found:

1) the peaks at low energy transfers (< 320 cm^{-1}) are almost identical

    to the lattice frequencies of pure nickel, and they deduced that

    each hydrogen is bound to just one nickel atom.

2) the mean square amplitude of the bound proton was found to exceed

    that of nickel by $0.04 \pm .02 \text{Å}^2$.

3) a broad band at 1120 cm^{-1} was attributed to motion of hydrogen

    relative to the surface.

4) no broadening of the elastic line was observed.

Asada et al.[34] have studied hydrogen adsorbed on platinum and they

concluded that

1) there was an intense band at 400 cm^{-1} associated with a vibration

    of the adsorbed hydrogen relative to the surface.

2) at lower energies (< 400 cm^{-1}) the i.n.s. spectrum is complex and

    does not merely resemble the density of states of the bulk platinum.

3) no broadening of the elastic peak was observed.

Model Compounds: I.R. and Raman[35,36] studies have shown that for transition metal hydrides the ν(M-H) occurs in the region 1600-2200 cm^{-1} and δ(M-H) in the region 600-900 cm^{-1}. For any particular metal the spread is rather narrower e.g. Pt has ν(M-H) usually in the region 1950 → 2280 and δ(M-H) at c.a. 800 cm^{-1}, though the stretching frequency can vary appreciably with the nature of the trans ligand. In comparable complexes the ν(Pd-H) is lower than in the corresponding Pt complex, thus implying a lower force constant for the vibration. Where there are bridging hydrogen atoms the hydrogen vibrations occur at lower frequencies e.g. $HOsCo_3(CO)_{12}$ {1109 cm^{-1}}[37] $[HTi(\pi-C_5H_5)_2]_2$ {1450 cm^{-1}}.[38]

Sintering: Metal catalysts show changes in surface area during use or treatment at high temperatures. This process is known as sintering. The sintering of both supported[39] and unsupported[40] platinum has been investigated. Baird et al.[40] concluded that treatment of Pt black, at room temperature, with hydrogen produced little sintering but that higher temperature treatments lead to extensive sintering and consequent loss of surface area.

Surface Cleaning: For the i.n.s. measurements we require a large surface area so that very high temperature pretreatments are not possible. LEED and Auger electron spectroscopy[41] data indicate that if the temperature is high enough ($>800°$C) atomically clean platinum surfaces can be generated by using gaseous hydrogen to remove surface oxygen. This temperature is far too high for us to use because of the sintering which would result.

There is more than one phase of adsorbed oxygen on platinum. Measurements have shown that at 195K there is rapid adsorption of 95% of the gas and the remaining 5% adsorbs over some tens of minutes.[42,43]

This last phase is not removed by reaction with hydrogen at 195K though it does react slowly at 393K. The temperature at which the surface was exposed to oxygen influences the subsequent reaction with hydrogen. The higher the temperature of exposure to oxygen the higher the temperature required for removal by reaction with hydrogen.

For very small platinum particles the extent of oxygen uptake is suppressed and this is a consequence of the enhanced electron affinity of such small particles relative to the need for electron transfer to the adsorbed oxygen.

c) Experimental

Platinum black was cleaned as described in chapter III and in this respect our samples are very similar to those used by other authors. Platinum black for the experiments was purchased from Englehard Ltd.

The successful removal of at least some of the surface oxide was indicated by the formation of water on the first adsorption of hydrogen. Addition of hydrogen and pumping out of the sample was completed several times and there was never any visible indication of water formation after the first addition. We also found that upon exposing a clean surface to air there was always a very significant exothermic reaction.

Because of the importance of the temperatures at which the i.n.s. experiments were performed we have summarised the information concerning the experiments, the spectrometers used and the temperatures of measurement in table 1.

Table 1: Summary of Run Conditions for i.n.s. Experiments on the Pt-H_2 System *

	6H	B.F.D. Harwell	B.F.D.(IN1B) Grenoble
Pt Background	Ambient (H1)	90K (B1)	90K (I1)
Pt + H_2 adsorbed at 200°C	Ambient (H2)	90K (B2)	90K (I2)
Pt + H_2O	Ambient (H3)	-	-
Pt + H_2 + atmosphere	-	-	Ambient (I3)
Pt + HD(H_2+D_2)	Ambient (H4)	-	-
Pt + 30cm H_2	-	-	Ambient (I4)

* the index in the brackets gives the experiment number and letter.

Because we wished to examine, initially, the least complex Pt + H_2 system we decided to investigate a sample on which only the δ state existed. In order to acomplish this we adsorbed hydrogen when the sample temperature was 200°C. Under these conditions the data of Tsuchiya et al.[19] indicate that the δ state is the only one which can be formed. We have also run mass spectra of the gases desorbed on heating a Pt-H sample at various temperatures. For this experiment the sample was prepared as we have described earlier for the i.n.s. experiments, except that it (10gm.Pt) was held in a 50 c.c. glass bulb to which was connected a glass break seal. After sealing off from the vacuum line the sample was

connected (via a ground glass joint) to the mass spectrometer. When the air had been pumped out of the inlet system the glass break seal was broken (using ball bearings) and a sample of the gas phase was admitted to the spectrometer. The sample was then heated and at intervals the mass spectrum of gas phase was obtained.

d) Background Subtractions

These are particularly difficult for the Pt-H$_2$ system because the Pt has a moderately large absorption cross section (at 1060 μs/m σ_{abs} = 4.24 barns) and this is important because we have some 100 grams of Pt in the beam. The absorption cross-section is energy dependent and in fact to an excellent degree of approximation it is proportional to ^{1}/V where V is the velocity of the neutron. Fairly obviously the cross section of the sample is greater than the background, and so a larger proportion of the neutrons are going to gain energy from the sample and hence have a reduced probability of absorption after scattering. Because the absorption cross-section is energy dependent the effect will vary from point to point. It is therefore not valid to simply subtract the background counts from the sample counts to give the scattered counts due to the presence of adsorbed hydrogen. The problem is rather more acute when one includes the effect of a scattering and absorbing sample container. For our initial experiments we used a silica sample holder. As explained in chapter III this has a fairly large cross section. For the later experiments we used an aluminium cell and the scattering from this is almost negligible.

Techniques for correcting for absorption in the sample and sample cell and for scattering by the sample cell have been developed for elastic scattering by Paalman and Pings.[44] A computer program based on

their work has been written by Dr. J.H. Clarke[45] and we have modified

this to include the case of inelastic scattering. Further details are

given in the appendix.

In order to use the program it is necessary to know the quantity

of adsorbed gas and because we do not yet know exactly how much gas is

adsorbed we have unfortunately not been able to apply this correction

to date. This is naturally an undesirable state of affairs, but the

lack of correction is likely to have three effects

a)   incorrect subtraction of the two spectra i.e. sample - background.

b)   the relative intensities of the peaks will not be correct.

c)   band centres will be shifted slightly but this will certainly be a

       very small effect and can be ignored compared with the instrumental

       resolution.

None of these factors will result in the generation of intense bands in

the difference spectrum, which were not present in the sample spectrum.

Our results therefore will be correct as far as band positions are

concerned, but we will not be able to make accurate intensity comparisons.

e)   Results and Discussion

1)   Time-of-flight spectra

Fig. 3 shows the t. of f. spectrum of hydrogen adsorbed on Pt at

200°C. The spectrum was obtained at ambient temperature and the back-

ground has been subtracted. For comparison purposes the spectrum in

fig. 4 is the spectrum, of hydrogen adsorbed on platinum, obtained by

Asada et al.[34] A pressure of 39cm Hg was used in their experiment and

the spectrum (fig. 4) represents the sum of spectra obtained at six

different scattering angles. In some respects our conclusions are at

variance with those of these authors. We find no evidence for large
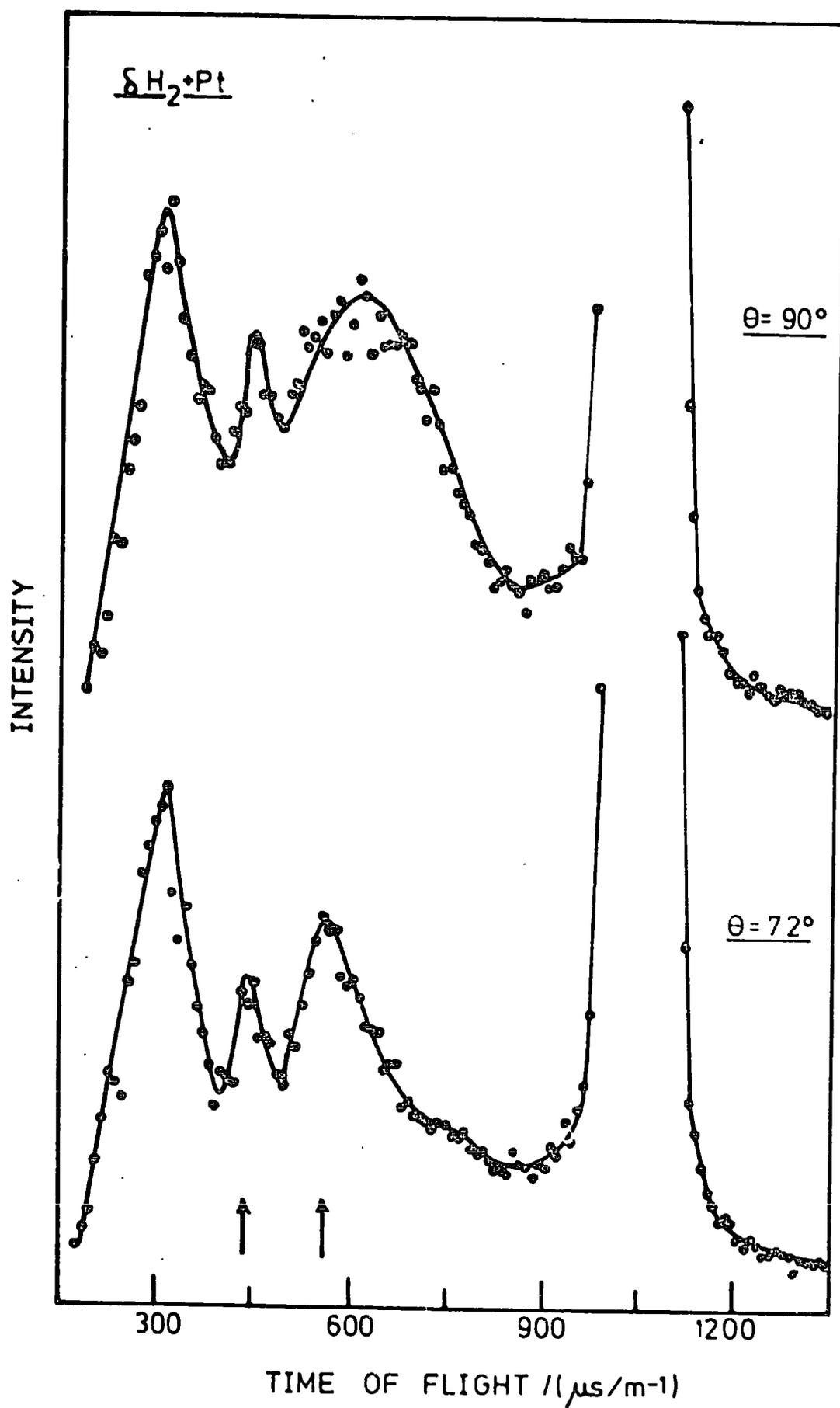
Fig. 3 T.of.F. Data for H_2 (δ State) Adsorbed on Pt.
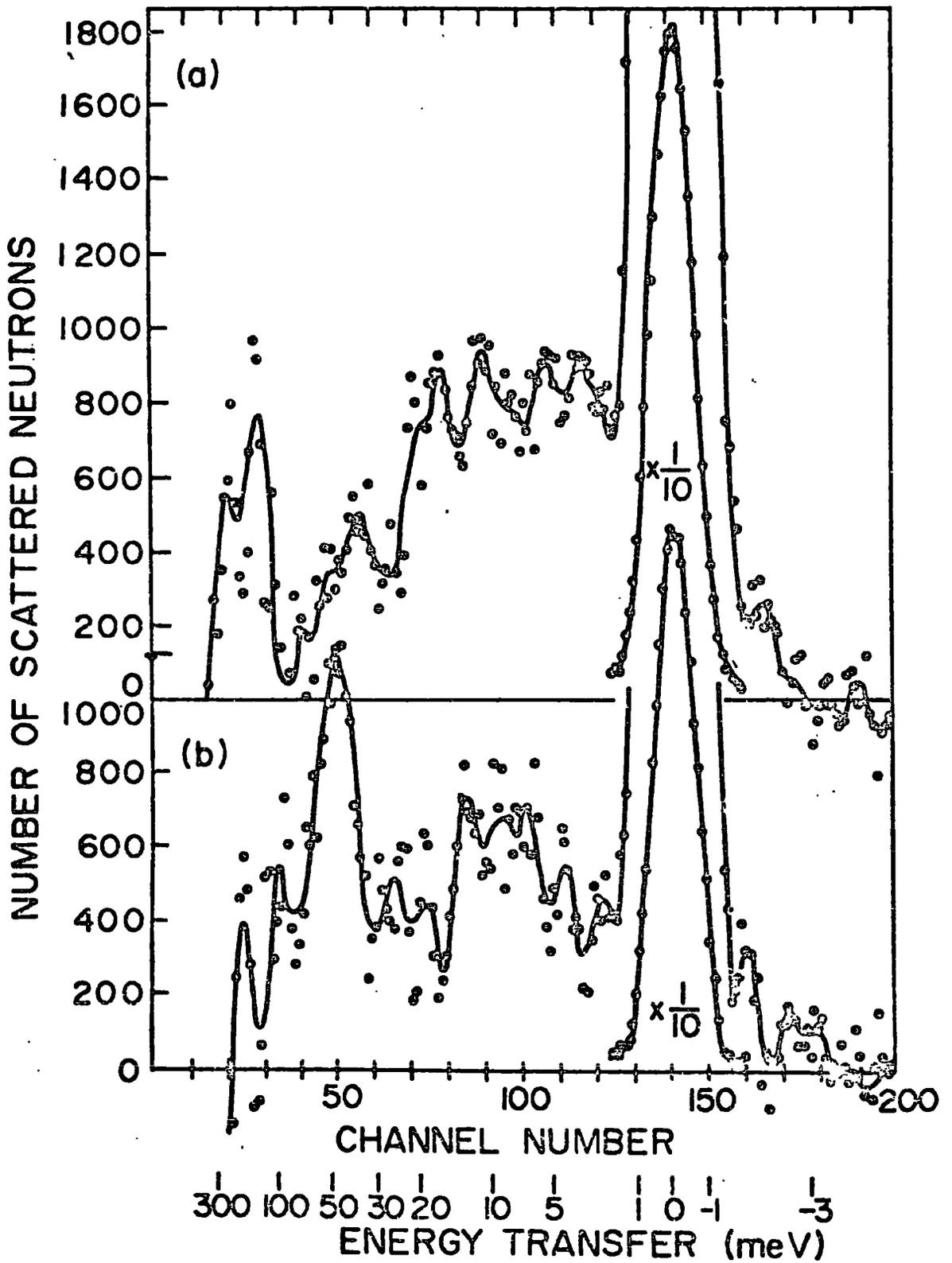
Fig. 4 I.N.S. Spectrum of H_2 + Pt Obtained by Asada et al.

numbers of separate features at low energy and we disagree with the

statement that the low energy spectrum is unlikely to be due to the

enhancement of the scattering from the Pt phonon spectrum caused by the

large cross-section of the hydrogen atoms. Rather we find that the two

lowest energy maxima, at 169 $\pm$ 8 and 97 $\pm$ 4 cm^{-1} correspond very closely

to those obtained for the density of states of bulk platinum.[46] The

bulk frequencies are indicated by the arrows in fig. 3. In this respect

our results are similar to those recently presented for Raney Nickel.[33]

Our data, as shown, is from just two scattering angles and the positions

of the peaks agree with the data from the other angles of detection.

The better accuracy of our data is indicated by the smooth variation in

intensity at all places remote from the peak positions. A comparison of

the total collected counts at c.a. 400 cm^{-1} indicates that Asada et al.

achieved 1200 counts as a total of six angles and our spectra e.g. 72°

has 1150 counts in that one angle at the same energy.

We do agree with Asada et al. that there is an intense peak at

403 $\pm$ 25 cm^{-1} which does not occur in the spectrum of the background.

Fig. 5 shows the i.n.s. spectrum of some Pt black samples after

various treatments and of a Pt sheet. The samples were in fact

5a) Pt cleaned with D$_2$ and degassed at 200°C.

5b) Pt not cleaned with hydrogen but degassed at 200°C.

5c) Pt sheet.

All of the spectra were obtained at ambient temperatures. It can

be seen that in figs. 5a, b, there is intensity beyond the lattice cut-

off (200 cm^{-1}). This band occurs at 350 cm^{-1}. It does not appear

entirely to be a combination band of Pt phonon modes because its

305.

Fig. 5 I.N.S. Spectra of

a) Pt Cleaned with D_2

b) Degassed Pt

c) Pt sheet
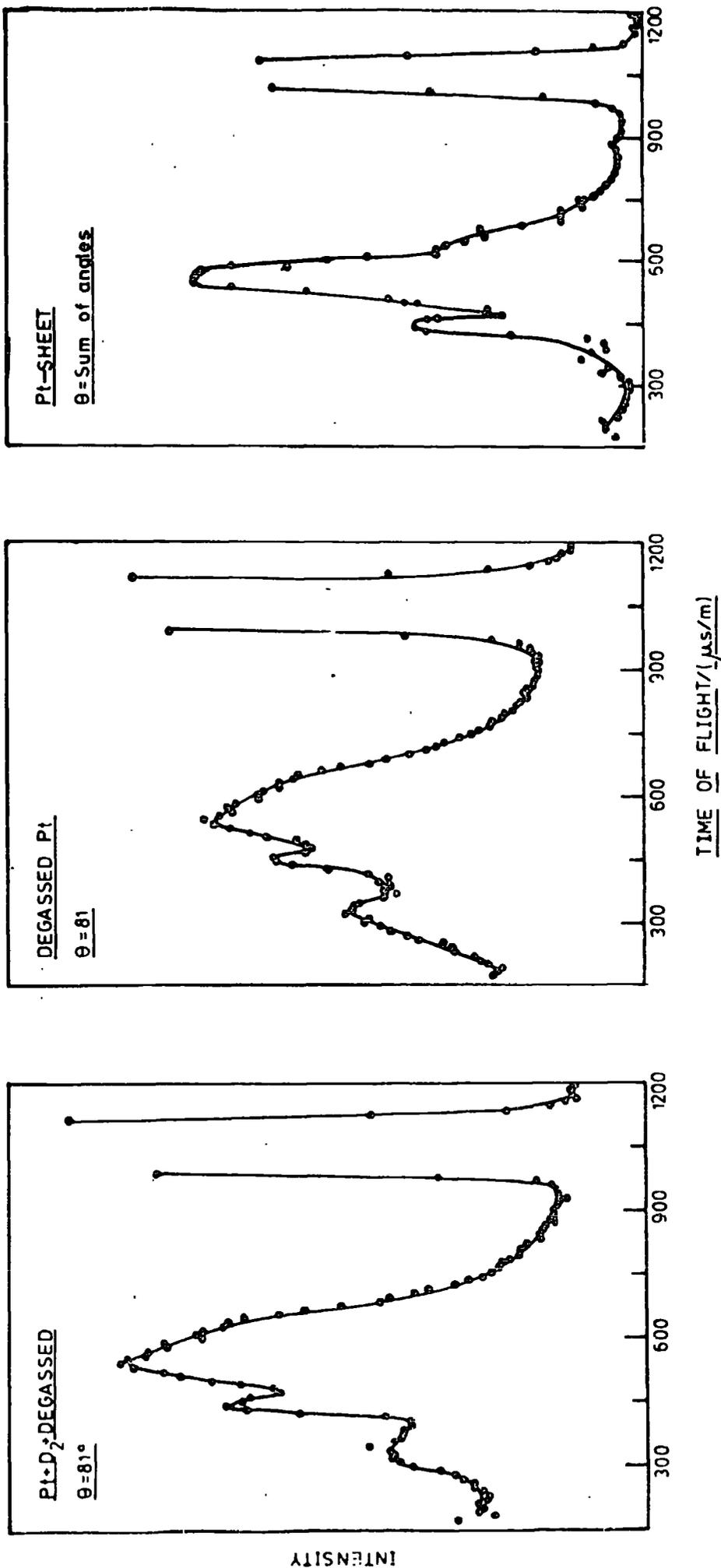
intensity, relative to the two lower energy peaks, depends upon the pre-treatment of the surface e.g. the intensity is reduced by c.a. 30 → 40% after cleaning with D_2 and degassing (c.f. figs. 5a,b). The i.n.s. spectrum of the silica is not peaked in this region (though there is a band at c.a. 300 cm^{-1}), therefore the 350 cm^{-1} band must correspond to some surface impurity. Because Pt and SiO_2 have small incoherent cross sections we must include the possibility that the band is due to a non-hydrogenous material e.g. Pt-oxide or adsorbed CO or N_2 as well as H_2 or H_2O or perhaps some impurity resulting from the preparation of the powder.

A similar situation was found for Raney Nickel i.e. transitions were observed above the lattice cut-off, though in that case the higher energy transitions were attributed to magnon scattering.

It is possible that at least some of the intensity at 350 cm^{-1} is due to Pt oxide on the surface and that the decrease in intensity on cleaning with D_2 is due to the formation of heavy water and hence the removal of the oxide. The presence of the band, after cleaning, may indicate a) that there is more than one type of oxygen on a platinum surface and at least one type reacts at most only slowly with adsorbed hydrogen or b) the sample container has a residual partial pressure of oxygen which is sufficient to partly re-form the oxide layer during the degassing and sealing-off procedures c) the residual intensity is due to some other adsorbed material.

If we consider the figures from our example in chapter I then we have approximately 30 atoms in the bulk for each surface atom. It is possible to observe a band due to an adsorbed species of low cross section provided that its mass is low and its amplitude of vibration is

large (see chapter I). A further important possibility is that the band is due to impurity in the bulk material. The Pt powder is produced by chemical precipitation and the manufacturers agree that there could be .1% impurity, some of which will be chlorine. If we have in fact a .1% impurity which is all chlorine then this is equivalent to a ratio of Pt:Cl atoms of 180:1. However, the ratio of σ_T/M for Cl to the same parameter for Pt is 31:1. Thus we have

$$\frac{\left(\text{concentration} \times \frac{\sigma_{inc}}{M}\right)_{Pt}}{\left(\text{concentration} \times \frac{\sigma_{inc}}{M}\right)_{Cl}} = \frac{180}{1} \times \frac{1}{27.8}$$

$$\approx 5.8$$

It is therefore just possible that we could observe the chlorine modes. Furthermore, the metal – halogen stretches occur at[57] c.a. 350 cm^{-1} (terminal Cl) and 315 cm^{-1} (bridging Cl) in $Pt_2Cl_6^{2-}$ so they are in the correct region for our observation.

Two factors mitigate against the 340 cm^{-1} peak being due to adsorbed water.

A) within the resolution of the spectrometer (see chapter III) the positions of the peaks in the spectrum of the uncleaned Pt surface (fig. 5b) and that of Pt cleaned with D_2 are the same. This is perhaps not very significant because the band could be due to $Pt-OH_2$ stretch which would have a relatively small shift on deuteration (the uncleaned surface would presumably contain H_2O while the cleaned one contained D_2O). Because the incoherent cross section of D is so much smaller than H we would also expect the intensity of the 340 cm^{-1} band relative to the lower peaks to change more than it in fact does.

B)   Fig. 6 shows the spectrum of adsorbed H_2O on Pt. For this experiment 0.3 cc of water was adsorbed onto the cleaned platinum black. The intense peak occurs at c.a. 460 cm^{-1} i.e. at considerably higher frequency than the 350 cm^{-1} peak in the background.

From this discussion it appears reasonable to assign the band at 403 cm^{-1} in the spectrum of hydrogen adsorbed on Pt, to a vibration of hydrogen relative to the surface. Perhaps in fact to the Pt-H stretch which would then be very much lower in frequency than found in unbridged Pt-hydrides (1950 $\rightarrow$ 2280 cm^{-1})[35,36,47] because of the probable interstitial nature of the hydrogen adsorbed on Pt under these conditions.

In order to ascertain whether or not we were observing dissociative chemisorption we decided to obtain the i.n.s. spectrum of adsorbed HD. It is known that rapid exchange takes place over a Pt surface so we adsorbed a quantity of $H_2 + D_2$ which had been pre-mixed in the ratio 1:4 respectively. The cleaning procedure was carried out with the same mixture. The spectrum of adsorbed D_2 would be very weak compared to HD or H_2 and so if the adsorbed phase is molecular we would expect to observe two bands, one due to H_2 at 400 cm^{-1} and a further band with a shift of $\sqrt{2/3}$ due to HD (predicted therefore at 3265 cm^{-1}). As can be seen from fig. 7, which shows the spectrum of the adsorbed $H_2 + D_2$, it contains only a single peak at 400 cm^{-1}. This strongly indicates that the adsorbed phase involves H atoms and not H_2 molecules.

2)   Beryllium Filter Detector Spectra

We have also obtained the spectrum of H_2 + Pt on the B.F.D. (Harwell) spectrometer (expts. B1 and B2) and the results are shown in fig. 8 and table 2. The Pt-H_2 system in fact appears more complex than was evident from the t. of f. spectra as there appear to be bands at

Fig. 7 Time of Flight Spectrum of $H_2 + D_2 + Pt$

$\underline{H_2 + D_2 + Pt}$

$\underline{AMBIENT}$

$\underline{\theta = 54°}$

INTENSITY

TIME OF FLIGHT/(μs/m)

Fig. 6 Time of Flight Spectrum of $H_2O + Pt$

$\underline{H_2O + Pt}$

$\underline{AMBIENT}$

$\underline{\theta = 74°}$

INTENSITY

TIME OF FLIGHT/(μs/m)
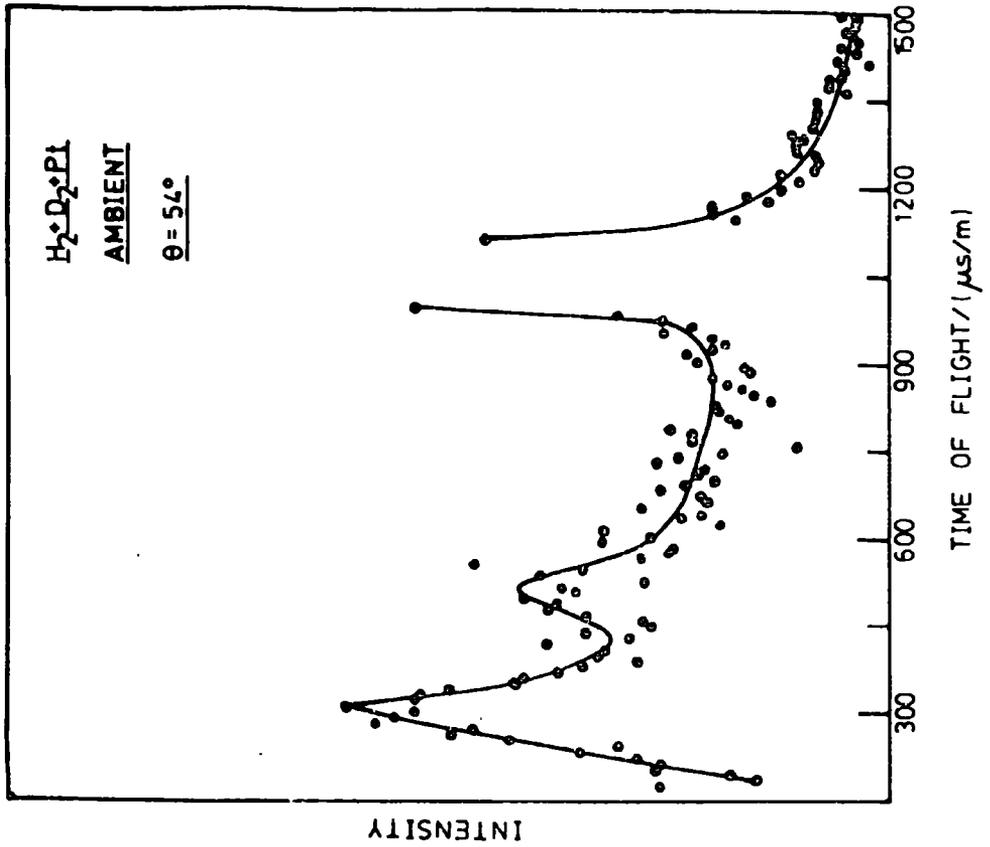
Fig. 8 B.F.D. (Harwell) Spectrum of H$_2$ + Pt

INCIDENT NEUTRON ENERGY/cm^{-1}

311.
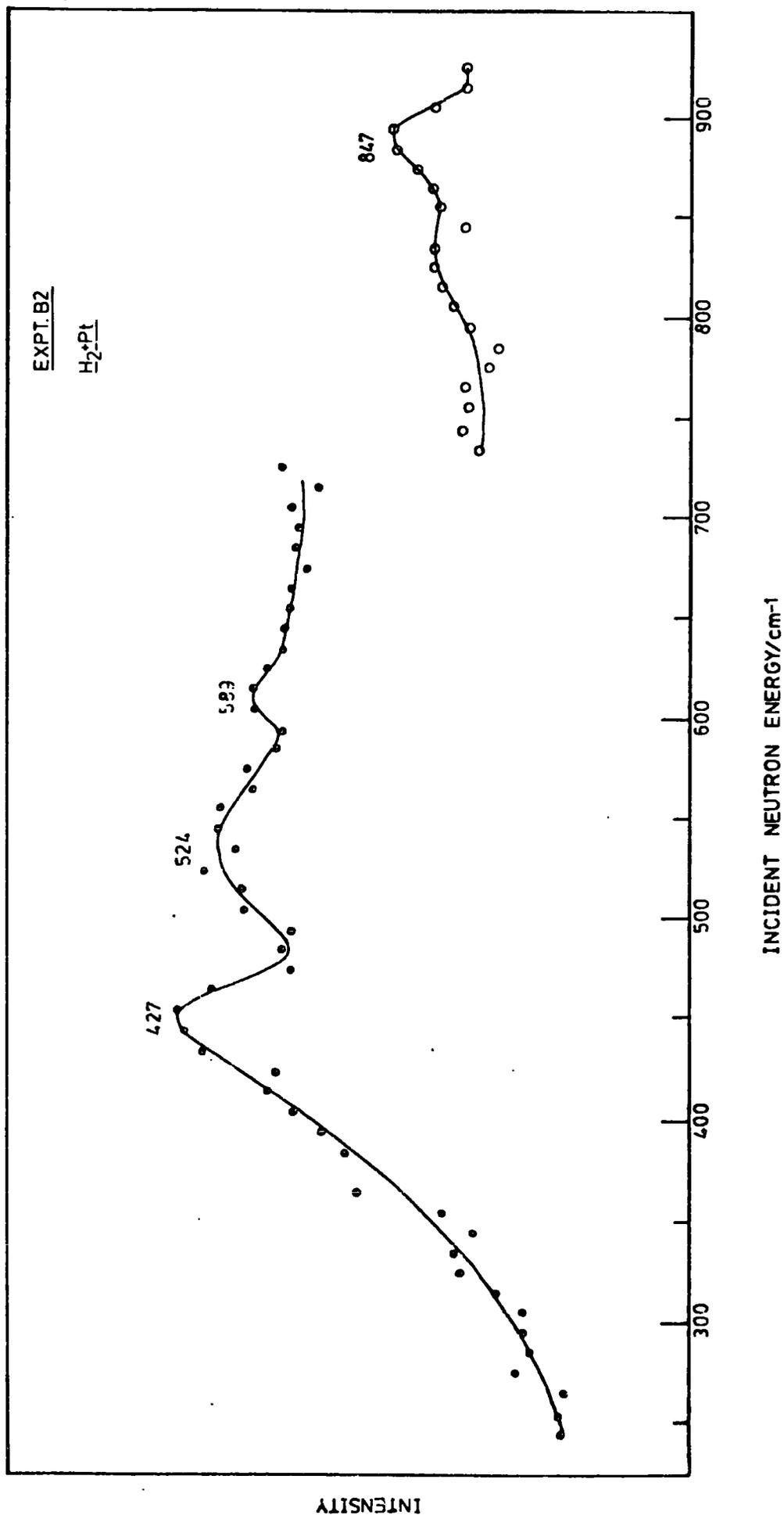
Table 2a <u>Summary of i.n.s. Results for H_2 and H_2O Adsorbed on Pt Black (cm^{-1})</u>

$H_2 + Pt^a$ B.F.D. Harwell[d] (B2)	$H_2 + Pt +$ atmosphere $IN1B^b$ (I3)	$H_2 + Pt^e$ $IN1B^b$ (I4)	$H_2 + Pt^d$ $IN1B^d$ (I2)	$H_2 + Pt^a$ $6H^b$ (H2)	$H_2O + Pt$ $6H^b$ (H3)	ice[49]	water[50]
427 ± 14			411 ± 12	403 ± 25	460 ± 30	160	169
						190	
524 ± 14	524 ± 30	532 ± 30	500 ± 12			220	
						280	
589 ± 14							
						650	492
847 ± 14	871 ± 50	840 ± 50	863 ± 50			900	
		1040 ± 50					
	1306 ± 50	1307 ± 50	1290 ± 50				
	1630 ± 50	1694 ± 50	1766 ± 100				
		2300 ± 120					

a) adsorbed at 200°C

b) spectrum run at ambient temperature

c) room temperature adsorption

d) spectrum run at 90K

e) 30 cms pressure H_2

Table 2b Spectral Ranges Covered (cm^{-1})

Experiment	Lowest Energy	Highest Energy
I2	290	4030
I3	360	2110
I4	360	3200
B2	200	900
H2	0	600
H3	0	600

higher energies than 403 cm^{-1}. It is necessary to remember that the

two spectrometers have very different resolution functions (chapter III)

and that the B.F.D. spectrometer involves neutron energy loss. At this

stage we thought it possible that we were observing extra bands as a

result of interactions between the adsorbed atoms, however, experiments

using the B.F.D. spectrometer at Grenoble (IN1B) made it necessary to

re-assess our data. The results (expt. I2) obtained using the IN1B

spectrometer and a sample prepared as described earlier are shown in

fig. 9. There are several distinct spectral features (table 2). The

band observed in the t. of f. spectra at 403 cm^{-1} was observed, however,

it was not the most intense band in the spectrum (fig. 9). The most

intense peak is found at 500 $\pm$ 12 cm^{-1}. Weaker bands were observed at

863 $\pm$ 50, 1290 $\pm$ 50 and 1766 $\pm$ 100 cm^{-1}. It would be very difficult to

explain the difference, in the region of overlap, between the B.F.D. spectra

obtained at Harwell and Grenoble (c.f. figs. 8 and 9) if they were in fact

the same system. Fig. 10a shows the result of what was in fact a "failed"

experiment. The sample was cleaned as usual and 30 torr of hydrogen was

adsorbed. Unfortunately the sample cell leaked and as there was not

time to repeat the preparations the cell was sealed using a teflon spray

and the i.n.s. spectrum obtained (expt. I4, fig. 10a). Afterwards the

cell was opened and the sample was left in contact with atmosphere for

10 hours before the spectrum was re-taken (expt. I3, fig. 10b). As can

be seen (fig. 10b and table 2) the results from expt. I3 (Pt + H$_2$ +

atmosphere) are _very_ similar to those obtained with the adsorbed hydrogen

(expt. I2). The sample which was opened to the atmosphere must contain

a large quantity of adsorbed H$_2$O because of the ease with which oxygen

reacts with adsorbed H$_2$. The band at 1630 $\pm$ 50 cm^{-1} must then be the

characteristic ν_2 vibration of water.

Fig. 9 B.F.D. Spectrum of H_2 + Pt

EXPT. 12
H₂+Pt

500cm⁻¹

863cm⁻¹

1290cm⁻¹

1766cm⁻¹

411cm⁻¹

INTENSITY

INCIDENT NEUTRON ENERGY/meV

50   100   150   200   250
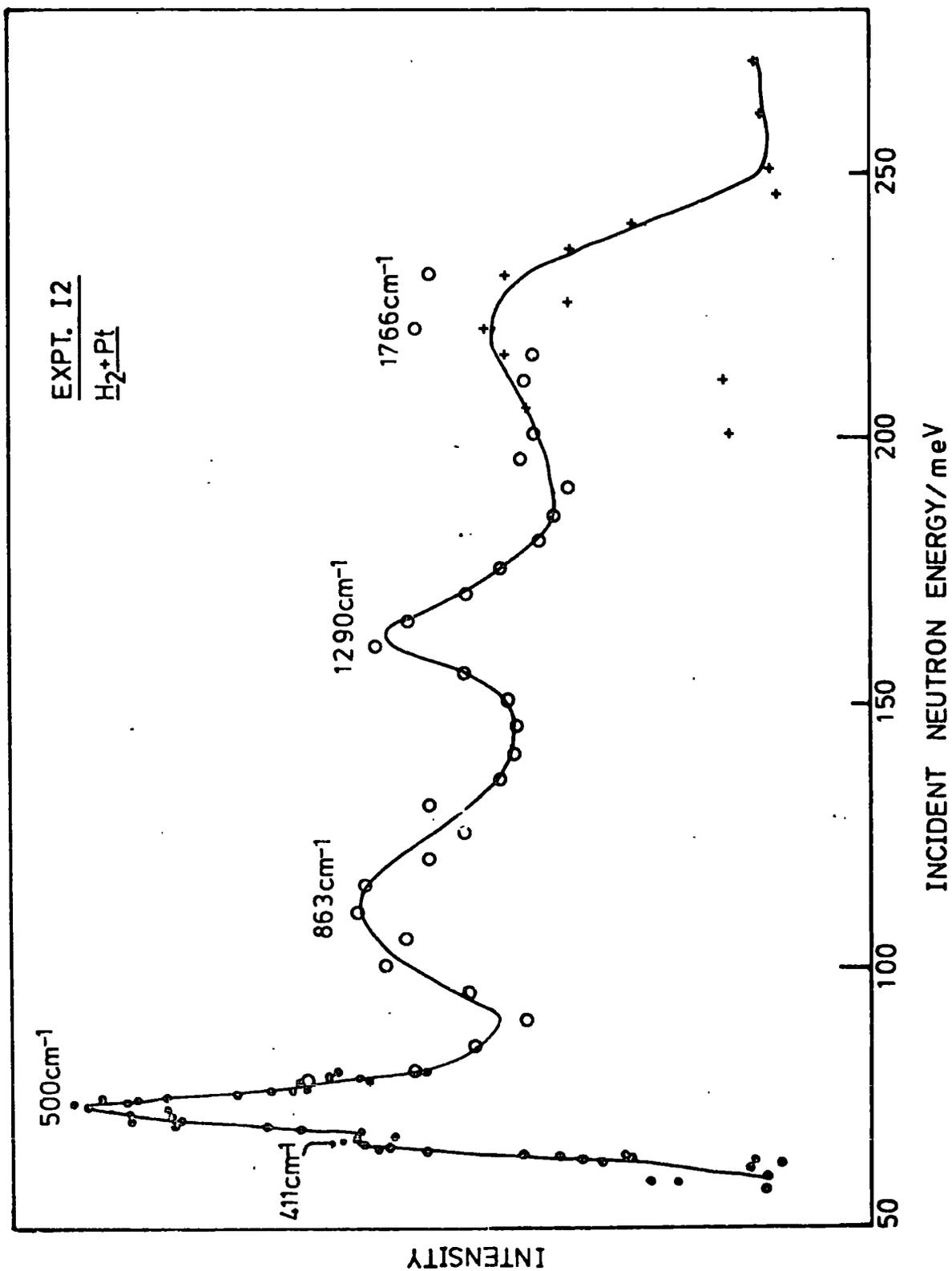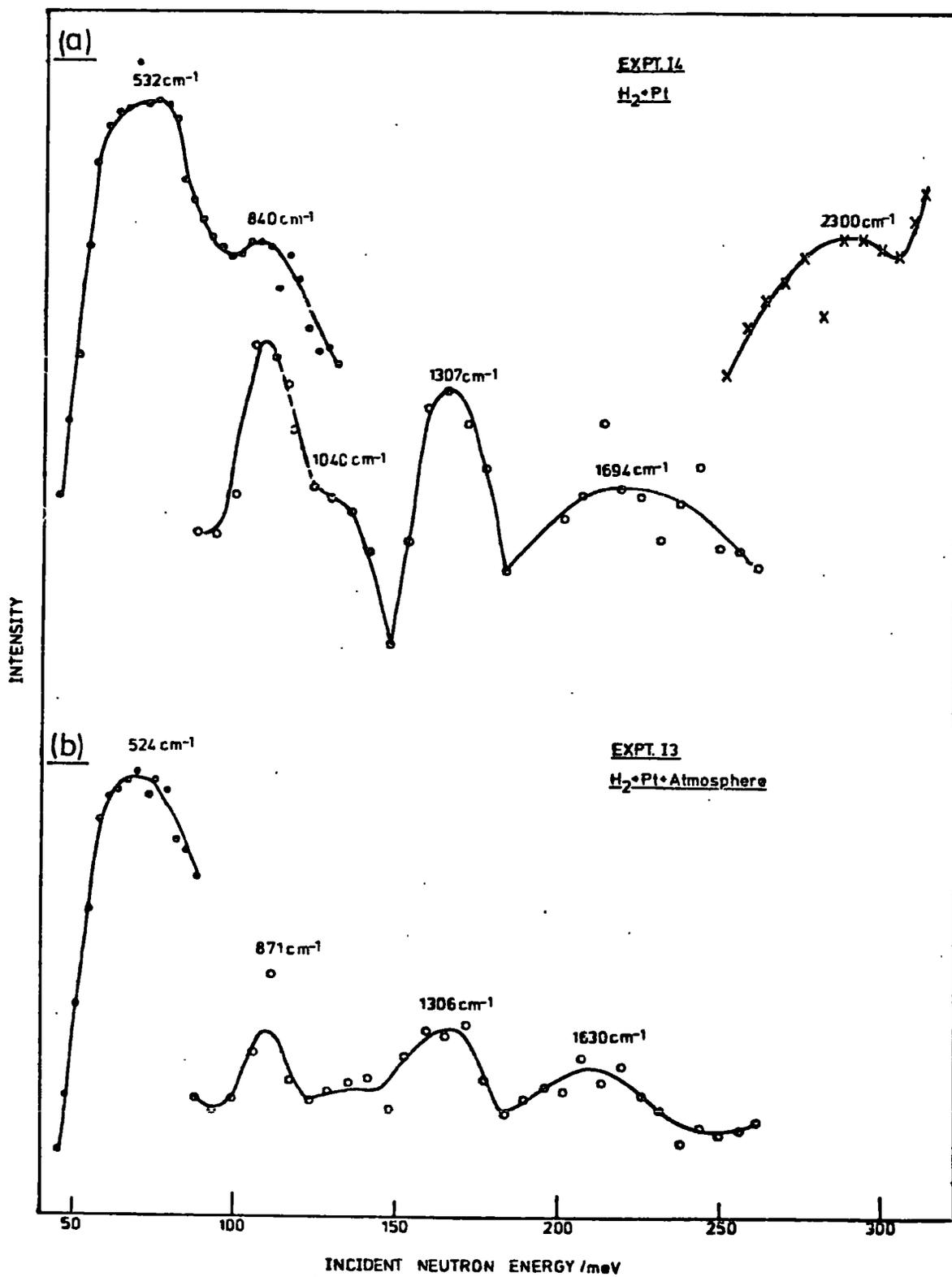
Fig. 10 B.F.D. Spectra (IN1B) of

a) Pt + 30 torr H_2

b) Pt + H_2 + Atmosphere

The adsorption of water on platinum has recently been studied by Sergeev et al.[48] who made isotherm determinations on Pt black and i.r. measurements on a sample supported on Al_2O_3. They obtained two forms of water from their isotherm measurements - an irreversibly bound form (at 25°C) which existed at low pressures of H_2O and a reversibly bound form. The infra-red results (8-10mm Hg of water) showed a band at 1630 cm^{-1} which was assigned to the characteristic ν_2 vibration of the water molecule. In the lower frequency region (expt. I3) there is a band centred at 524 cm^{-1} with no sign of a shoulder at 403 cm^{-1}. The existence of a band at 403 cm^{-1} cannot be ruled out because the 524 cm^{-1} band is broad and a copper monochromator was used for this experiment so that the experimental conditions are not directly comparable with the experiment I2 (fig. 9).

Fig. 10a shows the spectrum obtained with 30 cms Hg of H_2 adsorbed on the sample (expt. I4). With the exception of a possible shoulder at 1040 $\pm$ 50 cm^{-1} and a weak shoulder at 2300 $\pm$ 120 cm^{-1} this spectrum is identical to the spectrum of Pt + H_2 obtained more recently (expt. I2; fig. 9) and to the sample opened to the atmosphere (fig. 10b). The band at 2300 $\pm$ 120 cm^{-1} (expt. I4) because of the higher pressure of the adsorption, may correspond to the i.r. band at 2120 cm^{-1} assigned to an "r" type adatom. It would appear therefore that some hydrogen was still present on the surface.

We are therefore faced with the possibilities that our samples contain
a)   only adsorbed H_2O, or
b)   co-adsorbed H_2O and H_2.
The water may exist as "islands" of water or as a hydrate. We can discount the existence of islands of water in our sample because the i.n.s. spectra

at ambient and liquid nitrogen temperatures are almost identical. This

is important because the i.n.s. spectrum of Ice[49] is different from

that of liquid water[50] (table 2) particularly as regards the existence

of intense bands at 653 and 492 cm^{-1} respectively. We are left with

the conclusion that the adsorbed water exists as discrete molecules and

not as separate "islands" of water on the surface.

There have been several i.n.s. and other investigations of hydrates

of various metals[51,52,53] and fig. 11 shows data which we have collected

for $Ni(H_2O)_6(NO_3)_2$ and $Co(H_2O)_6(NO_3)_2$. The spectra are complex and

table 3 lists the bands expected in the lower frequency region. Table 4

lists some assignments available for hydrates, though of course we really

need data on hydrated Pt species.

Table 3: H_2O and $M-H_2O$ vibrations in hydrates

OH   sym str.
OH   antisym str.
OH_2 sciss
OH_2 rock
OH_2 wag   } expected 1000 → 250 cm^{-1}
M-O stretch
OH_2 twist
O-M-O defs.   expected < 250 cm^{-1}
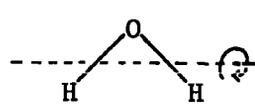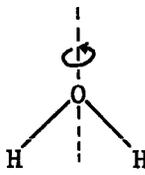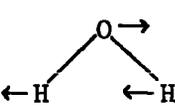
Wag   Twist   Rock

These results explain several features of our results with

adsorbed H_2O on Pt. First of all the absence of intense lower energy
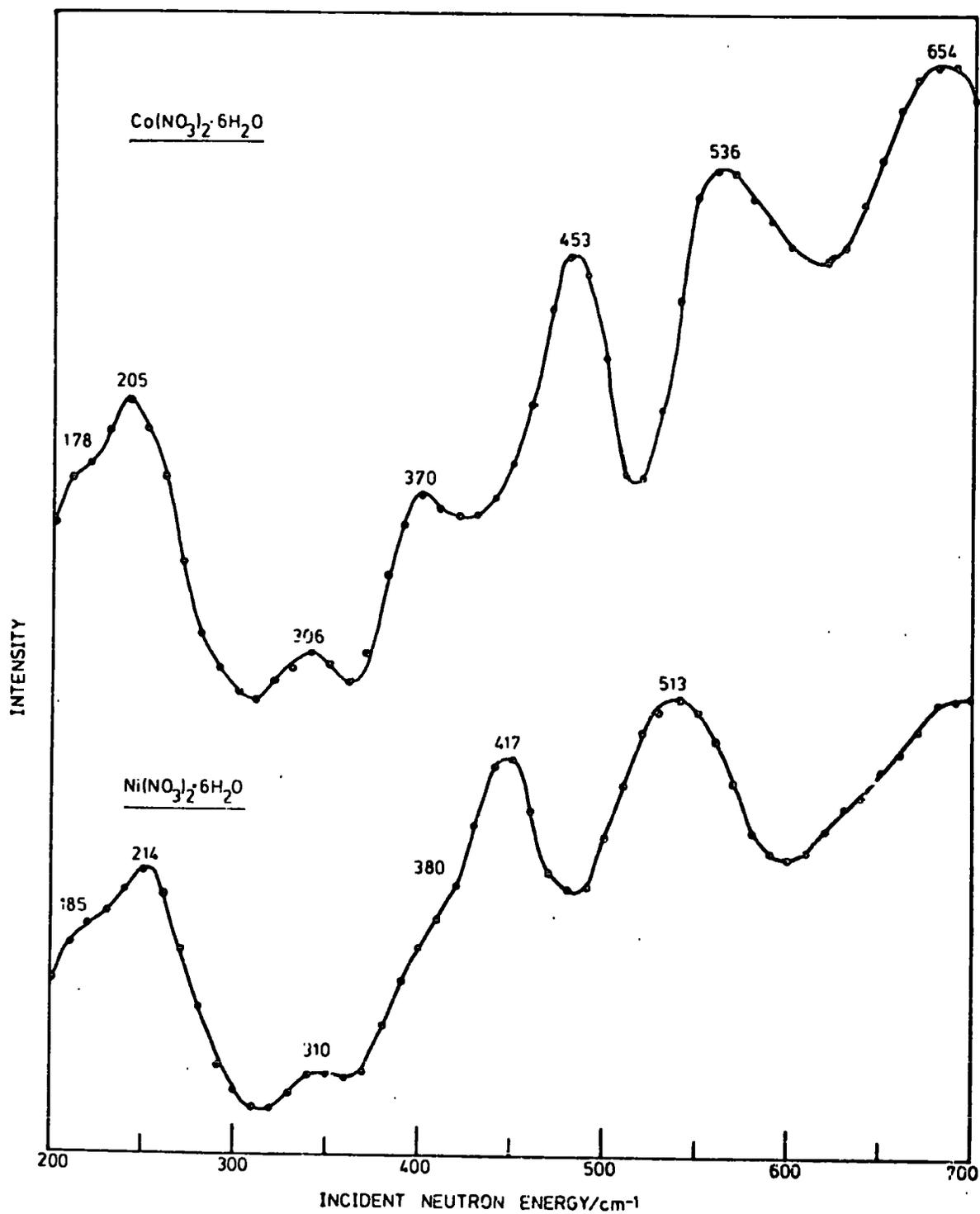
Fig. 11 B.F.D. Spectra of Metal Hydrates

Table 4: Examples of assignments for Metal hydrates (cm^{-1})

a)[52]

Compound	rock	wag	$\nu(M-O)$
$[Cr(H_2O)_6]Cl_3$	800	541	490
$[Ni(H_2O)_6]SiF_6$	755	645	405
$[Cu(H_2O)_4]SO_4 \cdot H_2O$	887,855	535	440

b)[53]

Compound	Librations	$\nu(M-O)$
$CoCl_2 \cdot 6H_2O$	776,656,560,464	341
$NiCl_2 \cdot 6H_2O$	728,650,584,480,396	350
$FeCl_2 \cdot 4H_2O$	725,552,456	379,320
$MgSO_4 \cdot 7H_2O$	665,595,484	380

bands (below 450 cm^{-1}) is not really surprising because the low energy

bands in the hydrates are due to O-M-O deformations which are not possible

in the adsorbed phase and to lattice vibrations. Modes arising from the

hindered translations of the water molecules are expected to be weak

(see chapter IV). The appearance of only a single band in the t. of f.

spectrum of adsorbed water also corresponds with our results for the

hydrates (fig. 12). The lower energy band in each of the hydrate spectra

is the O-M-O deformation. Experiments using the B.F.D. Spectrometer,

however, show that the higher energy t. of f. band is in fact several

bands (fig. 11). Unfortunately we have not had the opportunity to

obtain the B.F.D. spectrum of H_2O adsorbed on platinum.
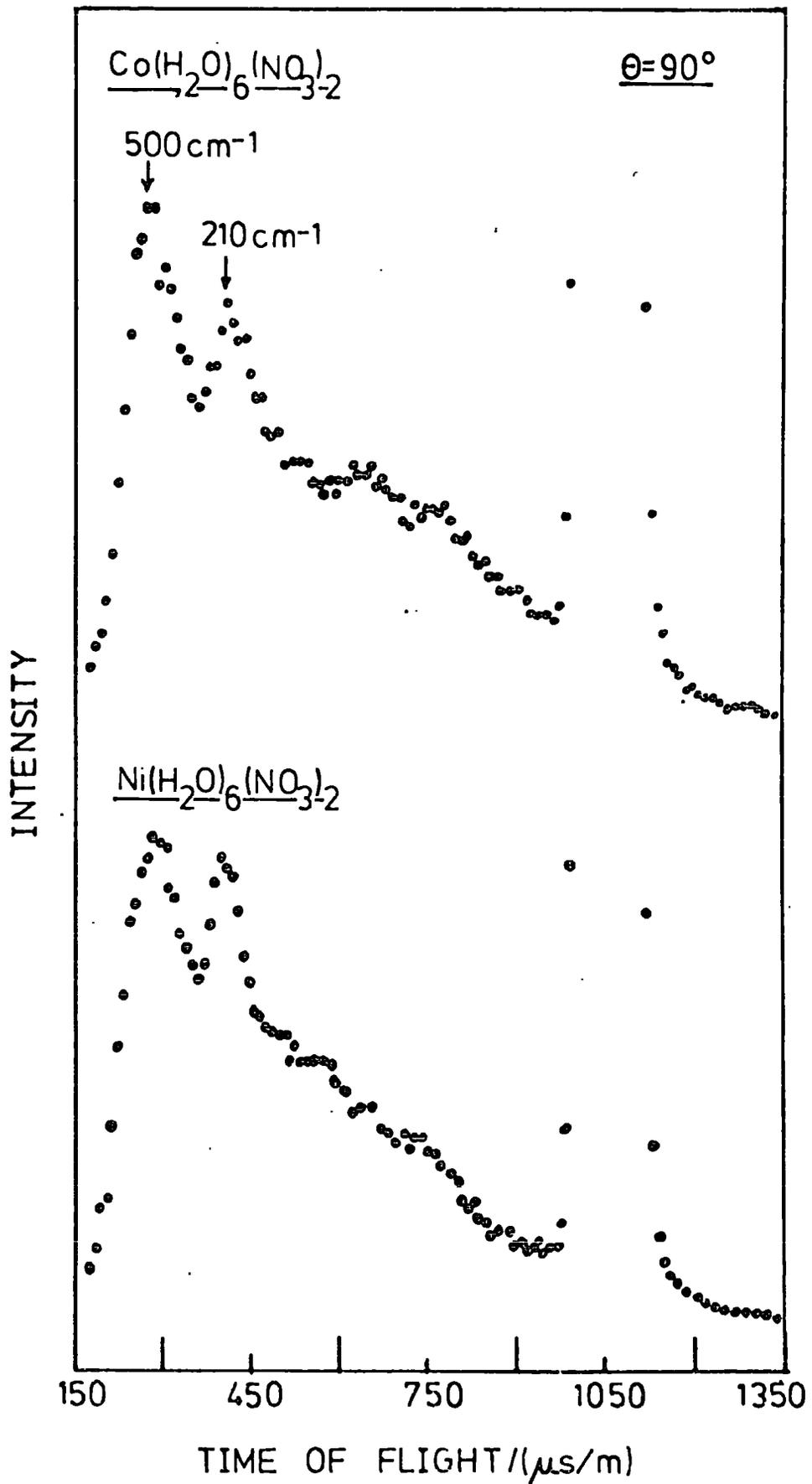
Fig. 12 T.of.F. Data for Metal Hydrates

A very strong indication that we are observing both H_2O and H_2

adsorbed on Pt is the observed difference between the Harwell and

Grenoble B.F.D. spectra (figs. 8 and 9). The difference is not

explicable in terms of difference in resolution or in momentum

transfer (Q) dependence because the values are almost identical in

both cases. We consider that the difference is in the ratio of

adsorbed H_2/H_2O on the two samples. The Harwell sample, which yielded

equally intense (measured by their peak heights) bands at 427 ± 14 and

$524 \pm 14 \; cm^{-1}$ was put into a helium atmosphere in the nitrogen cryostat

within an hour of sealing off the sample after the adsorption. The

Grenoble sample, however, was prepared in England and taken to Grenoble

so that there was a lapse of several days between the adsorption and

running the experiment. We feel, therefore, that this sample was the

most likely to become contaminated and a comparison of figs. 8 and 9

with the spectrum of Pt + H_2 + atmosphere (expt. I3; fig. 10b), bears

this out. A leakage of oxygen would of course increase the proportion

of H_2O to H_2. The sample cell was helium leak tested both before and

after the experiment (I2) and no leaks were found. There does, of

course, remain the possibility that the glass break-seals were the

source of any leakage. A comparison of the intensities in the bands

obtained in experiments I3 and I4 would be very useful because bands

associated with H_2O should increase and those associated with H_2

should decrease in intensity on opening the sample cell to the

atmosphere. Unfortunately after exposing the sample to the atmosphere

the general background level increased and the true level of background

is difficult to determine. The only really significant change is the

apparent disappearance of the shoulder at $1040 \; cm^{-1}$ on admitting the

atmosphere to the cell. The spectrum (fig. 10b) corresponding to Pt +

H_2 + atmosphere is less well defined than the other B.F.D. (IN1B)

spectra which is perhaps explained by the probable multiplicity of adsorbed species.

f)   Conclusions

1)   Results of Experiments

We have obtained i.n.s. spectra of Pt black containing co-adsorbed H_2 and H_2O. The characteristic v_2 vibration of H_2O was observed. We have also observed a band at 403 cm^{-1} which we assign to a vibration of a hydrogen atom relative to the surface. The hydrogen is atomic and probably corresponds to the interstitial "δ" or "s" form which has been shown to be i.r. inactive.

Evidence that we have in fact obtained entirely the δ state was gained by heating one of our samples and analysing the gas phase using a mass spectrometer. No gas was liberated below $200^{\circ}C$. Above this temperature strong peaks due to hydrogen were obtained and at a temperature of $250^{\circ}C$ water also appeared in the spectrum. The T.P.D. work of Tsuchiya et al. indicates that only the δ phase is stable above $100^{\circ}C$. The observation of water in the mass spectrum is not conclusive evidence, in its own right, that water also existed on the surface of our i.n.s. samples. This is because the sample used in the mass spectrometer experiment was prepared at Durham and we do not, as yet, have available pumping equipment equivalent to that used for the surface preparations at Harwell.

We can discount the possibility that we are observing an excitation of hydrogen absorbed in the bulk platinum because the solubility is so low. In our sample of 100 grams of platinum the total quantity of absorbed hydrogen cannot exceed 10^{-5} moles. However, it is still

tempting to compare the excitation energy we have observed at 403 cm^{-1} with those found for α Pd-H (552 $\pm$ 16 cm^{-1}) and β Pd-H (460 cm^{-1}).[54] These are obviously very much more similar - implying similar bonding - than the vibration frequency of the singly bonded hydrogen found on the surface of Raney Nickel (1129 cm^{-1}).[33] Recent experiments using reflection-absorption infrared spectroscopy[55] have shown that bands due to hydrogen adsorbed on palladium hydride occur at 760 and 880 cm^{-1}. Furthermore low energy electron scattering measurements[56] for hydrogen adsorbed on tungsten (100) noted two transitions, at 556 and 1089 cm^{-1}. No bands were observed at c.a. 4440 cm^{-1} where the H-H stretch occurs, indicating that the chemisorption was dissociative. Because a hydrogen atom bound to a single W atom was expected to have a stretching frequency of c.a. 2420 cm^{-1} and no band was observed at this frequency, the authors concluded that the hydrogen is multiply bonded to several W atoms. The relative intensity of the two bands indicated that they were not simply a transition and its first overtone so they were assigned to vibrations parallel (556 cm^{-1}) and perpendicular (1089 cm^{-1}) to the surface. For $WH_2(\pi-C_5H_5)$[35] the W-H stretches occur at 1896 and 1912 cm^{-1}.

To summarise we have observed five i.n.s. bands for a surface which contains adsorbed hydrogen and water (expt. I2). From the different relative intensities of the peaks in two experiments we have assigned the band at 403 cm^{-1} to a hydrogen mode and that at 500 cm^{-1} to a Pt-H_2O mode. The band at 1766 $\pm$ 100 is probably the ν_2 water vibration. We are left, therefore, with the bands at 863 cm^{-1} and 1290 cm^{-1}. The 1290 cm^{-1} cannot be an intramolecular mode of the H_2O molecule (table 2) and so it is either a harmonic (3 x 403 cm^{-1}) or perhaps a second fundamental hydrogen mode. If it is a second fundamental then the results are very similar to those described above for W. The width of

the quasi-elastic peak for the H on Pt was identical to that of the

resolution function of the instrument. This indicates that surface

diffusion must be slow and hence perhaps contrary to our earlier remarks,

two vibrational modes are to be expected (assuming that the two

hindered translations are degenerate). However, because of the low

resolution of the measurement and in the absence of corrections for

absorbtion of neutrons by the sample too much reliance cannot be placed

on this observation.

The band at 863 cm^{-1} (table 2, expt. I2) is in the correct region

for it to be a librational mode of the water molecule (table 4). (A

band at 620 cm^{-1} has been observed for H_2O adsorbed on W).[56] The other

possibility is that the 863 cm^{-1} band is the first overtone of the band

at 403 cm^{-1}, particularly because we know that because of the high

momentum transfers overtones can be intense when using the IN1B

spectrometer (chapter II).

These results do pose a further interesting question. We have the

following data for adsorbed hydrogen.

Ni	W	Pt		
		either		or
	556cm^{-1}	400cm^{-1}		40⁰ cm^{-1}
1129cm^{-1}	1089cm^{-1}	-	one or both	863 ⎤ cm^{-1} 1290 ⎦

If the mode at 400 cm^{-1} (H + Pt) is a Pt-H bend and one of the other

modes is the stretch then the results are fairly similar to those found

for W. Why then is it that no low frequency band was found for Ni + H?

The other alternative is that the 400 cm^{-1} is in fact the v(Pt-H) for

the interstitial species and its very low frequency is a consequence of

its being bonded to several Pt atoms.

g)   Further experiments and experimental procedure

Naturally we wish to examine a surface free of impurities and free

of water. In order to achieve this we must discover finally the origin

of the band at 350 cm^{-1} in the spectrum of the platinum black. To this

end it is planned to obtain the i.n.s. spectrum of platinum oxide. If

the peak is due to the oxide then we will need to determine whether it is

possible to fully clean one of our samples by hydrogen adsorption and

pumping.

Even if the sample is fully cleaned by our procedure we must still

take every precaution against the admission of oxygen into the system.

We have recently obtained a minimass 80 mass spectrometer. A mass

spectrum obtained using this instrument indicates that the partial

pressure of oxygen in the system we have been using is 3 x 10^{-6} torr

when equilibrium has been reached. When one considers the very large

surface area that we have present it would take a very long time (c.a.

100 hours) at this pressure for a full oxide layer to form. In point

of fact our samples are sealed off within a few hours of cleaning so

that only a small percentage of the surface should be recontaminated.

In order to improve this further we have designed and built an all-

metal ultra-high vacuum system (chapter III). After the initial

evacuation the pumping is continued on a completely closed system.

So far we have achieved pressures below 10^{-8} torr in the unbaked

system and after baking the pressure should be very significantly lower.

We will also be able to continuously monitor the gas phase using the

mass spectrometer.

We would also like to be able to monitor the pressure inside the sample cell after sealing-off from the pumping system. So far we have not been able to obtain a vacuum gauge which is both small enough and robust enough to be fitted to our sample cell.

In future we also plan to measure the actual quantities of gases adsorbed.

h)   The future

We feel that using i.n.s. spectroscopy we have been able to obtain data for adsorbed gases which is probably not obtainable using any other technique. These experiments are as yet in their initial stages but we have learned a great deal about the experimental procedures etc. required. Despite the difficulties mentioned in this chapter we feel that this is a very interesting and important line of research and it is one which we will pursue in the future.

Appendix

Let

I_T^{Pt} = true intensity of scattering from the Pt : corrected

for absorption cross section and container scattering

I_E^{Pt+C} = observed intensity of scattering from Pt + container

I_E^{C} = observed intensity of scattering for container

I_E^{Pt+H+C} = observed intensity of scattering from Pt + H + container

I_T^{Pt+H} = true intensity of scattering from Pt + H

Then we obtain according to the methods of Paalman and Pings

$$I_T^{Pt} = k_1 I_E^{Pt+C} - k_2 I_E^{C}$$

$$I_T^{Pt+H} = k_3 I^{Pt+H+C} - k_4 I_E^{C}$$

where the k_i's are constants to be calculated by the computer program.

Thus $I_T^{H} = I_T^{Pt+H} - I_T^{Pt}$

$$= k_3 I_E^{Pt+H+C} - k_1 I_E^{Pt+C} - I_E^{C}(k_4 - k_2)$$

Hence the considerable simplification if $I_E^{C} \approx 0$.

328.

References

1. G.A. Somorjai, Principles of Surface Chemistry, Prentice-Hall Inc. New Jersey, 1972.

2. M. Green, Solid State Surface Science Vol. 1., Marcel Dekker, New York, 1969.

3. J.C.P. Mignolet., J. Chim. Phys. Physicochim. Biol., 54, 19, (1957).

4. W.M.H. Sachtler and G.J.H. Dorgels, Phys. Chem. 25, 69, (1960).

5. R. Suhrmann, G. Wedler and H. Gertsch, Z. Phys. Chem., 17, 350, (1958).

6. R. Lewis and R. Gomer, Surface Sci., 17, 333, (1969).

7. V. Ponec, J. Catal., 6, 362, (1966).

8. a) T. Toya, Progr. Theor. Phys. Suppl., 23, 250, (1962).

   b) T. Toya, J. Res. Inst. Catal., Hokkaido Univ., 10, 236, (1962).

   c) T. Toya and J. Horiuti, J. Res. Inst. Catal., Hokkaido Univ., 16, 605, (1968).

9. T. Toya, J. Res. Inst. Catal., Hokkaido Univ., 8, 209, (1960).

10. J. Horiuti and T. Toya, Kinetika i Kataliz, 4, 3, (1963).

11. F.S. Brown, R.C. Brown and N.H. March, Phys. Lett., 47A(6), 489, (1974).

12. R.E. Norberg, Phys. Rev., 86, 745, (1952).

13. G.C. Bond, Plat. Metal Rev., 10, 87, (1966).

14. M. Primet, J.M. Basset, M.V. Mathieu and M. Prettre, J. Catal., 28, 368, (1975).

15. W.A. Pliskin and R.P. Eishens, Z. Phys. Chem., 24, 11, (1960).

16. D. Eley, D.M. Moran and C.H. Rochester, Trans. Faraday Soc., 64, 2168, (1968).

17. L.T. Dixon, R. Barth and J.W. Gryder, J. Catal., 37, 368, (1975).

18. K. Christmann, G. Ertl and T. Pignet, Surface Sci., 54, 365, (1976).

19. S. Tsuchiya, Y. Amenomiya and R.J. Cvetanovic, J. Catal., 19, 245, (1970).

20. S. Tsuchiya, Y. Amenomiya and R.J. Cvetanovic, J. Catal., 20, 1, (1971).

21. J.J. Stephan, V. Ponec and W.M.H. Sachtler, J. Catal., 37, 81, (1975).

22. Z. Paal and S.J. Thompson, J. Catal., 30, 96, (1973).

23. H.U.D. Wresendanger, J. Catal., 2, 538, (1963).

24. W.J. Rootsaert, L.L. Van Reijen and W.M.H. Sachtler, J. Catal., 1, 416, (1962).

25. J.D. Clewley, J.F. Lynch and T.B. Flanagan, J. Catal., 36, 291, (1975).

26. L.T. Dixon, R. Barth, R.J. Kokes and J.W. Gryder, J. Catal., 37, 376, (1975).

27. M. Smutek, S. Černý and F. Buzek, Advan. in Catal., 24, 343, (1975).

28. D.A. King, Surface Sci., 47, 384, (1975).

29. M. Primet, J.M. Basset and M.V. Mathieu, Faraday Trans. I., 70, 293, (1974).

30. T. Ito, T. Kadowaki and T. Toya, Proc. 2nd Int. Conf. on Solid Surfaces, 1974. Japan J. Appl. Phys. Suppl. 2, Pt. 2, (1974) p.257.

31. J.L. Bonardet, J.P. Fraissard and L.C. De Menorval, 6th Int. Cong. on Catalysis, London 1976, p.1.

32. Z. Paal, T. Baird and S.J. Thompson, Trans. Faraday Soc., 69, 50, (1973).

33. R. Stockmeyer, H.M. Conrad, A. Renouprez and P. Fouilloux, Surface Sci., 49, 549, (1975).

34. H. Asada, T. Toya, H. Motohashi, M. Sakamoto and Y. Hamaguchi, J. Chem. Phys., 63(9), 4078, (1975).

35. D.M. Adams, Metal-Ligand and Related Vibrations, Edward Arnold Ltd., London, 1967.

36. F.R. Hartley, The Chemistry of Palladium and Platinum, Applied Science Publishers, London 1973.

37. J. Knight and M.J. Mays, J. Chem. Soc. A., 711, (1970).

38. J.E. Bercaw and H.H. Brintzinger, J. Amer. Chem. Soc., 91, 7301, (1969).

39. P.C. Flynn and S.E. Wanke, J. Catal., 37, 432, (1975).

40. T. Baird, Z. Paal and S.J. Thompson, J.C.S. Faraday I., 69, 50,(1973).

41. W.H. Weinberg, R.M. Lambert, C.M. Comrie and J.W. Linnett in Proc. 5th Int. Cong. Catal., Ed. J.W. Hightower, North Holland,Amsterdam (1973), p.513.

42. J.R. Anderson, Structure of Metallic Catalysts, Academic Press London, (1975).

43. M. Akhtar and F.C. Tompkins, Trans. Faraday Soc., 67, 2454, (1971).

44. H.H. Paalman and C.J. Pings, J. Appl. Phys., 33(8), 2635, (1962).

45. J.H. Clarke, A.E.R.E. Report R-8121 (1976), (H.M.S.O.).

46. D.H. Dutton and B.N. Brockhouse, Can. J. Phys., 50(23), 2915, (1972).

47. U. Belluco, Organometallic and co-ordination Complexes of Platinum, Academic Press, London and New York 1974.

48. S.I. Sergeev, N.A. Shurmovskaya, L.A. Fokina and R.Kh. Burshtein, Elektrokhimiya, 2(2), 274, (1975).

49. H. Prask, H. Boutin and S. Yip, J. Chem. Phys., 48(8), 3367, (1968).

50. Ed. P.A. Egelstaff, Thermal Neutron Scattering, Academic Press London 1965.

51. J.R. Ferraro, Low-Frequency Vibrations of Inorganic and Co-ordination Compounds, Plenum Press, New York, 1971.

52. K. Nakamoto, Infrared Spectra of Inorganic and Co-ordination Compounds, Wiley Interscience New York, 1970.

53. H.J. Prask and H. Boutin, J. Chem. Phys., 45(9), 3284, (1966).

54. M.R. Chowdhury and D.K. Ross, Solid State Comm., 13, 229, (1973).

55. I. Ratajczykowa, Surface Sci., <u>48</u>, 549, (1975).

56. F.M. Propst and T.C. Piper, J. Vac. Sci. and Technol., <u>4(2)</u>, 53, (1967).

57. D.M. Adams, P.J. Chandler and R.G. Churchill, J. Chem. Soc.(A), 1272,
     (1967).